CHAPTER - 4

Results and discussion

CHAPTER IV
RESULTS AND DISCUSSION

4.0 INTRODUCTION

The results pertaining to the study **"Synthesis, Characterisation And Utilisation of Water Soluble Polyvinyl Alcohol-Selected Amino Acid Composites as Corrosion Inhibitors for Mild Steel in Acid Medium"** are presented and discussed in the light of the objectives set forth. The present study aims to synthesise derivatives of water soluble polyvinyl alcohol-selected amino acid composites and analyze the inhibitive nature of the polyvinyl alcohol-selected amino acid composites on mild steel in 1M HCl medium.

Efforts are taken to discuss the results in the three phases.

Phase I: Synthesis and characterisation of water soluble polyvinyl alcohol-selected amino acid composites.

PhaseII: Utilisation of polymer composites as corrosion inhibitors-Weight loss methods and electrochemical measurements.

PhaseIII: Analysing the surface of mild steel in the presence and absence of polyvinyl alcohol- selected amino acid composites by surface analytical techniques.

PHASE - I

4.1 SYNTHESIS AND CHARACTERISATION OF THE SYNTHESISED WATER SOLUBLE POLYVINYL ALCOHOL-SELECTED AMINO ACID COMPOSITES

In the present work, the synthesis of polyvinylalcohol-selected amino acid composites (PVAALA, PVAVAL, PVAGLU, PVAGLN, PVATYR and PVATRP composites) in electrolytic medium (0.5M oxalic acid) is presented. At the same time, its spectroscopic (FTIR and UV-Visible spectra), thermal properties (TG/DTA, DSC and XRD) and Morphological (SEM-EDXA) characterization as well as evaluation of its protective character against corrosion on mild steel is reported.

4.1.1 CHARACTERIZATION OF POLYVINYL ALCOHOL-SELECTED AMINO ACID COMPOSITES

4.1.1.1 Elemental Analysis

In order to confirm the chemical composition of the synthesized compounds CHN analysis has been carried out on the water soluble polymer composites (PVAALA, PVAVAL, PVAGLN, PVAGLU, PVATYR AND PVATRP) using the instrument Vario EL III CHNS serial number 11035060. The percentage of carbon, hydrogen and nitrogen was determined by CHN analysis. Chemical composition of

PVAALA, PVAVAL, PVAGLN, PVAGLU, PVATYR AND PVATRP polymer composites are summarized in Table-2.

Table-2 Result of elemental analysis of the prepared polyvinyl alcohol-selected amino acid composites

S.No	Sample	% Element Composition		
		C (%)	H (%)	N (%)
1	PVAALA	19.86	11.09	17.01
2	PVAVAL	18.04	13.09	19.08
3	PVAGLN	19.79	13.01	16.88
4	PVAGLU	20.02	10.96	15.76
5	PVATYR	21.33	10.36	16.8
6	PVATRP	18.23	9.98	18.91

4.1.1.2 Conductivity Studies

Conducting polymers are unique in that, they are organic chains of alternative double and single bonded sp^2 hybridization atoms, which endow the polymer with metal like semiconductive properties. Conductivity is a measure of electrical conduction and thus a measure of the ability of a material to pass a current. Generally, materials with conductivities less than 10^{-8} S/cm and 10^3 S/cm are considered semiconductors and materials with conductivities greater than 10^3 S/cm are considered conductors.

The conductivity measurements are carried out using standard four point probe techniques at room temperature for all the synthesized polymer composites. From the results, PVAGLU and PVAGLN composites showed the conductivity value of -1.93 $\times 10^2$ S/cm (I=0.005) and 2.09 $\times$ 10^4 S/cm (I=0.002) respectively. To find out whether the polymer composites PVAALA, PVAVAL, PVATYR and PVATRP are semiconductors, measured in the frequency range 10^2 -10^6 Hz at room temperature.

The powders of PVAALA, PVAVAL, PVATYR and PVATRP composites so obtained were crushed and finely ground in agate mortar. The composite powders were pressed to form pellets of 10 mm diameter and 2-2x5 mm thickness by applying pressure of 90 Mpa in hydraulic press. The pellets of PVAALA, PVAVAL, PVATYR and PVATRP, composites were coated with silver paste on either side. Copper electrodes were placed on both the surfaces to obtain a better contact. The electric resistivity of PVAALA, PVAVAL, PVATYR and PVATRP, composites were measured using impedance analyzer.

Impedance spectroscopy is employed to establish the conduction mechanism, observing the participation of the polymer chain, mobility and carrier generation processes. The conductivities of the polymer complexes are calculated from the bulk resistance obtained by the intercepts of the typical impedance curves for room temperatures. The impedance curves of PVAALA, PVAVAL, PVATRY and

PVATRY composites are presented in table-3. The disappearance of the semicircular portion in the impedance curve leads to a conclusion that the current carriers are ions and this leads to further conclude that the total conductivity is mainly the result of ion conduction **(Hema et al., 2008).**

The conductivity value of polymer composites - PVAALA, PVAVAL, PVATYR, PVATRP composites are found to be $5.9 \times 10^{-8}\ \Omega$, $2.9 \times 10^{-9}\ \Omega$, $1.5 \times 10^{-2}\ \Omega$, and $1.42 \times 10^{-8}\ \Omega$. Normally the conductivity values of 10^{3} to 10^{-8} S/cm are described as semiconductors. Hence PVAALA, PVAVAL, PVATYR, PVATRP composites are found to be semiconductors.

Table-3 Room temperature conductivity values of polyvinyl alcohol-selected amino acids composites

S.NO.	Polymer	Conductivity values (S/cm)	Conductors/ semiconductors
1.	PVAALA	5.9×10^{-8}	semiconductor
2.	PVAVAL	2.9×10^{-9}	semiconductor
3.	PVAGLN	2.1×10^{4}	conductor
4.	PVAGLU	-1.9×10^{2}	conductor
5.	PVATYR	1.5×10^{-2}	semiconductor
6.	PVATRP	1.4×10^{-8}	Semiconductor

4.2 CHARACTERIZATION OF POLYVINYL ALCOHOL-ALALINE COMPOSITE

4.2.1 CHARACTERISATION OF PVAALA USING FTIR SPECTRA DATA

To characterize the synthesized PVAALA composite, the FTIR analysis of PVA, ALA and PVAALA has been carried out (Figure-12a). The bands pertaining to PVA and Alanine (ALA) and PVAALA composite as shown in table-4 are shifted to the following wave numbers as given in table-4. The FTIR spectra obtained for Alanine could go hand to hand with the **(Lydia Caroline et al., 2009)**. The spectral changes are therefore clear evidence for the formation of polymer composite between PVA & ALA has occurred. The important peaks are assigned and discussed with references (**Yuan-Hiang Yu *et al.,* 2003, srimathi *et al.,* 2011).**

PVA Vs PVAALA

A broad and strong peak centred at 3299 cm^{-1} is due to the stretching vibrations of -OH stretching from the inter and intra molecular hydrogen bonds in PVA. The adsorption peak at 2923 cm^{-1} assigned to -C-H stretching from alkyl group in PVA has been shifted to 2962 and 2850 cm^{-1} in PVAALA composite. A peak at 1723 cm^{-1} associated with C=O stretching vibration and carbonyl group which can easily bond with hydrogen of PVA backbone is found to be shifted to a lower wave number in (1905 cm^{-1} and 1742 cm^{-1}) (amide I band(C=O stretching)) in the PVAALA composite. The absorption peak due to CH_3 bending deformation, C-O stretching and OH in plane bending observed in PVA at 1417 cm^{-1} is found to be shifted to a

lower wave number (1417 cm^{-1}) in PVAALA composite. A band at 1371 cm^{-1} associated with C–H/OH bending is found in PVA. This peak shifted to 1374cm^{-1} in the PVAALA composite. A sharp band at 1080 cm^{-1} and 1022 cm^{-1}due to C-O stretching and C-O-C stretching in PVA backbone is found to be shifted to 1096 cm^{-1} in the PVAALA composite. The absorption band at 838 cm^{-1}, 1251 cm^{-1} and 925 cm^{-1} corresponds to CH_2 rocking vibrations and C-H out of plane deformation of PVA.

ALA Vs PVAALA

A broad and strong peak centred at 3194 cm^{-1} is due to the stretching vibrations of NH_3^+ asymmetric stretching, solid state stabilized a zwitterions structure with NH_3^+ and COO^- and N-H group of polyalanine is hydrogen bonding with -O-H group of PVA in PVAALA composite. A band at 2989 cm^{-1} corresponds to -C-H stretching from alkyl group of ALA. A peak at 2594 cm^{-1} in ALA indicates the presence of combination band of NH_3^+ bending. Bands at 2118 and 1576 cm^{-1} of ALA are due to NH_3^+ degenerative deformation and NH_3^+ symmetric deformation (combination NH deformation and CN stretching). This band is shifted to 2013 and 1591 cm^{-1} in the PVAALA composite. A peak at 1452 and 1413 cm^{-1} is due to CH_3 bending deformation and C-O stretching of ALA. This band is shifted to 1417 cm^{-1} in the PVAALA composite. The band at 1107 cm^{-1} is due to COO^- symmetric stretching and C-C-C stretching in ALA. The peaks at 918 and 840cm^{-1} are related to C-H out of plane deformation and CH_2 rocking vibration in ALA. Another peak at 1355 cm^{-1} is also related to symmetric stretching of COO^- in ALA. This is also present in the PVAALA composite. A peak at 1223/1010 cm^{-1} due to the rocking of NH_3^+ /C-C-N stretching in ALA is shifted to a lower wave number 1278/1096 cm^{-1} in PVAALA composite. A peak at 763 cm^{-1} is related to special NH wagging and COO^-bending in ALA. This is shifted to 790 cm^{-1} in PVAALA composite. A band at 643 cm^{-1} is due to the COO- scissoring of ALA. This is shifted to 627 cm^{-1} in PVAALA composite. The changes in the vibrational frequencies of the above mentioned peaks in the FTIR spectrum of PVA, ALA and PVAALA confirmed the formation of PVAALA composite.

4.2.2 UV-VISIBLE ABSORBANCE SPECTRUM OF PVAALA COMPOSITE

The chemical structure of the synthesised polyvinyl alcohol-Alanine composite has been identified using UV-Vis analysis. Figure-12c and table-5 represents the UV-Vis absorption spectra of PVA, Alanine and PVAALA composite **(Shanker Ram et *al.,* 2004, Lydia Caroline *et al.,* 2009)**. PVA, Alanine and PVAALA composite are almost transparent in the wavelength region of 190-1100nm. Figure-12c shows the absorption spectrum of L-Alanine. The cut off wavelength is absorption at 220nm.

Figure-12 Characterization of PVAALA Composite

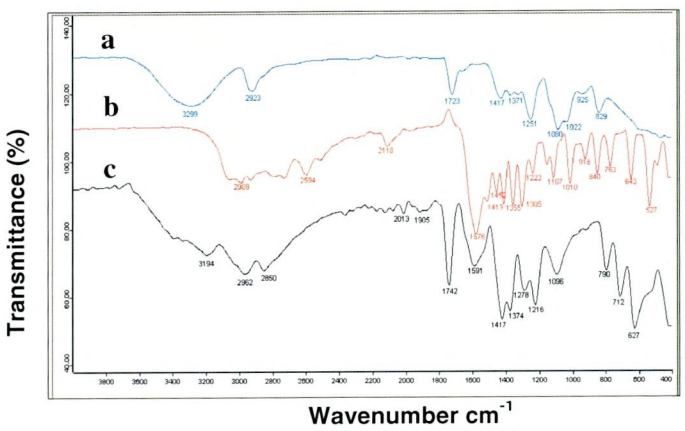

Fig. 12a FTIR Spectra of (a) PVA (b) Alanine (c) PVAALA composite

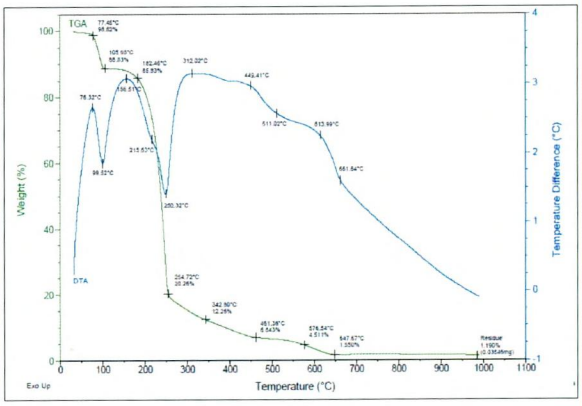

Fig. 12b TG and DTA thermograms of PVAALA composite

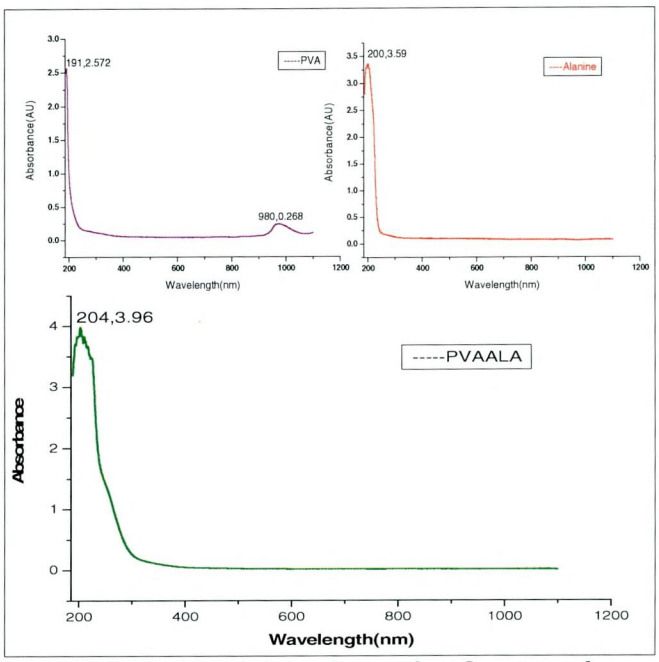

Fig. 12c UV-visible absorption Spectra of (a) PVA (b) Alanine (c) PVAALA composite

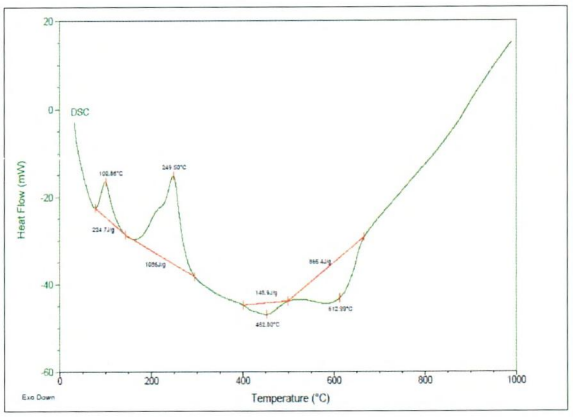

Fig. 12d DSC traces of PVAALA composite

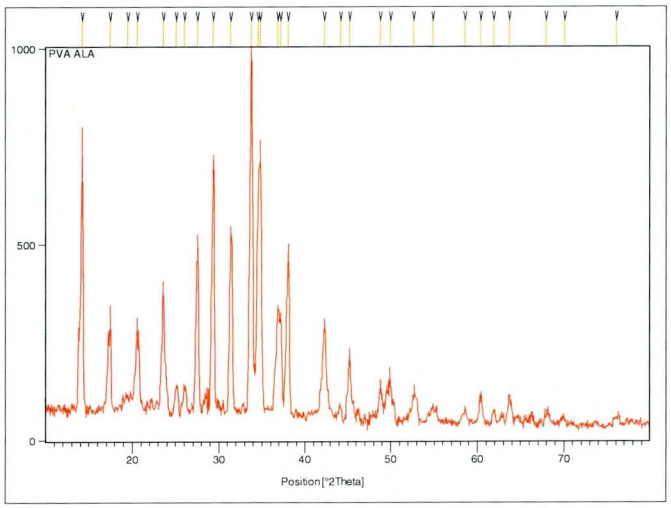

Fig. 12e X-ray Diffraction pattern of PVAALA composite

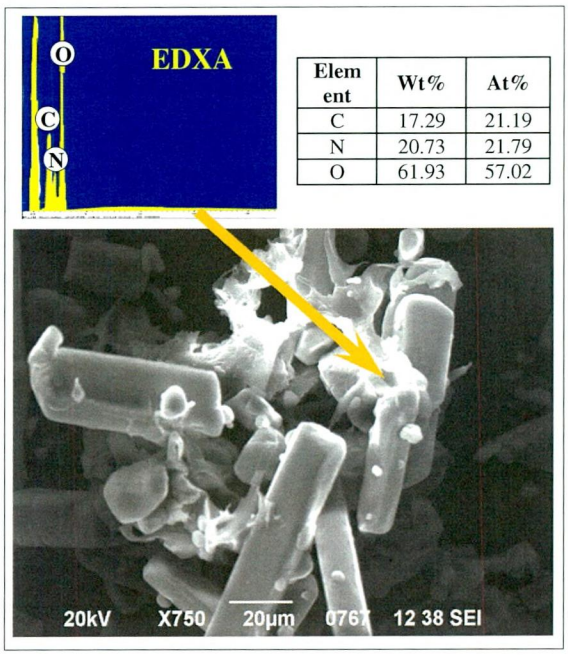

Element	Wt%	At%
C	17.29	21.19
N	20.73	21.79
O	61.93	57.02

Fig. 12f SEM-EDXA micrograph of PVAALA composite

Table: 4 FTIR Peak assignments for PVA, Alanine (ALA) and PVAALA composite

S. No.	PVA (cm^{-1})	Alanine (ALA) (cm^{-1})	PVAALA Composite (cm^{-1})	Assignment
1.	3299	-	-	OH str. (inter and intra molecular hydrogen bonds)
2.	-	-	3194	NH_3^+ asym. str., zwitterions structure, bonded N-H str.
3.	2923	2989	2962, 2850	-C-H str. from alkyl group
4.	-	2594	-	Combination band of NH_3^+ bending
5.	-	2118	2013	NH_3^+ degenerative def.
6	1723	-	1905, 1742	C=O str. Vib., amide I band(C=O str.)
7.	-	1576	1591	NH_3^+ sym. def., combination of NH def. and CN str.
8.	1417	1452,1413	1417	CH_3 bending def. + C-O str. +OH in plane bending
9.	1371	1355,1305	1374	Sym. str. of COO^-, C–H/OH bending
10.	1251	1223	1278, 1216	CH_2 rocking, rocking of NH_3^+
11.	-	1107	-	COO^- sym. str., C-C-C str.
12.	1080, 1022	1010	1096	C-O str. + C-O-C str. , C-C-N str.
13.	925	918	-	C-H out of plane def.
14.	829	840	-	CH_2 rocking vib.
15.	-	763	790, 712	NH wag., COO^-bending
16.	-	643	627	COO- scissoring
17.	-	527	-	COO^- rocking, NH_3^+ torsional

Table-5 Wavelength and absorption maxima of PVA, Selected Amino acid, polymer composite

S.NO.	PVA, AA and Polymer composite	Wavelength(nm) of PVA, AA and Polymer composite	Assignment (transition)
1.	PVA	200, 960,	n-π*
2.	Alanine	210, 220	n-π*
3.	PVAALA	220, 260	n-π* and π-π*
4.	Valine	210	n-π*
5.	PVAVAL	220, 260, 960	n-π* and π-π*
6.	Glutamine	220	n-π*
7.	PVAGLN	220, 960	n-π*
8.	Glutamic acid	210	n-π*
9.	PVAGLU	220, 960	n-π*
10.	Tyrosine	220, 240, 260, 280	n-π* and π-π*
11.	PVATYR	220, 280, 310	n-π* and π-π*
12.	Tryptophan	260, 2.80, 300	n-π* and π-π*
13.	PVATRP	220,960	n-π* and π-π*

There is no significant adsorption in the range 300-1100 nm. This is an advantage of using amino acids, where the absence of strongly conjugated bands leads to wider transparency range in the visible and UV spectral region. From L-Alanine when the absorbance is monitored from 190 to 300 nm, the absorption is

evident below 240 nm. It is assigned to electronic excitation in the COO^- group of L-Alanine. The bands at 200 and 220 nm could be connected with the transitions π-π^* transition respectively. The presence of chromophores, namely amino group and carboxyl groups in the L-Alanine structure, makes it transparent in the UV-Visible region. PVA was found to absorb strongly in the 200-400 nm region. The optical absorption (UV/Visible) spectrophotometric scans in the wavelength range of 200-1400 nm of PVAALA composite is shown in the figure-12c. The observed spectra are characterized by main absorption edge, 220 and 260 nm for the PVAALA composite curve and it slightly shifted towards shorter wavelength with Alanine content. The shift of the absorption edge in the PVAALA composite reflects the variation in the energy band gap, which arises due to the variation in crystallinity within the polymer matrix. The band at 220 nm in the UV spectra is assigned to n-π^*. Another absorption shoulder is observed at about 260 nm and it may be attributed to π-π^* which comes from unsaturated bonds mainly C=O. From the above results, it can be inferred that the PVAALA composite was obtained using the polyvinyl alcohol and Alanine.

4.2.3 THERMOGRAVIMETRIC AND DIFFERENTRIAL THERMAL ANALYSIS (TG/DTA ANALYSIS)

To find out the thermal characteristics of PVAALA, PVAVAL, PVATYR, PVATRP, PVAGLN and PVAGLU composites, differential thermal analysis (DTA) and thermogravimetric analysis (TGA) were carried out simultaneously in a thermal analyzer (SDTQ600V8.3 Build 101). The sample was heated at a rate of 20°C/min in protected nitrogen gas between 20°C and 1100°C, 4.7690 mg (PVAVAL), 2.9380 (PVAGLN), 2.3810 mg (PVATRP), 2.9490 mg (PVAGLU), 2.9800 mg (PVAALA) and 2.480 mg (PVATYR) of the samples have been taken to carry out the experiment. Figure12-18 shows the thermograms illustrating simultaneously recorded TGA and DTA. The relation between temperature and weight loss of the polymer composite samples in the TG/DTA curves is shown in figure 12-18.

4.2.3.1 TG/DTA ANALYSIS OF POLYVINYL ALCOHOL-ALANINE (PVAALA) COMPOSITE

The thermal degradation behaviour of PVAALA composite has been examined by TGA as shown in the Figure-12b. It can be noted that PVAALA composite exhibits two weight loss stages at 77-105°C, 182-254°C followed by a final decomposition of the PVAALA composite around 1000°C. The first weight loss of the polymer occurring between the temperature range 77-105°C is 9.79%, which may be attributed to the loss of physically adsorbed and hydrogen bond linked water molecules at the first stage (or) is due to the evaporation of physically weakly and

chemically strongly bound water. In the second stage the weight loss occurred in the ranges 182-254°C. This may be due to breakdown of the PVAALA backbone.

In the two phases, the weight loss of PVAALA composite in the temperature range of 182-254°C is around 65.57%, which is due to extensive degradation of PVA chain and the pyrolysis is completed in a clear and visible step, which may include the following aspects **(Wanjun *et al.*, 2006).**

(a) Amino acids form, via dehydration, intermediates dipeptides as well as poly (amino acids) in the solid/liquid phase. The dipeptides are high thermal reactivity and low volatility, which keeps them in the thermal zone until they react further and form cyclic dipeptides piperazine-2, 5-diones.

(b) Amino acids, intermediate peptides, together with formed cyclic dipeptides, form both low molecular weight volatile products and other higher molecular weight (and sometimes volatile) products.

(c) Amino acids and their pyrolysis products evaporate or sublimate at high temperatures.

For the samples exposed to air prior to TG analysis, the weight losses in the first, second and third stages can be respectively attributed to the expulsion of water molelcules from the PVAALA composites or the moisture absorbed from the air, the decomposition of hyrdoxide groups and the splitting of the main chain PVA followed by decomposition of the polymer backbone. No effort has been made to confirm the decomposition products as it is well known that the decomposition leads to evolution of low molecular weight alkanes, alkenes, aldehyde, ketone etc and also acetaldehyde and acetic acid in case of pure PVA(**Yuan-Hiang Yu *et al.*, 2003).** The maximum weight loss of L-alanine in the temperature range 205-365°C.

The DTA-plot shows an endothermic peak at 99°C due to the release of water and an endothermic peak at 250°C due to the melting point of PVAALA composite. This is probable due to the decomposition of PVA and L-Alanine for PVAALA composite. Prolonged heating upto 1000°C does not produce any weight loss.

4.2.4 DIFFERENTIAL SCANNING CALORIMETRY OF PVAALA COMPOSITE

Differential Scanning Calorimetry (DSC) thermogram of PVA and PVAALA composite are presented in figure-12d-13. The endothermic peak at 100°C is attributed to water loss, represent the energy required to vaporize water present in the PVAALA composite (figure 12d). Two major endothermic peaks are found at about 193°C and 321°C are shown in figure -12d.

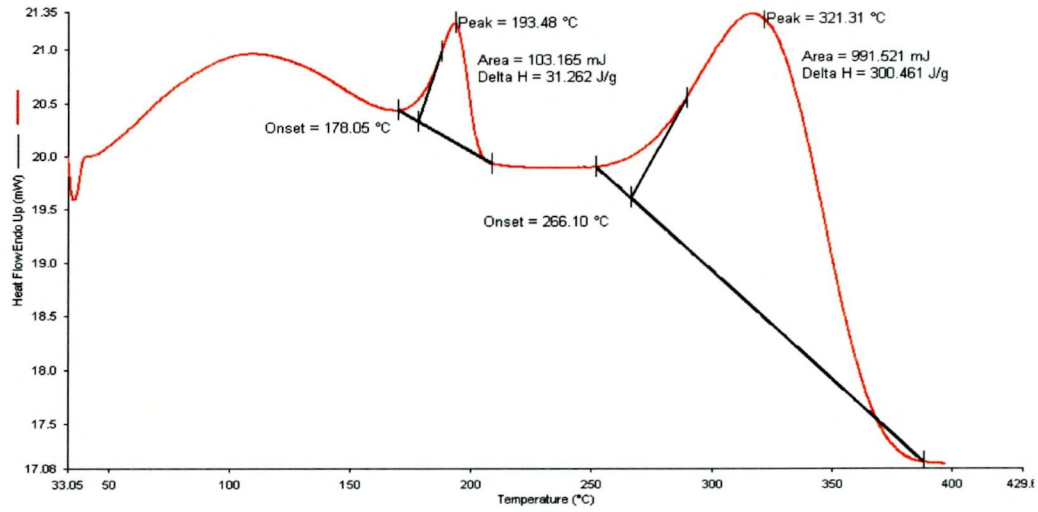

Figure-13 Differential scanning calorimetry of PVA

The peak 193°C peak represents melting temperature of semi crystalline PVA polymer (**Yuan-Hiang Yu *et al.*, 2003).** Under such circumstances self-decomposition, which is mainly the dehydration reaction should also occur in the local segments of the PVA molecular chain. The main PVA should be transformed to poly acetylene $(C\text{-}CH{=}CH\text{-})_n$ without the presence of any oxygen. The optical appearance of the PVA changed from transparent to a yellow-brown color. The reacted PVA is free from oxygen. The 321°C peak is related to another decomposition reaction of the reacted PVA free from oxygen as mentioned above (figure-13). It is well established that crystalline and amorphous phases in variable amounts coexist in most of the polymeric materials. PVA is one of the partially crystalline polymer exhibiting both the glass transition (characteristics of amorphous phase) and melting transition (characteristics of crystalline phase) supporting the above argument. PVA exhibited a relatively large and sharp endothermic curve, with a peak at 193°C and 321°C which is crystalline, had endothermic curve.

Suriya Kumar *et al.*, (2008) reported previously that the endothermic peaks at 299°C and 301°C were observed for pure L-alanine. The endothermic peak at 249°C corresponds to the melting point of PVAALA composites. The characteristics peak of crystalline polymer fraction of PVA is at about 321°C. Comparing the area of the endothermic to that of PVAALA composite suggests that the PVA crystallization is decreased after blending with alanine. From the DSC graph (figure-12d), it is observed an endothermic peak at 100°C and 249°C which appear in DTA and this same of two results (DTA and DSC) may be due to the same rate at heating of PVAALA composite sample.

4.2.5 XRD OF POLYVINYL ALCOHOL – ALANINE COMPOSITE (PVAALA)

XRD analysis studies of PVAALA composite are presented in figure-12e. Earlier reports show that the XRD results of PVA (19.5º, 23.7ºand 27.8º) in the crystal region **(Yuan-Hiang Yu *et al.,* 2003)**. L-Alanine exhibits eight mean peak reflections at 14.5 º, 16º, 21º, 29.5º, 31º, 33º, 35º and 37º. L-Alanine crystallize in the orthorhombic crystal system with a lattice parameters a=6.032Å, b=12.343Å º, c=5.784Å and space group p212121 with the reported values **(Aravindan et al., 2008)** and they also reported that the neutral alanine molecule exists as a zwitterions, where the carboxyl group is dissociated (COO^-) and the amino group is protonated (NH_3^+). The structure of L-alanine alaninium nitrate is held together by a three dimensional hydrogen-bond network. The full hydrogen bonding capabilities of the amino groups of the two-alanine molecules are realized. The alanine O atoms that are not already involved in the very strong intra-dimer hydrogen bonds accept H atoms from neighboring NH_3^+ groups. The hydrogen bonding NH_3^+ and COO^- moieties is the additional major force in the crystal lattice. There are already numerous reports on enhancement of nonlinear optical efficiency due to protonation and acid base chemistry.

From the entire reported spectra, moderately sharp peaks of PVA membrane can be noticed, indicating its semi-crystalline nature. Accordingly, the PVAALA composite (figure-12e) also exhibited semi-crystalline nature. From the spectra of PVAALA composite, distinct bonds at 2θ=20°, 23° and 27° corresponding to crystal 1, which is responsible for separation, as it comprises of functional groups such as -NH_2 and –OH, has not undergone any significant change after adding more amount of PVA. A slight reflection in the d-spacing values from 4.2979 Å, 3.76067Å and 3.23260 Å of PVAALA composites of ratios 10:1 is an indication of shrinkage in cell size or intersegmental spacing, which could improve the selective permeation property of the membrane. From these patterns, it is clear that the uncrosslinked PVA membrane exhibit more crystalline domains than the cross linked ones. The crystallinity has decreased with increasing alanine contents in the crosslinking agents. This results implies that the increase of the cross linking of the PVA membrane decrease the crystallinity of the membrane, which results in a compressing of the amorphous region. This suggests the compactness of the crosslinked PVAALA composite which signals good separation performance. This, XRD studies confirm crosslinking of PVAALA composite **(Aravindan et al., 2008)**.

4.2.6 SEM-EDXA OF PVAALA COMPOSITE

The effect of the component ratio of 10% PVA and 1% Alanine on the morphologies of pure PVA-Alanine composite is investigated, as shown in figure-12f at ×750 magnifications. The SEM micrographs clearly illustrate the morphological dependence on the PVA and Alanine content in the composite **(Yuan-Hiang Yu *et al.,* 2003)**. Several PVA and Alanine components, in the PVAALA composite as measured by an energy dispersive x-ray detector (EDX) attached to SEM **(Dae Sik Kim *et al.,* 2004)**. SEM image of the PVAALA composite shows non-agglomerated uniformly distributed polyalanine particles in PVA component. SEM photograph of the PVAALA composite are presented in figure-12f.

The PVAALA composite have a globular growth of the polymer with white coral like islands. These islands may be formed due to interaction of polyalanine and PVA polymer chains. The SEM image (figure-12f) clearly reveals the presence of binary phase. Figure-12f shows the EDXA analysis of PVAALA composite. This spectrum shows the EDXA analysis of PVAALA composite. This spectrum shows the presence of C, O and N in the PVAALA composite. EDXA analysis of the phases shows the presence of nitrogen atoms only in the minor phases. Based on these analyses, the structure of the PVAALA polymer composite may be proposed as one in which polyalanine chain are randomly distributed in the PVA matrix. SEM- EDXA offered valuable information concerning the elemental composition of the PVAALA composite, but also concerning the choice of materials used of the PVA and L-Alanine. The PVA and polyalanine phases are held together by hydrogen bonds OH of PVA and N-H of the polyamides.

4.3 CHARACTERIZATION OF POLYVINYL ALCOHOL-VALINE COMPOSITE

4.3.1 CHARACTERISATION OF PVAVAL USING FTIR SPECTRA DATA

To characterize the synthesized PVAVAL composite, the FTIR analysis of PVA, VAL and PVAVAL have been carried out (Figure-14a). The important peaks are assigned and discussed with references. The bands pertaining to PVA and Valine (VAL) and PVAVAL composite as shown in table-6 are shifted to the following wave numbers as given in table-6 The FTIR spectra obtained for Valine could go hand to hand with the **(Kirubavathi *et al.,* 2008).** The spectral changes are therefore clear evidence that the formation of polymer composite between PVA & VAL has occurred **(Yuan-Hiang Yu *et al.,* 2003, srimathi *et al.,* 2011).**

PVA Vs PVAVAL

A broad and strong peak centred at 3299 cm^{-1} is due to the stretching vibrations of -OH stretching from the inter and intra molecular hydrogen bonds in PVA. The absorption peak at 2923 cm^{-1} assigned to -C-H stretching from alkyl group in PVA has been shifted to 2915 and 2846 cm^{-1} in PVAVAL composite. A peak at 1718 cm^{-1} associated with C=O stretching vibrations of PVA backbone is found to be shifted to a lower wave number in (1889cm^{-1}) (amide I band(C=O stretching)) in the PVAVAL composite. The absorption peak due to CH_3 bending deformation , C-O stretching and OH in plane bending observed in PVA at 1417 cm^{-1} is found to be shifted to a lower wave number (1413 cm^{-1}) in PVAVAL composite. A band at 1367 cm^{-1} associated with C–H/OH bending is found in PVA. A sharp band at 1080 cm^{-1} due to C-O stretching, C-O-C stretching and C-C-N stretching in PVA backbone is found to be shifted to 1080 cm^{-1} in the PVAVAL composite. The absorption band at 1251 cm^{-1} corresponds to CH_2 rocking vibrations of PVA. This band is shifted to 1293 cm^{-1} in the PVAVAL composite. The band at 941cm^{-1} results from an angular deformation outside the plane of O-H bond of PVA. The absorption band at 838 cm^{-1} corresponds to CH rocking vibrations of PVA.

VAL Vs PVAVAL

The protonation of amino group can be proved because of the presence of strong bands at 1266 cm^{-1}(NH_3^+ rocking mode) and at 3148cm^{-1} due to NH_3^+ asymmetric stretching of VAL. A broad and strong peak centred at 3194 cm^{-1} is due to the stretching vibrations of NH_3^+ asymmetric stretching, solid state stabilized a zwitterions structure with NH_3^+ and COO^- and N-H group of polyvaline is hydrogen bonding with -O-H group of PVA in PVAVAL composite. A band at 2927 cm^{-1} corresponds to -C-H stretching from alkyl group of VAL. The combination band of NH_3^+ bending and NH_3^+ degenerative deformation is evident from a sharp medium band at 2617 cm^{-1} and 2087 cm^{-1} in the VAL. This band is shifted to 2122 cm^{-1} in the PVAVAL composite. Bands at 1560 cm^{-1} and 1503 cm^{-1} of VAL are due to NH_3^+ symmetric deformation (combination NH deformation and CN stretching) is found to be shifted to higher wavelength at 1587cm^{-1} of PVAVAL. The peak at 1266 cm^{-1} are due to CH_2 rocking and rocking of $NH_3^+$of VAL. This band is shifted to 1293cm^{-1} in the PVAVAL composite. Another peak at 1061cm^{-1} is also related to C-O stretching, C-O-C stretching and C-C-N stretching in VAL is shifted to a higher wave number 1080cm^{-1} in PVAVAL composite. The peak at 937 cm^{-1} and 825cm^{-1} are related to C-H out of plane deformation and CH_2 rocking vibration. A peak at 763/703cm^{-1} and 658 cm^{-1} are related to CH_2 rocking vibration / NH wagging and COO^-bending in VAL. This is shifted to 794 /705cm^{-1} and 623cm^{-1} in PVAVAL. The rocking, wagging and

Figure-14 Characterization of PVAVAL Composite

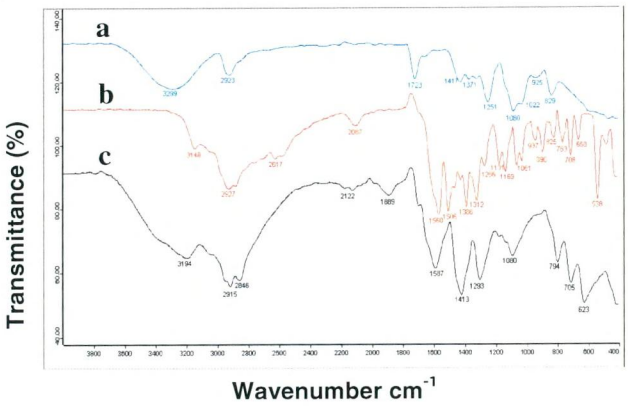

Fig. 14a FTIR Spectra of (a) PVA (b) Valine (c) PVAVAL composite

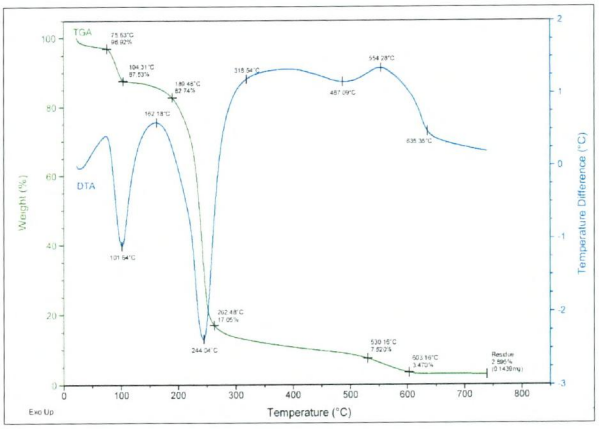

Fig. 14b TG and DTA thermograms of PVAVAL composite

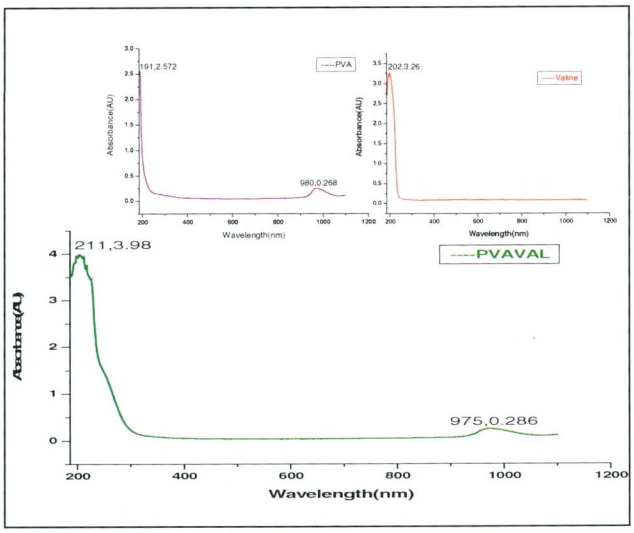

Fig. 14c UV-visible absorption Spectra of (a) PVA (b) Valine (c) PVAVAL composite

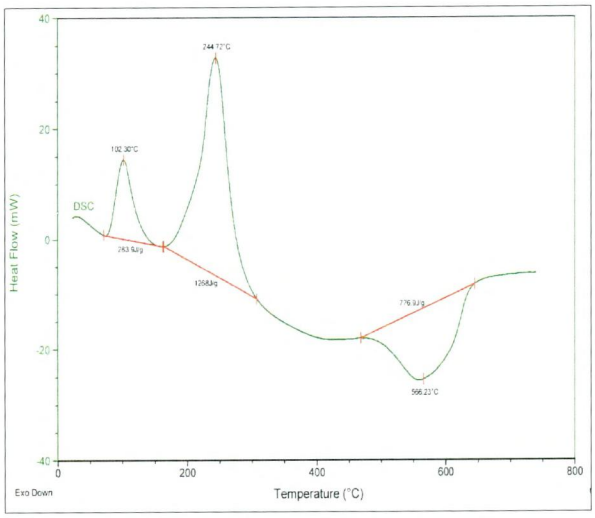

Fig. 14d DSC traces of PVAVAL composite

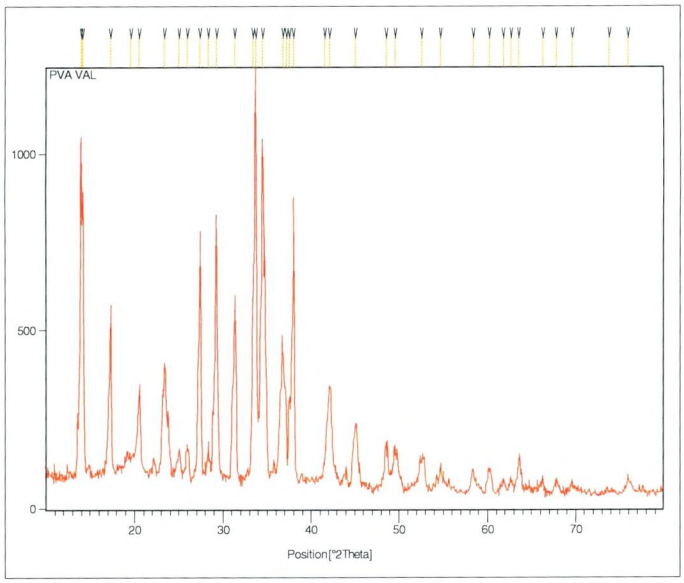

Fig. 14e X-ray Diffraction pattern of PVAVAL composite

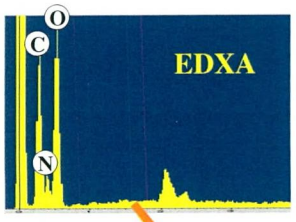

Element	Wt%	At%
C	27.55	32.91
N	16.71	17.11
O	55.74	49.98

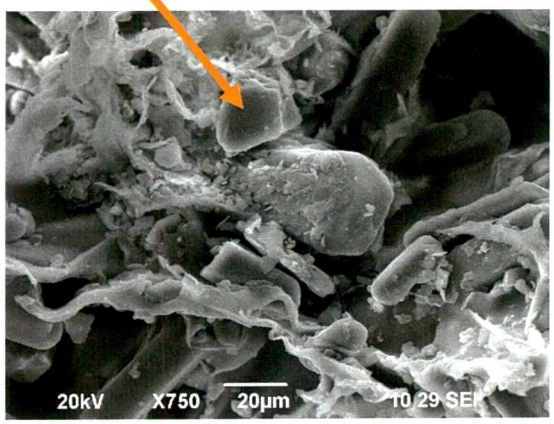

Fig. 14f SEM-EDXA micrograph of PVAVAL composite

scissoring in plane and out of plane deformation modes of COO^- ionized carboxylic group and NH_3^+ torsional are expected at 538cm^{-1} in VAL. Hence the PVAVAL composite formation is confirmed from FTIR spectra.

Table: 6 Assignment of FTIR absorption bands (in wave number) of PVA, Valine (VAL) and PVAVAL composite

S. NO.	PVA (cm^{-1})	Valine (VAL) (cm^{-1})	PVAVAL Composite (cm^{-1})	Assignment
1.	3299	-	-	OH str. (inter and intra molecular hydrogen bonds)
2.	-	3148	3194	NH_3^+ asym. str., zwitterions structure, bonded N-H str.
3.	2923	2927	2915,2846	-C-H str. from alkyl group
4.	-	2617	-	Combination band of NH_3^+ bending
5.	-	2087	2122	NH_3^+ degenerative deformation
6	1723	-	1889	C=O Str. Vib., amide I band(C=O str.)
7.	-	1560, 1506	1587	NH_3^+ sym. def., combination of NH def. and CN str.
8.	1417	-	1413	CH_3 bending def. + C-O str. +OH in plane bending
9.	1371	1386, 1312	-	Sym. str. of COO^-, C–H/OH bending
10.	1251	1266	1293	CH_2 rocking, rocking of NH_3^+
11.	-	1169,1131	-	COO^- sym. str., C-C-C str.
12.	1080, 1022	1061	1080	C-O str. + C-O-C str. , C-C-N str.
13.	925	937	-	C-H out of plane def.
14.	829	825	-	CH_2 rocking vib.
15.	-	763, 703	794, 705	NH wag., COO^-bending
16.	-	658	623	COO- scissoring
17.	-	538	-	COO^- rocking, NH_3^+ torsional

4.3.2 UV-VISIBLE ABSORBANCE SPECTRUM OF PVAVAL COMPOSITE

The UV-Vis transmission spectrum (figure-14c and table-5) of the PVA, Valine, and PVAVAL composite has been recorded in the range 190-1100 nm using AGILENT (8453) **(Shanker Ram et *al.*, 2004, Moitor *et al.*, 2010)**. When the transmittance is monitored from longer to shorter wavelength, L-Valine has optical transparency from 210 to 1100 nm. PVA absorbs strongly in the 200-400 nm region, while the adsorption band at 960 nm is assigned as the polaron band. The UV-Vis absorption spectrum of the PVAVAL composite is shown in figure-14. PVA, Valine and PVAVAL composite are almost transparent in the wavelength region of 190-1100 nm. The UV-Vis absorbance spectrum of PVAVAL composite depicts three absorption bands around 220 nm, 260 nm and 960 nm. The absorption band at 220 nm and 260 nm arises from π-π^* electron transition. The absorption band at 960 nm is assigned as the polaron band. The shift of the absorption edge in the PVAVAL composite reflects the variation in the energy band gap, which arises due to the variation in crystallinity within the polymer matrix **(Moitor *et al.*, 2010)**.

4.3.3 TG/DTA ANALYSIS OF POLYVINYL ALCOHOL-VALINE (PVAVAL) COMPOSITE

The therogravimetric curves of the PVAVAL composite revealed three main weight loss regions as shown in figure-14b. The first region, at a temperature of 75-104°C is due to the evaporation of physically weak and chemically strong bound water. The weight loss is about 9.36 %. The second transitional region, at around 189-262°C appears due to the breakdown of the PVAVAL composite backbone. The weight loss is about 62%. The second stages are due to the decomposition of hydroxide group. The second peak at 189-262°C is due to the dissociation of both inter and intra molecular forces with slight PVA backbone degradation. The PVA chain with low molecular weight underwent degradation at lower temperature. The valine material is fully decomposed at 260°C as reported earlier (**Yuan-Hiang Yu *et al.,* 2003),** The total weight loss in this stage corresponds to about 65.69%. The remaining weight after the polymer decomposed in PVAVAL composite is due to the residual char. However PVAVAL composite show lower weight loss in relation to PVA suggesting their higher thermal stability

Two endothermic peaks at 101°C and 244°C are shown. The first one with its endothermic peak minimum at 101°C is due to the release of water molecules and second one with its endothermic peak at 244°C is due to the melting point of PVAVAL composite. Overall, the degradation peaks of the cross-linked PVAVAL composite sample are less intense and shift towards higher temperatures. It can be concluded that improved thermal stability is probably due to the additive effect of the ammonium per sulphate filler and the chemical cross linking reaction of between PVA and L-Valine **(Kirubavathi *et al.,* 2008)**.

4.3.4 DIFFERENTIAL SCANNING CALORIMETRY OF PVAVAL COMPOSITE

Differential Scanning Calorimetry curves of PVA and PVAVAL composite are shown in figure-14d. The endothermic peak at 102ºC attributed to water loss, represents the energy required to vaporize water present in the PVAVAL composite. Two major endothermic peaks are found at about 193ºC and 321ºC. The 193ºC peak represents melting temperature of semi crystalline PVA polymer (**Yuan-Hiang Yu *et al.,* 2003).** PVA exhibited a relatively large and sharp endothermic curve, with peaks at 193ºC and 321ºC. The melting point of PVAVAL composite is 244ºC, while the melting temperature of the pure PVA is 321ºC. DTA curves show an endothermic peak at around 269ºC which corresponds to the melting point of the L-valine which was earlier reported (**Moitor *et al.,* 2010).** The melting temperature depression is caused by morphological and chemical modifications. The morphological changes

involve the thickness of the crystallites and the degree of crystallinity. The chemical changes are results of the crosslinking and of the branching due to the grafting o the cross linker, of course, the chemical changes affect the morphological ones. The melting temperature depression and the peak broadening suggest that the PVA molecules are highly constrained by the entanglement of the PVAVAL composite due to the crosslinking of the PVA blend with L-valine **(Yang *et al.,* 1996)**.

4.3.5 XRD OF POLYVINYL ALCOHOL – VALINE COMPOSITE (PVAVAL)

The X-ray diffraction pattern of the PVAVAL composite is shown in figure-14e. Earlier reports show that the X-ray diffractogram of PVA reveals a sharp crystalline peak at d=4.53 Å (2θ = 19.6°) and a shoulder at d=3.86 Å (2θ = 23.0) typical of crystalline PVA **(Yuan-Hiang Yu *et al.,* 2003)**. Least square refinement of 25 reflections in the range 20-30° reveal the lattice parameters as a=9.701 Å, b=5.261 Å, c=11.953 Å and β= 90.66°. Systematic extinctions were compatible with the space group P21. The XRD pattern of pure PVA shows a characteristic peak for an orthorhombic lattice centred at 2θ = 20° indicating its semicrystalline nature. On the incorporation of L-valine into PVA the intensity of this peak decrease gradually, suggesting a decrease in the degree of crystallinity of PVA. The crystalline nature of PVA results from the strong intermolecular interaction between PVA chains through the intermolecular hydrogen bonding. This interaction between PVA and L-Valine leads to the decrease of the intermolecular hydrogen bonding between the PVA chains and thus the crystalline degree. Hema et al., (2009) established a correlation between the intensity of the peak and the degree of crystallinity. They observed that the intensity of XRD pattern decreases as the amorphous nature increases with the addition of dopant. The observed higher decrease in crystallinity after L-valine treatment signifies formation of cross-linked product on membrane surface **(Moitor *et al.,* 2010).**

4.3.6 SEM-EDXA OF PVAVAL COMPOSITE

SEM photograph for the top view of the 10%PVA 1%Valine (VAL) [PVAVAL] composite polymer membranes at ×750 magnifications, is shown in figure-14f. The surface morphology of the PVAVAL composite polymer show good uniformity and the added PVA fillers are dispersed well into PVAVAL composite polymer matrix. The orientation of the polyvaline and PVA crystallites **(Yuan-Hiang Yu *et al.,* 2003)** has been detected by X-ray diffraction. The image clearly reveals the presence of binary phase in which polyvaline chains (minor phase) are randomly distributed in the PVA matrix. Polyvaline micro domains are dispersed within PVA matrix in the blend film with relatively good interfacial adhesion between the two components.

The surface morphology of PVAVAL composite using energy dispersive spectroscopy (EDXA) technique is shown in figure-14f **(Dae Sik Kim *et al.,* 2004)**. The PVAVAL composite exhibited a clear carbon, oxygen and nitrogen. Among the two phases the EDX analysis, shows the presence of nitrogen atom in the minor phase only which is due to the incorporated polymerized polyvaline chain in the PVA matrix.EDX results reveal that carbon, oxygen and nitrogen are solely concentration at topographically heterogeneity on the PVAVAL composite.

4.4 CHARACTERIZATION OF POLYVINYL ALCOHOL-GLUTAMIC ACID COMPOSITE

4.4.1 CHARACTERISATION OF PVAGLU USING FTIR SPECTRA DATA

To characterize the synthesized PVAGLU composite, the FTIR analysis of PVA, GLU and PVAGLU were carried out (Figure-15a). The important peaks are assigned and discussed with references **(Guan Huei Ho *et al.,* 2006).** Figure-15a shows the FTIR spectra of PVA, Glutamic acid ant their respective polymer composite PVAGLU and the frequencies are listed in table-7. The frequencies mentioned in the table justify the formation of PVAGLU composite (**Yuan-Hiang Yu *et al.,* 2003, srimathi *et al.,* 2011).**

PVA Vs PVAGLU

A broad and strong peak centred at 3299 cm^{-1} is due to the stretching vibrations of -OH stretching from the inter and intra molecular hydrogen bonds in PVA. A strong peak centred at 3019 cm^{-1} is due to the NH_3^+ symmetric stretching in PVAGLU. The adsorption peak at 2923 cm^{-1} assigned to -C-H stretching from alkyl group in PVA has been shifted to 2973 and 2852 cm^{-1} in PVA GLU composite. A peak at 1723 cm^{-1} associated with C=O stretching vibration and carbonyl group which can easily bond with hydrogen of PVA backbone is found to be shifted to a lower wave number in (1884 cm^{-1} and 1702 cm^{-1}) (amide I band(C=O stretching)) in the PVAGLU composite. The absorption peak due to CH_3 bending deformation, C-O stretching and OH in plane bending observed in PVA at 1417 cm^{-1} is found to be shifted to a lower wave number (1415 cm^{-1}) in PVAGLU composite. A band at 1371 cm^{-1} associated with C–H/OH bending is found in PVA. A sharp band at 1080 cm^{-1} and 1022 cm^{-1}due to C-O stretching and C-O-C stretching in PVA backbone is found to be shifted to 1082cm^{-1} in the PVA GLU composite. The absorption band at 838 cm^{-1}, 1251 cm^{-1} and 925 cm^{-1} corresponds to CH_2 rocking vibrations and C-H out of plane deformation of PVA.

Table: 7 Comparison of observed vibrational frequencies for PVA, Glutamic acid (GLU) and PVAGLU composite

S. NO.	PVA (cm^{-1})	Glutamic acid (GLU) (cm^{-1})	PVAGLU Composite (cm^{-1})	Assignment
1.	3299	-	-	OH str. (inter and intra molecular hydrogen bonds)
2.	-	-	3190	NH_3^+ asym. str., zwitterions structure, bonded N-H str.
3.	-	3019	-	NH_3^+ sym. str.
4.	2923	2934,2736	2973,2852	-C-H str. from alkyl group
5.	-	2081	2136	NH_3^+ degenerative def.
6	1723	1826	1884,1702	C=O str. Vib., amide I band(C=O str.)
7.	-	1632	-	COO^- asym.str.
8.	-	-	1581	NH_3^+ sym.def., combination of NH def. and CN str.
9.	1417	1419	1415	CH_3 bending def.+ C-O str.+OH in plane bending
10.	1371	1337, 1302	-	Sym. str. of COO^-, C–H/OH bending
11.	1251	1248, 1202	1283	CH_2 rocking, rocking of NH_3^+
12.	1080, 1022	1043	1082	C-O str. + C-O-C str. , C-C-N str.
13.	925	942	-	C-H out of plane def.
14.	829	853	-	CH_2 rocking vib.
15.	-	799, 702	795, 710	NH wag., COO^-bending
16.	-	659	632	COO- scissoring
17.	-	527	-	COO^- rocking, NH_3^+ torsional

GLU Vs PVAGLU

A broad and strong peak centred at 3190 cm^{-1} is due to the stretching vibrations of NH_3^+ asymmetric stretching, solid state stabilized a zwitterions structure with NH_3^+ and COO^- and N-H group of polygultamic acid is hydrogen bonding with -O-H group of PVA in PVAGLU composite. A band at 2934 and 2736 cm^{-1} corresponds to -C-H stretching from alkyl group of GLU. A peak at 3019 cm^{-1} in GLU indicates the presence of NH_3^+ symmetric stretching. A peak at 1826 cm^{-1} associated with C=O stretching vibration and carbonyl group which can easily bond with hydrogen GLU is found to be shifted to a lower wave number in (1884 cm^{-1}) in the PVAGLU composite. Bands at 1632 and 1581 cm^{-1} of GLU are due to COO^- asymmetric stretching and NH_3^+ symmetric deformation (combination NH deformation and CN stretching). A peak at 1419 cm^{-1} is due to CH_3 bending deformation and C-O stretching of GLU. This band is shifted to 1415 cm^{-1} in the PVA GLU composite. The band at 1107 cm^{-1} is due to COO^- symmetric stretching and C-C-C stretching in GLU. The peaks at 918 and 840cm^{-1} are related to C-H out of plane deformation and CH_2 rocking vibration in GLU. Another peak at 1355 cm^{-1} is also related to symmetric stretching of COO^- in GLU. This is also present in the PVA GLU composite. A peak at 1248/1043 cm^{-1} due to the rocking of NH_3^+ /C-C-N stretching in GLU is shifted to a lower wave number 1283/1082 cm^{-1} in PVA GLU composite. A peak at 799 cm^{-1} is related to special NH wagging and COO^-bending in GLU. This was shifted to 795 cm^{-1} in PVA GLU composite. A band at 659 cm^{-1} is due to the COO- scissoring of GLU.

Figure-15 Characterisation of PVAGLU Composite

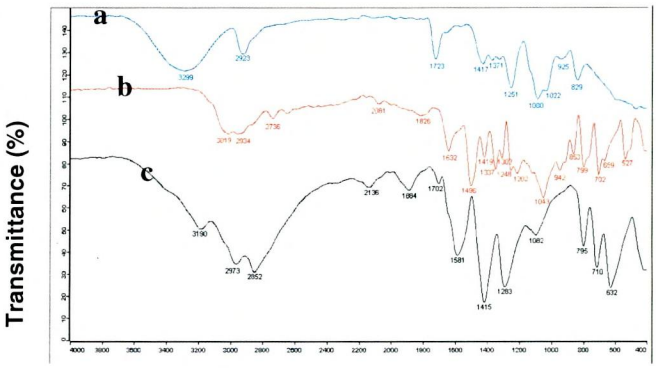

Fig. 15a FTIR Spectra of (a) PVA (b) Glutamic acid (c) PVAGLU composite

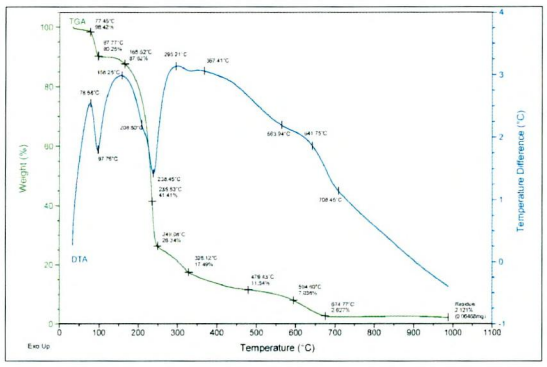

Fig. 15b TG and DTA thermograms of PVAGLU composite

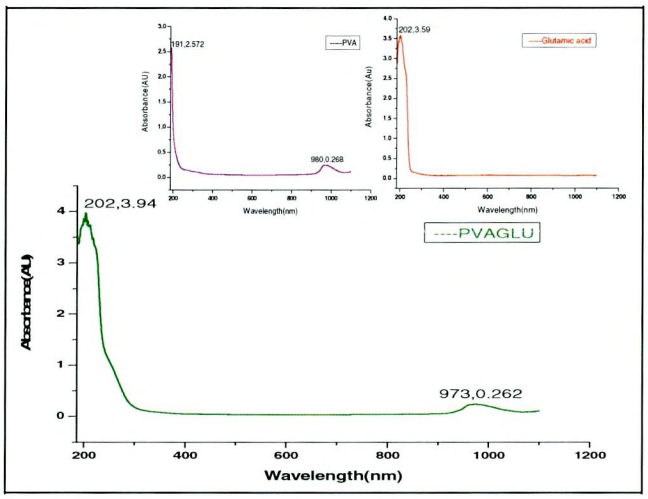

Fig. 15c UV-visible absorption Spectra of (a) PVA (b) Glutamic acid (c) PVAGLU composite

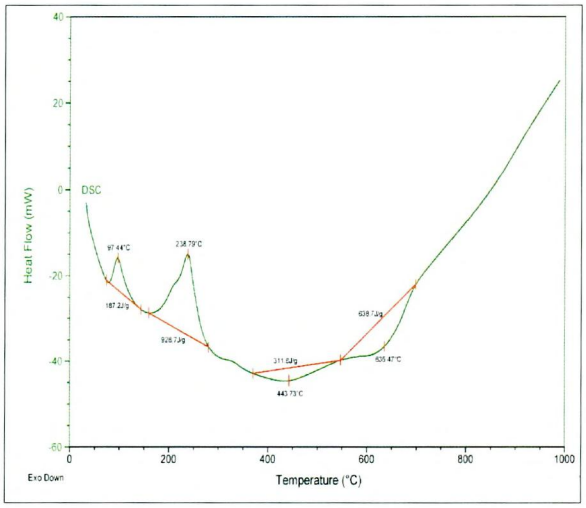

Fig. 15d DSC traces of PVAGLU composite

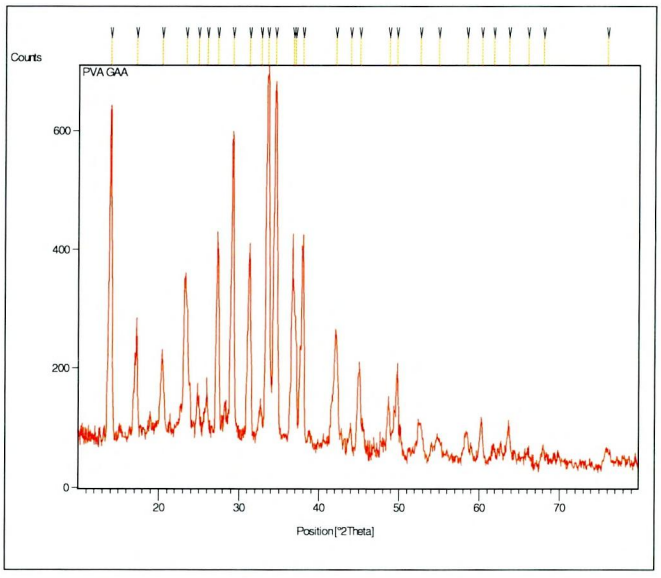

Fig. 15e X-ray Diffraction pattern of PVAGLU composite

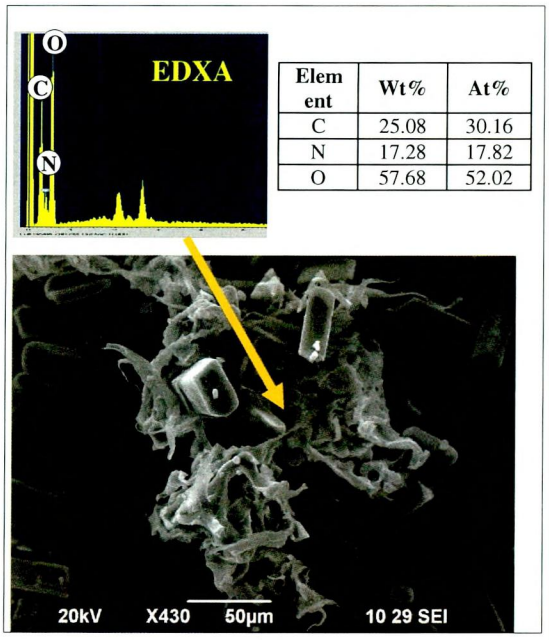

Element	Wt%	At%
C	25.08	30.16
N	17.28	17.82
O	57.68	52.02

Fig. 15f SEM-EDXA micrograph of PVAGLU composite

This was shifted to 632 cm^{-1} in PVA GLU composite. The absorption band at 853 cm^{-1}, 1248 cm^{-1} and 942 cm^{-1} corresponds to CH_2 rocking vibrations and C-H out of plane deformation of GLU. The changes in the vibrational frequencies of the above mentioned peaks in the FTIR spectrum of PVA, GLU and PVA GLU confirm the formation of PVA GLU composite.

4.4.2 UV-VISIBLE ABSORBANCE SPECTRUM OF PVAGLU COMPOSITE

UV-Visible transmittance spectrum was recorded in solution state in the range 190-1100nm using double beam spectrophotometer of PVA, Glutamic acid, PVAGLU composite and it is shown in figure-15c and table-5 represents the UV-Vis absorbance band of PVA, Glutamic acid and PVAGLU composite **(Shanker Ram et *al.,* 2004**, **Kumararaman *et al.,* 2011)**. At 210 nm, a sharp fall of transmittance to zero is observed indicating a single transition in the near UV region of L-Glutamic acid. The material is found to be transparent to all radiations in the wavelength range of 210-1100 nm. PVA absorbs strongly in the 200-400 nm region, while the adsorption band at 960 nm is assigned as the polaron band as shown in figure. The UV-Vis absorbance spectrum of PVAGLU composite is shown in figure-15. The absorbance peak at 220 nm is assigned to the π-π^* transition on the basis of the studies of the PVAGLU composite. It could be attributed to poor conjugation along the composite chain since Glutamic acid blocks along the polymer chain. The steric effect of the –COOH group along the polymer chain causes loss of coplanarity of the π system reducing charge delocalization between the polymer chains. The band is attributed to another polaron transition of the PVAGLU composite and the peak at 960 nm is observed. This bands could be assigned to the n-π^* transition due to the presence of non-bonding electrons on the carboxylate groups.

4.4.3 TG/DTA ANALYSIS OF POLYVINYL ALCOHOL-GLUTAMIC ACID (PVAGLU) COMPOSITE

The TG spectrum of a composite (PVAGLU) is given in figure-15b. In general, two degradations are observed in the composite. The first weight loss in the trace at about 77-97°C is primarily due to moisture present due to hygroscopic character of PVA. While in the second one the breakdown of the polymer backbone takes place (**Yuan-Hiang Yu *et al.,* 2003).** The thermal degradation of PVAGLU composite starts at about 77°C and continues upto 249°C with 72.08 % weight loss. The second transitional region 165-249°C appears due to the degradation of the side chain of the PVAGLU composite. The total weight loss corresponding to this stage is about 61.28 %. It is reported earlier **(Fouad et al., 2009)** that the two profiles reveal the occurrence of a first decomposition step taking place in the 250-300°C range and

involving a weight loss of around 50 and 70% of the initial mass respectively. The small weight loss (<3%) observed on the poly (γ-Glutamic acid) trace below 200°C is the release of water absorbed during sample handling because of the highly hydrophilic nature of the poly-acid. The subsequent weight loss at 200-220°C was a result of the decomposition due to a release of CO_2 from carboxyl residue of L-Glutamic acid. Cyclic thermal measurements between room temperature and 150°C exhibited reversible mass changes due to the adsorption and desorption of water. This thermal behaviour of the release and uptake of water molecules is not stepwise but continuous, which may indicate that the two adsorbed water molecules are strongly linked to each other in the L-Glutamic acid crystal.

The DTA trace indicates a weak endothermic curve starting at about 97°C which may also be assigned to isomorphic transformation (or) to the release of water, as there is corresponding weight loss in TGA trace. This is followed by an endothermic peak at 238°C due to its melting point of PVAGLU composite. From the studies it can be noted that crosslinking has caused a major impact on the thermal stability of the PVAGLN composite. Hence, crosslinked PVAGLU composite can be safely used for preparation application upto a temperature of 249°C **(Sebastián Muñoz Guerra *et al.,* 2008).**

4.4.4 DIFFERENTIAL SCANNING CALORIMETRY OF PVAGLU COMPOSITE

DSC is useful in the investigation of solid-state interactions, hence thermograms were generated for both PVA and PVAGLU composite (figure-13,15d). The endothermic peak at 97ºC, attributed to water loss, represents the energy required to vaporize water present in the PVAGLU composite. PVA exhibited a relatively large and sharp endothermic curve, with a peak at 193ºC and 321ºC (figure-13) (**Yuan-Hiang Yu *et al.,* 2003).** It has been reported that the melting point of the L-gultamic acid was at 185°C.The DSC results showed an endothermic peak at 238ºC, which is due to the melting point of the PVAGLU composite followed by the degradation. The melting temperature peak did not change much with different degrees of crosslinking. However, PVAGLU composite showed higher melting temperature peaks with higher degrees of crosslinking, their melting temperature peaks decreased to almost the same as that of the plain PVA. The interesting phenomenon may result from the change of the crystalline morphology induced by L-Glutamic acid moieties or between the mechanisms of crystallinity. Furthermore, the more the L-Glutamic acid moieties in PVA matrixes, the lower their melting temperature peaks. When heated above melting point, the plain PVA curve showed to be in unstably endothermic form at 193ºC and 321ºC, while crosslinked PVAGLU

curve appeared to be fairly flat. The results provide information about their thermal stabilities and it can be seen that cross linked PVAGLU composites are more stable at high temperature than plain PVA **(Adoor *et al.*, 2006).**

4.4.5 XRD OF POLY VINYL ALCOHOL-GLUTAMIC ACID COMPOSITE (PVAGLU)

The composite of PVA and L-Glutamic acid produced in the present work were subjected to X-ray diffraction (XRD) analysis. Earlier reports show that in the PVA sample, there are two peaks at $2\theta = 10.7°$ and $21.1°$ **(Yuan-Hiang Yu *et al.*, 2003)**. The XRD patterns of the two form of L-Glutamic acid reveal characteristics peaks at $18.1°$ and $10.2°$ (2θ) corresponding to α-form and β-form, respectively. The X-ray diffraction measurement was performed to examine the crystalline nature of PVAGLU composite. Figure-15e depicts the diffraction scans for the membrane samples of PVAGLU composite polymer membranes and earlier reported PVA as shown above. PVAGLU composite exhibit a semicrystalline structure with a peak angle at 2θ of $20°$. However, the intensity of the PVA peak dramatically decreases when L-Glutamic acid was added to the membrane system. This implies that the crystalline region within the PVAGLU composite polymer membrane has become dominated.

The crystalline peak is nearly visible as the PVAGLU ratio gets to 10:1. The crystalline hump indicates that the PVAGLU composite polymer membranes are crystalline polymer in general. Hence there is significant motion of polymer chain existing in the crystalline phase while the amorphous phase is conducting. The crystalline characteristic of PVAGLU composite polymer membranes can greatly enhance the electric conductivity due to the formation of cross linked product in the polymer matrix **(Yuxin Mo *et al.*, 2011)**.

4.4.6 SEM-EDXA OF PVAGLU COMPOSITE

The integral morphologies of the synthesised PVAGLU composite are shown by SEM image (figure-15f). It can be observed that the PVAGLU composite has an non-agglomerate structure with the small primary particles. It is shown that the primary particles size of PVAGLU composite is in the range of 50μm. The earlier report depicts the scanning electron microscope photographs of the used L-Glutamic acid was a large of orthorhombic shape particle. The SEM of PVA derivation **(Yuan-Hiang Yu *et al.*, 2003)** exhibited a polyphasic microporous structure. L-Glutamic acid was successfully integrated into the polymer matrix with no visible agglomerate formation at low particle amounts.

Figure-15f shows the SEM pictures of PVAGLU composite with different volume fraction. The magnified SEM photograph of polyhedral shape crystal reveal the closely and regularly packed by flake structures. A rectangle crystal which was

loosely and irregularly accumulated by some fine rod-shaped structures was also found in the presence of Glutamic acid. The Glutamic acid particles are randomly distributed throughout the PVA matrix. L-Glutamic acid is a dimorphic amino acid with a meta-stable-α form, having prismatic crystals, and stable β-form with characteristic needle shaped crystals has earlier reported. This SEM images clearly visualizes the presence of small ratio of secondary phases (polymerized Glutamic acid) distributed and get adherent on the polyvinyl alcohol matrix. Elemental mapping via EDXA provides further insight into the chemical identity of these special features present on the surface and in the bulk. The EDX spectrum of PVAGLU composite (figure-15) shows the characteristic peaks of the elements constituting of nitrogen, oxygen and carbon. EDX analyses of the two phases show the presence of nitrogen atom only in the minor phases. The hydrogen bonding is the force that holds the polyamides of Glutamic acid to PVA matrix **(Dae Sik Kim *et al.,* 2004).**

4.5 CHARACTERIZATION OF POLYVINYL ALCOHOL-GLUTAMINE COMPOSITE

4.5.1 CHARACTERISATION OF PVAGLN USING FTIR SPECTRA DATA

To characterize the synthesized PVAGLN composite, the FTIR analysis of PVA, GLN and PVAGLN has been carried out (Figure-16a). The important peaks are assigned and discussed with references **(Bharthasarathi *et al.,* 2010)**. FTIR spectra of PVA, Glutamine (GLN) and PVAGLU are depicted in the figure-16a. & the respective frequencies of the synthesised inhibitor are also highlighted in the table-8. Table-8 clearly reveals the major peaks associated with PVA and GLN are present in the recorded in the FTIR spectra of the synthesised PVAGLN. Hence from FTIR spectroscopy the formation of PVAGLN has been confirmed (**Yuan-Hiang Yu *et al.,* 2003, srimathi *et al.,* 2011).**

PVA Vs PVAGLN

A broad and strong peak centred at 3299 cm^{-1} is due to the stretching vibrations of -OH stretching from the inter and intra molecular hydrogen bonds in PVA. The absorption peak at 2923 cm^{-1} assigned to -C-H stretching from alkyl group in PVA has been shifted to 2958 and 2842 cm^{-1} in PVAGLN composite. A peak at 1723 cm^{-1} associated with C=O stretching vibrations of PVA backbone is found to be shifted to a lower wave number in (1893cm^{-1}) (amide I band(C=O stretching)) in the PVAGLN composite. The absorption peak due to CH_3 bending deformation , C-O stretching and OH in plane bending observed in PVA at 1417 cm^{-1} is found to be shifted to a lower wave number (1413 cm^{-1}) in PVAGLN composite. A band at 1371 cm^{-1} associated with C–H/OH bending is found in PVA. A sharp band at 1084 cm^{-1} due to C-O stretching, C-O-C stretching and C-C-N stretching in PVA backbone is

found to be shifted to 1080 cm^{-1} in the PVAGLN composite. The absorption band at 1251 cm^{-1} corresponds to CH_2 rocking vibrations of PVA. This band is shifted to 1293 cm^{-1} in the PVAGLU composite. The band at 929 cm^{-1} results from an angular deformation outside the plane of O-H bond of PVA. The absorption band at 836 cm^{-1} corresponds to CH rocking vibrations of PVA.

GLN Vs PVAGLN

The protonation of amino group can be proved because of the presence of strong bands at 1266 cm^{-1}(NH_3^+ rocking mode) and at 3148cm^{-1} due to NH_3^+ asymmetric stretching of GLN. A broad and strong peak centred at 3163 cm^{-1} is due to the stretching vibrations of NH_3^+ asymmetric stretching, solid state stabilized a zwitterion structure with NH_3^+ and COO^- in GLN. This band is shifted to 3186 cm^{-1} and N-H group of polyglutamine is hydrogen bonding with -O-H group of PVA in the PVAGLN composite. A band at 2857 cm^{-1} corresponds to -C-H stretching from alkyl group of GLN. The combination band of NH_3^+ bending and NH_3^+ degenerative deformation is evident from a sharp medium band at 2617 cm^{-1} and 2029 cm^{-1} in the GLN. This band is shifted to 2145 cm^{-1} in the PVAGLN composite. Bands at 1518 cm^{-1} of GLN are due to NH_3^+ symmetric deformation of PVAGLN composite. The peak at 1293 cm^{-1} are due to CH_2 rocking and rocking of $NH_3^+$of PVAGLN composite. The peak at 1471 cm^{-1} are due to CH_3 bending deformation, C-O Stretching and OH in plane bending of GLN composite. This band is shifted to 1413 cm^{-1} in the PVAGLN composite. Another peak at 1088 cm^{-1} is also related to C-O stretching, C-O-C stretching and C-C-N stretching in GLN is shifted to a higher wave number 1080cm^{-1} in PVAGLN composite. The absorption band at 1618 cm^{-1}, 1312 cm^{-1} and 1154 cm^{-1} corresponds to COO^- asymmetric stretching, Symmetric stretching of COO^- /Symmetric bending of CH_3/ C–H/OH bending and COO^- symmetric stretching/ C-C-C stretching of GLN. The peak at 1518 cm^{-1} is due to NH_3^+ symmetric deformation (combination NH deformation and CN stretching) of PVAGLN composite. The absorption band at and 925 cm^{-1} corresponds to CH_2 rocking vibrations and C-H out of plane deformation of PVA. The peak at 995 cm^{-1} and 844cm^{-1} are related to C-H out of plane deformation and CH_2 rocking vibration. A peak at 767cm^{-1} and 658 cm^{-1} are related to CH_2 rocking vibration / NH wagging and COO^-bending in GLN. This is shifted to 794 /705cm^{-1} and 635 cm^{-1} in PVAGLN. The rocking, wagging and scissoring in plane and out of plane deformation modes of COO^- ionized carboxylic group and NH_3^+ torsional are expected at 592 cm^{-1} in GLN. PVAGLN composite formation is well evidenced from FTIR.

Figure-16 Characterization of PVAGLN Composite

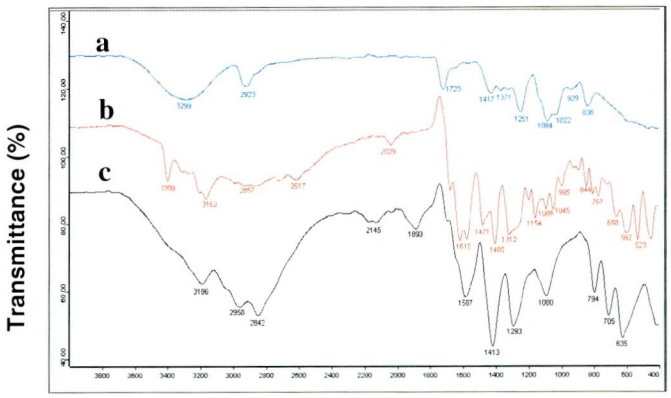

Fig. 16a FTIR Spectra of (a) PVA (b) Glutamine (c) PVAGLN composite

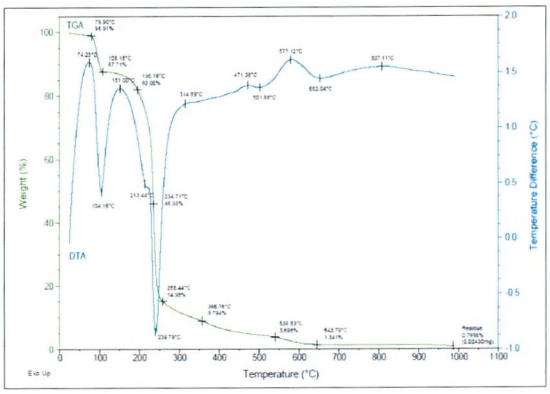

Fig. 16b TG and DTA thermograms of PVAGLN composite

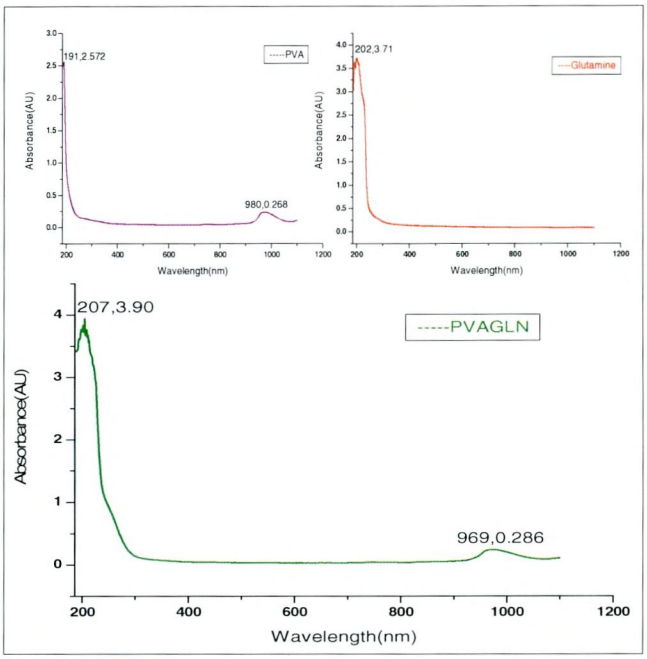

Fig. 16c UV-visible absorption Spectra of (a) PVA (b) Glutamine (c) PVAGLN composite

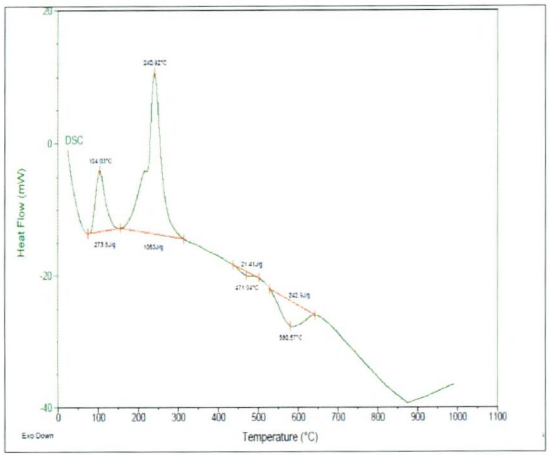

Fig. 16d DSC traces of PVAGLN composite

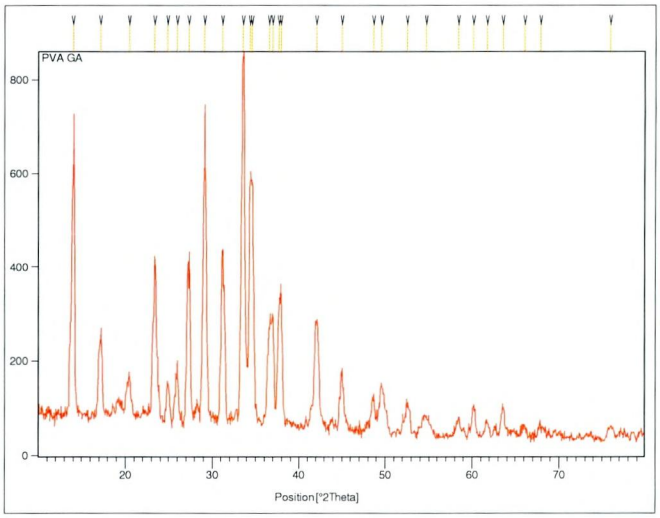

Fig. 16e X-ray Diffraction pattern of PVAGLN composite

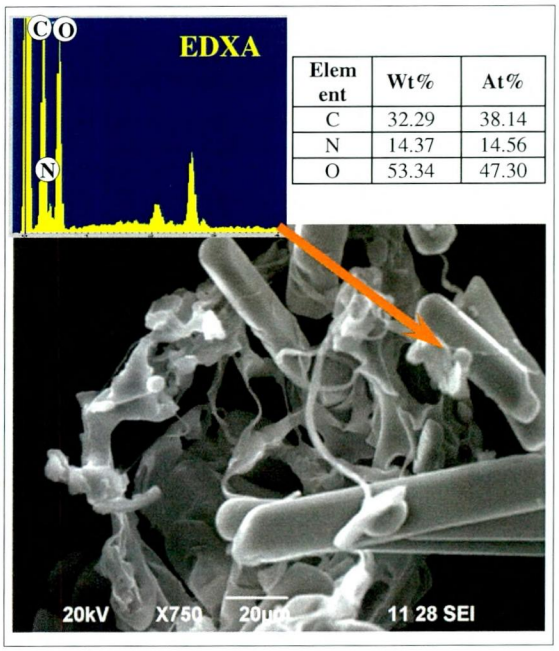

Element	Wt%	At%
C	32.29	38.14
N	14.37	14.56
O	53.34	47.30

Fig. 6 SEM-EDXA micrograph of PVAGLN composite

Table- 8 FTIR spectra band assignment of PVA, Glutamine (GLN) and PVAGLN composite

S. NO	PVA (cm^{-1})	Glutamine (GLN) (cm^{-1})	PVAGLN (cm^{-1})	Assignment
1.	-	3399	-	N-H str.
2.	3299	-	-	OH str.(inter and intra molecular hydrogen bonds)
3.	-	3163	3186	NH_3^+ asym. str., amide (bonded N-H str.)
4.	2923	2857	2958,2842	-C-H str. from alkyl group
5.	-	2617	-	Combination band of NH_3^+ bending
6	-	2029	2145	NH_3^+ degenerative def.
7.	1723	-	1893	C=O str.vib., amide I band(C=O str.)
8.	-	1618	-	COO^- asym. str.
9.	-	-	1518	NH_3^+ sym. def., combination NH def. and CN str.
10.	1417	1471, 1405	1413	CH_3 bending def. + C-O Str. +OH in plane bending
11.	1371	1312	-	Sym. str. of COO^-, C–H/OH bending
12.	1251	-	1293	CH_2 rocking, rocking of NH_3^+
13.	-	1154	-	COO^- sym.str., C-C-C str.
14.	1084,1022	1088, 1045	1080	C-O str. + C-O-C str. , C-C-N str.
15.	929	995	-	C-H out of plane def.
16.	836	844	-	CH_2 rocking vib.
17.	-	767	794, 705	NH wag., COO^-bending
18.	-	658	635	COO- scissoring
19.	-	592, 523	-	COO^- rocking, NH_3^+ torsional

4.5.2 UV-VISIBLE ABSORBANCE SPECTRUM OF PVAGLN COMPOSITE

The UV-Vis transmittance spectrum has been recorded in the range of 190-1100nm covering the entire UV and Visible region as shown in table-5 for PVA,GLN and PVAGLN composite **(Shanker Ram et *al.*, 2004, Bharthasarathi *et al.*, 2010).** The UV-Visible absorbance spectrum of L-Glutamine is shown in figure-16c. The spectrum has been recorded in the range 190-1100 nm, the cut-off wavelength is found to be 220 nm. The absorbance is very low and steady from 220 to 1100 nm. PVA absorbs strongly in the 200-400 nm region, while the absorption band at 960nm is assigned as the polaron band. Figure-16 depicts the light transmittance curve of PVAGLN composite. The observed spectra are characterized by a absorption edge around 220 nm for shorter wavelength, which arises due to the variation in crystallinity within polymer matrix. The band at 220 nm in the UV spectra is assigned to n-π^*. Another absorption shoulder observed at about 220-230 nm and it may be attributed to the π-π^* which can be attributed to unsaturated bonds mainly C=O. The UV-Vis spectra of the PVAGLN composite has been measured in the range of 200-1100 nm showing two distinct regions. The first one is specific for the ranging from 200nm to 400 nm, matching the transitions of π-π^*or n-π^* of PVA, Glutamine and PVAGLN composite. The appearance of the second peak at 960nm may be attributed to the evolution of a polaron bond of PVAGLN composite.

4.5.3 TG/DTA ANALYSIS OF POLYVINYL ALCOHOL-GLUTAMINE (PVAGLN) COMPOSITE

The thermograms of polyvinyl alcohol – Glutamine (PVAGLN) composite is shown in figure-16b. The initial decomposition temperature is observed in the temperature rage 79-108°C, it may be attributed to loss of moisture, volatilization of the solvent and adsorbed HCl. The second weight loss step (195-234°C) is associated with the degradation of ester unit of PVA (82 %) hydrolysed PVA is used. The second and third minor weight loss steps (195-258°C) are ascribed to the dissociation of both inter and intra molecular forces with slight PVA backbone degradation. The PVA chain with low molecular weight underwent degradation at lower temperature. The final weight loss step can be explained on the basis of degradation of PVA backbone completely. It is earlier reported (**Yuan-Hiang Yu *et al.,* 2003)** that the two profiles reveal the occurrence of a first decomposition step taking place in the 250-300°C range and involving a weight loss of around 50 and 70% of the initial mass respectively. The small weight loss (<3 %) observed on the polyglutamine trace below 200°C is the release of water absorbed during sample handling because of the highly hydrophilic nature of the poly acid **(Jen Ming yang *et al.,* 2004)**.

The DTA-plot shows an endothermic peak at 104°C due to the release of water. The endothermic peak at around 240°C (or) 239°C corresponds to the melting point of the PVAGLN composite, which is also observed in DSC curve. The sharpness of the endothermic peak how's the good degree of crystallinity and purity of the sample. Above the melting point, only gradual weight loss is observed as the temperature is increased. It is seen that at different stages that various gaseous fractions like CO, CO_2, NH_3 etc., are evolved, leading to a bulk decomposition of the compound 1100°C.

4.5.4 DIFFERENTIAL SCANNING CALORIMETRY OF PVAGLN COMPOSITE

Figure-16d shows typical Differential Scanning Calorimetry (DSC) traces of PVA and PVAGLN composite. The endothermic peak at 104ºC is attributed to water loss, represents the energy required to vaporize water present in the PVAGLN composite. The DSC curve for PVA shows endotherms at 193ºC and 321ºC, which corresponds to its melting point (**Yuan-Hiang Yu *et al.,* 2003).** It has been reported that the melting point of the L-glutamine was at 200°C. DSC traces which includes the PVAGLN composite segment, exhibited two obvious ranges: the stage with a temperature lower than 104ºC, which corresponds to the evaporation of water absorbed through a hydrogen bond between PVAGLN backbone and water. The

enthalpy with a temperature higher than 150ºC may be due to possible esterification of-OH and –COOH, the amidation $–NH_2$ and –COOH in PVAGLN composite, and the decomposition of PVAGLN composite, as well as the possible crosslinking between polyvinyl alcohol and L-glutamine. For the PVAGLN composite, the temperature with the most heat flow shifts towards a lower temperature with an increase of PVA, indicating that the decomposition of the L-Glutamine side chain plays a significant role in the decomposition of the PVAGLN composite. The cross linked PVAGLU composite show melting transitions (highest peak) at 240ºC. The results indicated that the structure of PVAGLN composite is approximately similar to PVA and L-Glutamine **(Kanokporn Juntanon *et al.,* 2008).**

4.5.5 XRD OF POLY VINYL ALCOHOL-GLUTAMINE COMPOSITE (PVAGLN)

X-ray diffraction patterns of the PVAGLN composite are presented in figure-16e. From the XRD of the PVA, it is clear that, PVA is well known as a crystalline polymer, and the diffraction peak at about 2θ = 11.4º and 19.4º corresponded to the PVA crystalline phase has been reported **(Yuan-Hiang Yu *et al.,* 2003)**. Figure-16e shows the diffraction pattern of the 10% PVA polymer membranes that are cross-linked by 1% - Glutamine solution. It is well known that the PVA polymer exhibits a semi-crystalline structure with a large peak at a 2θ angle of 20º. As can be seen clearly in figure, a large peak at 2θ of 20º for the PVAGLN composite polymer membrane is obtained. But it can also clearly seen that the peak intensity of the PVA polymer membrane greatly reduced when the membranes are further cross-linked by L-Glutamine. It is well known that the hydroxyl group of PVA chemically react with –COOH and $–NH_2$ of the L-Glutamine to form amine, ester and peptides linkages. Indeed, this chemically crosslinking reaction on the PVAGLN composite provides greater chemical, thermal and mechanism stabilities. It can be observed that cross-linked PVAGLN composite greatly augmented the domain of crystalline region (i.e., the degree of amorphous is decreased). This indicates that the cross-linked PVAGLN becomes more cystalline. Notably, it is found that the degree of crystalline of the composite membranes increases as both the L-glutamine fillers and the cross linking reaction are added into and treated on the PVA polymer, respectively **(Chun-Chen Yang et al., 2009).**

4.5.6 SEM-EDXA OF PVAGLN COMPOSITE

SEM photographs of the surface morphology of the PVAGLN composite polymer membranes are shown in figure-16f respectively. As seen in figure, the surface morphology of the PVAGLN composite polymer sample shows a lot of large irregular L-Glutamine aggregates or chunks that are randomly distributed on the top

surface. It was found that the dimension of those L- L-Glutamine particles embedded in PVA matrix **(Yuan-Hiang Yu *et al.,* 2003)** was about 20μm. This indicated that the L-Glutamine particle filler were not completely dispersed well within the polymer matrix due to L-Glutamine filler having flake –like irregular structure. As a whole, the hydrophilic PVA polymer and the L-Glutamine filler are compatible when the content of L-Glutamine filler is less than 1%.

The SEM micrograph has been used to investigate the morphology of the PVAGLN composite. Polyvinyl alcohol shows a semi crystalline morphology. The composite however display two features, one of amorphous and other of crystalline domain. The crystalline morphology may result from intra molecular hydrogen bonded a PVA and polyglutamine units. The composite particles show rough pattern on one side and comparatively smoother pattern on the other side as seen in figure-16f. Among them, smaller granular particles dispersed around the sharp edged particles with lamellar structure on one side are noticed for the composite. The composite of PVA with polyglutamine reveal the presence of small void in their SEM pictures. The difference in morphology for the composite of PVA with L-Glutamine may be associated with different monomer relativities. This SEM images clearly visualizes the presence of small ratio of secondary phases (polymerized Glutamine) distributed and get adherent on the polyvinyl alcohol matrix. The elemental composition of PVAGLN composite was identified through EDX elemental mapping (figure-16). The elements carbon, hydrogen and nitrogen are attributed to the PVAGLN composite. EDX analyses of the two phases reveal the presence of nitrogen atom only in the minor phases. The hydrogen bonding is the force that holds the polyamides of Glutamine to PVA matrix **(Dae Sik Kim *et al.,* 2004)**.

4.6 CHARACTERIZATION OF POLYVINYL ALCOHOL-TYROSINE COMPOSITE

4.6.1 CHARACTERISATION OF PVATYR USING FTIR SPECTRA DATA

To characterize the synthesized PVATYR composite, the FTIR analysis of PVA, TYR and PVATYR has been carried out (Figure-17a). The assignment of FTIR band frequencies tabulated in table-9. The FTIR absorption spectral values recorded for Tyrosine are in close agreement with the values reported earlier **(Narayana moolya et al., 2006)** The important peaks are assigned and discussed with references (**Yuan-Hiang Yu *et al.,* 2003, Srimathi *et al.,* 2011).**

PVA Vs PVATYR

The analysis of PVA, Tyrosine (TYR) & PVATYR composite confirm the PVATYR composite formation. A broad and strong peak centred at 3299 cm^{-1} is due to the stretching vibrations of -OH stretching from the inter and intra molecular

hydrogen bonds in PVA. The adsorption peak at 2923 cm^{-1} assigned to -C-H stretching from alkyl group in PVA has been shifted to 2952 and 2852 cm^{-1} in PVATYR composite. A peak at 1723 cm^{-1} associated with C=O stretching vibration and carbonyl group which can easily bond with hydrogen of PVA backbone is found to be shifted to a lower wave number in (1884 cm^{-1}) (amide I band(C=O stretching)) in the PVATYR composite. The absorption peak due to CH_3 bending deformation, C-O stretching and OH in plane bending observed in PVA at 1417 cm^{-1} is found to be shifted to a lower wave number (1419 cm^{-1}) in PVATYR composite. A band at 1371 cm^{-1} associated with C–H/OH bending is found in PVA. A sharp band at 1080 cm^{-1} and 1022 cm^{-1}due to C-O stretching and C-O-C stretching in PVA backbone is found to be shifted to 1082 cm^{-1} in the PVATYR composite. A peak at 1251 cm^{-1} is related to CH_2 rocking, rocking of NH_3^+in TYR. This is shifted to 1279 cm^{-1} in PVATYR composite. The absorption band at 838 cm^{-1} and 925 cm^{-1} corresponds to CH_2 rocking vibrations and C-H out of plane deformation of PVA.

TYR Vs PVATYR

A broad and strong peak centred at 3197 cm^{-1} is due to the stretching vibrations of NH_3^+ asymmetric stretching, solid state stabilized a zwitterion structure with NH_3^+ and COO^- and N-H group of polytyrosine is hydrogen bonding with -O-H group of PVA in PVATYR composite. A band at 2880 cm^{-1} corresponds to -C-H stretching from alkyl group of TYR. A peak at 2601 cm^{-1} in TYR indicates the presence of combination band of NH_3^+ bending. Bands at 2132 and1698 cm^{-1} of TYR are due to NH_3^+ degenerative deformation and COO^- asymmetric stretching/Substituted benzene ring. A peak at 1417cm^{-1} is due to CH_3 bending deformation and C-O stretching of TYR. This band is shifted to 1419 cm^{-1} in the PVATYR composite. The band at 1155 cm^{-1} is due to COO^- symmetric stretching and C-C-C stretching in TYR. The peaks at 973 and 876 cm^{-1} are related to C-H out of plane deformation and CH_2 rocking vibration in TYR. Another peak at 1357 cm^{-1} is also related to Symmetric stretching of COO^- in TYR. This is also present in the PVATYR composite. A peak at 1251/1080 cm^{-1} due to the rocking of NH_3^+ /C-C-N stretching in TYR is shifted to a lower wave number 1279/1082 cm^{-1} in PVATYR composite. A peak at 787 m^{-1} is related to special NH wagging and COO^-bending in TYR. This was shifted to 795 cm^{-1} in PVATYR composite. A band at 640 cm^{-1} is due to the COO- scissoring of TYR. This is shifted to 628 cm^{-1} in PVATYR composite. The changes in the vibrational frequencies of the above mentioned peaks in the FTIR spectrum of PVA, TYR and PVATYR confirmed the formation of PVATYR composite. The rocking, wagging and scissoring in plane and out of plane deformation modes of COO^- ionized carboxylic group and NH_3^+torsional are expected at 566 cm^{-1} in TYR.

Figure-17 Characterization of PVATYR Composite

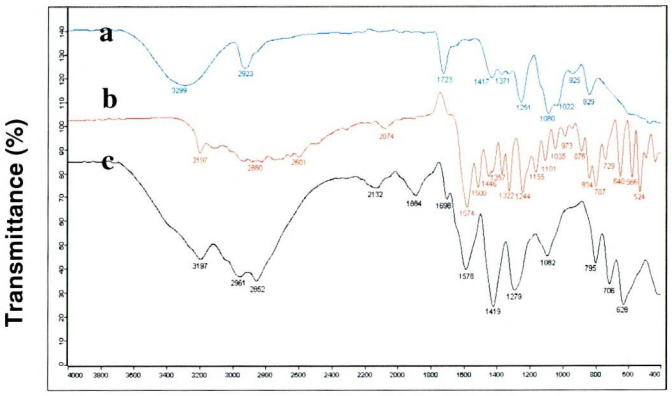

Fig. 17a FTIR Spectra of (a) PVA (b)) Tyrosine (c) PVATYR composite

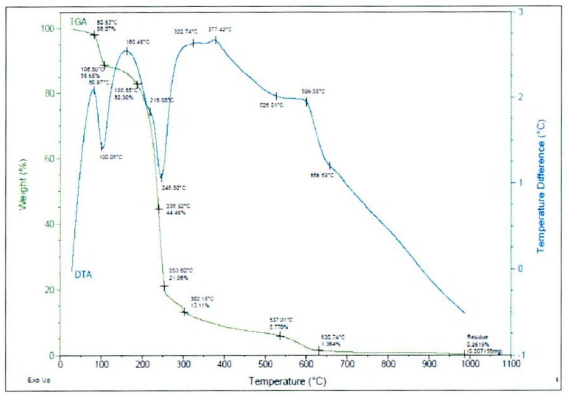

Fig. 17b TG and DTA thermograms of PVATYR composite

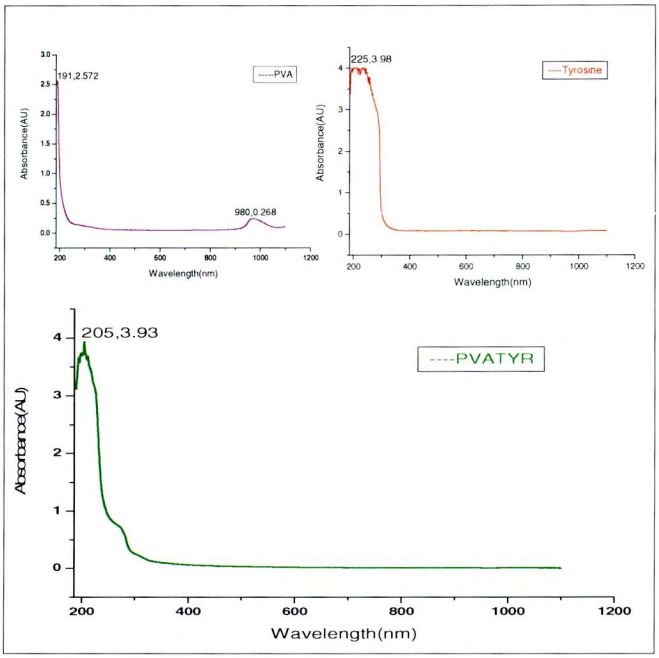

Fig. 17c UV-visible absorption Spectra of (a) PVA (b) Tyrosine (c) PVATYR composite

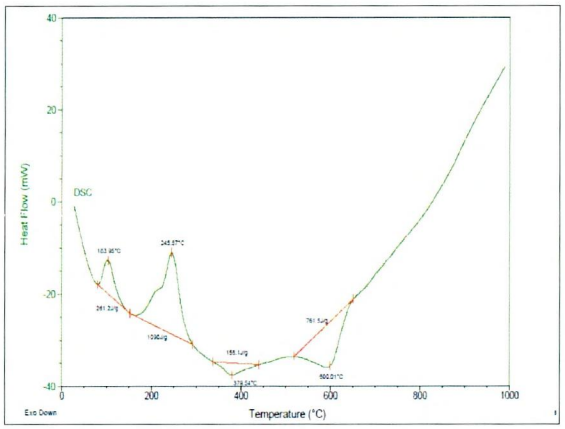

Fig. 17d DSC traces of PVATYR composite

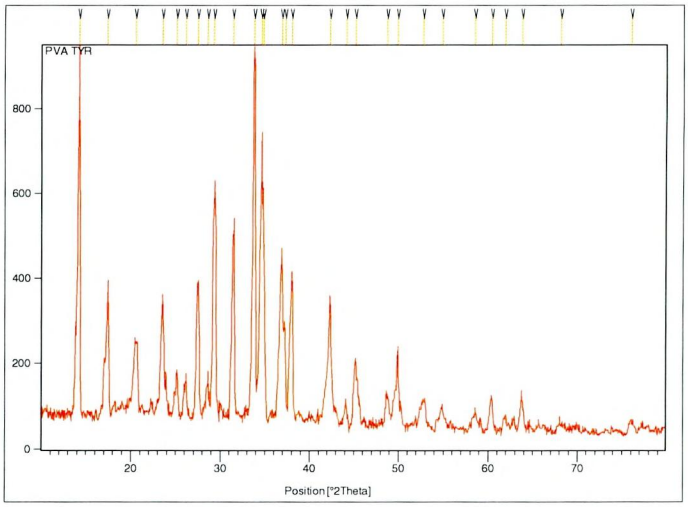

Fig. 17e X-ray Diffraction pattern of PVATYR composite

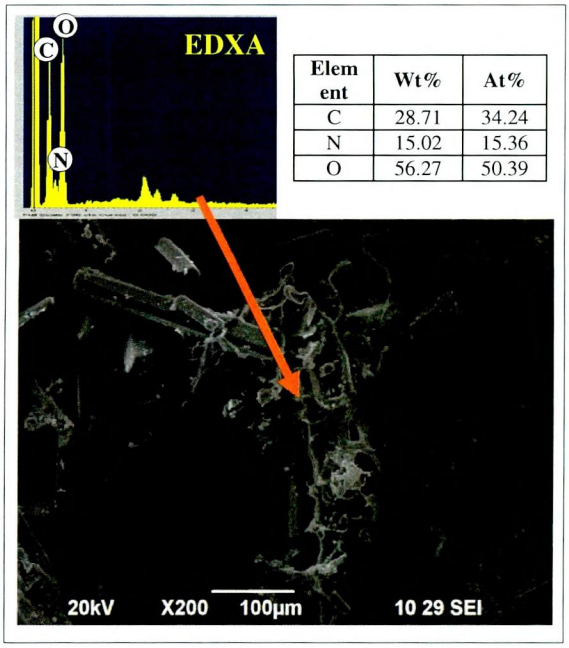

Element	Wt%	At%
C	28.71	34.24
N	15.02	15.36
O	56.27	50.39

Fig. 17f SEM-EDXA micrograph of PVATYR composite

Table: 9 Assignments of vibrational frequencies observed in FTIR spectra of PVA, Tyrosine (TYR) and PVATYR composite

S. NO	PVA (cm^{-1})	Tyrosine (TYR) (cm^{-1})	PVATYR (cm^{-1})	Assignment
1.	3299	-	-	OH str. (inter and intra molecular hydrogen bonds)
2.	-	3197	3197	NH_3^+ asym. str., zwitterions structure , bonded N-H str.
3.	2923	2880	2952, 2852	-C-H str. from alkyl group
4.	-	2601	-	Combination band of NH_3^+ bending
5.		2074	2132	NH_3^+ degenerative def.
6	1723	-	1884	C=O Str. Vib., amide I band(C=O str.)
7.	-	-	1698	COO^- asym. str. , Substituted benzene ring
8.	-	1574, 1500	1578	NH_3^+ sym. def., combination NH def. and CN str.
9.	1417	1446	1419	CH_3 bending def. + C-O Str. +OH in plane bending
10.	1371	1357, 1322	-	Sym. str. of COO^-, C–H/OH bending
11.	1251	1244	1279	CH_2 rocking, rocking of NH_3^+
12.	-	1155, 1101	-	COO^- sym. str., C-C-C str.
13.	1080, 1022	1035	1082	C-O str. + C-O-C str. , C-C-N str.
14.	925	973	-	C-H out of plane def.
15.	829	876, 834	-	CH_2 rocking vib.
16.	-	787, 729	795, 706	NH wag., COO^-bending
17.	-	640	628	COO- scissoring, Aromatic C-H out of plane bending
18.	-	566, 524	-	COO^- rocking, NH_3^+ torsional

4.6.2 UV-VISIBLE ABSORBANCE SPECTRUM OF PVATYR COMPOSITE

The UV-Vis analysis has been measured using AGILENT (8453 spectrophotometer in the wavelength range of 190-1100nm of PVA, Tyrosine and PVATYR composite as shown in figure-17c and table-5 **(Shanker Ram et *al.*, 2004**, **Narayana moolya et al., 2006)**. Figure-17c shown the UV spectrum of Tyrosine. The strongest adsorption peak at 220, 240, 260 and 280nm all corresponds to the aromatic ring of the Tyrosine. The cut-off wavelength is observed at 280nm. There is no significant absorption in the range 300-1100. This is an advantage of using amino acids, where the absence of strongly conjugated bonds leads to wider transparency range in the visible and UV spectral region. It is seen that a strong absorption band occurs at 290nm and the absorption is due to the n-π^* transition. The lower cut off wavelength at 240nm and is due to the π-π^* transition. After that, no absorption takes place in the entire visible region. It is clear that the spectrum of pure PVA exhibits an absorption edge (AE) around 200 and 960nm as shown in figure-17c. The absorption band at 200nm arises from π-π^* electron transition within PVA backbone, while the absorption band at 960nm is assigned as the polaron band. The UV-Visible absorption of PVATYR composite is shown in figure-17c. It is clear that the spectrum of pure PVA exhibits an adsorption edge (AE) around (260nm) indicates the semicrystalline nature of PVA. The UV-Visible spectrum of the PVATYR composite

has three bands, the first at 220nm, the second at 280nm and the third at 310nm associated with the $n \rightarrow \pi^*$ and π-π^* transition responsible for adsorption in C= O compounds can be traced to the "lone pair" of electrons is represented in the molecular orbital theory by a pair of electrons in an orbital confined largely to one atom and not appreciably involved in a bond formation. One of these electrons may be excited into an empty π^* orbital of the C=O group which gives rise to $n \rightarrow \pi^*$ transition (290nm) because $n \rightarrow \pi$ transition in C=O are symmetry forbidden, the absorption are weak. In summary, the UV-Visible data presented above provide strong support for the formation of the composite between PVA and Tyrosine. This result is confirmed by XRD. Figure-17c shows a shift in adsorption edge towards the higher wavelengths. These shifts in the absorption edge indicate the formation of inter/intra molecular hydrogen bonding mainly between Tyrosine with that of the adjacent OH groups of PVA. The bonds reflect the variation of the energy band gap which arises due to the variation in crystallinity within the polymer matrix.

4.6.3 TG/DTA ANALYSIS OF POLYVINYL ALCOHOL-TYROSINE (PVA) COMPOSITE

The TG spectrum of a composite (PVATYR) is given in figure-17b. The stability of the polymers is evaluated by 9.39% and 61.84% weight loss at minimum temperature. The results disclosed that, the polymer are stable upto 253° and start degrading thereafter in nitrogen. The thermal stability of the PVATYR composite increases with decreasing spacer length. The degradation occurs in two-step manner; the first step between 80-106°C corresponds to the vaporization of the absorbed surface and interlayer water (weight loss is 9.39%). The second and third step between 185-238°C, 238-253°C may be due the expulsion of water molecules from the polymer matrix or the moisture absorbed from the air, the decomposition of hydroxide groups, the splitting of the main chain of PVA and thermal degradation (or) decomposition of main chain of PVA. It is reported earlier (**Yuan-Hiang Yu *et al.*, 2003)** that from 250°C onwards, a steady decrease in weight has been observed upto 500°C which signifies the decomposition of tyrosine **(Anandan *et al.*, 2011)**

From DTA curve, it is observed that the material undergoes an irreversible endothermic transition at about 160° where the decomposition starts. The PVATYR composite material is completely decomposed at 245°C. The weight loss curve is very sharp and it starts at 160° and ends at 245°. This weight loss is due to the liberation of volatile substances. The sharpness of the endothermic peak shows good degree of crystallinity. The peak at 245°C indicates a phase change from liquid to vapour state as evidence from the loss of weight in the TG curve. These results

suggest that the introduction of tyrosine into the PVA chains enhances the thermal stability of the given PVATYR composite materials, which may be attributed to the high thermal stability of the tyrosine and the nature of crosslinking network between the tyrosine phase and PVA bulk.

4.6.4 DIFFERENTIAL SCANNING CALORIMETRY OF PVATYR COMPOSITE

Typical Differential Scanning Calorimetry results of PVA and PVATYR composite are shown of figure-13, 17d. The endothermic peak at 103°C is attributed to water loss, represents the energy required to vaporize water present in the PVATYR composite. The DSC thermogram of pure PVA exhibits a melting temperature 198°C and thermal degradation of 321°C (**Yuan-Hiang Yu *et al.*, 2003).** An endothermic peak, due to the melting of the crystalline phase present in the polymer can be observed at 191°C in PVA. It had been reported that the melting point of the L-Tyrosine was at 295°C. DSC curves of PVATYR composite are shown in figure-17. There is an endothermic peak at 103°C, following the first scan, the characteristic peak was PVAGLN composite in the second scan. The presence of this first scan peak results from the dissociation process of interaction hydrogen bonding of PVATYR composite. The peak temperature increased significantly from 103°C to 245°C. A melting endothermic peak at 245°C, is associated with crystalline polymer fraction of PVAGLN composite. The homogeneous nature of PVA and L-Tyrosine represents gave relatively large and sharp melting endotherms with a melting temperature peak(Tm) observed around 321°C and 295°C. However upon composite, a decrease in endothermic peak was observed. The tendency that melting temperature of the PVATYR composite shared 245°C small than that of PVA, which upon cross linking, reduced to 201 – 240°C, this implies the comparable, but reduced relatively crystallinity due to crosslinking **(Anjali Devi *et al.*, 2006).**

4.6.5 XRD OF POLY VINYL ALCOHOL-TYROSINE (PVATYR)

The XRD spectra of Poly Vinyl Alcohol-Tyrosine composite (powder) is presented in figure-17e. The x-ray diffraction measurement is preformed to examine the crystalline nature of PVATYR composite. Earlier reports show that the observed PVA spectrum alone reveals a semi-crystalline feature. It is vital to note that there are two halos cited at 19.5° and 40.5°. The first one has a clear crystalline peak at a scattering angle 2θ = 19.5 that corresponds to (101) spacing. The second halo has a low intensity and broad shape and corresponds to non-crystalline zones within the crystalline polymer matrix **(Yuan-Hiang Yu *et al.*, 2003)**. According to X-ray data, the unit cell of zwitter ionic L-Tyr contains two different oriented molecules, supposing a co-linear disposition of γ OH, γ_s NH_3^+ and δ_s NH_3^+ transition moments. The o.p (β_1)

phenyl ones in the frame of the two molecules are mutual oriented at a angle of 78.4°, avoiding their simultaneously elimination of the reduction procedure. The phenyl i.p. modes of both rings are near to co-linear oriented closing an angle of 14.3°. Hence presented are assumptions are confirmed by applications of the reduction procedure resulted to:

i. The elimination of γ OH stretching mode at 3202 cm^{-1} (Indicated the disappearance of maxima at 1525 and 1515 cm-1 (δ_s NH_3^+ and γ_s COO-) In addition, the multiple γ_s NH_3^+ maximum between 3100 and 2411cm^{-1} is strongly reduced in the obtained reduced spectrum.

ii. The simultaneously vanishing of a peak at 1613 and 1593 cm^{-1} is established, assigning the character of the second maximum as δ NH_3^+.

iii. On the other hand, the elimination of o.p. band at 840cm-1 (11-γ CH), a arises the second peak at 844 cm^{-1} belonging to same vibration mode of the second l-Tyrosine molecule with the reported value.

By comparing, the XRD of PVATYR composite obtained with PVA and L-Tyrosine it can be seen that the intensity of the PVA crystalline diffraction peak is decreased. The intensity of the diffraction and also the size of the crystals of PVA are determined by the number of PVA chains packing together. The complexation of PVA chains with L-Tyrosine leads to a decrease in the intermolecular interaction between the PVA chains and thus the degree of crystallinity. It seemed that the complication of PVA chains L-Tyrosine would confine the growth of the L-Tyrosine particle. No impurities such as Cl, NO, NO_2 are detected in XRD patterns. The difference between the crystal size calculated from XRD and particle size from SEM may be due to the change of aggregation of the crystal and smaller particles such that, the data of XRD reflected the size of the crystal while the data of SEM was obtained by the aggregation of the particle. Also, this difference may be due to the high surface energy of the nanometer size crystals. These facts suggest that the high viscosity of polymer matrix would prevent these particles from aggregating. **(Zhimin Liu *et al.,* 2008)**

4.6.6 SEM-EDXA OF PVATYR COMPOSITE

SEM photographs of the cross- sectional views of the PVATYR composite polymer membrane with 1% Tyrosine and the 10% PVA polymer were well compatible. As seen in figure-17f, magnification at ×200, the Tyrosine fillers are uniformly embedded into the PVA matrix. It is found that Tyrosine aggregates or chunks are formed in the PVATRY composite. A few Tyrosine aggregates or chunks with indicate tyrosine particles not completely dispersed into the PVA polymer **(Yuan-**

Hiang Yu *et al.,* 2003). This SEM images clearly visualizes the presence of small ratio of secondary phases (polymerized tyrosine) distributed and get adherent on the polyvinyl alcohol matrix.

In addition, a SEM equipped with EDXA has been used for the morphological analysis and to determine the elemental composition of the PVATYR composite as shown in the figure-17 (**Dae Sik Kim *et al.,* 2004).** In order to verify the chemical components of PVATYR composite, elemental analysis were performed to identify the major composition of the PVATYR composite. EDX analyses of the two phases were carried and it show the presence of nitrogen atom only in the minor phases. The hydrogen bonding is the is the force that holds the polyamides of tyrosine to PVA matrix.

4.7 CHARACTERIZATION OF POLYVINYL ALCOHOL-TYRPTOPHAN

4.7.1 CHARACTERISATION OF PVATRP USING FTIR SPECTRA DATA

To characterize the synthesized PVATRP composite, the FTIR analysis of PVA, TRP and PVATRP has been carried out (Figure-18a). The important peaks are assigned and discussed with references **(Cakira *et al.,* 2010)**. The formation of the synthesised PVATRP and Tryptophan (TRP) were identified using FTIR analysis. Table-10 shows the absorption bands of the active groups. The main final groups and their FTIR frequencies for TRP and PVATRP are presented in the table-10. The shift in the position of the characteristic peaks confirms the formation of the polymer composited (**Yuan-Hiang Yu *et al.,* 2003, srimathi *et al.,* 2011).**

PVA Vs PVATRP

A broad and strong peak centred at 3299 cm^{-1} is due to the stretching vibrations of -OH stretching from the inter and intra molecular hydrogen bonds in PVA. The absorption peak at 2923 cm^{-1} assigned to -C-H stretching from alkyl group in PVA has been shifted to 2965 and 2841 cm^{-1} in PVATRP composite. A peak at 1723 cm^{-1} associated with C=O stretching vibrations of PVA backbone is found to be shifted to a lower wave number in (1888 cm^{-1}) (amide I band(C=O stretching)) in the PVATRP composite. The absorption peak due to CH_3 bending deformation , C-O stretching and OH in plane bending observed in PVA at 1417 cm^{-1} is found to be shifted to a lower wave number (1407 cm^{-1}) in PVATRP composite. A band at 1371 cm^{-1} associated with C–H/OH bending is found in PVA. A sharp band at 1080 cm^{-1} due to C-O stretching, C-O-C stretching and C-C-N stretching in PVA backbone is found to be shifted to 1082 cm^{-1} in the PVATRP composite. The absorption band at 1251 cm^{-1} corresponds to CH_2 rocking vibrations of PVA. This band is shifted to 1275 cm^{-1} in the PVATRP composite. The band at 925 cm^{-1} results from an angular

deformation outside the plane of O-H bond of PVA. The absorption band at 829 cm^{-1} corresponds to CH rocking vibrations of PVA.

TRP Vs PVATRP

The protonation of amino group can be proved because of the presence of strong bands at 1266 cm^{-1}(NH_3^+ rocking mode) and at 3019 cm^{-1} due to NH_3^+ asymmetric stretching of TRP. A broad and strong peak centred at 3201 cm^{-1} and 3054 is due to the stretching vibrations of NH_3^+ asymmetric stretching, solid state stabilized a zwitterions structure with NH_3^+ and COO^- and amide (N-H group of polytryptophan is hydrogen bonding with -O-H group of PVA)in PVATRP composite. A strong peak centred at 3399 cm^{-1} is due to the stretching vibrations of NH stretching vibration of indole ring in PVATRP composite. A band at 2927 cm^{-1} corresponds to -C-H stretching from alkyl group of TRP. The NH_3^+ degenerative deformation is evident from a sharp medium band at 2058 cm^{-1} in the TRP. This band is shifted to 2132 cm^{-1} in the PVATRP composite. Bands at 1574cm^{-1} of TRP are due to NH_3^+ symmetric deformation (combination NH deformation and CN stretching) is found to be shifted to higher wavelength at 1578 cm^{-1} of PVATRP. The peak at 1221 cm^{-1} are due to CH_2 rocking and rocking of $NH_3^+$of TRP. This band is shifted to 1275 cm^{-1} in the PVATRP composite. Another peak at 1093cm^{-1} is also related to C-O stretching, C-O-C stretching and C-C-N stretching in TRP is shifted to a higher wave number 1082 cm^{-1} in PVATRP composite. The peak at 992 cm^{-1} and 849 cm^{-1} are related to C-H out of plane deformation and CH_2 rocking vibration. A peak at 733cm^{-1} and 613 cm^{-1} are related to CH_2 rocking vibration / NH wagging and COO^-bending in TRP. This is shifted to 795 /706cm^{-1} and 624cm^{-1} in PVATRP. The rocking, wagging and scissoring in plane and out of plane deformation modes of COO^- ionized carboxylic group and NH_3^+ torsional are expected at 500 cm^{-1} in TRP. FTIR spectral data of the polymer composite with reference to PVA and TRP confirmed the formation of PVATRP composite.

4.7.2 UV-VISIBLE ABSORBANCE SPECTRUM OF PVATRP COMPOSITE

The absorbance spectrum was recorded on a AGILENT (8453) UV-Vis spectrophotometer in the wavelength range 200-1100 nm in solution from using solvent (water). Figure-18c and table-5 shows the UV-Vis spectra of the PVA, Tryptophan and PVATRP composite **(Shanker Ram et *al.,* 2004**, **Cakira *et al.,* 2010).** The tryptophan solution has been observed with noticeable absorbance at 260,280, and 300 nm, which is assigned to conjugated double bond of benzene ring that easily generated π-π^* transition. UV-Vis spectrum of tryptophan exhibits three maximum absorption bands at 260, 280 and 300 nm, respectively. The aromatic amino acids are responsible for the ultraviolet absorption of most proteins with

maxima between 275 and 285 nm as shown in earlier reports. Tryptophan is known to have a strong spectroscopic signature at 280 nm that arises due to excitation of π-π* transitions in the indole part of the molecule. Most commercial PVA absorbs strongly in the 200-400 nm region, while the absorption band at 960nm is assigned as the polaron band as shown in figure. The appearance of the peak at 960nm may be attributed to the evolution of a polaron band.

Figure-18 shows the UV-Vis spectra of PVATRP composite. The PVATRP composite solution was observed with noticeable absorbance at 220 and 960 nm. The transmittance is high in the visible region. There is no significant absorption in the range 220-1100 nm. This is an advantage of the use of amino acids where the absence of strongly conjugated bonds leads to wider transparency range in the visible and UV spectral regions of PVATRP composite. Most commercial PVA absorbs strongly in the 200-400 nm region is also in the PVATRP composite. The appearance of the peak at 960 nm may be attributed to the evolution of a polaron bond of PVATRP composite. When the absorbance is monitored from longer to shorter wavelength, the absorption is found to be nearly zero in the entire visible region of the spectrum due to the delocalization of electronic cloud through charge transfer (CT) axis.

Table-10 Observed FTIR bands (cm-1) and their assignments for PVA, Tryptophan (TRP) and PVATRP composite

S.NO.	PVA (cm^{-1})	Tryptophan (TRP) (cm^{-1})	PVATRP (cm^{-1})	Assignment
1.	-	3399	-	NH str.vib. of indole ring
2.	3299	-	-	OH str. (inter and intra molecular hydrogen bonds)
3.	-	-	3201	NH_3^+ asym.str., zwitterions structure , bonded N-H str.
4.	-	3019	3054	NH_3^+ sym. str.
5.	2923	-	2965, 2841	-C-H str.from alkyl group
6	-	2058	2132	NH_3^+ degenerative def.
7.	1723	-	1888	C=O Str. Vib., amide I band(C=O str.)
8.	-	1647	-	COO^- asym. str. , Substituted benzene ring
9.	-	1574	1578	NH_3^+ sym. def., combination NH def. and CN str.
10.	1417	1407	1407	CH_3 bending def. + C-O str. +OH in plane bending
11.	1371	1345	-	Sym. str. of COO^-, C–H/OH bending
12.	1251	1221	1275	CH_2 rocking, rocking of NH_3^+
13.	-	1144	-	COO^- sym. str., C-C-C str.
14.	1080, 1022	1093	1082	C-O str. + C-O-C str. , C-C-N str.
15.	925	992, 911	-	C-H out of plane def.
16.	829	849	-	CH_2 rocking vib.
17.	-	733	795, 706	NH wag., COO^-bending
18.	-	613	624	COO- scissoring, Aromatic C-H out of plane bending
19.	-	500	-	COO^- rocking, NH_3^+ torsional

Figure-18 Characterization of PVATRP Composite

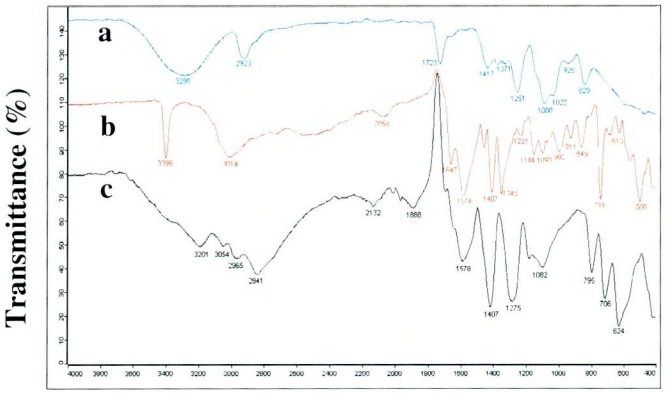

Fig. 18a FTIR Spectra of (a) PVA (b) Tyrptophan (c) PVATRP composite

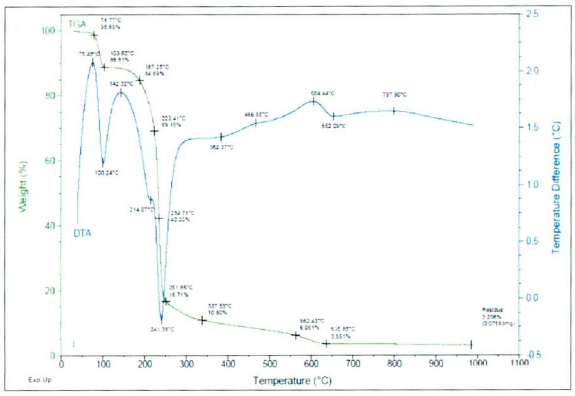

Fig. 18b TG and DTA thermograms of PVATRP composite

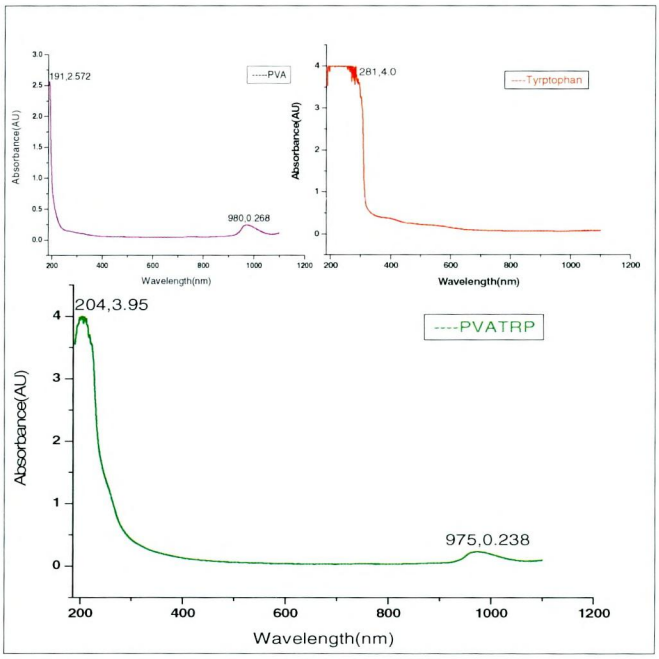

Fig. 18c UV-visible absorption Spectra of (a) PVA (b) Tyrptophan (c) PVATRP composite

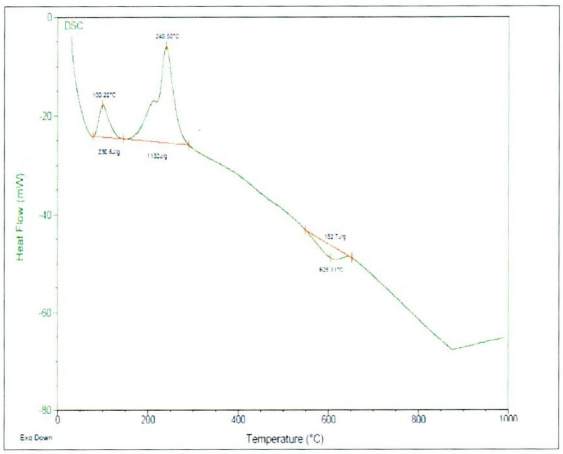

Fig. 18d DSC traces of PVATRP composite

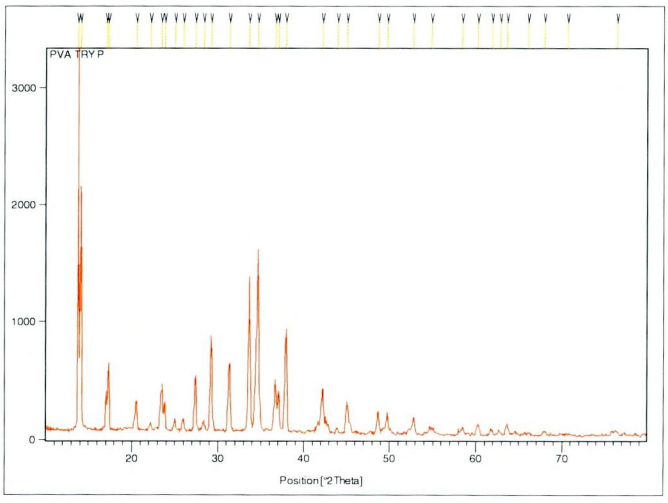

Fig. 18d X-ray Diffraction pattern of PVATRP composite

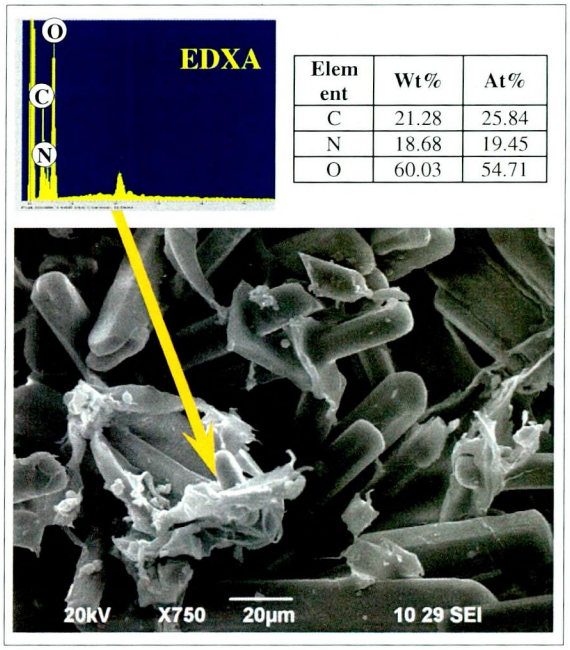

Element	Wt%	At%
C	21.28	25.84
N	18.68	19.45
O	60.03	54.71

Fig.18e SEM-EDXA micrograph of PVATRP composite

In summary, the UV-Vis data presented for all invesgated water soluble PVA-selected amino acids composite provide strong support for the formation of polymer composite between PVA and selected amino acids.

4.7.3 TG/DTA ANALYSIS OF POLYVINYL ALCOHOL-TRYPTOPHAN (PVATRP) COMPOSITE

Thermogravimetric analysis is carried to estimate the percentage weight loss of the polyvinyl alcohol – tryptophan (PVATRP) composite against temperature as shown in figure-18b. The initial decomposition temperature of PVATRP composite is 78-103°C is due to the removal of moisture and water molecules. The second , third and fourth step between 187-251°C, it is reported that is pure PVA decomposition occurred in two stages and it was thermally stable upto 265°C with weight loss of around 15% (**Yuan-Hiang Yu *et al.,* 2003).**

The DTA curve shows an endothermic peak at around 100°C due to the release of water and moisture. The sharp endothermic peak at 241°C is due to the decomposition of the sample desired by its DTA analysis, indicates that is exactly coincides with the decomposition in TG analysis. It is observed from DTA curve that a sharp peak appears at 241°C. The endothermic event in the PVATRP composite sample corresponds to the experimentally determined melting point. The remaining weight after the PVATRP composite decomposition is due to the residual char. However PVATRP composite membranes show lower weight loss is relation to PVA suggesting their higher thermal stability **(Tripathi *et al.,* 2009).**

4.7.4 DIFFERENTIAL SCANNING CALORIMETRY OF PVATRP COMPOSITE

The DSC diagram of the PVA and PVATYR, composite are shown in figure-13, 18d. The endothermic peak at 100ºC is attributed to water loss and represents the energy required to vaporize water present in the PVATRP composite. A melting endothermic peak at 193ºC is associated with the crystalline polymer fraction of PVA. The characteristic peak of crystalline polymer fraction of PVA is at about 193ºC and a thermal degradation temperature of 321ºC (**Yuan-Hiang Yu *et al.,* 2003).** It is found that the melting temperature, of the PVATRP composite shifted toward lower temperature when L-Tryptophan filler were added into PVA polymer matrix. An endothermic peak is observed at about 240ºC indicating the PVATRP composite melting temperature. It has been reported that the melting point of the L-Tryptophan was at 282°C, the DSC curves of PVATRP composite showed with endothermic peak with melting temperature at 240ºC and this indicates the presence of some degree of crystallinity order in polymer backbone. These results suggest that the introduction of L-tryptophan into the PVA chains enhances the thermal stability of the given PVATRP

composite materials, which may be attributed to the high thermal stability of L-tryptophan and the nature of crosslinking network between the L-tryptophan and PVA bulk. Melting endotherm of PVA is around 200ºC followed by dehydration and crosslinking of the polymer above 300°C producing polygene structure and volatile products. Ultimately PVA decomposes into carbon and hydrocarbons on heating above 450ºC. However, the DSC thermogram clearly exhibit that the PVATRP composite materials successfully combine the physical properties of both the components **(Tripathi et al., 2009).**

4.7.5 XRD OF POLY VINYL ALCOHOL-TRYPTOPHAN (PVATRP)

The x-ray diffraction measurement was performed to examine the crysatllinity of the PVATRP polymer composite. Figure-18e shows the diffraction scans for sample of PVATRP polymer composite. Earlier reports shows that PVA exhibits a typical diffraction peak at 2θ = 20º due to mixture of (101) and (200) crystalline phase **(Yuan-Hiang Yu *et al.,* 2003)**. XRD pattern of pure PVA shows a characteristic peak for a orthorhombic lattice centered at 2θ = 20º indicating its semi-crystalline nature (8). An initial indexing from the new powder XRD peaks suggests an orthorhombic unit cell of the new polymorph of L-Tryptophan with lattice parameters a=19.771Å, b=10.363Å, C=9.962Å, which is different from the known crystalline form of the Tryptophan(orthorhombic 16.81º, 17.9º,6.904º) with the reported values. If there were no or weak interaction between PVA and L-Tryptophan molecules in the composite membrane, each component and x-ray diffraction (XRD) patterns would express a simple addition of patterns of PVA and L-Tryptophan, with the same ratio (10:1) as that for composite. Figure-18 represents XRD patterns of crosslinked PVATRP composite membrane along with PVA and L-Tryptophan. The diffraction scan of the L-Tryptophan sample shows two peaks at 16.81º and 17.9º. For the PVA sample, there are two peaks at 2θ = 10.7º and 21.1º (30). Comparing L-Tryptophan, PVA is more crystalline than L-Tryptophan. In the PVA membrane, the high crystallinity was mainly caused by intra molecular hydrogen bonding. The peak at 2θ =10.7º of PVA almost disappears in the PVATRP composite with incorporation of L- Tryptophan. This indicates the occurrence of strong interaction between PVA and L-Tryptophan in the composite membranes at 70-80 wt % of L-Tryptophan. From the figure, it can be observed that compared to the PVA and L-Tryptophan membrane, the composite membrane shows a relatively obtuse and broad peak around 21º, indicating a decrease in the crystallinity of the composite. With an increase L-Tryptophan in the composite, the crystallinity decreases, which is expressed for L-Tryptophan is less crystalline than PVA. Figure-18e, shows the X-ray spectra of PVATRP before and

after crosslinking. Since L-Tryptophan molecules are bigger in size than PVA molecules, the composite of PVA inside the Tryptophan network can make the structure less compact. This also resulted in the decrease in crystallinity after the PVATRP composite formation. This implied that the interactions among PVA and Tryptophan resulted in the destroying the crystalline domain, thereby increasing the motion of PVA chains, losing the polymer chain packing and decreasing chain rigidity.

In a way, it was to be expected that the PVATRP composite from PVA and L-Tryptophan would be partially crystalline materials, because the PVATRP composite mode with both pure L-Tryptophan and PVA, showed partially crystalline structures. PVA has a flexible structure, which favors close molecular packing and crystallization and the crystallization of L-Tryptophan is due to its tendency to re-naturation. Maria et al., (2008), observed that films made with blend of PVA and L-Tryptophan presented partially amorphous structures, even though this biopolymer is a completely crystalline material. In general, a decrease in the intensity of the crystallinity peak (at 2θ =20°) of the PVATRP composite produced with PVA with the highest degree of hydrolysis was observed in this work.

4.7.6 **SEM-EDXA OF PVATRP COMPOSITE**

SEM micrographs for the polymer membrane with composition ratio of PVA: TRP = 10:1 is shown in figure-18f. It shows uniform surface morphology. The cross-section micrograph also exhibits uniform layer structure morphology. It has been found that the surface morphology of the PVATRP composite polymer sample show many different sizes of PVATRP composite aggregates or chunks that are randomly distributed on the top surface. It can be seen that the dimension of this Tryptophan embedded in PVA chunks is about 50μm. The presence of the PVA and Tryptophan particles has been confirmed using energy-dispersive X-ray analysis (EDXA). It has been noted that the L-Tryptophan particles are embedded in PVA matrix. These phenomena indicate that the well distributed OH ligands on the PVA chains complexed **(Yuan-Hiang Yu *et al.*, 2003)** with L-Tryptophan ions in an oxalic solution could assure even seeding of the Tryptophan, and the grids formed with PVA chains, determined by the PVA concentration might confine the L-Tryptophan seeds growing with confinement of the PVA tend to be clustered. Taken as a whole, the results of SEM demonstrate the good miscibility was sustained by the hydrogen bonds and intermolecular interaction between PVA and Tryptophan.

Moreover, result of EDX analysis evidenced uniform hydrogen, oxygen and nitrogen atom distributed through the polymer cross- section, which further supports heterogeneity of the PVATRP composite as shown in the figure-18 **(Dae Sik Kim *et***

***al.,* 2004).** EDX analysis of the two phases are carried out and its shows the presence of nitrogen atom only in the minor phases. The hydrogen bonding holds the polyamide of L-Tryptothan to PVA matrix. The elemental composition of the same cross- sections was examined by single point EDX and EDX mapping. The mordant layers appear to certain carbon, oxygen, and nitrogen, amongst other elements, suggesting the presence of PVATRP composite.

Figure-19 Proposed structure based on the characterisation of the investigated PVA-selected amino acid composites are depicted below

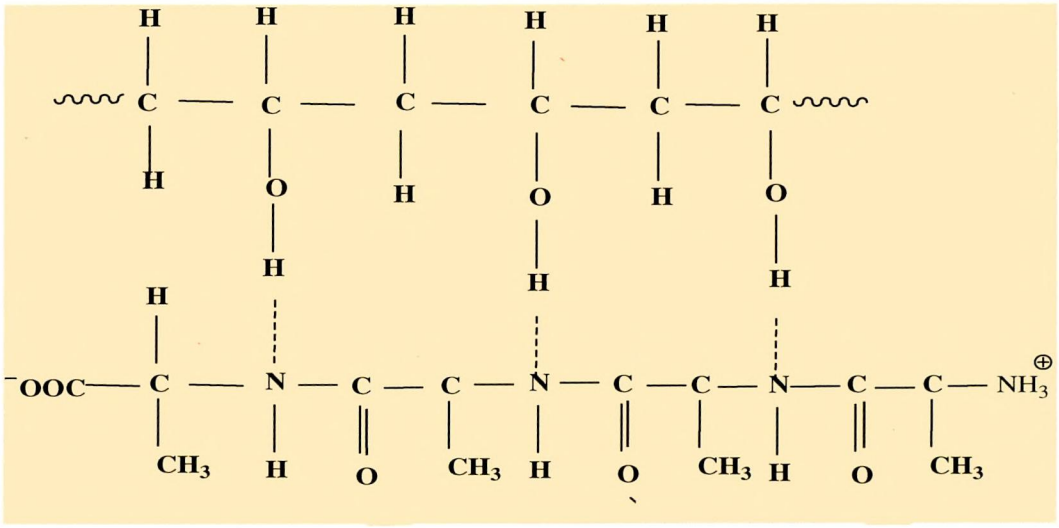

PVAALA

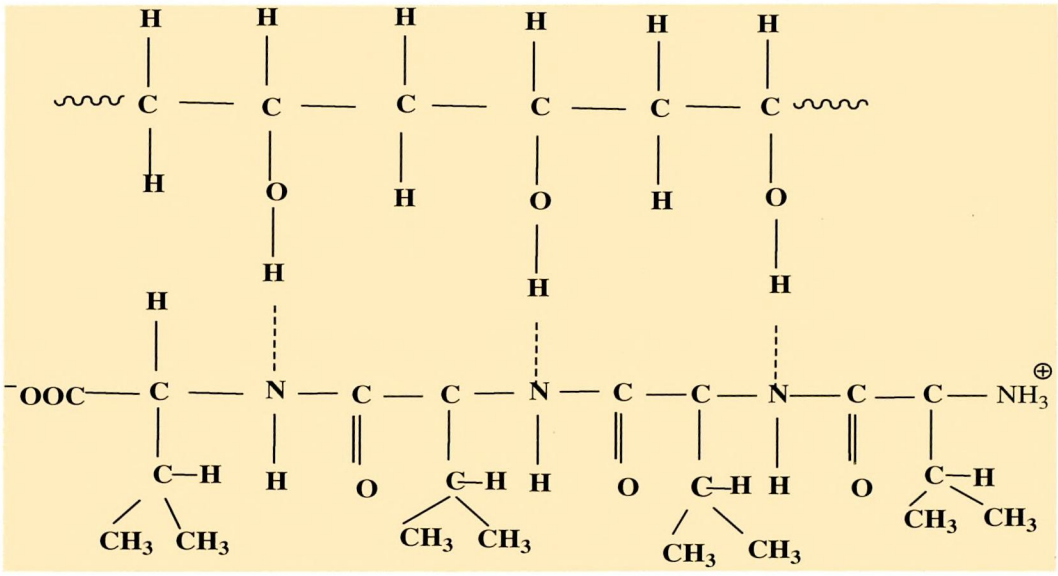

PVAVAL

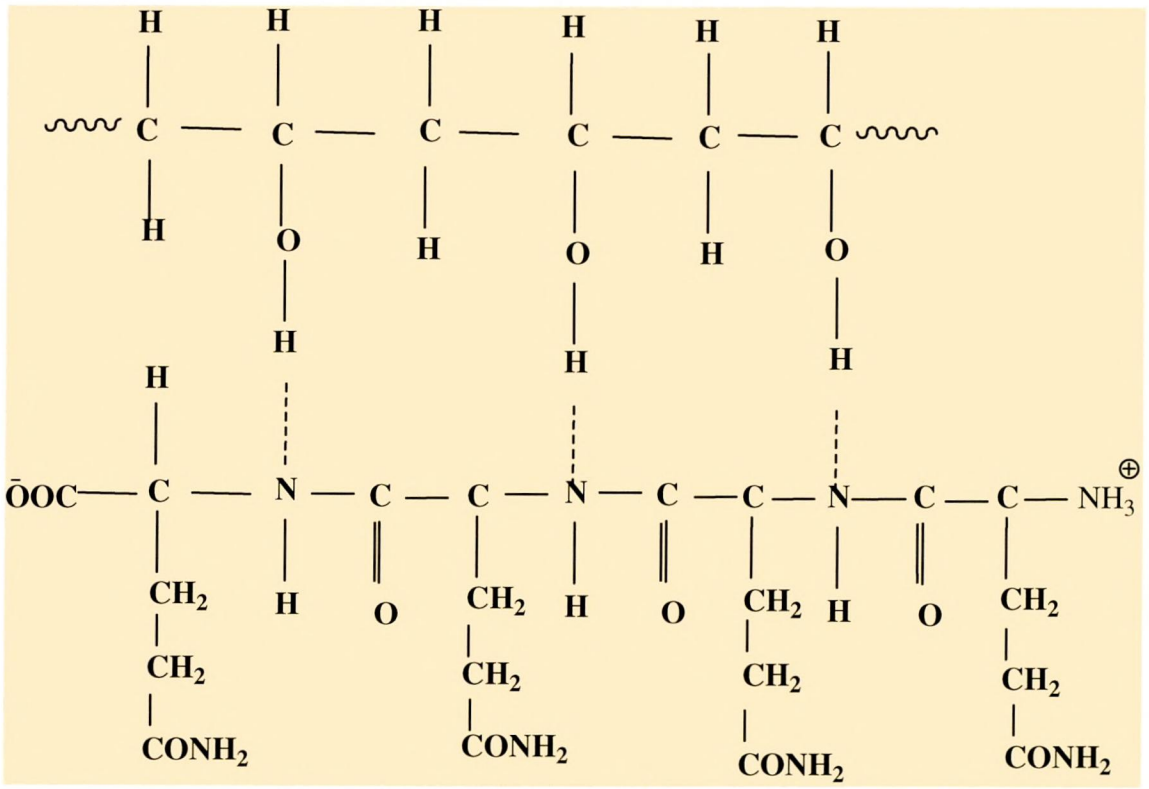

PVAGLN

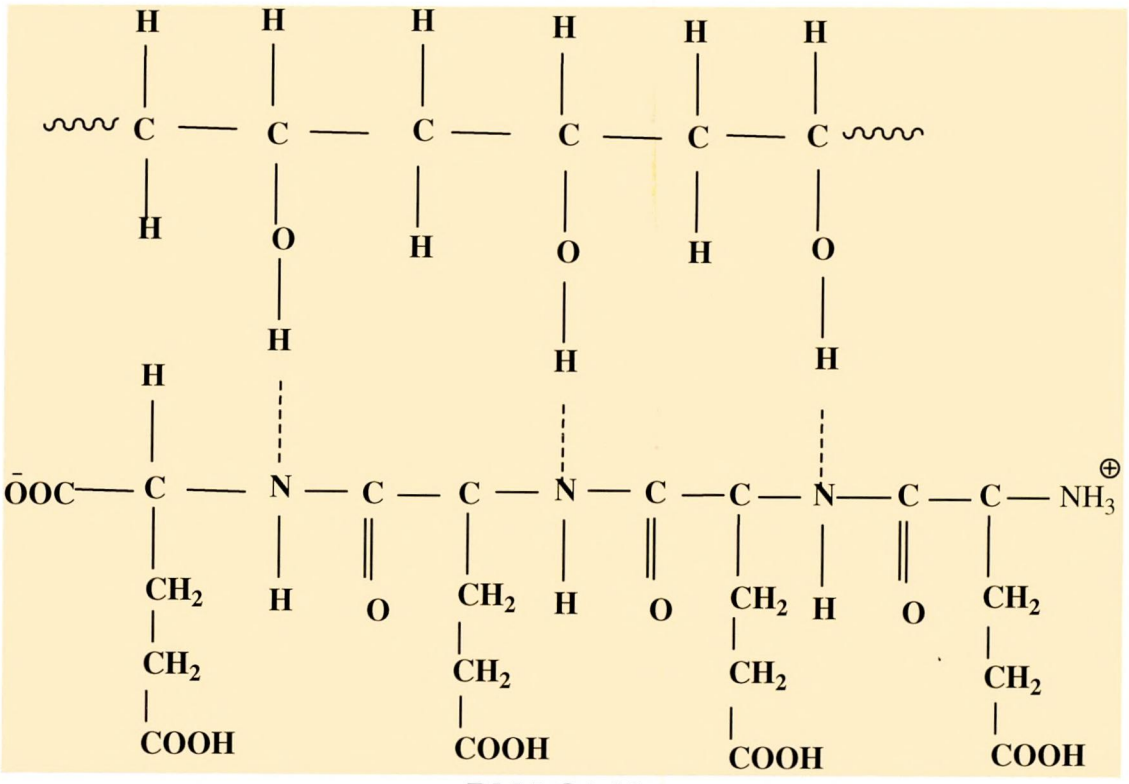

PVAGLU

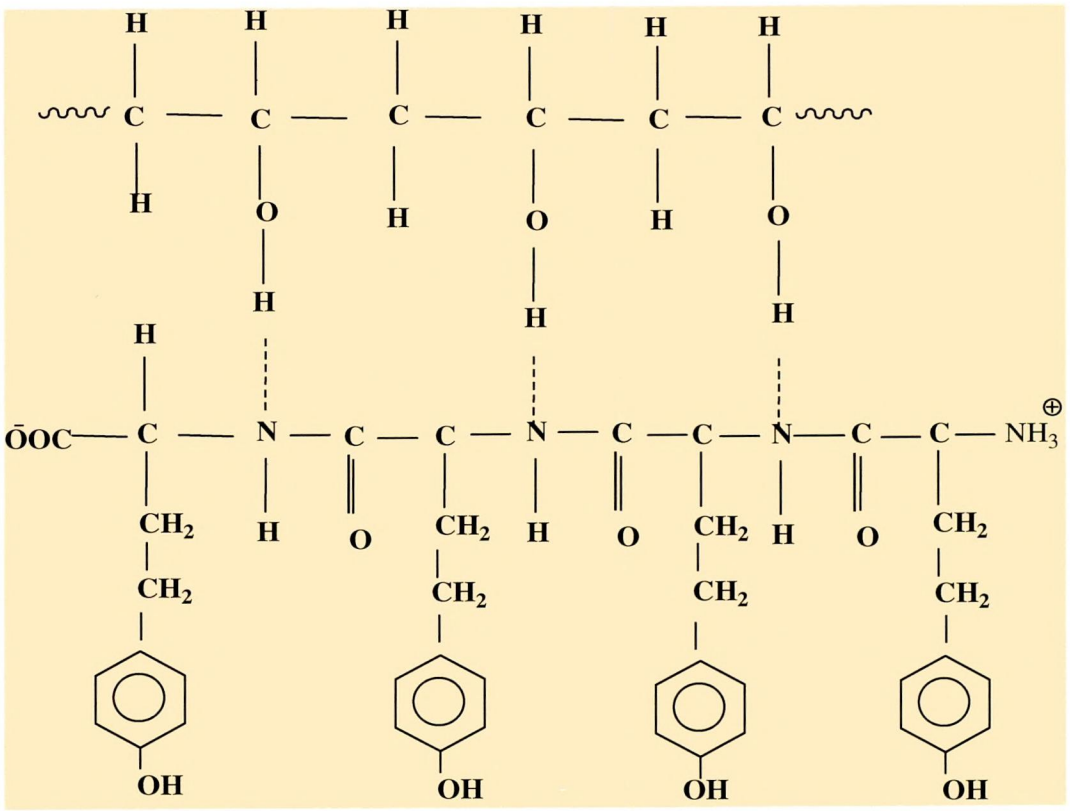

PVATYR

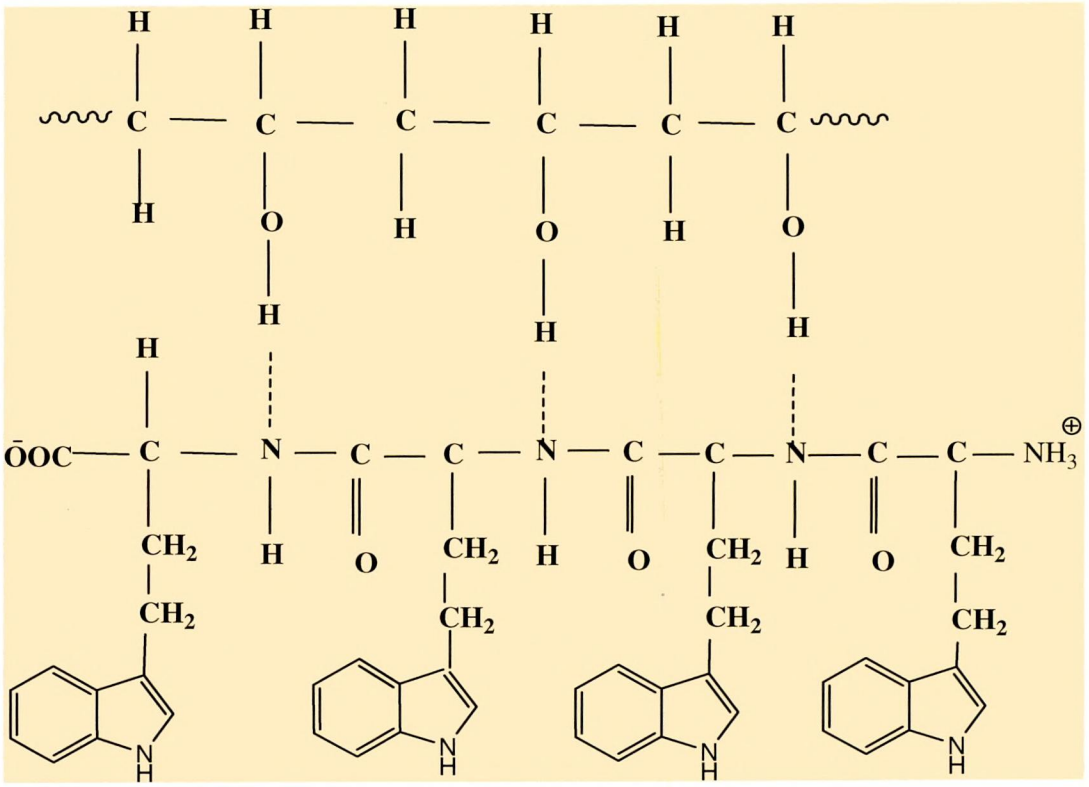

PVATRP

PHASE II

UTILISATION OF POLYMER COMPOSITES AS CORROSION INHIBITORS – WEIGHT LOSS METHODS AND ELECTROCHEMICAL MEASUREMENTS

The weight loss method is widely used in laboratory and factory due to its simple equipment and accurate data of average corrosion rate, whereas the electrochemical measurements give instantaneous corrosion rates. To assess the effectiveness of the inhibitors (PVAALA, PVAVAL, PVAGLU, PVAGLN, PVATYR and PVATRP composites) in minimising corrosion and to ascertain the mode of inhibition the following techniques were utilised.

a) **Weight loss method:** The following parameters are investigated:

- **Effect of concentration (0.06 % to 0.60 %)**
- **Effect of immersion time (½ h, 1 h, 3 h, 6 h, 12 h, 24 h and 48 h)**
- **Temperature variation (303 K, 313 K, 323 K, 333 K, 343 K)**

b) **Electrochemical Measurements:** The following techniques are carried out in this method

- **Potentiodynamic polarization method (Tafel polarisation)**
- **Linear polarisation resistance method**
- **Electrochemical impedance spectroscopic technique**.

4.8 WEIGHT LOSS METHOD

4.8.1 Effect of concentration of PVAALA and PVAVAL composites on mild steel corrosion

Table-11 reflect the values of inhibition efficiency (IE) and corrosion rate (CR) obtained from weight loss measurements at different concentrations of PVAALA and PVAVAL composites at room temperature (30°C) respectively. From the weight loss values, IE (%) and surface coverage (θ) of each concentration are calculated. It has been found that inhibition efficiency of PVAALA and PVAVAL composites increase with increase in concentration (figure-20) at all immersion time. This indicates that the presence of PVAALA and PVAVAL composites inhibit the corrosion of mild steel in 1M HCl and the extent of corrosion inhibition depend on the concentration of the PVAALA and PVAVAL composites present. The maximum inhibition efficiency for PVAALA and PVAVAL composites for each compound was achieved at 0.6 %. Further increase in concentration did not cause any appreciable change in the performance of the inhibitors. A maximum inhibition efficiency of 93.4 % and 95.0 % of PVAALA and PVAVAL composites was noted at 0.6 % concentration at 6 h.

Table-11 Effect of Concentration of PVAALA/ PVAVAL composites on mild steel corrosion in 1M HCl at various time intervals

S.No	Conc. of inhibitor (%) PVAALA	Immersion Time (in hour)													
		0.5		1		3		6		12		24		48	
		CR (mpy)	IE (%)	CR (mpy)	IE (%)	CR (mpy)	IE (%)	CR (mpy)	IE (%)	CR (mpy)	IE (%)	CR (mpy)	IE (%)	CR (mpy)	IE (%)
1.	Blank	1463.5	-	2093.0	-	2276.0	-	2408.0	-	1871.6	-	1600.0	-	978.5	-
2.	0.06	570.8	61.0	567.2	72.9	382.4	83.2	611.6	74.6	686.9	63.3	609.6	61.9	674.2	31.1
3.	0.12	488.8	66.6	477.2	77.2	366.5	83.9	207.1	91.4	535.3	71.4	433.6	72.9	596.9	39.0
4.	0.18	442.0	69.8	470.9	77.5	346.0	84.8	192.6	92.0	529.7	71.7	427.2	73.3	524.5	46.4
5.	0.24	434.7	70.3	445.8	78.7	316.4	86.1	190.2	92.1	505.3	73.0	299.2	81.3	486.3	50.3
6.	0.30	428.8	70.7	412.3	80.3	284.5	87.5	190.2	92.1	486.6	74.0	284.8	82.2	391.4	60.0
7.	0.36	361.5	75.3	332.8	84.1	270.9	88.1	175.8	92.7	481.0	74.3	265.6	83.4	364.0	62.8
8.	0.42	357.1	75.6	332.8	84.1	257.2	88.7	171.0	92.9	424.9	77.3	262.4	83.6	353.2	63.9
9.	0.48	346.9	76.3	326.5	84.4	243.5	89.3	171.0	92.9	423.0	77.4	259.2	83.8	287.7	70.6
10.	0.54	305.9	79.1	314.0	85.0	239.0	89.5	166.2	93.1	205.9	89.0	256.0	84.0	239.7	75.5
11.	0.60	276.6	81.1	247.0	88.2	227.6	90.0	158.9	93.4	187.2	90.0	241.6	84.9	150.7	84.6

S.No.	Conc. of inhibitor (%) PVAVAL	Immersion Time(in hour)													
		0.5		1		3		6		12		24		48	
		CR (mpy)	IE (%)	CR (mpy)	IE (%)	CR (mpy)	IE (%)	CR (mpy)	IE (%)	CR (mpy)	IE (%)	CR (mpy)	IE (%)	CR (mpy)	IE (%)
1.	Blank	1463.5	-	2093.0	-	2276.1	-	2408.0	-	1871.6	-	1600.0	-	978.5	-
2.	0.06	548.8	62.5	933.5	55.4	264.0	88.4	207.1	91.4	452.9	75.8	481.6	69.9	502.9	48.6
3.	0.12	543.0	62.9	920.9	56.0	248.1	89.1	190.2	92.1	329.4	82.4	371.2	76.8	397.3	59.4
4.	0.18	512.2	65.0	638.4	69.5	239.0	89.5	173.4	92.8	329.4	82.4	361.6	77.4	391.4	60.0
5.	0.24	487.4	66.7	527.4	74.8	216.2	90.5	163.7	93.2	314.4	83.2	310.4	80.6	374.8	61.7
6.	0.30	483.0	67.0	372.6	82.2	214.0	90.6	161.3	93.3	265.8	85.8	302.4	81.1	360.1	63.2
7.	0.36	472.7	67.7	372.6	82.2	211.7	90.7	144.5	94.0	243.3	87.0	278.4	82.6	345.4	64.7
8.	0.42	405.4	72.3	314.0	85.0	198.0	91.3	144.5	94.0	265.8	85.8	278.4	82.6	332.7	66.0
9.	0.48	386.4	73.6	305.6	85.4	182.1	92.0	130.0	94.6	168.4	91.0	265.6	83.4	306.3	68.7
10.	0.54	300.0	79.5	274.2	86.9	170.7	92.5	130.0	94.6	168.4	91.0	206.4	87.1	297.5	69.6
11.	0.60	279.5	80.9	270.0	87.1	159.3	93.0	120.4	95.0	104.8	94.4	153.6	90.4	271.0	72.3

Figure -20 Inhibition efficiency as a function of time and concentration of PVAALA /PVAVAL composites on mild steel acid corrosion

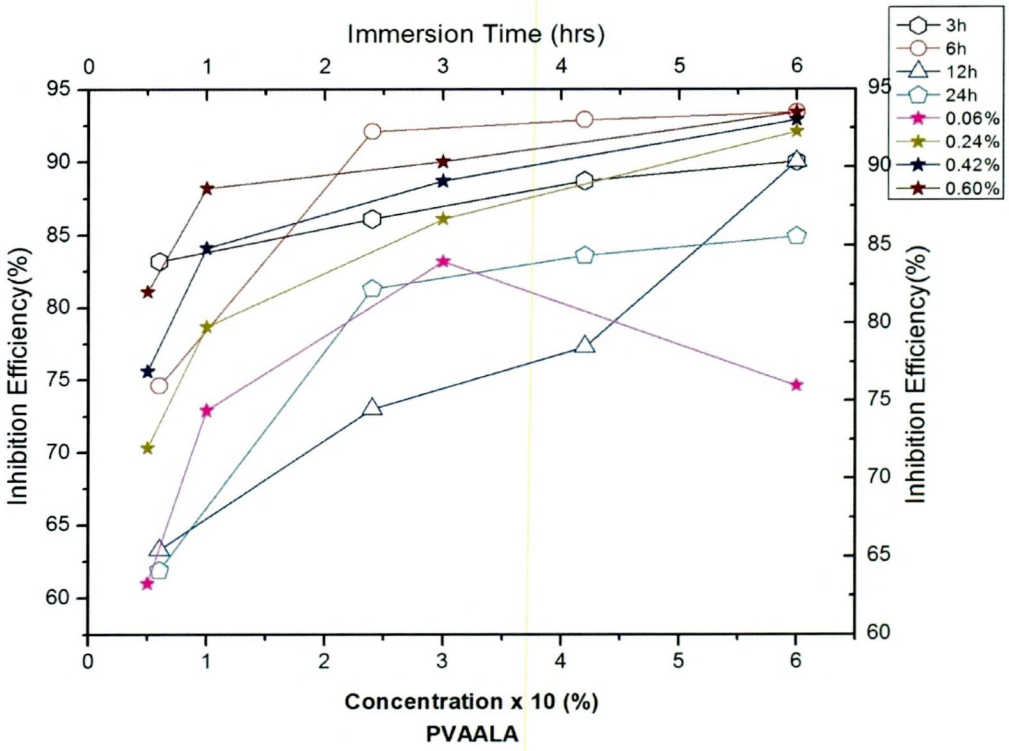

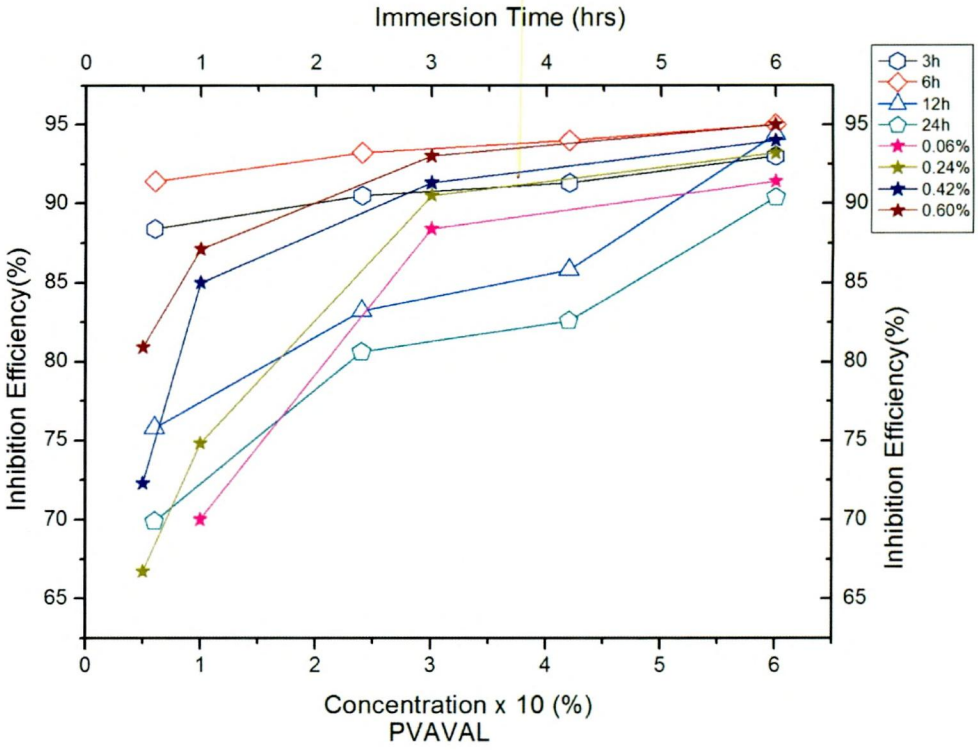

One possible mechanism of inhibition action of inhibitors is the adsorption of the inhibitor onto the metal surface which blocks the metals surface and this does not permit the corrosion process to takes place. The adsorption process is made possible due to the presence of hetero atoms such as oxygen, nitrogen and sulphur atoms, which are regarded as centres of adsorption.

PVAALA and PVAVAL composites contain nitrogen and oxygen atoms and methyl groups in this structure having lone pair and π- electrons. The inhibitive action of inhibitor can be accounted by the interaction between the lone pair of electrons in the nitrogen atom of amino group and positively charged metal surface. The presence of methyl groups leads to an enhancement of electron density at the nitrogen atom of amino group. This in turn leads to an increase in the value of the inhibition efficiency.

4.8.2 Effect of exposure time (PVAALA and PVAVAL composites):

In order to study the stability of adsorbed inhibitor film at mild steel /acid solution interface with time, weight loss measurements were conducted at 303 K for ½,1,3,6,12,24 and 48 h in 1 M HCl containing various concentrations of PVAALA and PVAVAL composites. The effect of exposure time on inhibition efficiency is shown in figure 20.

In the presence of PVAALA composite, the inhibition efficiency increases from 81.1 % (½ h) to 93.4 % (6 h) then slightly decreases to 90.0 % (12 h) and further reduced to 84.9 % at 24 h and stabilised at 48 h furnishing 84.6 % inhibition efficiency. Analysis of the table 11 reveals the stability of adsorbed layer on the mild steel surface with time of immersion.

Inspection of the figures reveals that of PVAVAL composite inhibition efficiency increases from 80.9 % at 1/2h to 95.0 % at 6 h. After 6 h, as the exposure time increases, a slight decrease in inhibition is observed and the value of IE is stabilised at 24 h affording an inhibition efficiency of 90.4 %. At 48 h exposure time, IE is reduced to 72.3 %. This is probably due to decreased adsorption and increased desorption. Shriver et al **(Singh *et al.*, 2010)** explained that decrease in inhibition for long period of immersion can be attributed to the depletion of available inhibition molecules in the solution due to chelate formation between iron and the inhibitor ligands. Thus it can be concluded that the studied compounds are efficient corrosion inhibitors for mild steel in molar hydrochloric acid solution. At low concentration (0.06 %) inhibition efficiency decreased continuously with immersion time but at higher concentration (0.60 %) inhibition efficiency was almost constant for different immersion times.

Inspection of data furnished in Table 1 and 3 infer that PVAALA and PVAVAL composites effectively function well up to 12 h and 24 h at 0.6% concentration respectively (inhibition efficiency of PVAALA composite – 84.9 % and PVAVAL composite – 90.4 % at 24 h). It also exhibits its inhibitive action at 48 h furnishing reasonable inhibition efficiency. The increase in inhibition efficiency with respect to time of immersion indicates the stability of adsorbed layer on mild steel surface.

4.8.3 Effect of concentration of PVAGLN AND PVAGLU composites on mild steel corrosion

The corrosion rate (CR) of mild steel in 1M HCl solution at various concentrations of PVAGLN and PVAGLU composites (at room temperature) are given in table-12. Investigation of results listed in table-12 infer that, as the concentration of PVAGLN and PVAGLU composites increases the IE of the studied PVAGLN and PVAGLU composites also increases at all periods of immersion. Maximum inhibition efficiencies of PVAGLN and PVAGLU composites were found to be 94.4 % (6 h) and 95.5 % (6 h) at 0.6% concentration respectively. Further increase in concentration of PVAGLN and PVAGLU composites does not show an increase in efficiency. However the IE at 12 h immersion period was found to be 88.1% for PVAGLN and 90.1% for PVAGLU Composites which infers the stability of adsorbed layer on mild steel surface. This may be due to the total coverage of the metal surface of the inhibitor molecules. Analysis of the table-12 also indicates that increase in immersion time at 24 h and 48 h decrease the inhibition efficiency of PVAGLU and PVAGLN composites.

A plausible mechanism for corrosion inhibition of mild steel in 1M HCl by PVAGLN and PVAGLU composites may be explained on the basis of adsorption behaviour. The adsorption of the PVAGLN and PVAGLU composites molecule with the metal surface is through the already adsorbed chloride ion. In acidic solutions, the diamine molecule exists as cations and adsorb through electrostatic interactions between the positively charged PVAGLN and PVAGLU composites cations and adsorbed chloride ions. Owing to the acidicity of the medium, PVAGLN and PVAGLU composites can exist as a neutral species or in the cationic form. Thus, the adsorption of the neutral PVAGLN and PVAGLU composites could occur due to the formation of links between the d-orbital of iron atoms, involving the displacement of water molecules from the metals surface, and the lone sp^2 electron pairs present on the N and/or O atoms. Moreover, the presence of electron releasing character of -OH group may be attributed to the increased electron density leading to electron transfer mechanism from functional group to metal surface.

Table-12 Effect of Concentration of PVAGLN/ PVAGLU composites on mild steel corrosion in 1M HCl at various time intervals

S.No	Conc. of inhibitor (%) PVAGLN	Immersion Time (in hour)													
		0.5		1		3		6		12		24		48	
		CR (mpy)	IE (%)	CR (mpy)	IE (%)	CR (mpy)	IE (%)	CR (mpy)	IE (%)	CR (mpy)	IE (%)	CR (mpy)	IE (%)	CR (mpy)	IE (%)
1.	Blank	1463.5	-	2093.0	-	2276.1	-	2408.0	-	1871.6	-	1600.0	-	978.5	-
2.	0.06	361.5	75.3	378.8	81.9	243.5	89.3	515.3	78.6	473.5	74.7	296.0	81.5	448.1	54.2
3.	0.12	358.6	75.5	368.4	82.4	236.7	89.6	209.5	91.3	393.0	79.0	257.6	83.9	418.8	57.2
4.	0.18	355.6	75.7	347.4	83.4	234.4	89.7	183.0	92.4	344.4	81.6	225.6	85.9	406.1	58.5
5.	0.24	355.6	75.7	343.3	83.6	225.3	90.1	168.6	93.0	310.7	83.4	212.8	86.7	344.4	64.8
6.	0.30	355.6	75.7	299.3	85.7	191.2	91.6	158.9	93.4	288.2	84.6	212.8	86.7	343.4	64.9
7.	0.36	336.6	77.0	293.0	86.0	191.2	91.6	156.5	93.5	275.1	85.3	209.6	86.9	340.5	65.2
8.	0.42	272.2	81.4	284.7	86.4	188.9	91.7	149.3	93.8	262.0	86.0	209.6	86.9	334.6	65.8
9.	0.48	166.8	88.6	265.8	87.3	170.7	92.5	137.3	94.3	254.5	86.4	204.8	87.2	288.7	70.5
10.	0.54	150.7	89.7	265.8	87.3	166.2	92.7	134.9	94.4	252.7	86.5	201.6	87.4	269.1	72.5
11.	0.60	130.3	91.1	144.4	93.1	143.4	93.7	134.9	94.4	222.7	88.1	195.2	87.8	258.3	73.6

S.No.	Conc. of inhibitor (%) PNAGLU	Immersion Time (in hour)													
		0.5		1		3		6		12		24		48	
		CR (mpy)	IE (%)	CR (mpy)	IE (%)	CR (mpy)	IE (%)	CR (mpy)	IE (%)	CR (mpy)	IE (%)	CR (mpy)	IE (%)	CR (mpy)	IE (%)
1.	Blank	1463.5	-	2093.0	-	2276.1	-	2408.0	-	1871.6	-	1600.0	-	978.5	-
2.	0.06	560.5	61.7	351.6	83.2	252.7	88.9	166.2	93.1	278.9	85.1	372.8	76.7	442.3	54.8
3.	0.12	550.3	62.4	305.6	85.4	248.1	89.1	137.3	94.3	260.2	86.1	326.4	79.6	383.6	60.8
4.	0.18	521.0	64.4	297.2	85.8	198.0	91.3	125.2	94.8	241.4	87.1	312.0	80.5	342.5	65.0
5.	0.24	260.5	82.2	286.7	86.3	168.4	92.6	125.2	94.8	235.8	87.4	289.6	81.9	329.8	66.3
6.	0.30	250.3	82.9	267.9	87.2	163.9	92.8	120.4	95.0	217.1	88.4	268.8	83.2	325.8	66.7
7.	0.36	248.8	83.0	257.4	87.7	157.1	93.1	118.0	95.1	213.4	88.6	265.6	83.4	295.5	69.8
8.	0.42	247.3	83.1	240.7	88.5	152.5	93.3	115.6	95.2	211.5	88.7	240.0	85.0	283.8	71.0
9.	0.48	228.3	84.4	238.6	88.6	145.7	93.6	115.6	95.2	205.9	89.0	238.4	85.1	247.6	74.7
10.	0.54	225.4	84.6	232.3	88.9	145.7	93.6	113.2	95.3	190.9	89.8	238.4	85.1	226.0	76.9
11.	0.60	206.4	85.9	230.2	89.0	132.0	94.2	108.4	95.5	185.3	90.1	230.4	85.6	185.9	81.0

Figure-21 Variation of time of immersion and concentration of PVAGLU/PVAGLN with inhibition efficiency

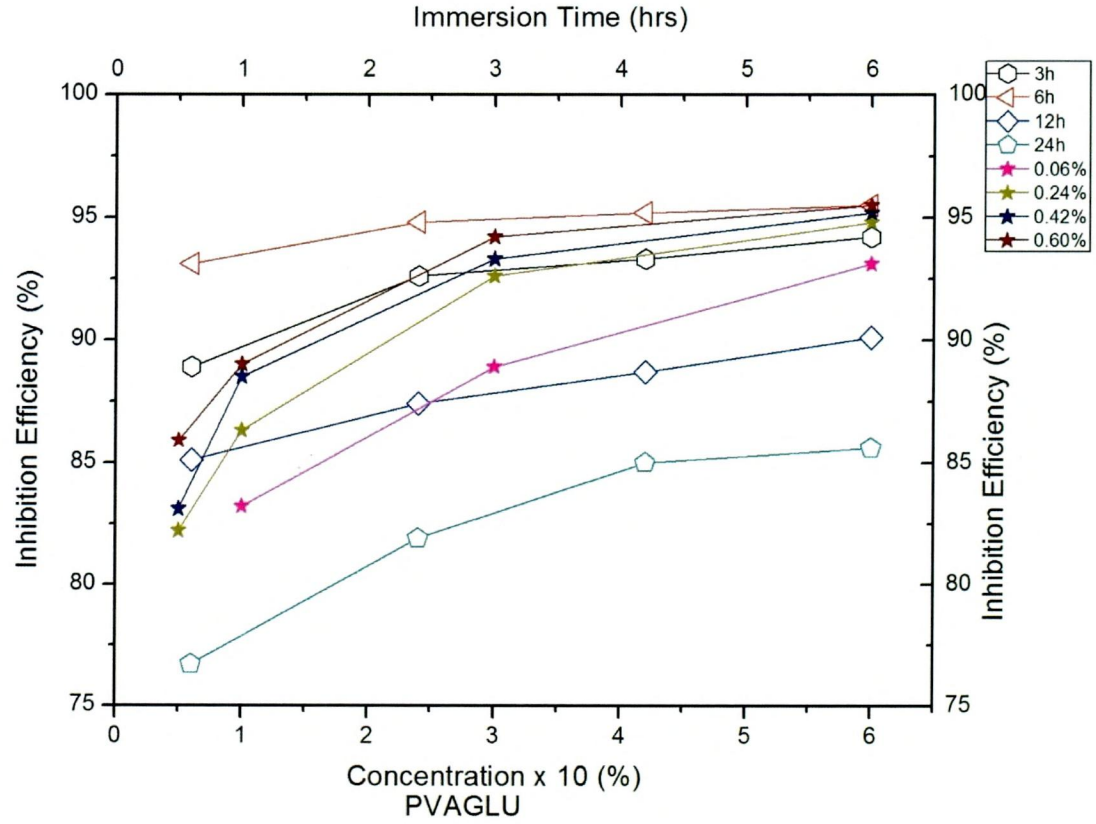

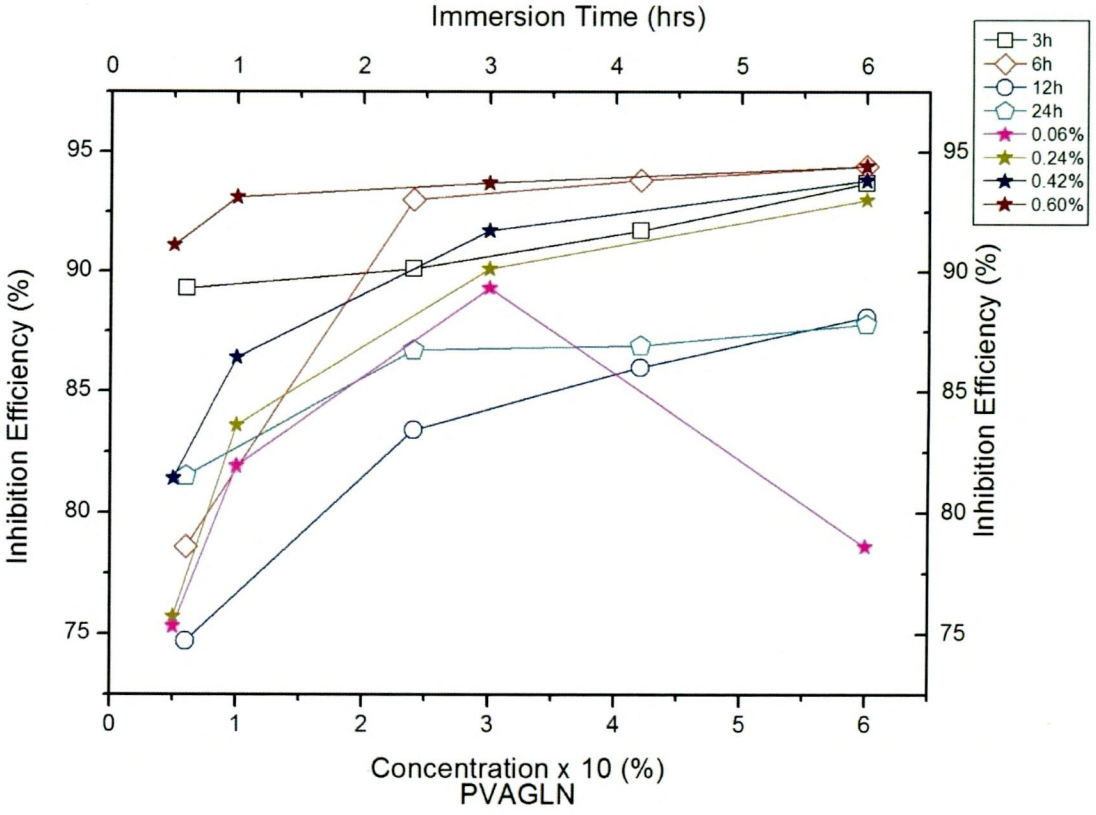

Also, the larger molecular size can be considered which ensures greater coverage of the metallic surface. The hydrophobic groups (CH_2-CH_2) in PVAGLN and PVAGLU composites may act as an effective barrier from the aggressive medium **(Tebbii *et al.*, 2005)**.

4.8.4 Effect of immersion time of PVAGLN AND PVAGLU composites on mild steel corrosion

In order to assess the stability of inhibitive behaviour of PVAGLN and PVAGLU composites on a time scale, weight loss measurements are performed in 1M HCl in the absence and presence of PVAGLN and PVAGLU composites at 0.6 % concentration for ½, 1, 3, 6, 12, 24 and 48 h of immersion time at temperature 303 K. Inhibition efficiencies were plotted against immersion time as seen from figure -21. The figure shows that inhibition efficiency of the PVAGLN and PVAGLU composites were increased with increasing immersion time from ½ to 6 h. The increase in inhibition efficiency upto 6 h reflects the strong adsorption of constituents present in the PVAGLN and PVAGLU composites on mild steel surface, resulting in a more protective layer formed at mild steel/ hydrochloric acid solution interface. This may be due to the formation of barrier film which prevents the attack of acid on metal surface. Desorption of synthesised polymer composites- PVAGLU and PVAGLN composites resulted at 12h, 24h and 48 h. Despite the desorption, mild steel surface could be covered by polymer composites furnishing around 80% in the presence of the polymer composites. This behaviour can be discussed on the basis that prolonged immersion of mild steel in acid solution **(Zakvi and Mehta, 1987)**.

a) allows the cathodic or hydrogen evolution kinetics to increase presumably or more cathodic or carbon containing sites are exposed by the corrosion process.
b) increase the concentration of ferrous ions which decrease the corrosive nature of the acid.

4.8.5 Effect of concentration of PVATYR and PVATRP composites on mild steel corrosion

The values of percentage inhibition efficiency and corrosion rate obtained from weight loss method at different concentrations of studied PVATYR and PVATRP composites at 30°C are summarized in table-13. Analysis of the table and figure-22, it has been found that PVATRY and PVATRP composites inhibits the corrosion of mild steel in hydrochloric acid solution at all concentrations used in this study that is 0.06-0.60 %. It is evident from the table that the corrosion rate decreased with the addition of PVATYR and PVATRP composites. The inhibition efficiency increases with increasing concentration to reach a maximum of 96.6 % (12 h) for PVATYR

Table-13 Effect of Concentration of PVATYR/PVATRP composites on mild steel corrosion in 1M HCl at various time intervals

S.No	Conc. of inhibitor (%) PVATYR	Immersion Time (in hour)													
		0.5		1		3		6		12		24		48	
		CR (mpy)	IE (%)	CR (mpy)	IE (%)	CR (mpy)	IE (%)	CR (mpy)	IE (%)	CR (mpy)	IE (%)	CR (mpy)	IE (%)	CR (mpy)	IE (%)
1.	Blank	1463.5	-	2093.0	-	2276.1	-	2408.0	-	1871.6	-	1600.0	-	978.5	-
2.	0.06	547.4	62.6	560.9	73.2	591.8	74.0	358.8	85.1	441.7	76.4	416.0	74.0	338.6	65.4
3.	0.12	523.9	64.2	560.9	73.2	578.1	74.6	332.3	86.2	293.8	84.3	416.0	74.0	264.2	73.0
4.	0.18	518.1	64.6	517.0	75.3	534.9	76.5	286.6	88.1	273.3	85.4	406.4	74.6	215.3	78.0
5.	0.24	507.8	65.3	475.1	77.3	534.9	76.5	257.7	89.3	235.8	87.4	400.0	75.0	205.5	79.0
6.	0.30	485.9	66.8	473.0	77.4	446.1	80.4	240.8	90.0	230.2	87.7	393.6	75.4	203.5	79.2
7.	0.36	469.8	67.9	464.7	77.8	380.1	83.3	202.3	91.6	219.0	88.3	392.0	75.5	203.5	79.2
8.	0.42	463.9	68.3	460.5	78.0	373.3	83.6	202.3	91.6	190.9	89.8	369.6	76.9	188.8	80.7
9.	0.48	431.7	70.5	460.5	78.0	371.0	83.7	175.8	92.7	177.8	90.5	328.0	79.5	184.0	81.2
10.	0.54	383.4	73.8	420.7	79.9	361.9	84.1	154.1	93.6	144.1	92.3	316.8	80.2	156.6	84.0
11.	0.60	346.9	76.3	414.4	80.2	143.4	93.7	98.7	95.9	63.6	96.6	310.4	80.6	118.4	87.9

S.No.	Conc. of inhibitor (%) PVATRP	Immersion Time(in hour)													
		0.5		1		3		6		12		24		48	
		CR (mpy)	IE (%)	CR (mpy)	IE (%)	CR (mpy)	IE (%)	CR (mpy)	IE (%)	CR (mpy)	IE (%)	CR (mpy)	IE (%)	CR (mpy)	IE (%)
1.	Blank	1463.5	-	2093.0	-	2276.1	-	2408.0	-	1871.6	-	1600.0	-	978.5	-
2.	0.06	480.0	67.2	450.0	78.5	318.7	86	604.4	74.9	471.6	74.7	609.6	74.8	481.4	50.8
3.	0.12	420.0	71.3	431.2	79.4	268.6	88.2	351.6	85.4	443.6	76.1	433.6	76.3	406.1	58.5
4.	0.18	377.6	74.2	424.9	79.7	266.3	88.3	320.3	86.7	396.8	78.2	427.2	78.8	335.6	65.7
5.	0.24	377.6	74.2	362.1	82.7	248.1	89.1	313.0	87.0	370.6	79.9	299.2	80.2	322.9	67.0
6.	0.30	370.3	74.7	337.0	83.9	248.1	89.1	289.0	88.0	350.0	81.0	284.8	81.3	291.6	70.2
7.	0.36	360.0	75.4	330.7	84.2	227.6	90.0	264.9	89.0	340.6	82.3	265.6	81.8	261.3	73.3
8.	0.42	336.6	77.0	305.6	85.4	202.6	91.1	252.8	89.5	336.9	83.3	262.4	82.0	238.8	75.6
9.	0.48	301.5	79.4	286.7	86.3	188.9	91.7	255.3	89.4	329.4	83.9	259.2	82.4	231.9	76.3
10.	0.54	238.6	83.7	215.6	89.7	166.2	92.7	233.6	90.3	312.6	84.0	256.0	83.3	219.2	77.6
11.	0.60	209.3	85.7	146.5	93.0	122.9	94.6	221.5	90.8	295.7	87.5	241.6	84.2	197.7	79.8

Figure-22 Dependence of concentration and time of immersion with inhibition efficiency of PVATYR and PVATRP

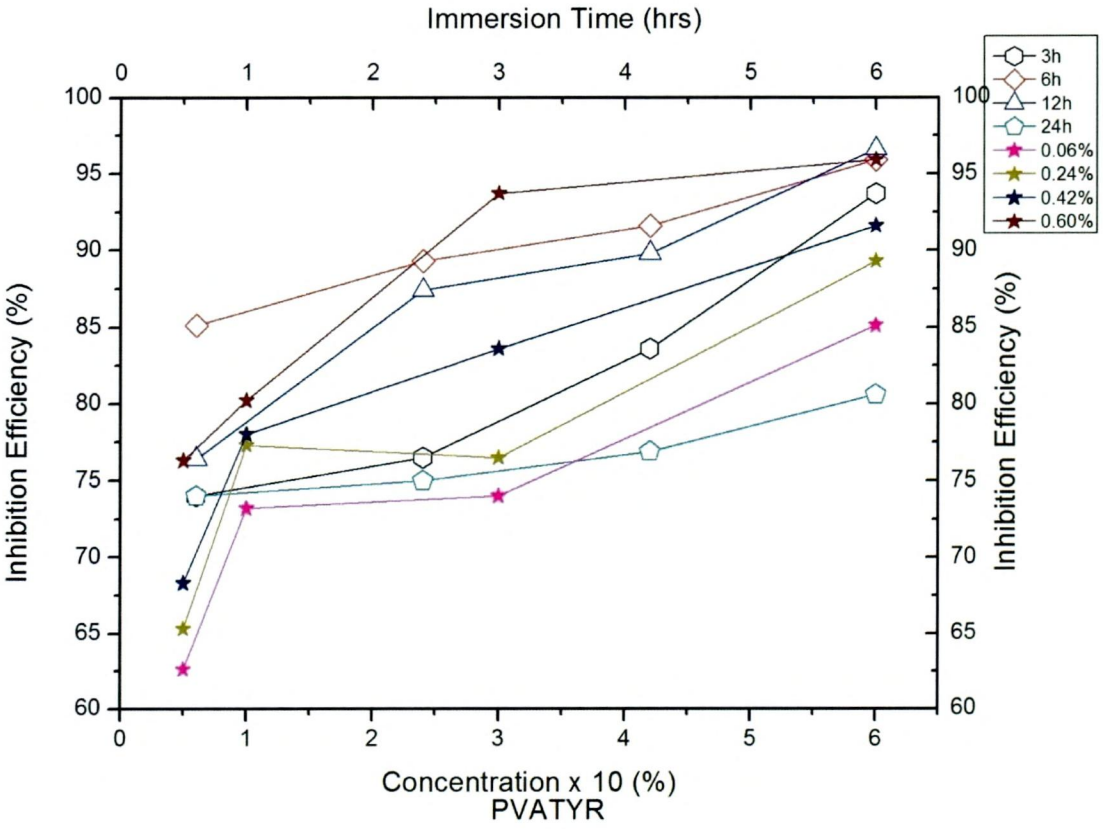

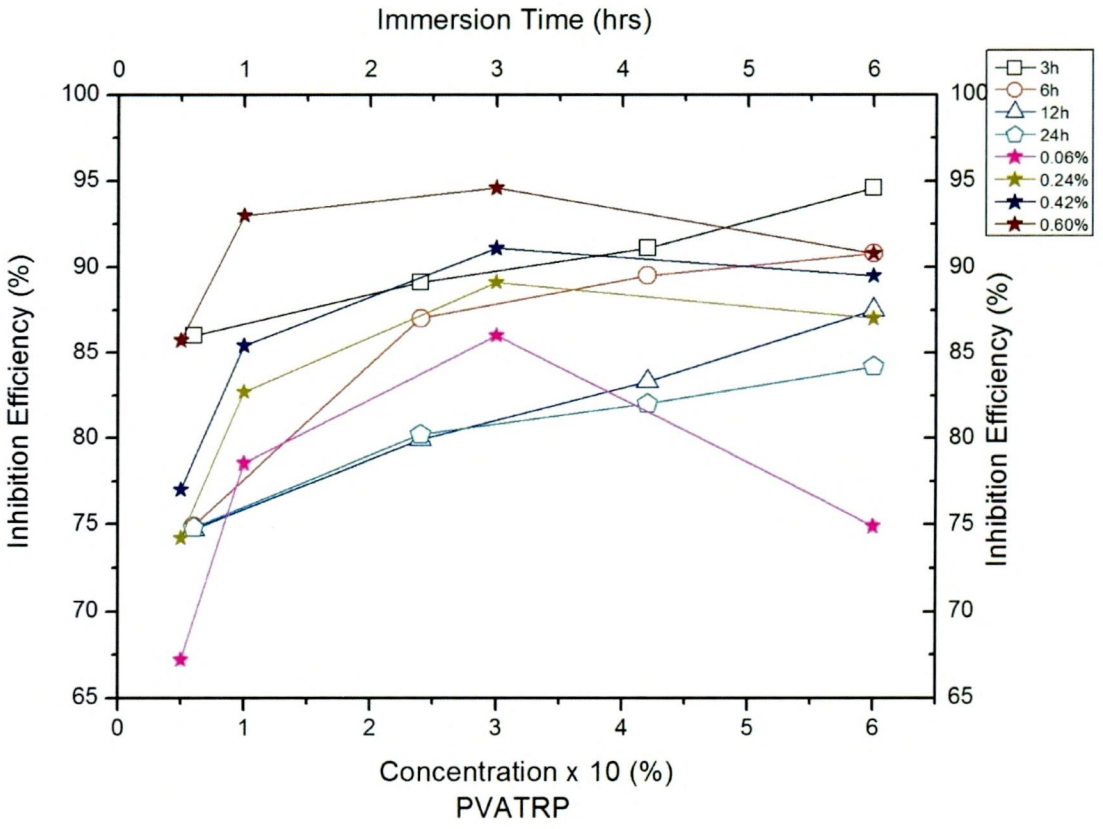

composite and 90.8 % (6 h) for PVATRP composite at 0.6 % respectively. The stability of the adsorbed layer of PVATYR and PVATRP composites on mild steel surface prevents the corrosion of mild steel surface upto 12 h in the case of PVATYR composite and 6 h in the case of PVATRP composite. Desorption of polymer composites at 12 h, 24 h and 48 h took place.

The inhibition of corrosion of mild steel in 1M HCl by these compounds can be explained in terms of adsorption on the metal surface. These compounds can be adsorbed on the metal surface by means of i) interation between π-electrons of the benzene rings and the metal surface ii) interaction of the ion pairs of electrons of nitrogen(or) oxygen and the metal surface **(Sudha *et al.,* 2004)**.

4.8.6 Effect of immersion time for mild steel corrosion using PVATYR and PVATRP

The variation of inhibition efficiency of both PVATYR and PVATRP composites on mild steel acid corrosion with different immersion time is shown in figure-22. The inhibition efficiency of the inhibitors was found to increase with increasing time of immersion upto 12 h, furnishing a maximum inhibition efficiency of 96.6 % and 87.5 % in the presence of PVATYR and PVATRP composite respectively and there after the inhibitor efficiency decreases. However the adsorbed layer was stabilized at 24 h, resulting in 80.6 % and 84.2 % in the presence PVATYR and PVATRP composites respectively. Analysing the table-13, the stability of the adsorbed layer was maintained at higher concentration PVATYR and PVATRP composites at 24 h and 48 h of immersion. In the current investigation, PVATYR and PVATRP composites function effectively upto 48h of immersion at higher concentration.

It is generally accepted that the first step in the adsorption of an organic inhibitor on a metal surface usually involves the replacement of water molecules adsorbed at the metal surface.

$$Inh_{(sol)} + X\,H_2O_{(ads)} \leftrightarrow Inh_{(ads)} + XH_2O_{(sol)} \qquad (32)$$

The second step is occurrence of metal-inhibitor complexes with freshly generated Fe^{2+} ions on the mild steel surface.

$$Fe \rightarrow Fe^{2+} + 2e^{-} \qquad (33)$$

$$Fe^{2+} + Inh_{(ads)} \rightarrow Fe\,(Inh)^{2+}_{(ads)} \qquad (34)$$

Thus it is possible to suggest that at low concentrations, the amount of inhibitor molecules in the solution is insufficient to form a compact complex with the metal ions. As the concentration is increased, more inhibitor molecules become available for complex formation.

The inhibition process is based on the adsorption of the amino acid molecules at the active sites and/or deposition of corrosion products on the metal surface. So an increase in the efficiency of inhibition with the inhibitor concentration indicates that more its molecules are adsorbed on the metal surface, thus leading to a greater surface coverage (**Zor *et al.*, 2007).**

Considering that adsorption is essentially controlled by electrostatic attraction, as the immersion time increases, more chlorides will be adsorbed on the surface helping to the formation of the inhibitor layers. However as soon as all the active sites become saturated with inhibitor, the development of the inhibitor layer is gradually slows down. Furthermore, with time it seems the inhibiting effect decreases probably because some defects exist on the film leading to the access of aggressive anions to the mild steel/ inhibitor interface. The formation of this weaker site can be explained with basis in literature, where the decrease of the inhibition efficiency was attributed to the formation of hemi micelles aggregates by the initially deposited inhibitor molecules, reducing the effective area covered by the inhibitor. Figure 20-22 depicts the surface of the sample after 24 and 48 h and it is clearly shown that the amount of corrosion products increases from 24 to 48 h **(Aitchikh *et al.*, 2005)**.

In most of the polymer composites the inhibition efficiency is found to increase with increase in immersion time upto to 12 h. After that there is a slight decline in inhibition efficiency upto the examined immersion time. This can be explained on the following basis. There is a competition between the formation of $FeCl_2$ (and also $FeCl_3$) and Fe-polymer composites on the anodic sites of the metal surface. Perusal of the results suggests that the formation of $FeCl_2$ is favoured when compared with the formation of Fe-polymer composites complex **(Selvaraj *et al.*, 2004).**

4.8.7 Performance evaluation of studied polyvinyl alcohol-selected amino acid composites at 0.6 % concentration for optimum time of immersion

To substantiate the enhanced corrosion inhibition character of water soluble polymer composites under study, weight loss measurements of mild steel in 1M HCl in the presence of 0.6 % concentration of polyvinyl alcohol-selected amino acid composites (PVAALA, PVAVAL, PVAGLU, PVAGLN, PVATYR and PVATRP composites) at optimum time of immersion studies are conducted and the experimental results are clearly demonstrated in the figure-23.

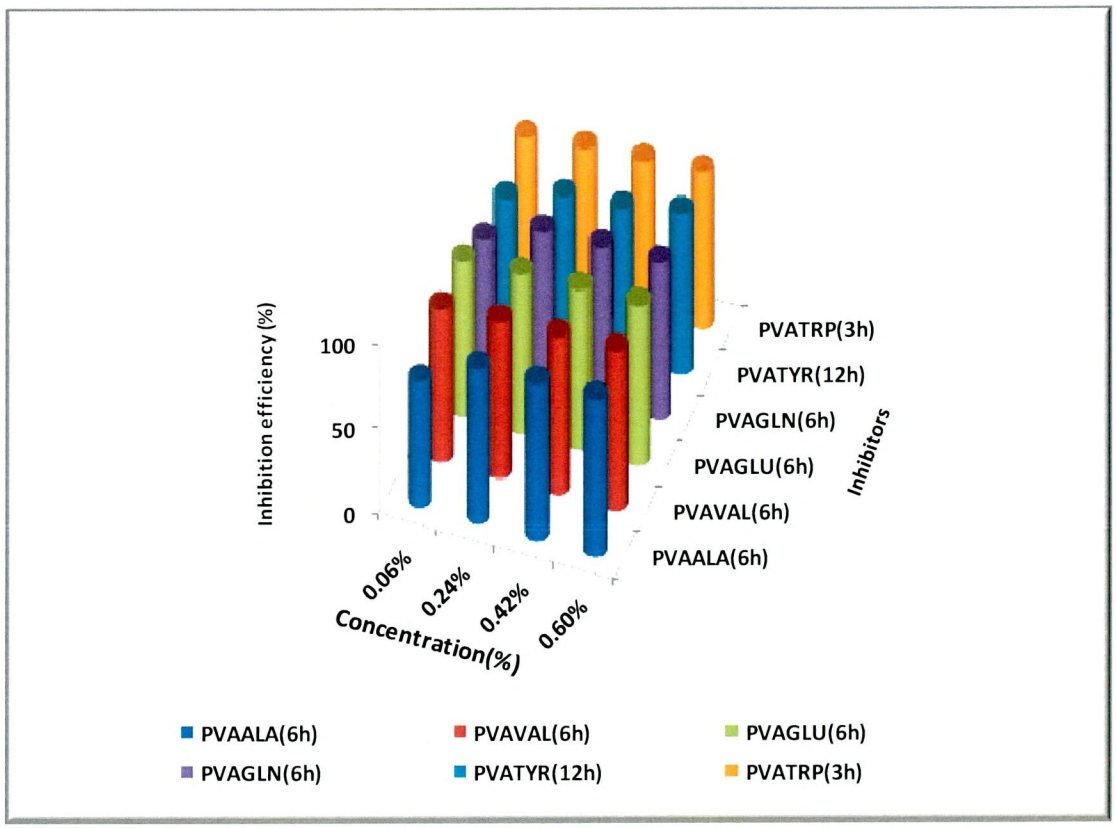

Figure -23 Inhibition efficiency of various inhibitors at optimum time of immersion in 1M HCl medium (by weight loss methods)

4.8.7 EFFECT OF TEMPERATURE (PVAALA and PVAVAL COMPOSITES)

Temperature has a great effect on the rate of metal corrosion. The weight loss of mild steel in 1M HCl solution with and without the addition of inhibitors was determined at room temperature and higher temperatures. For the studied inhibitors, the weight loss decreased by increasing the concentration of each inhibitor at the studied temperatures of concentration of each inhibitor at the studied temperatures of 303 K-343 K, so that PVAALA and PVAVAL composite inhibits the corrosion of mild steel in the acidic environment. Figure-24 and Table 14 presents the variation of the inhibitor efficiency versus temperature of the PVAALA and PVAVAL composite from 303-343 K.

It is evident from the table that the corrosion rate decreases with increasing inhibitor concentration but increases with rise in temperature. Table 14 also reveals that inhibition efficiency increases with increasing inhibitor concentration, reaching a maximum of 87.3 % and 91.5 % of PVAALA (333 K) and PVAVAL (313 K) composites respectively. This may be due to the adsorption of PVAALA and PVAVAL composites on the mild steel surface through non-bonding electron pair of oxygen and nitrogen (**Obi-Egbedi et al., 2011).** The inhibition efficiencies for 0.6% PVAALA

composite were 81.1 %, 84.5 %, 78.2 %, 87.3 % and 77.1 % at 30°C, 40°C, 50°C, 60°C and 70°C. The above results show that PVAALA composite functions well as inhibitor in the range 30 to 70°C. Analysis of table-14 reveals that PVAVAL composite works well as inhibitor in the range 313K-333K, affording 91.5 %, 91.2 % and 82.1 % at 0.60 % concentration of the PVAVAL composite.

After 333 K the IE is found to decrease but stabilized to 77 % at higher concentration. A plausible explanation for this may be that adsorption and desorption of inhibitive molecules continuously occur at the metal surface and equilibrium exists between these two processes at a particular temperature. With increase in temperature, the equilibrium between the adsorption and desorption processes are shifted leading to a higher desorption rate than adsorption. This exposes the metal surface for further attack **(Ebenso and Oguzie, 2005).**

The corrosiveness of acid is hugely limited in the presence of inhibitor concentration. **Bouklah *et al.,* (2006b)** considers the increase of IE (%) with temperature increases as the change in the nature of the adsorption mode, the inhibitor is being physically adsorbed at lower temperatures, while chemisorption is favoured as temperature increases. This is due to increase in the surface coverage by an inhibitor. Thus, at a high degree of coverage, the diffusion through the surface layer containing the inhibitor and corrosion products becomes the rate-determining step of the metal dissolution process.

4.8.8 EFFECT OF TEMPERATURE (PVAGLN and PVAGLU COMPOSITES)

The effect of temperature on the weight loss and the corrosion rate of mild steel coupons in 1 M HCl without inhibitor (blank) and with various concentrations of PVAGLN and PVAGLU composites were examined at 303-343 K and the results are presented in tables 15 and figures-25. The values of inhibition efficiency in 1M HCl solution containing various concentrations of PVAGLN and PVAGLU composites inhibitors at the tested temperatures.

Values of inhibition efficiency of PVAGLN and PVAGLU composites increase with increase in concentration at all investigated temperatures. Analysis of the table indicate that as the temperature increases inhibition efficiency increases upto 313 K affording an efficiency of 92.3 % for PVAGLN and 87.4 % for PVAGLU and then decreases. However it stabilised at 343 K to give an efficiency of 74.8 % (PVAGLN) and 83.1 % (PVAGLU) respectively. Results presented in table-15 infer that 91.1 %, 92.3 %, 87.8 % and 88.3 % are the inhibition efficiency afforded by PVAGLN composite at 303 K, 313 K, 323 K and 333 K, where as PVAGLU composite furnished around 85 % at all studied temperatures

Table-14 Variation of Inhibition efficiency of PVAALA/PVAVAL composites on mild steel corrosion as a function of temperature in 1M HCl

S.No.	Conc. of inhibitor (%) PVAALA	Temperature(in Kelvin)									
		303K		313K		323K		333K		343K	
		CR (mpy)	IE (%)	CR (mpy)	IE (%)	CR (mpy)	IE (%)	CR (mpy)	IE (%)	CR (mpy)	IE (%)
1.	Blank	2250.3	-	7387.5	-	12242.1	-	18901.3	-	29990.3	-
2.	0.06	570.8	61	1596.1	78.3	5118.5	58.2	4230.1	77.6	11133.5	62.9
3.	0.12	488.8	66.6	1414.7	80.9	4623.0	62.2	3424.2	81.9	9999.7	66.7
4.	0.18	442.0	69.8	1404.7	81	3825.0	68.8	3325.7	82.4	9703.1	67.6
5.	0.24	434.7	70.3	1359.7	81.6	3625.3	70.3	2787.5	85.3	9535.2	68.2
6.	0.30	428.8	70.7	1352.8	81.7	3419.9	72.1	2644.9	86	9158.4	69.5
7.	0.36	361.5	75.3	1346.7	81.8	3096.7	74.7	2588.2	86.3	7739.6	74.1
8.	0.42	357.1	75.6	1336.2	81.9	2883.5	76.4	2566.9	86.4	7380.9	75.4
9.	0.48	346.9	76.3	1306.5	82.3	2825.9	76.9	2528.5	86.6	7158.9	76.1
10.	0.54	305.9	79.1	1190.5	83.9	2793.6	77.1	2499.3	86.8	6875.0	77
11.	0.60	276.6	81.1	1148.7	84.5	2667.2	78.2	2387.2	87.3	6851.5	77.1

S.No.	Conc. of inhibitor (%) PVAVAL	Temperature(in Kelvin)									
		303K		313K		323K		333K		343K	
		CR (mpy)	IE (%)	CR (mpy)	IE (%)	CR (mpy)	IE (%)	CR (mpy)	IE (%)	CR (mpy)	IE (%)
1.	Blank	2250.3	-	7387.5	-	12242.1	-	18901.3	-	29990.3	-
2.	0.06	843.8	62.5	1071.1	86.8	3701.6	83.5	4376.2	76.2	10353.8	62.8
3.	0.12	834.8	62.9	975.1	87.4	2923.1	83.8	4176.9	78.6	9380.6	68.3
4.	0.18	787.6	65	919.3	87.5	2610.5	84.5	3878.6	78.8	9064.2	68.6
5.	0.24	749.3	66.7	784.1	87.7	2547.7	84.7	3465.2	80.1	8396.6	69.7
6.	0.30	742.6	67	746.6	89.4	2499.7	87	3165.2	80.4	8364.6	70.7
7.	0.36	726.8	67.7	710.8	89.5	2311.3	88.3	3145.1	81.6	8080.0	76.3
8.	0.42	623.3	72.3	708.2	90.1	2072.8	88.8	2864.3	81.7	7971.8	76.7
9.	0.48	594.1	73.6	706.5	90.2	1964.2	89.7	2693.3	81.8	7932.6	77.3
10.	0.54	461.3	79.5	631.5	91	1933.2	90.6	2497.1	82	7581.5	77.4
11.	0.60	429.8	80.9	566.9	91.5	1499.3	91.2	2211.9	82.1	7547.1	77.7

Figure-24 Temperature effect on mild steel corrosion in the presence of PVAALA and PVAVAL composites

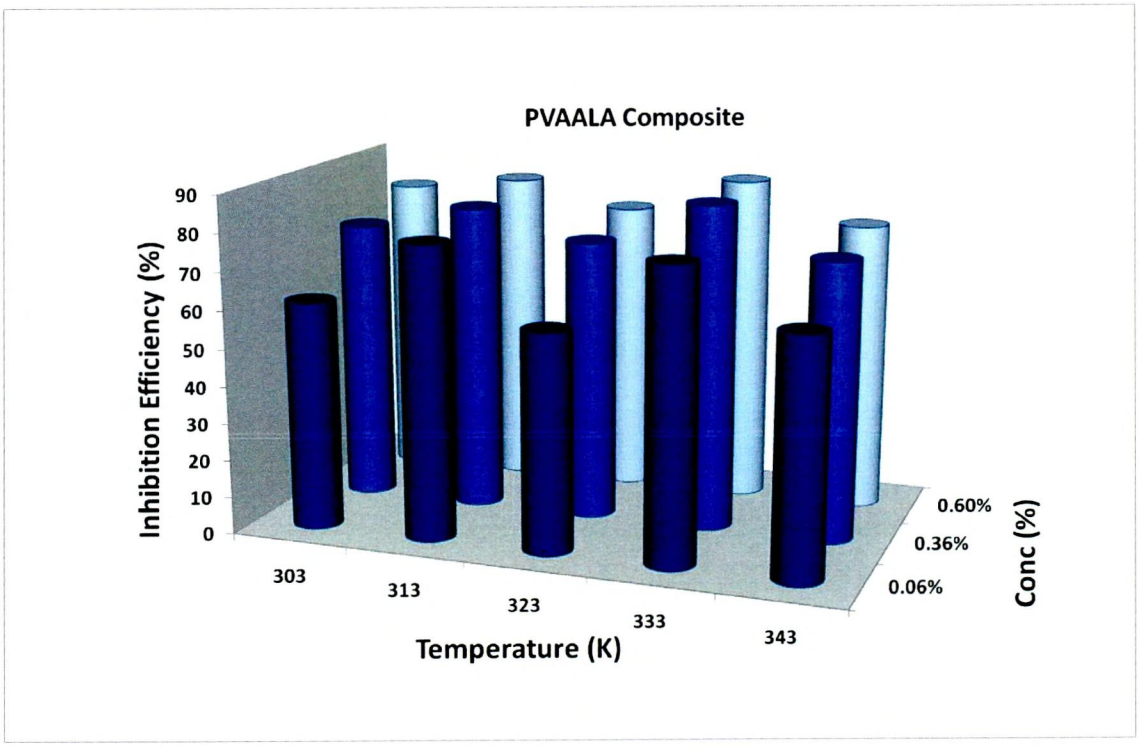

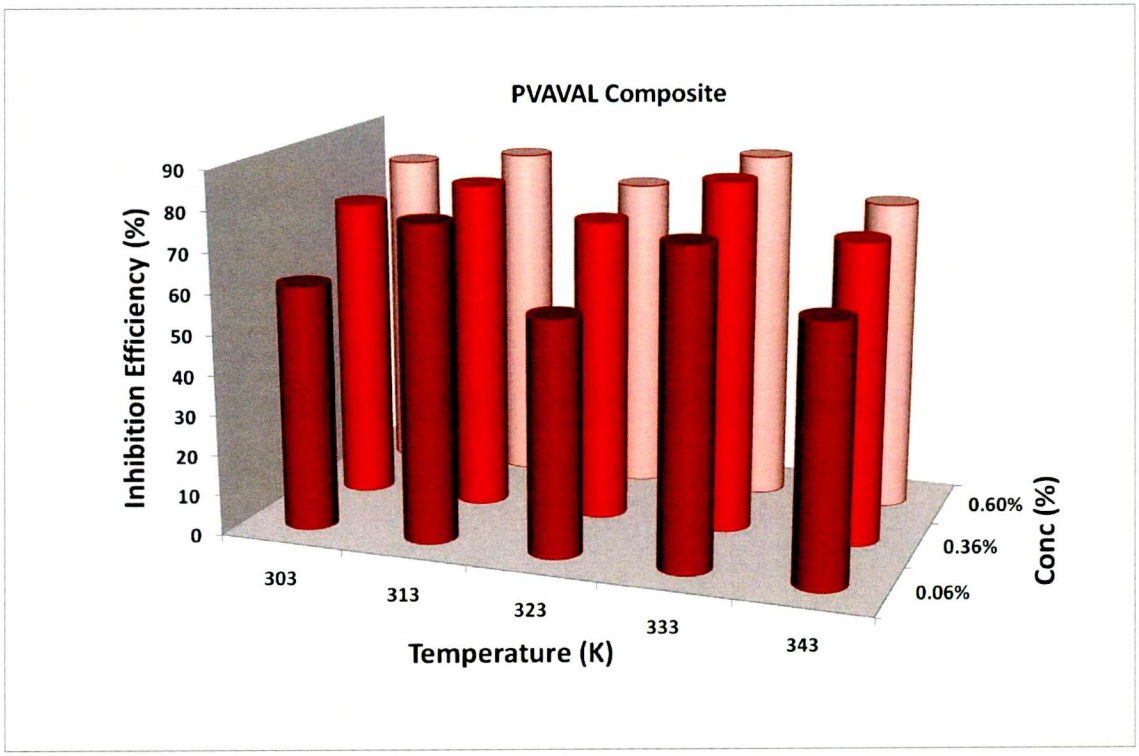

This trend in the inhibition properties of PVAGLN and PVAGLU composites with increase of temperature may be connected with two effects: decreasing strength of adsorption (shifting the adsorption and desorption equilibrium towards desorption) and roughening of the mild steel surface which results from enhanced corrosion while it decreases with rising of temperature supporting the occurrence of physical adsorption **(Abd El Rehim et al., 2010)**, but chemical adsorption could not be excluded due to uniform inhibition efficiency at all temperature.

Table -15 Variation of Inhibition efficiency of PVAGLN/PVAGLU composites on mild steel corrosion as a function of temperature in 1M HCl

S. No.	Conc. of inhibitor (%) PVAGLN	Temperature(in Kelvin)									
		303K		313K		323K		333K		343K	
		CR (mpy)	IE (%)	CR (mpy)	IE (%)	CR (mpy)	IE (%)	CR (mpy)	IE (%)	CR (mpy)	IE (%)
1.	Blank	2250.3	-	7387.5	-	12242.1	-	18901.3	-	29990.3	-
2.	0.06	361.5	75.3	1071.1	85.5	3701.6	69.6	4376.2	76.8	10353.8	65.5
3.	0.12	358.6	75.5	975.1	86.8	2923.1	76.1	4176.9	77.9	9380.6	68.7
4.	0.18	355.6	75.7	919.3	87.6	2610.5	78.7	3878.6	79.4	9064.2	69.8
5.	0.24	355.6	75.7	784.1	89.4	2547.7	79.2	3465.2	81.7	8396.6	72
6.	0.30	355.6	75.7	746.6	89.9	2499.7	79.6	3165.2	83.3	8364.6	72.1
7.	0.36	336.6	77	710.8	90.4	2311.3	81.1	3145.1	83.4	8080.0	73.1
8.	0.42	272.2	81.4	708.2	90.4	2072.8	83.1	2864.3	84.8	7971.8	73.4
9.	0.48	166.8	88.6	706.5	90.4	1964.2	84	2693.3	85.8	7932.6	73.5
10.	0.54	150.7	89.7	631.5	91.4	1933.2	84.2	2497.1	86.8	7581.5	74.7
11.	0.60	130.3	91.1	566.9	92.3	1499.3	87.8	2211.9	88.3	7547.1	74.8

s.no.	Conc. of inhibitor (%) PVAGLU	Temperature(in Kelvin)									
		303K		313K		323K		333K		343K	
		CR (mpy)	IE (%)	CR (mpy)	IE (%)	CR (mpy)	IE (%)	CR (mpy)	IE (%)	CR (mpy)	IE (%)
1.	Blank	2250.3	-	7387.5	-	12242.1	-	18901.3	-	29990.3	-
2.	0.06	861.8	61.7	1805.4	75.6	1980.7	83.6	4381.0	76.8	9324.2	68.9
3.	0.12	846.1	62.4	1576.9	78.7	1935.4	84.2	4340.2	77	7684.9	74.4
4.	0.18	801.1	64.4	1513.5	79.5	1903.1	84.5	3888.2	79.4	7634.3	74.5
5.	0.24	400.5	82.2	1385.5	81.2	1866.5	84.7	3723.8	80.2	7043.4	76.5
6.	0.30	384.8	82.9	1238.5	83.2	1858.6	84.8	3650.1	80.7	6834.5	77.2
7.	0.36	382.3	83	1133.0	84.7	1855.2	84.8	3357.9	82.2	6628.7	77.9
8.	0.42	380.3	83.1	1123.4	84.8	1808.9	85.2	3343.1	82.3	5684.9	81
9.	0.48	351.0	84.4	1065.8	85.6	1769.2	85.5	3267.2	82.7	5366.6	82.1
10.	0.54	346.5	84.6	1025.3	86.1	1758.3	85.6	3060.5	83.7	5229.7	82.5
11.	0.60	317.3	85.9	927.6	87.4	1653.7	86.5	2830.7	85	5076.2	83.1

Figure 25 Effect of temperature and concentration of PVAGLU and PVAGLN composites on mild steel acid corrosion

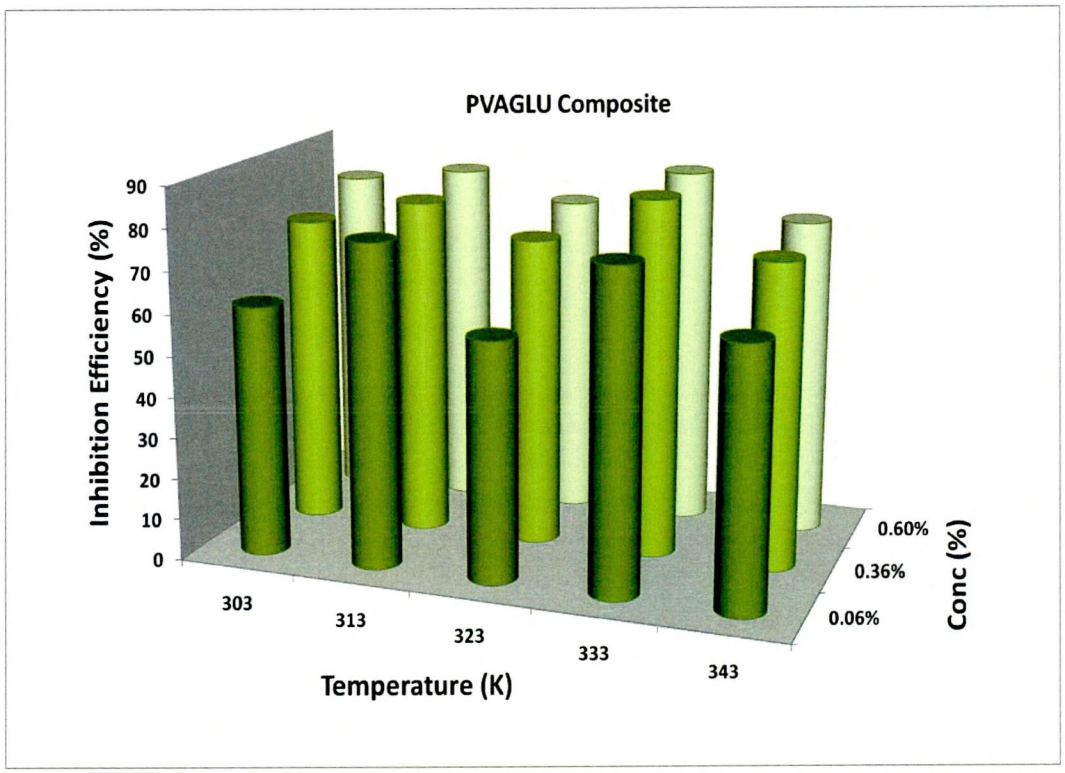

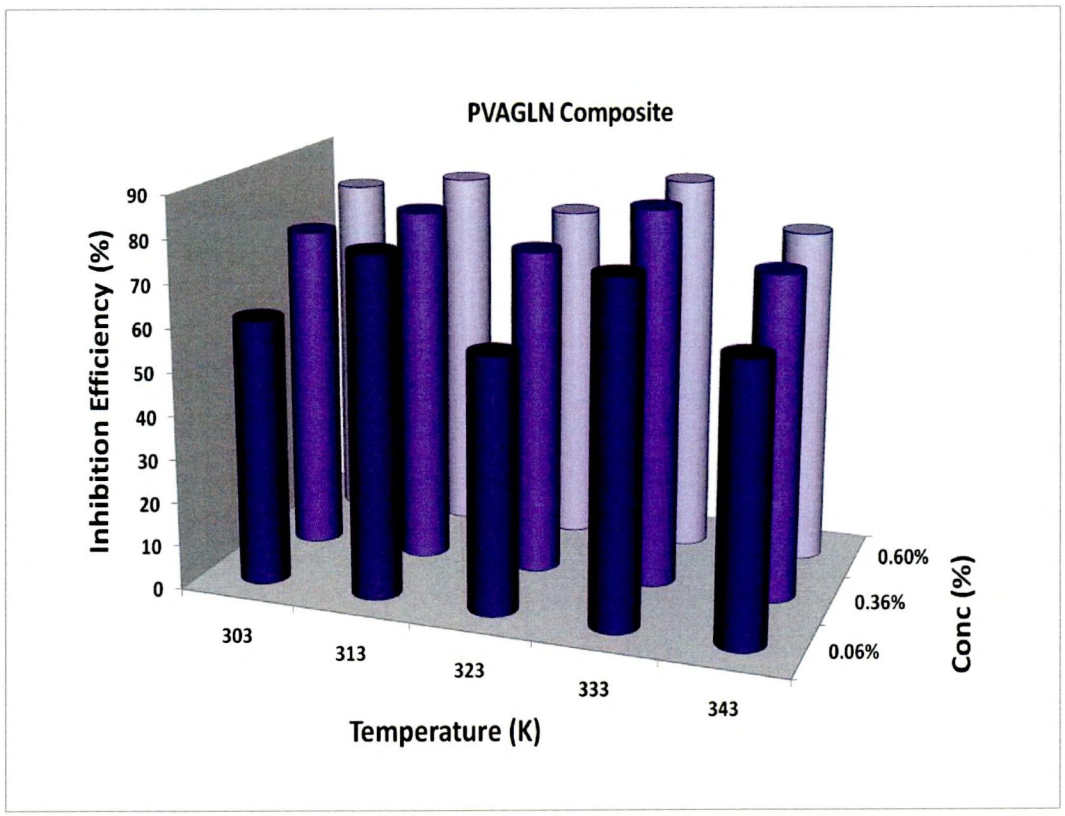

4.8.9 EFFECT OF TEMPERATURE (PVATRP and PVATRY COMPOSITES)

The effect of temperature on the inhibited acid-metal reaction is very complex, because many changes occur on the metal surface such as rapid etching, description of inhibitor and inhibitor itself may undergo decomposition . The change of corrosion rate at various concentrations of the PVATRP and PVATRY composites during ½ h of immersion at different temperatures are studied in 1M HCl. It is clear from tables-16 and Figure -26, that the increase of corrosion rate is more pronounced with the rise of temperature for blank solution.

In the presence of PVATRP and PVATRY composites, the corrosion rate of mild steel decreases at any given temperature as inhibitor concentrations due to the increase of the degree of surface coverage. In contrast at constant inhibitor concentration, the corrosion rate increases as temperature rises. However it is noted that the efficiency depend on the temperature and decreases with the rise of temperature from 303 K to 343 K. Data presented in table-16 using PVATYR composite as corrosion inhibitor indicate that as the temperature increases inhibition efficiency increases upto 333 K, then a slight decrease in inhibition efficiency at 323 K immediately after that the increase in temperature favours enhancement in inhibition efficiency at 333 K (90.2 %) and then stabilises to 82.1 % at 343 K .This behaviour can be interpreted on the basis that an increase in temperature resulted in the adsorption of adsorbed molecules from the metal surface. PVATYR composite exhibits as a good composite inhibitor at higher temperatures.

Temperature study results given in table-16 infer inhibition efficiency of PVATRP composite increases as the temperature rises upto 313 K (87.5 %), then a slight decline in inhibition efficiency at 333 K (82.5 %) followed by stabilisation of inhibition efficiency at 343 K furnishing a maximum inhibition efficiency of 86.4 % at higher concentration. It can be concluded that PVATRP composite works out as a promising inhibitor at all studied temperatures. PVATYR composite furnished a maximum of 90.2% inhibition efficiency at 333K. PVATRP composite could afford 86% inhibition efficiency at all studied temperatures.

This may be ascribed to the following reason: The adsorption and desorption of inhibitive molecules continuously occur at the metal surface and equilibrium exists between these two molecules processed at particular temperature. With the increase in temperature the equilibrium between adsorption and desorption process are shifted leading to higher desorption rate than adsorption. The desorption at elevated temperature thus exposing the metal surface for further attack **(Mohammed Ajmal *et al.,* 1998)**. In 1 M HCl solutions, an increase or decrease in the inhibitors efficiency depending on its concentration is detected with increasing temperature indicating that

adsorption of inhibitor species on mild steel surface at these conditions is not merely physical or chemical adsorption, but a comprehensive adsorption (physical and chemical adsorption) **(Ehteram A Noor, 2007)**.

4.8.10 Performance evaluation of studied polyvinyl alcohol-selected amino acid composites at 0.6% concentration for temperature

To establish the enhanced corrosion inhibition character of water soluble polymer composites under study, the results of weight loss measurements of mild steel in 1M HCl in the presence of 0.6% concentration of polyvinyl alcohol-selected amino acid composites (PVAALA, PVAVAL, PVAGLU, PVAGLN, PVATYR and PVATRP composites) at optimum temperature studies are conducted and the experimental are clearly demonstrated in figure-27.

Table 16 Variation of Inhibition efficiency of PVATYR/PVATRP composite on mild steel corrosion as a function of temperature in 1M HCl

S. No.	Conc. of inhibitor (%) PVATYR	Temperature(in Kelvin)									
		303K		313K		323K		333K		343K	
		CR (mpy)	IE (%)	CR (mpy)	IE (%)	CR (mpy)	IE (%)	CR (mpy)	IE (%)	CR (mpy)	IE (%)
1.	Blank	2250.3	-	7387.5	-	12242.1	-	18901.3	-	29990.3	-
2.	0.06	841.6	62.6	1668.5	77.4	5512.2	60.0	4050.7	78.6	7912.6	73.6
3.	0.12	805.6	64.2	1561.2	78.9	4415.0	63.9	3957.6	79.1	7362.2	75.5
4.	0.18	796.6	64.6	1479.2	80	3412.0	72.1	3296.8	82.6	6819.7	77.3
5.	0.24	780.8	65.3	1217.6	83.5	3376.7	72.4	3048.3	83.9	6578.9	78.1
6.	0.30	747.1	66.8	1161.8	84.3	3241.5	73.5	2947.9	84.5	6348.7	78.8
7.	0.36	722.3	67.9	1140.8	84.6	2951.5	75.9	2615.3	86.2	5937.0	80.2
8.	0.42	713.3	68.3	1092.9	85.2	2891.7	76.4	2308.7	87.8	5912.6	80.3
9.	0.48	663.8	70.5	1067.6	85.5	2667.8	78.2	1987.7	89	5739.1	80.9
10.	0.54	589.6	73.8	1053.6	85.7	2559.4	79.1	1848.2	89.6	5677.1	81.1
11.	0.60	533.3	76.3	1012.2	86.3	2450.0	80.0	1947.6	90.2	5371.8	82.1

S. No.	Conc. of inhibitor (%) PVATRP	Temperature(in Kelvin)									
		303K		313K		323K		333K		343K	
		CR (mpy)	IE (%)	CR (mpy)	IE (%)	CR (mpy)	IE (%)	CR (mpy)	IE (%)	CR (mpy)	IE (%)
1.	Blank	2250.3	-	7387.5	-	12242.1	-	18901.3	-	29990.3	-
2.	0.06	480.0	67.2	2160.9	70.7	4780.0	61	6477.8	63.2	11036.7	65.7
3.	0.12	420.0	71.3	1915.3	74	3886.9	68.2	5752.5	76.1	7179.0	69.6
4.	0.18	377.6	74.2	1927.5	74.1	3128.5	74.4	5541.5	78.1	6569.8	70.7
5.	0.24	377.6	74.2	1659.8	76.2	3032.2	75.2	4987.6	79.2	6224.8	73.6
6.	0.30	370.3	74.7	1524.6	79.4	2898.3	76.3	4604.3	80.6	5820.6	75.6
7.	0.36	360.0	75.4	1360.6	81.6	2853.8	76.7	3979.8	80.7	5778.3	78.9
8.	0.42	336.6	77	1257.3	83	2700.7	77.9	3916.1	81.7	5495.7	79.3
9.	0.48	301.5	79.4	1250.8	83.1	2286.0	81.3	3145.1	82.4	5288.1	83.4
10.	0.54	238.6	83.7	1178.3	84.1	2225.3	81.8	2973.7	82.4	5285.5	84.3
11.	0.60	209.3	85.7	926.3	87.5	2033.1	83.4	2573.0	82.5	5237.5	86.4

Figure-26 Inhibition efficiency of PVATYR and PVATRP at various concentration and temperatures

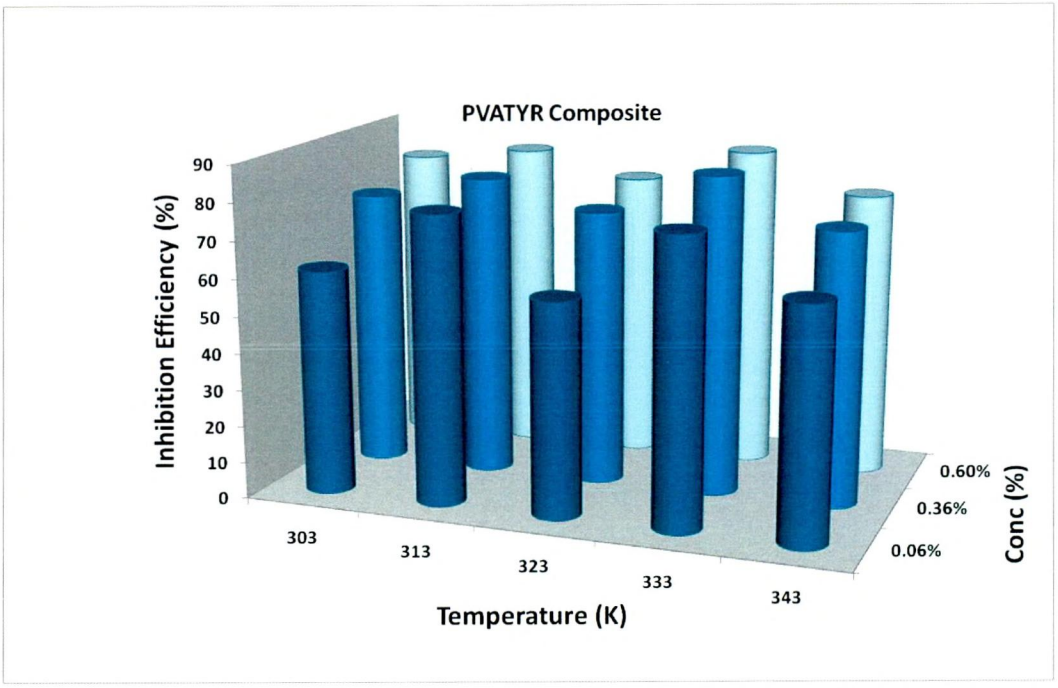

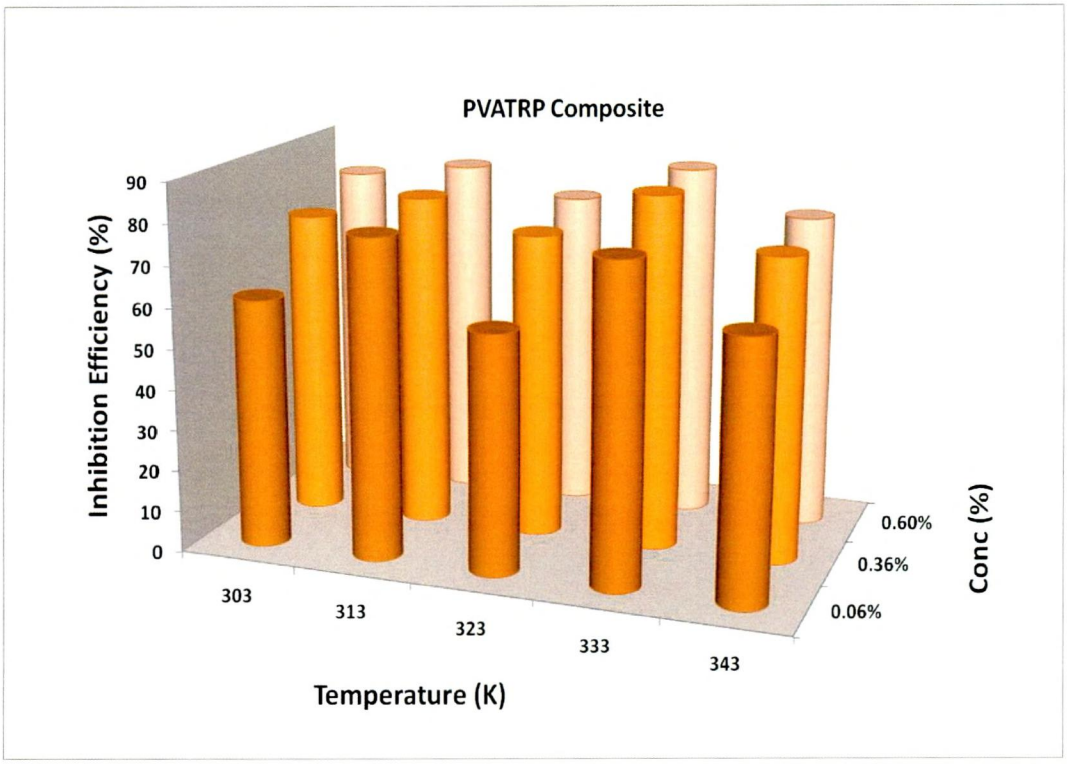

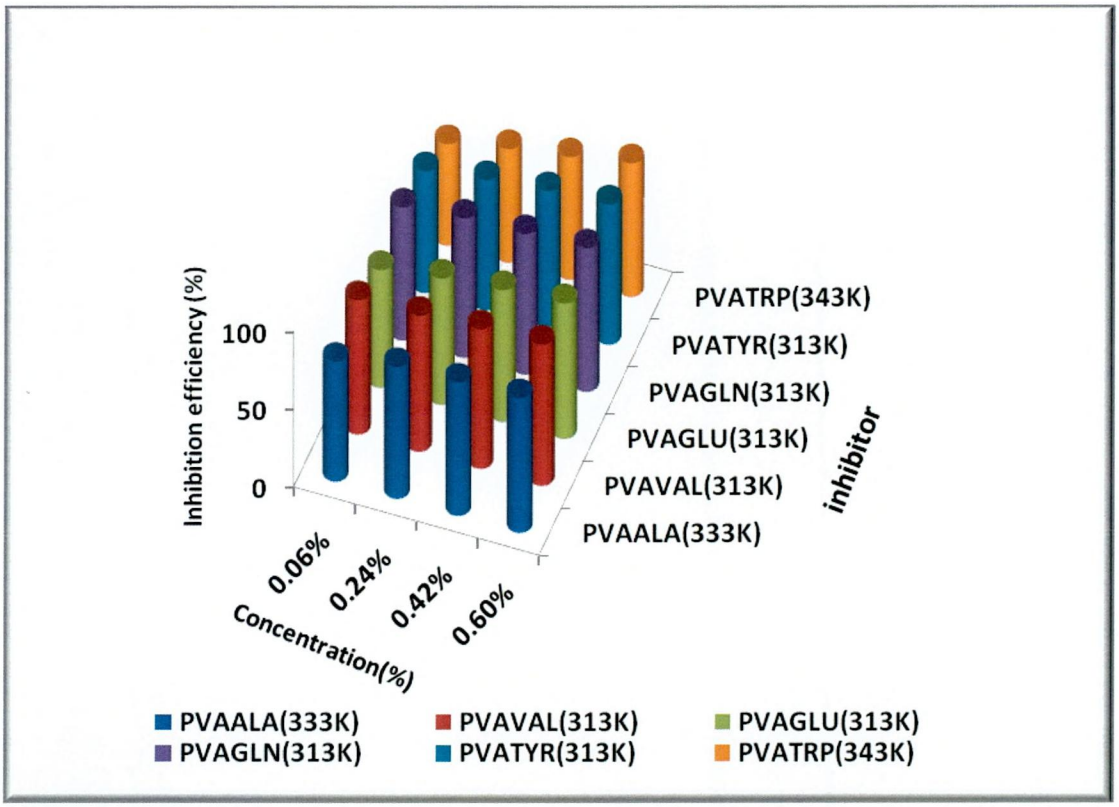

Figure-27 Inhibition efficiency of various inhibitors at optimum temperature in 1M HCl medium (by weight loss method)

Performance evaluation of studied polymer composites (0.6% concentration) using weight loss method is depicted in the figure -27

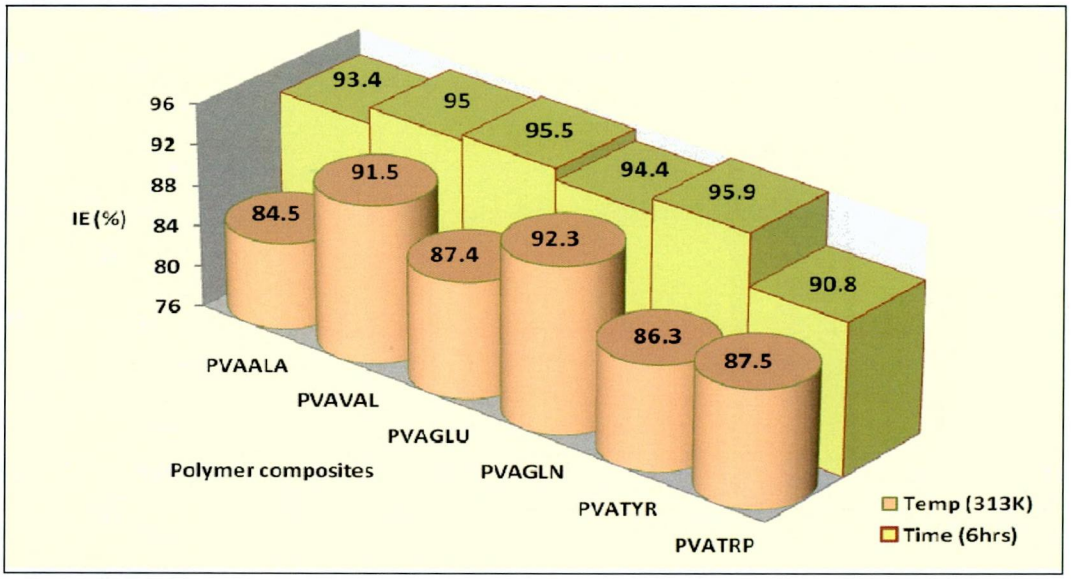

Figure 27a Performance evaluations of Polymer composites using weight loss method

4.8.11 To establish the inhibition efficiency of studied polyvinyl alcohol-selected amino acid composites versus amino acid and PVA at 0.6% concentration for 3 h immersion time

Efforts are also made to prove the enhanced inhibition efficiency of polyvinyl alcohol-selected amino acid composites with reference to PVA and amino acids (ALA, VAL, GLN, GLU, TYR and TRP) individually. Weight loss method of mild steel in the presence of studied concentration of PVA, amino acids, polyvinyl alcohol-selected amino acid composites at 3h immersion studies was conducted and the results are representation pictorially. It is clear from the pictorial representation that, polyvinyl alcohol-selected amino acid composites (PVAALA (90.0 %), PVAVAL (93.0 %), PVAGLN (93.7 %), PVAGLU (94.2 %), PVATYR (93.7 %) and PVATRP (94.6 %)) exhibit higher inhibition efficiency with reference to PVA (86.9 %) and amino acids (ALA(37.8 %), VAL (58.2 %), GLN (47.6 %), GLU (52.4 %), TYR (69.5 %) and TRP (89.9 %)) as shown in the figure-28. This justifies the need for polymerisation of PVA with selected amino acids and the utilisation of the same as corrosion inhibitors for mild steel in acidic medium.

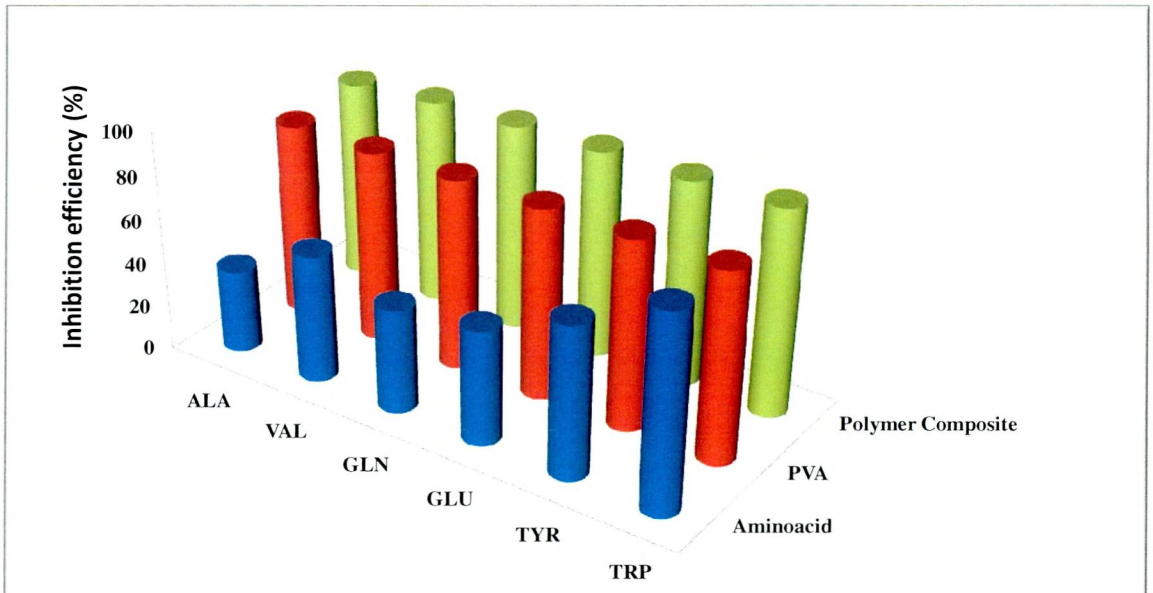

	ALA	VAL	GLN	GLU	TYR	TRP
Aminoacid	37.8	58.2	47.6	52.4	69.5	89.9
PVA	86.9	86.9	86.9	86.9	86.9	86.9
Polymer Composite	90	93	93.7	94.3	93.7	94.6

Analysing the results of weight loss method and based on the inhibitive properties of the examined polyvinyl alcohol – selected amino acid composites, these inhibitors can be ranked as follows: at room temperature PVATYR (12 h) > PVAGLU (6 h) > PVAVAL (6 h) > PVATRP(3 h) > PVAGLN (6 h) > PVAALA (6 h) (at 0.60 % concentration) and at various temperature PVAGLN (313 K) > PVAVAL (313 K) > PVATYR (333 K) > PVATRP (313 K) > PVAGLU (313 K) > PVAALA (333 K) (at 0.60 % concentration).

4.9 ADSORPTION ISOTHERMS

In acid corrosion, generally, it is assumed that inhibitors act through a process of adsorption on the metal surface. The adsorption of the inhibitor may determine a structural change of the double layer, thus reducing the rate of electrochemical-partial reactions. Moreover, adsorption that particularly takes place at the active sites of the metal surface may hinder the reactivity of the metal in the process of dissolution. On the other hand, if the adsorption is followed by reaction of hydration or reduction or polymerization of the inhibitor itself, thick layers may form that behave as a true physical barrier. In any case, the knowledge of the adsorption behavior of the inhibitors is important for the definition of its action mechanism.

An adsorption isotherm gives the relation between the coverage of an interface with the adsorbed species and the concentration of the species in solution. Interpretation of the performance of the adsorbent type of inhibitor can be enhanced by fitting the data in one of known adsorption isotherm.

According to Awady et al

$$S + YI \longleftrightarrow SI_Y \qquad (35)$$

where S is the substrate and K' is a constant. This leads to the relationship

$$\frac{\theta}{1-\theta} = K'[I]y \qquad (36)$$

where θ is the surface coverage

$$\frac{\theta}{1-\theta} = K'[I]^y \qquad (37)$$

The plot of log (θ/1-θ) Vs log C gives a straight line with a slope Y and intercept of K' if relation (33) is applicable.

Values of Y>1 imply the formation of multilayers of the inhibitor on the surface of the metal. Values of Y<1 mean inhibitor molecule will occupy more than one active sites.

The observed corrosion data in the presence of inhibitors, linear dependence of weight loss on immersion time, suggest that the corrosion inhibition of mild steel occurs through surface adsorption of inhibitors and /or their complexes.

For this reason, an attempt is also made to understand the nature of the interaction of these compounds on mild surface by adsorption characteristics.

The degree of surface coverage θ for different concentration of inhibited in both acids has been evaluated from weight loss values using the relation $\theta = CR_o - CR_i / CR_o$ where CR_o and CR_i are the corrosion rate in the absence and presence of the inhibitor respectively.

Goodness of Fit:

Data were tested graphically by fitting to various isotherms. Statistical estimation of correlation for the curve fitting of isotherms have been used to investigate the goodness of fit of the isotherms **(Schulthess *et al.*, 1996).**

A measure of the goodness of fit is the square of correlation coefficient. R^2 which shows the % of the total variation of the dependent variables can be explained by the independent variable Y. Symbolically

$$R^2 = \frac{\Sigma Y_1^2}{\Sigma Y_1} = \frac{\text{Explained variation}}{\text{Total variation}} \qquad (38)$$

The value of R^2 generally lies between 0 and 1 ($0 \leq R^2 \leq 1$). The closer the value of R^2 lines to 1, the better is the regression line to data and vice versa.

To test the overall significance of regression model, the technology of ANOVA is used, which is defined by the F value.

$$F = \frac{\text{Explained sum of square/degrees of freedom}}{\text{Residual sum of squares/ degrees of freedom}} \qquad (39)$$

A large F value will be evidence against the null hypothesis the explanatory variable have no effect of Y.

Adsorption isotherms are often shown to demonstrate the performance of polymer composite adsorbent-type inhibitors. Corrosion inhibitors are found to protect mild steel corrosion in acid solutions by adsorbing themselves on mild steel surface. Adsorption is a separation process involving two phases between which certain components can become differentially distributed. Adsorption can be described by two main types of interaction:

• **Physisorption** involves electrostatic forces between ionic charges or dipoles on the adsorbed species and the electric charge at the metal/solution interface. The heat of adsorption is low and therefore this type of adsorption is stable only at relatively low temperatures.

• **Chemisorption,** involves charge sharing or charge transfer from the inhibitor molecules to the metal surface to form a coordinate type bond. In fact, electron transfer is typically for transition metals having vacant low-energy electron orbital. Chemisorption is typified by much stronger adsorption energy than physical adsorption. Such a bond is therefore more stable at higher temperatures.

It is well recognized that the first step in inhibition of metallic corrosion is the adsorption of organic inhibitor molecules at the metal/solution interface. Furthermore, the adsorption depends on the molecules chemical composition, the temperature and the electrochemical potential at the metal/solution interface. So the adsorption of organic inhibitor molecules from the aqueous solution can be regarded as a quasi-substitution process between the organic compounds in the aqueous phase [$Org_{(sol)}$] and water molecules at the electrode surface [$H_2O_{(ads)}$]

$$Org_{(sol)} + x\ H_2O_{(ads)} \longleftrightarrow Org_{(ads)} + x\ H_2O_{(sol)} \qquad (40)$$

where x is the size ratio, that is, the number of water molecules replaced by one organic inhibitor. Basic information on the interaction between the inhibitor of the mild steel surface can be provided by the adsorption isotherm (**Noor et al., 2008**). In order to obtain the isotherm, the linear relation between degree of surface coverage (θ) values (θ = %I/100) and inhibitor concentration (C) must be found. Attempts were made to fit the θ values to various isotherms including Langmuir, Temkin, Freundlich, Frumkin, Flory-Huggins, El Awady kinetic thermodynamic and Bockris-Swinkel's adsorption isotherms.

In this section of study, the changes in the surface coverage and thereby the change in the inhibition efficiency is measured using different models at the same level of temperature. These models include Langmuir, Temkin, Freundlich, Frumkin, Flory-Huggins, El Awady kinetic thermodynamic and Bockris-Swinkel's adsorption isotherms.

Langmuir adsorption isotherm can be obtained according to equation (37) **(Eddy *et al.,* 2010)**

$$\text{Log } (C/\theta) = \log C - \log K \qquad (41)$$

where K is the equilibrium constant, C is the concentration of inhibitor and θ is the degree of surface coverage of the inhibitors. The plots of Langmuir adsorption isotherm is log (C/θ) Vs log C.

Temkin adsorption isotherm can be represented according to equation (38) **(Umoren *et al.*, 2007a)**

$$\exp(-2a\theta) = KC \qquad (42)$$

where 'a' is molecular interaction parameters, θ is the degree of surface coverage, K is the equilibrium constant of adsorption process and C is the concentration of the inhibitors. The plots of Temkin adsorption isotherm is θ Vs ln C.

Frumkin adsorption isotherm can be deduced according to equation (39) **(Oguzie et al., 2004)**

$$\ln\left[\frac{\theta}{C(1-\theta)}\right] = \ln K + 2a\theta \qquad (43)$$

where 'a' is the lateral interaction term describing the molecular interaction in the adsorbed layer, θ is the degree of surface coverage, K is the equilibrium constant of adsorption process and C is the concentration of inhibitors. The plots of Frumkin adsorption isotherm is θ Vs ln [θ/C (1- θ)].

Freundlich adsorption isotherm can be written according to equation (40) **(Umoren *et al.*, 2007a)**

$$\theta = K C^{1/n} \qquad (44)$$

where n is the adsorption intensity, C is the inhibitors concentration and K is the equilibrium constant of adsorption reaction. The plots of Freundlich adsorption isotherm is ln θ Vs ln C.

Flory-Huggins adsorption isotherm can be explained according to equation (41) **(Umoren *et al.*, 2007a)**

$$\log(\theta/C) = \log K + x \log(1-\theta) \qquad (45)$$

where θ is the degree of surface coverage, C is the concentration of the system studied x is the number of water molecule replaced by one inhibitor molecule and K is the equilibrium constant for the adsorption process. The plot of Flory-Huggins adsorption isotherm is log (θ/C) Vs log (1-θ).

El Awady kinetic thermodynamic adsorption isotherm can be described according to equation (42) **(Uwah et al., 2010)**

$$\log\left[\frac{\theta}{1-\theta}\right] = \log K' + y \log C \qquad (46)$$

where C is the concentration of the adsorbate θ is the degree of surface coverage and 1/y is the number of inhibitor molecules occupying one active sites. The plots of El Awady kinetic thermodynamic adsorption isotherm is log (θ/1- θ) Vs log C.

Bockris-Swinkel's adsorption isotherm can be arrived at using equation (43) **(Moretti et al., 2004)**

$$\frac{\left[\dfrac{\theta}{(1-\theta)^{x}}\right]}{\dfrac{[\theta + x(1-\theta)^{x-1}]}{x^{x}}} = KC \qquad (47)$$

Where θ is the degree of surface coverage, x is the number of water molecules substituted by one molecule of organic absorbate and K is the equilibrium constant of the adsorption process. The plot of Bockris-Swinkel's adsorption isotherm is θ log (θ/1-θ) Vs log C.

A particular model which has highest value of R^2 can be considered as the best model to explain the changes in performance of polymer composites adsorbent-type inhibitors. Similarly, the effect of the level of concentration on the IE can be estimated by coefficient of the equation and can be tested against the hypothesis. The model used takes the following form $\ln y = \alpha + \beta x$, where 'y' is the surface coverage, α is the intercept, β is the slope and 'x' is the concentration. The same model has applied for the seven adsorption isotherms to identify the most suitable model for the problem understudy using **Statistical Software Package SPSS 17.**

4.9.1 Adsorption isotherm behaviour of investigated inhibitors in acidic medium:

Values of adsorption parameters deduced from various adsorption isotherm and the estimated coefficients of studied inhibitors in 1M HCl are enlisted in Table-(17-22).

Table-17 Adsorption parameters deduced from various adsorption isotherms - PVAALA composite in 1M HCl

S.No.	Adsorption isotherms	Temp (K)	Slope	t	intercept	R^2	F
1.	Langmuir	303	0.885	109.19** (0.000)	0.076	1.000	11922.072** [0.000]
		313	0.976	263.278** (0.000)	0.074	1.000	69315.447** [0.000]
		323	0.866	128.673** (0.000)	0.072	1.000	16556.643** [0.000]
		333	0.951	214.076** (0.000)	0.045	1.000	45828.538** [0.000]
		343	0.906	94.485** (0.000)	0.094	1.000	8927.358** [0.000]
2.	Temkin	303	0.081	12.346** (0.000)	0.831	0.975	152.435** [0.000]
		313	0.019	6.271** (0.000)	0.844	0.912	39.329** [0.000]
		323	0.091	21.071** (0.000)	0.834	0.991	443.998** [0.000]
		333	0.041	11.569** (0.000)	0.900	0.971	133.837** [0.000]
		343	0.066	9.157** (0.000)	0.801	0.955	83.844** [0.000]
3.	Frumkin	303	-0.124	-6.472** (0.000)	1.011	0.916	41.882** [0.000]
		313	-0.021	-5.228** (0.000)	0.879	0.880	27.327** [0.000]
		323	-0.158	-11.900** (0.000)	1.069	0.973	141.621** [0.000]
		333	-0.056	-8.360** (0.000)	1.017	0.947	69.887** [0.000]
		343	-0.09	-5.750** (0.000)	0.916	0.897	33.058** [0.000]
4.	Freundlich	303	0.115	141.121** (0.000)	-0.175	0.981	199.413** [0.000]
		313	0.024	6.409** (0.000)	-0.169	0.951	41.077** [0.000]
		323	0.134	19.930** (0.000)	-0.165	0.990	397.210** [0.000]
		333	0.049	11.130** (0.000)	-0.103	0.969	123.870** [0.000]
		343	0.094	9.832** (0.000)	-0.216	0.961	96.672** [0.000]
5.	Flory-Huggins	303	2.781	8.015** (0.000)	2.014	0.943	64.233** [0.000]
		313	7.357	5.517** (0.000)	5.942	0.890	30.443** [0.000]
		323	2.816	16.971** (0.000)	1.981	0.986	288.014** [0.000]
		333	3.721	12.845** 0.000)	3.549	0.977	165.002** [0.000]
		343	3.501	7.211** (0.000)	2.347	0.931	51.995** [0.000]
6.	El-Awady kinetic thermodynamic	303	0.400	9.887** (0.000)	0.657	0.961	97.760** [0.000]
		313	0.129	5.795** (0.000)	0.729	0.899	33.578** [0.000]
		323	0.434	20.779** (0.000)	0.653	0.991	431.782** [0.000]
		333	0.294	13.288** (0.000)	0.915	0.978	176.570** [0.000]
		343	0.321	8.401** (0.000)	0.585	0.948	70.575** [0.000]
7.	Bockris-Swinkels	303	0.358	8.389** (0.000)	0.523	0.948	70.374** [0.000]
		313	0.135	5.690** (0.000)	0.613	0.895	32.372** [0.000]
		323	0.373	17.603** (0.000)	0.511	0.987	309.869** [0.000]
		333	0.309	13.541** (0.000)	0.811	0.979	183.368** [0.000]
		343	0.285	7.725** (0.000)	0.454	0.939	59.669** [0.000]

Figure within ( ) give t values; F Figure within [ ] give F ratio. ** - 1% level of significane, * - 5% level of significance.

Table-18 Adsorption parameters deduced from various adsorption isotherms - PVAVAL composite in 1M HCl

S.No.	Adsorption isotherms	Temp (K)	Slope	t	intercept	R^2	F
1.	Langmuir	303	0.891	41.096** (0.000)	0.096	0.998	1688.882** [0.000]
		313	0.976	295.945** (0.000)	0.037	1.000	87583.547** [0.000]
		323	0.958	154.581** (0.000)	0.036	1.000	23895.373** [0.000]
		333	0.967	407.498** (0.000)	0.077	1.000	166054.955** [0.000]
		343	0.904	95.622** (0.000)	0.086	1.000	9143.494** [0.000]
2.	Temkin	303	0.076	4.677** (0.002)	0.797	0.856	21.877** [0.002]
		313	0.021	7.038** (0.000)	0.918	0.928	49.536** [0.000]
		323	0.037	6.683** (0.000)	0.920	0.921	44.658** [0.000]
		333	0.026	13.819** (0.000)	0.837	0.980	190.952** [0.000]
		343	0.068	9.643** (0.000)	0.814	0.960	92.984** [0.000]
3.	Frumkin	303	-0.080	-2.141* (0.065)	0.871	-0.604	4.586* [0.065]
		313	-0.025	-5.169** (0.001)	0.976	-0.877	26.714** [0.001]
		323	-0.047	-3.917** (0.004)	1.024	-0.811	15.341** [0.004]
		333	-0.031	-11.517** (0.000)	0.886	-0.971	132.630** [0.000]
		343	-0.095	-5.950** (0.000)	0.944	-0.903	35.398** [0.000]
4.	Freundlich	303	0.109	5.016** (0.000)	-0.221	0.871	25.157** [0.000]
		313	0.024	7.123** (0.001)	-0.085	0.929	50.735** [0.001]
		323	0.042	6.796** (0.000)	-0.082	0.923	46.188** [0.000]
		333	0.033	13.787** (0.000)	-0.177	0.980	190.082** [0.000]
		343	0.096	10.198** (0.000)	-0.198	0.964	104.003** [0.000]
5.	Flory-Huggins	303	2.124	3.457** (0.009)	1.535	0.774	11.948** [0.009]
		313	4.255	6.213** (0.000)	4.632	0.910	38.600** [0.000]
		323	2.690	5.669** (0.000)	2.937	0.895	32.138** [0.000]
		333	7.284	13.100** (0.000)	5.628	0.977	171.618** [0.000]
		343	3.359	7.655** (0.000)	2.334	0.938	58.602** [0.000]
6.	El-Awady kinetic thermodynamic	303	0.374	4.242** (0.003)	0.585	0.832	17.998** [0.003]
		313	0.214	6.452** (0.000)	1.039	0.916	41.625** [0.000]
		323	0.330	6.042** (0.000)	1.031	0.906	36.503** [0.000]
		333	0.160	13.667** (0.000)	0.703	0.979	186.785** [0.000]
		343	0.336	8.901** (0.000)	0.618	0.953	79.232** [0.000]
7.	Bockris-Swinkels	303	0.332	3.914** (0.000)	0.457	0.810	15.316** [0.000]
		313	0.235	6.428** (0.000)	0.951	0.915	41.325** [0.000]
		323	0.358	5.9992** (0.000)	0.941	0.904	35.906** [0.000]
		333	0.162	13.548** (0.000)	0.585	0.979	183.554** [0.000]
		343	0.301	8.222** (0.000)	0.486	0.946	67.605** [0.000]

values; F Figure within [ ] give F ratio. ** - 1% level of significane, * - 5% level of significance.

Table-19 Adsorption parameters deduced from various adsorption isotherms - PVAGLN composite in 1M HCl

S.No.	Adsorption isotherms	Temp (K)	Slope	t	intercept	R^2	F
1.	Langmuir	303	0.917	35.950** (0.000)	0.048	0.997	1292.419** [0.000]
		313	0.968	421.854** (0.000)	0.031	1.000	177960.832** [0.000]
		323	0.914	134.659** (0.000)	0.047	1.000	18133.062** [0.000]
		333	0.938	175.286** 0.000)	0.047	1.000	30725.014** [0.000]
		343	0.943	368.363** (0.000)	0.112	1.000	135691.073** [0.000]
2.	Temkin	303	0.068	3.189* (0.013)	0.894	0.748	10.167* [0.013]
		313	0.028	13.580** (0.000)	0.931	0.979	184.406** [0.000]
		323	0.067	12.204** (0.000)	0.891	0.974	148.946** [0.000]
		333	0.051	10.830** (0.000)	0.894	0.968	117.293** [0.000]
		343	0.040	23.308** (0.000)	0.770	0.993	543.270** [0.000]
3.	Frumkin	303	-0.015	-0.315 (0.761)	0.846	0.111	0.099 [0.761]
		313	-0.039	-8.825** (0.000)	1.028	0.952	77.875** [0.000]
		323	-0.104	-6.136** (0.000)	1.088	0.908	37.654** [0.000]
		333	-0.072	-6.153** (0.000)	1.038	0.909	37.865** [0.000]
		343	-0.049	-18.950** (0.000)	0.828	0.989	359.094** [0.000]
4.	Freundlich	303	0.083	3.236* (0.012)	-0.111	0.753	10.471* [0.012]
		313	0.032	13.988** (0.000)	-0.070	0.980	195.672** [0.000]
		323	0.086	12.664** (0.000)	-0.109	0.976	160.370** [0.000]
		333	0.062	11.553** (0.000)	-0.109	0.971	133.470** [0.000]
		343	0.057	22.130** (0.000)	-0.259	0.992	489.745** [0.000]
5.	Flory-Huggins	303	1.090	2.545* (0.034)	1.279	0.669	6.479* [0.034]
		313	3.489	10.083** (0.000)	3.945	0.963	101.675** [0.000]
		323	2.500	7.893** (0.000)	2.267	0.941	62.300** [0.000]
		333	2.869	7.712** (0.000)	2.707	0.939	59.468** [0.000]
		343	6.852	22.497** (0.000)	4.198	0.992	506.105** [0.000]
6.	El-Awady kinetic thermodynamic	303	0.083	3.236* (0.012)	-0.111	0.753	10.471* [0.012]
		313	0.032	13.988** (0.000)	-0.070	0.980	195.672** [0.000]
		323	0.086	12.664** (0.000)	-0.109	0.976	160.370** [0.000]
		333	0.062	11.553** (0.000)	-0.109	0.971	133.470** [0.000]
		343	0.052	22.130** (0.000)	-0.259	0.992	489.745** [0.000]
7.	Bockris-Swinkels	303	0.515	2.984* (0.017)	0.825	0.726	8.905* [0.017]
		313	0.317	1.590** (0.000)	1.016	0.966	112.158** [0.000]
		323	0.414	8.438** (0.000)	0.741	0.948	71.198** [0.000]
		333	0.367	8.211** (0.000)	0.786	0.945	67.426** [0.000]
		343	0.170	23.551** (0.000)	0.390	0.993	554.657** [0.000]

Figure within ( ) give t values; F Figure within [ ] give F ratio. ** - 1% level of significane, * - 5% level of significance.

Table-20 Adsorption parameters deduced from various adsorption isotherms - PVAGLU composite in 1M HCl

S.No.	Adsorption isotherms	Temp (K)	Slope	t	intercept	R^2	F
1.	Langmuir	303	0.827	29.366** (0.000)	0.170	0.995	862.379** [0.000]
		313	0.937	293.657** (0.000)	0.047	1.000	86234.278** [0.000]
		323	0.989	529.758** (0.000)	0.064	1.000	280643.894** [0.000]
		333	0.956	225.593** (0.000)	0.067	1.000	5892.029** [0.000]
		343	0.921	154.844** (0.000)	0.065	1.000	23976.715** [0.000]
2.	Temkin	303	0.126	6.176** (0.000)	0.939	0.909	38.137** [0.000]
		313	0.051	17.985** (0.000)	0.893	0.988	323.465** [0.000]
		323	0.010	5.929** (0.000)	0.863	0.903	35.148** [0.000]
		333	0.036	10.106** (0.000)	0.856	0.963	102.126** [0.000]
		343	0.060	12.428** (0.000)	0.856	0.963	102.126** [0.000]
3.	Frumkin	303	-0.120	-1.156** (0.000)	1.087	0.378	1.336** [0.000]
		313	-0.076	-10.403** (0.000)	1.046	0.965	108.214** [0.000]
		323	-0.010	-5.354** (0.000)	0.880	0.884	28.670** [0.000]
		333	-0.045	-7.385** (0.000)	0.933	0.934	54.537** [0.000]
		343	-0.086	-7.529** (0.000)	1.000	0.936	56.691** [0.000]
4.	Freundlich	303	0.173	6.147** (0.000)	-0.038	0.908	37.782** [0.000]
		313	0.063	19.694** (0.000)	-0.109	0.990	387.842** [0.000]
		323	0.011	6.008** (0.000)	-0.148	0.905	36.091** [0.000]
		333	0.044	10.470** (0.000)	-0.153	0.965	109.622** [0.000]
		343	0.079	13.213** (0.000)	-0.150	0.978	174.580** [0.000]
5.	Flory-Huggins	303	1.311	5.086** (0.001)	1.345	0.874	25.864** [0.001]
		313	3.138	11.836** (0.000)	2.900	0.973	140.081** [0.000]
		323	12.318	5.434** (0.001)	10.636	0.887	29.524** [0.001]
		333	4.666	8.241** (0.000)	3.858	0.946	67.916** [0.000]
		343	3.247	9.108** (0.000)	2.604	0.955	82.963** [0.000]
6.	El-Awady kinetic thermodynamic	303	0.680	6.396** (0.000)	0.952	0.915	40.912** [0.000]
		313	0.346	13.336** (0.000)	0.883	0.978	177.852** [0.000]
		323	0.075	5.5751** (0.001)	0.795	0.892	31.085** [0.001]
		333	0.228	8.923** (0.000)	0.763	0.953	79.623** [0.000]
		343	0.339	10.459** (0.000)	0.744	0.965	109.381** [0.000]
7.	Bockris-Swinkels	303	0.639	6.433** (0.000)	0.823	0.915	41.379** [0.000]
		313	0.360	12.483** (0.000)	0.776	0.975	155.826** [0.000]
		323	0.080	5.532** (0.000)	0.685	0.890	30.605** [0.000]
		333	0.234	8.630** (0.000)	0.648	0.950	74.476** [0.000]
		343	0.331	9.624** (0.000)	0.621	0.959	92.612** [0.000]

Figure within ( ) give t values; F Figure within [ ] give F ratio.
**** - 1% level of significane, * - 5% level of significance.**

Table-21 Adsorption parameters deduced from various adsorption isotherms - PVATYR composite in 1M HCl

S. No.	Adsorption isotherms	Temp (K)	Slope	t	intercept	R^2	F
1.	Langmuir	303	0.924	62.982** (0.000)	0.125	0.999	3966.782** [0.000]
		313	0.948	225.860** (0.000)	0.051	1.000	51012.659** [0.000]
		323	0.874	103.250** (0.000)	0.066	1.000	10660.632** [0.000]
		333	0.934	170.118** (0.000)	0.033	1.000	28940.249** 0.000]
		343	0.953	586.752** (0.000)	0.077	1.000	344277.865** [0.000]
2.	Temkin	303	0.052	4.845** (0.001)	0.748	0.864	23.473** [0.001]
		313	0.042	12.241** (0.000)	0.886	0.974	149.844** [0.000]
		323	0.088	15.996** (0.000)	0.846	0.985	255.883** [0.000]
		333	0.055	11.374** (0.000)	0.923	0.970	129.373** [0.000]
		343	0.037	26.342** (0.000)	0.836	0.994	693.893** [0.000]
3.	Frumkin	303	-0.058	-3.191* (0.013)	(0.000)0 .800	-0.748	10.179* [0.013]
		313	-0.058	-8.525** (0.000)	0.999	-0.949	72.683** [0.000]
		323	-0.149	-9.192** (0.000)	1.078	-0.956	84.485** [0.000]
		333	-0.086	-5.557** (0.001)	1.117	-0.891	30.877** [0.001]
		343	-0.046	-19.572** (0.000)	0.909	-0.990	383.056** [0.000]
4.	Freundlich	303	0.076	5.155** (0.001)	-0.288	0.877	26.572** [0.001]
		313	0.056	12.281** (0.000)	-0.118	0.974	150.820** [0.000]
		323	0.126	14.888** (0.000)	-0.152	0.982	221.653** [0.000]
		333	0.066	11.946** (0.000)	-0.076	0.973	142.717** [0.000]
		343	0.047	28.964** (0.000)	-0.178	0.995	839.926** [0.000]
5.	Flory-Huggins	303	3.759	3.865** (0.005)	2.274	0.807	14.941** [0.005]
		313	3.780	11.365** (0.000)	3.432	0.970	129.164** [0.000]
		323	2.767	14.179** (0.000)	2.038	0.981	201.050** [0.000]
		333	2.311	8.126** (0.000)	2.445	0.944	66.026** [0.000]
		343	5.593	18.239** (0.000)	4.246	0.988	332.666** [0.000]
6.	El-Awady kinetic thermodynamic	303	0.076	5.155** (0.001)	-0.288	0.877	26.572** [0.001]
		313	0.052	12.281** (0.000)	-0.118	0.974	150.820** [0.000]
		323	0.126	14.888** (0.000)	-0.152	0.982	221.653** [0.000]
		333	0.066	11.946** (0.000)	-0.076	0.973	142.717** [0.000]
		343	0.047	28.964** (0.000)	-0.178	0.995	838.96** [0.000]
7.	Bockris-Swinkels	303	0.206	4.169** (0.003)	0.345	0.828	17.383** [0.003]
		313	0.301	11.976** (0.000)	0.754	0.973	143.417** [0.000]
		323	0.382	15.446** (0.000)	0.549	0.984	238.567** [0.000]
		333	0.456	8.706** (0.000)	0.922	0.951	75.801** [0.000]
		343	0.213	18.770** (0.000)	0.573	0.989	352.310** [0.000]

Figure within ( ) give t values; F Figure within [ ] give F ratio.
**** - 1% level of significane, * - 5% level of significance.**

Table-22 Adsorption parameters deduced from various adsorption isotherms - PVATRP composite in 1M HCl

S.No.	Adsorption isotherms	Temp (K)	Slope	t	intercept	R^2	F
1.	Langmuir	303	0.909	69.143** (0.000)	0.067	0.999	4780.791** [0.000]
		313	0.910	101.694** (0.000)	0.050	1.000	10341.719** [0.000]
		323	0.875	99.461** (0.000)	0.052	1.000	9892.555** [0.000]
		333	0.897	56.354** (0.000)	0.046	0.999	3175.824** [0.000]
		343	0.880	82.774** (0.000)	0.049	0.999	6851.527** [0.000]
2.	Temkin	303	0.069	6.280** (0.000)	0.852	0.912	39.437** [0.000]
		313	0.070	9.262** (0.000)	0.885	0.956	85.787** [0.000]
		323	0.090	15.417** (0.000)	0.874	0.984	237.687** 0.000]
		333	0.076	7.112** (0.000)	0.888	0.929	50.581** [0.000]
		343	0.090	9.786** (0.000)	0.885	0.961	95.758** [0.000]
3.	Frumkin	303	-0.084	-2.997* (0.017)	0.973	-0.727	8.979* [0.017]
		313	-0.104	-4.381** (0.002)	1.072	-0.840	19.191** [0.002]
		323	-0.161	-7.879** (0.003)	1.152	-0.941	62.077** [0.003]
		333	-0.112	-4.095** (0.006)	1.086	-0.823	16.772** [0.006]
		343	-0.141	-3.707** (0.000)	1.126	-0.795	13.739** [0.000]
4.	Freundlich	303	0.091	6.903** (0.000)	-0.155	0.925	47.654** [0.000]
		313	0.090	10.061** (0.000)	-0.116	0.963	101.224** [0.000]
		323	0.125	14.272** (0.000)	-0.120	0.981	203.700** [0.000]
		333	0.103	6.475** (0.000)	-0.106	0.916	41.921** [0.000]
		343	0.120	11.276** (0.000)	-0.112	0.970	127.147** [0.000]
5.	Flory-Huggins	303	2.214	4.316** (0.003)	1.857	0.836	18.631** [0.003]
		313	2.275	6.358** (0.000)	2.055	0.914	40.427** [0.000]
		323	2.415	11.779** (0.000)	1.956	0.972	138.734** [0.000]
		333	2.603	8.092** (0.000)	2.253	0.944	65.481** [0.000]
		343	1.903	6.170** (0.000)	1.689	0.909	38.072** [0.000]
6.	El-Awady kinetic thermodynamic	303	0.091	6.903** (0.000)	-0.155	0.925	47.654** [0.000]
		313	0.090	10.061** (0.000)	-0.116	0.963	101.224** [0.000]
		323	0.125	14.272** (0.000)	-0.120	0.981	203.700** [0.000]
		333	0.103	6.475** (0.000)	-0.106	0.916	41.921** [0.000]
		343	0.120	11.276** (0.000)	-0.112	0.970	127.147** [0.000]
7.	Bockris-Swinkels	303	0.374	4.700** (0.002)	0.614	0.857	22.088** [0.002]
		313	0.430	6.881** (0.000)	0.725	0.925	47.345** [0.000]
		323	0.433	12.508** (0.000)	0.635	0.975	156.462** [0.000]
		333	0.395	9.678** (0.000)	0.691	0.960	93.667** [0.000]
		343	0.492	6.708** (0.000)	0.700	0.921	44.997** [0.000]

Figure within ( ) give t values; F Figure within [ ] give F ratio.
**** - 1% level of significane, * - 5% level of significance.**

Analysing the values of F, the following table has been arrived at and the adsorption models followed by the studied inhibitors are represented in table-23. The highest values of F are also highlighted in Table -23.

Table -23 The results of Statistical SPSS 17 package on adsorption isotherms and the various adsorption models obeyed by the investigated inhibitors their highest F values and corresponding R^2 values

S.NO.	Polymer composite	Adsorption models	Highest value of F	R^2
1.	PVAALA	Langmuir	69315.447	1.000
2.	PVAVAL	Langmuir	166054.955	1.000
3.	PVAGLN	Langmuir	177960.832	1.000
4.	PVAGLU	Langmuir	280643.894	1.000
5.	PVATYR	Langmuir	344277.865	1.000
6.	PVATRP	Langmuir	10341.719	1.000

From the tables - 23 it can be noticed that Langmuir model has highest R^2 when compared to the other models. The highest R^2 indicates best fit of the model. This is supported by significant F value at 1% level of significance. From statistical analysis PVAALA, PVAVAL, PVAGLN, PVAGLU, PVATRY and PVATRP composites obey Langmuir models in 1M HCl medium. Langmuir adsorption isotherm for the investigated inhibitors is further explained.

4.9.2 LANGMUIR ADSORPTION ISOTHERM:

A direct relationship between inhibition efficiency (IE %) and the degree of surface coverage (θ) (%IE = 100 $\times$ θ) can be assumed for different concentration of the inhibitors. The degree of surface coverage (θ) for different concentrations of polyvinyl alcohol- selected amino acid composites are evaluated from weight loss method in 1M HCl at 303-343°C for ½ h immersion period. The data are tested graphically by fitting to various adsorption isotherms including Langmuir, temkin, Frumkin, Freundlich, Flory-Huggins, El-Awady kinetic thermodynamic and Bockics-Swinkels isotherms. The correlation coefficient (R^2) is used to determine the best fit isotherm which was obtained for Langmuir. According to this isotherm, θ is related to the inhibitor concentration by the following equation (48)

$$\theta = \frac{K_{ads} C_{inh}}{1 + K_{ads} C_{inh}} \qquad (48)$$

Where θ is the surface coverage, C_{inh} is the concentration, K_{ads} is the equilibrium constant for the adsorption /desorption process. This equation (48) can be rearranged to equation (49)

$$\frac{C_{inh}}{\theta} = \frac{1}{K_{ads}} + C_{inh} \qquad (49)$$

K_{ads} is related to the free energy to the free energy of adsorption $\Delta G^{*}ads$ by the adsorption

$$\log K_{ads} = -\log C_{H2O} - \frac{\Delta G^{*}ads}{2.303RT} \qquad (50)$$

Where C_{H2O} is the concentration of water expressed in % (the same as that of inhibitor concentration), R is the molar gas constant ($KJmol^{-1}K^{-1}$) and T is the absolute temperature (K). Figure- 29 shows the plots of log(C/θ) Vs log C and linear plots are obtained for different temperatures indicating that the adsorption of polyvinyl alcohol-selected amino acid composites followed Langmuir isotherm. The various adsorption parameters obtained from this isotherm are in table-17-22. It is seen from the table the correlation coefficients are very good and K values decreases with increasing temperature showing that the molecules of the inhibitor was physically adsorbed on the mild steel surface. Although the plots are linear as depicted by R^2 values (0.99-1.00) however, the slopes deviation from the value of unity as expected from the ideal Langmuir adsorption equation. This deviation may be explained on the basis of the interaction among adsorbed species on the surface of the metal. It has been postulated in the deviation of Langmuir isotherm equation that adsorbed molecules do not interact with one another, but this is not the case of large polymer composites (such as PVAALA, PVAVAL, PVAGLN,PVAGLU, PVATYR and PVATRP composites) having polar atoms or groups which can adsorbed on the cathodic and anodic sites of the metal surface. Such adsorbed species interact by mutal repulsion or attraction. It is also possible that the inhibitor studied can be adsorbed on the anodic and cathodic sites resulting in deviation from unit gradient.

From the intercepts of the straight lines on the C_{inh}/θ-axis (figure-29), K_{ads} can be calculated which is related to free energy of adsorption ΔG^{*}_{ads}, as given by equation (51)

$$\Delta G^{*}_{ads} = -RT \ln (55.5\ K_{ads}) \qquad (51)$$

The values of the free energy of adsorption, ΔG^{*}_{ads} are obtained from equation (47) and are given in table-24. Results presented in the table indicate that the values of ΔG^{*}_{ads} are negative in all cases and lies between -10.2 and -11.8 $KJmol^{-1}$.

Figure-29 Langmuir Adsorption isotherms of Polyvinyl alcohol – selected Amino acid composites

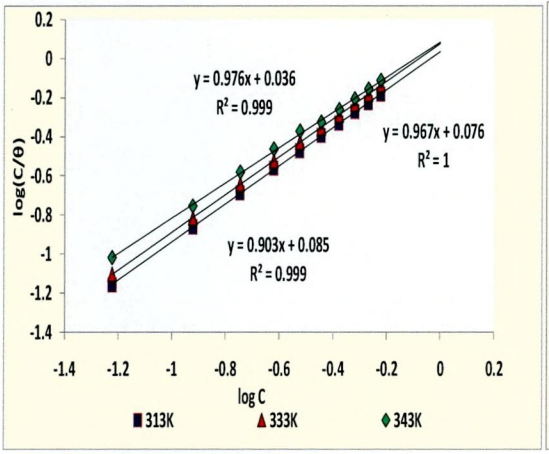

PVAALA

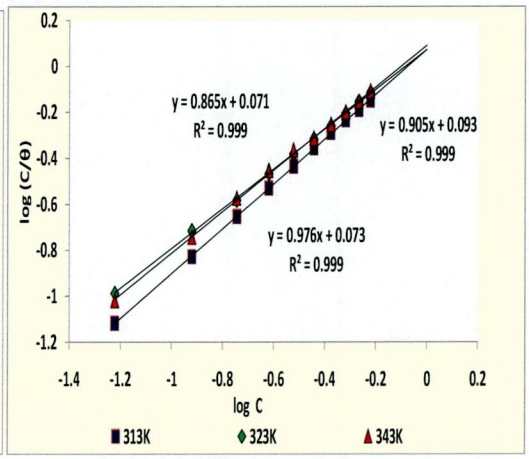

PVAVAL

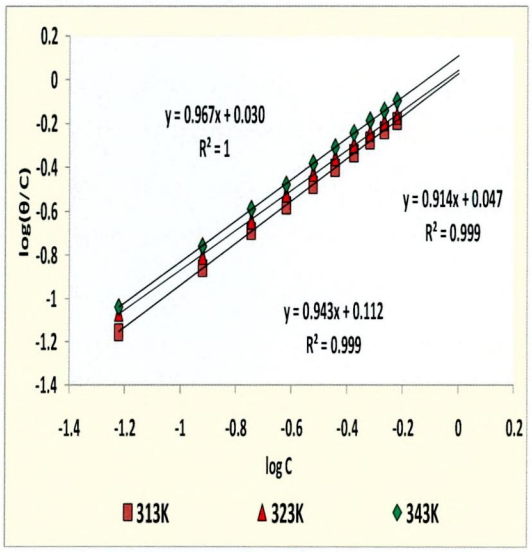

PVAGLN

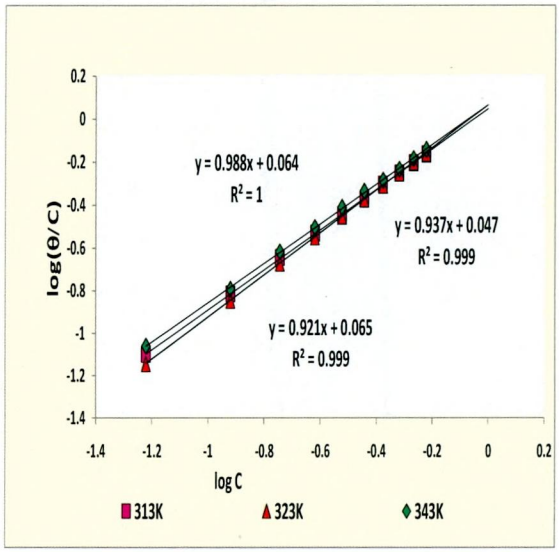

PVAGLU

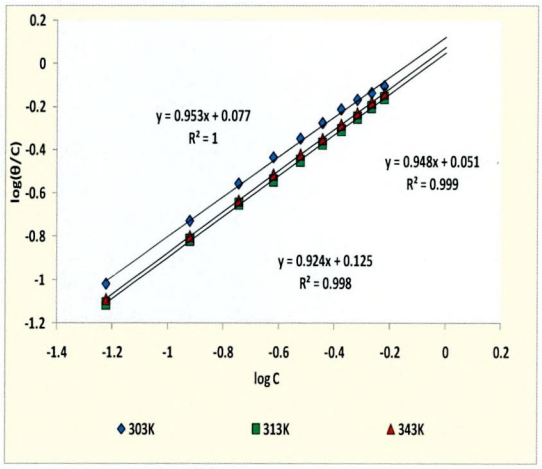

PVATYR

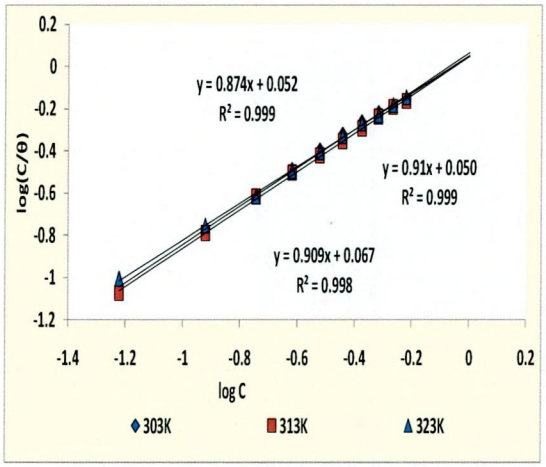

PVATRP

The negative values signify spontaneous adsorption of the inhibitors molecules via physical adsorption mechanism. It is also seen that values of ΔG^*_{ads} decreased with an increase in temperature, a phenomenon which indicates that the adsorption of the inhibitor onto mild steel surface was unfavorable with increasing experimental temperatures as a result of desorption of adsorbed inhibitors from the metal surface. Generally, values of $\Delta G^*_{ads} \leq -20$ KJmol^{-1} (as obtained in this study) signify physisorption, and values more negative than -40 KJmol^{-1} signify chemisorption, physisorption is consistent with electrostatic interaction between charged molecules and charged metal while chemisorption is consistent with charge sharing or transfer from the inhibitors components to the metal surface to form a co-ordinate type of bond **(solomon *et al.,* 2010).**

Table – 24 Deduced adsorption parameter using Langmuir adsorption isotherm

S.NO.	Inhibitors	ΔG^*_{ads} (KJmol^{-1})				
		303K	313K	323K	333K	343K
1.	PVAALA	-10.3	-10.6	-11.0	-11.2	-11.7
2.	PVAVAL	-10.4	-10.5	-10.9	-11.3	-11.7
3.	PVAGLU	-10.2	-10.6	-11.0	-11.3	-11.6
4.	PVAGLN	-10.2	-10.5	-10.9	-11.3	-11.8
5.	PVATYR	-10.4	-10.6	-11.0	-11.2	-11.7
6.	PVATRP	-10.3	-10.6	-10.9	-11.2	-11.6

4.9.3 El – Awady et al., Thermodynamic – Kinetic isotherm model:

It is necessary to determine empirically which adsorption isotherm fits best to the surface coverage data in order to use the corrosion rate measurements to calculate the thermodynamic parameters pertaining to inhibitor adsorption. El – Awady et al., Thermodynamic – Kinetic isotherm model may be formulated as equation (46). The binding constant K is given by

$$K = K'^{(1/y)} \qquad (52)$$

The data are given in table -25. The efficiency of the given inhibitors is a function of both magnitude of its binding constant K and the number of active sites (1/y) it is blocking with the former being the most important **(El-Awady *et al.,* 1992).** Large values of K mean better and strong interaction, while small values of K mean that the interaction between the inhibitors molecules and the metal is weaker. The reciprocal of y gives the number of inhibitor molecules occupying one active site (or the number of water molecules replaced by one molecule of inhibitor). Values of 1/y are more than unity indicating that each molecule of the inhibitor is attached to one active site of the mild steel surface **(Abd -El Rehim *et al.,*2001).** Inspection of table-17-22, show that K values decrease with increase in temperature. This is interpreted to

mean that weaker surface interaction results at higher temperatures. The values of 1/y obtained were greater than one. This implies that a given inhibitor molecule will occupy more than one active site on the surface of the metal **(El-Awady *et al.*, 1992).**

Table –25 Deduced adsorption parameter using El Awady thermodynamic-kinetic model

S.NO.	Inhibitors	(x=1/y)				
		303K	313K	323K	333K	343K
1.	PVAALA	2.5	7.7	2.3	3.4	3.1
2.	PVAVAL	2.7	4.7	3.0	6.3	3.0
3.	PVAGLN	2.0	3.5	2.4	2.8	5.2
4.	PVAGLU	1.5	2.9	13.4	4.4	3.0
5.	PVATYR	4.2	3.5	2.3	2.3	4.7
6.	PVATRP	2.6	2.3	2.1	2.4	2.0

4.10 Activation energy for inhibition process

Temperature dependence of the inhibitor efficiency and the comparison of the values of effective activation energy of the corrosion process both in the absence and in the presence of inhibitors lead to some conclusions concerning the mechanism of the inhibiting action.

The thermodynamic functions for the dissolution of mild steel in 1M HCl with and without polyvinyl alcohol- selected amino acid composites are obtained from Arrhenius equations (18) and (19) and explained in methods and materials (chapter III). The plot of log CR against 1/T for mild steel corrosion in 1M HCl in the absence and presence of different concentrations of polyvinyl alcohol- selected amino acid composites is presented in figure - 30. Linear plots are obtained. The values of E_a are then computed from the slope of the linear plots and are listed in table - 26. From the table, it is clearly seen that the Ea values are higher than the value of 53.3 $KJmol^{-1}$ obtained for the free acid solution indicating that the corrosion reaction of mild steel is inhibited by polyvinyl alcohol – selected amino acid composites (PVAALA, PVAVAL, PVAGLN, PVAGLU, PVATYR and PVATRP composites) hence supports phenomenon of physical adsorption. The increase in the activation energy in the presence of the additives signifies physical adsorption. Higher values of Ea in the presence of inhibitors can be correlated with increasing thickness of the double layer which enhances the Ea of the corrosion process **(Solomon *et al.*, 2010).**

Figure-30 Arrhenius plot for mild steel corrosion in 1M HCl in the absence and presence of different concentration of PVA-Selected Amino acid composites

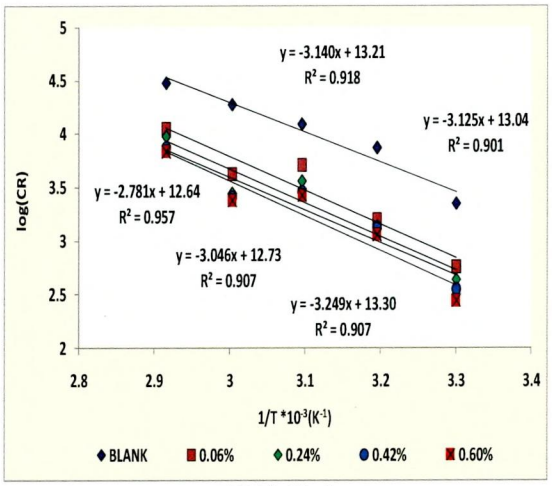

PVAALA

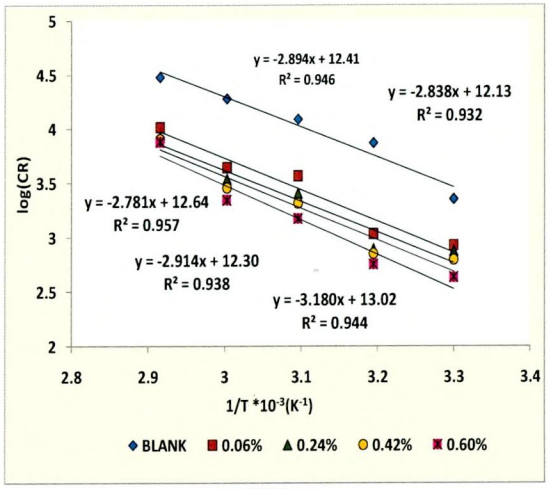

PVAVAL

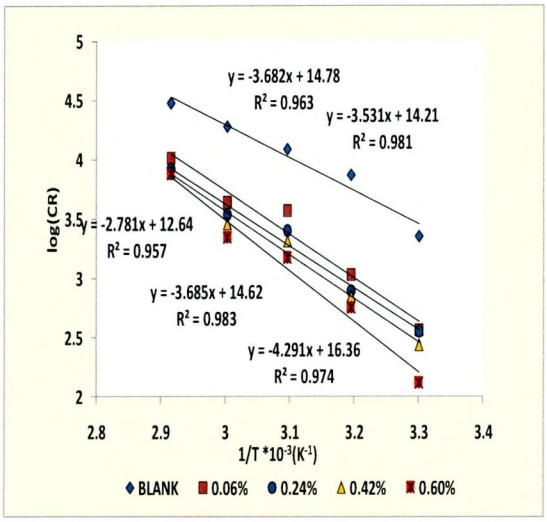

PVAGLN

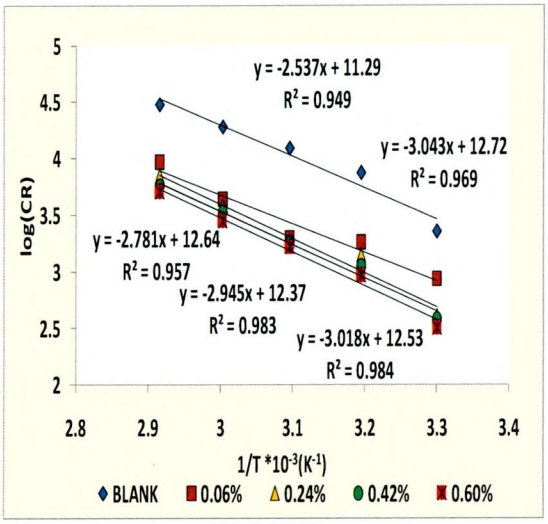

PVAGLU

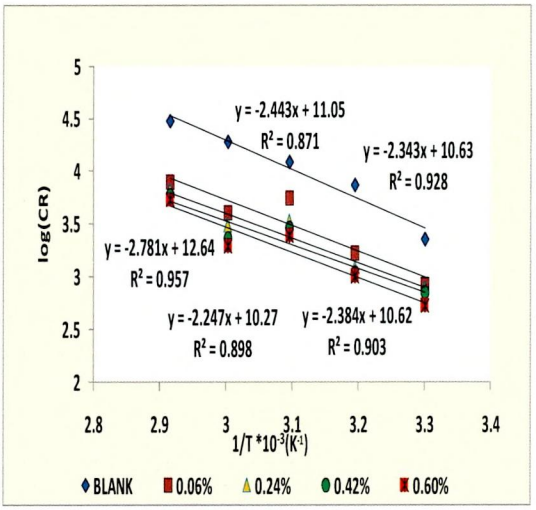

PVATYR

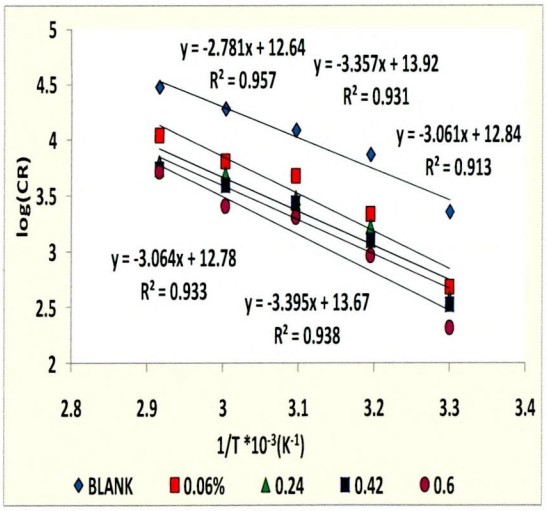

PVATRP

Linear plots are obtained, from the slope ($-E_a/2.303R$), activation energy (E_a) values are deduced and listed in Table 4. The temperature dependence of the inhibiting effect and the comparison of the values of the apparent activation energy of the corrosion process in the absence and presence of inhibitors can provide further evidence concerning the mechanism of the inhibiting action. The decrease of the inhibitor efficiency with temperature rise, which refers to a higher value of E_a, when compared to that in an acid without inhibitor, is interpreted as an indication for an electrostatic character of the inhibitor's adsorption. The lower value of E_a in an inhibited solution for PVATYR composite when compared to that of an uninhibited one shows that strong chemisorption bond between the inhibitor and the metal is highly probable. Unchanged or lower values of E_a in inhibited systems compared to the blank are reported to be indicative of chemisorption mechanism, whereas higher values of Ea suggest a physical adsorption mechanism. E_a values in the presence of PVAALA, PVAVAL, PVAGLU, PVAGLN and PVATRP composites were higher than that in its absence (blank). The higher values of E_a in the inhibited solution can be correlated with the increased thickness of the double layer, which enhances the activation energy of the corrosion process. The increase in activation energy after the addition of inhibitor to acid solution can indicate that physical adsorption (electrostatic interaction) occurs in the first stage. Indeed PVA-Amino acids molecule which contains N atoms in its structure can be protonated to form cation forms in acid medium. It is logical to assume that in this case the electrostatic cation adsorption is responsible for the good protective properties of this compound. However, the adsorption phenomenon of an organic molecule is not considered only as a physical or as chemical adsorption phenomenon, but a wide spectrum of conditions, ranging from the dominance of chemisorption or electrostatic effects may arise due to the complex nature of the corrosion inhibiting process. Physical adsorption in inhibition of corrosion of carbon steel in acidic solution is large but important because it is preceding stage of chemisorption of PVA-Amino acids on mild steel **(Obi-Egbedi *et al.,* 2010a)**. The higher Ea values in the presence of inhibitor compared to the blank solution indicates that the inhibitor will be effective at low temperatures, but efficiencies will be diminished at higher temperatures **(Umoren et al., 2006).**

4.10.1 Activation parameters – Entropy of Activation and Enthalpy of Activation

The relationship between log (CR/T) versus 1/T for mild steel corrosion in 1M HCl in the absence and presence of different concentrations of polyvinyl alcohol-selected amino acid composites are shown in figure-31.

Figure-31 Transition state plot for mild steel corrosion in 1M HCl in the absence and presence of different concentrations of Polyvinyl alcohol-selected Amino acid composites

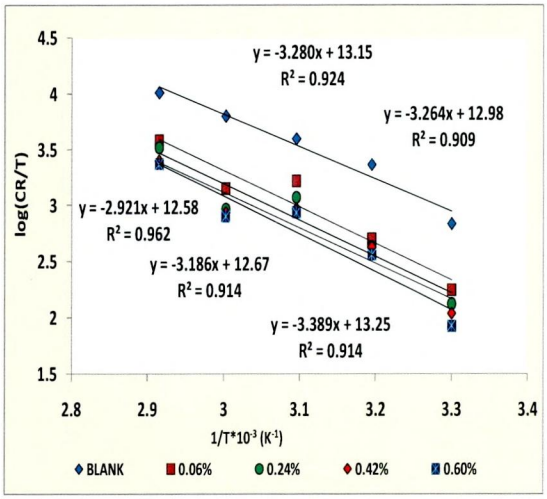

PVAALA

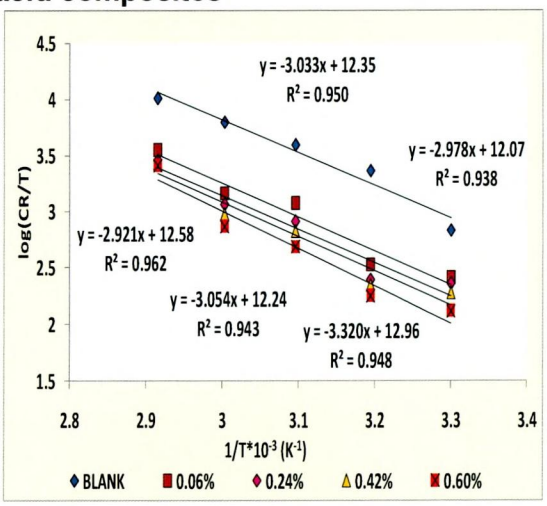

PVAVAL

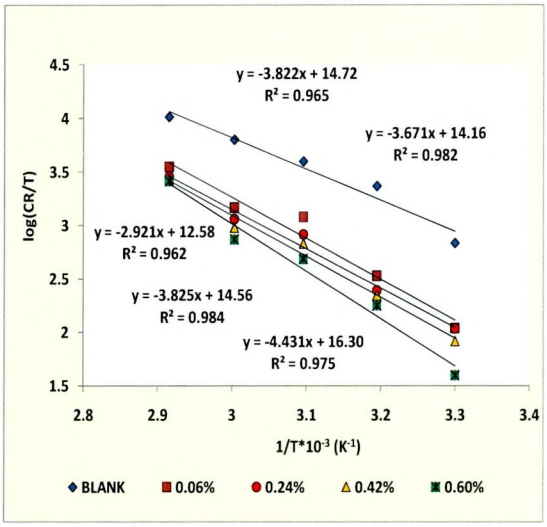

PVAGLN

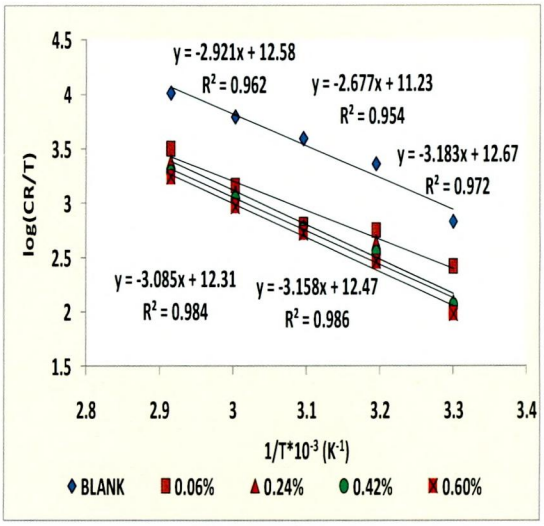

PVAGLU

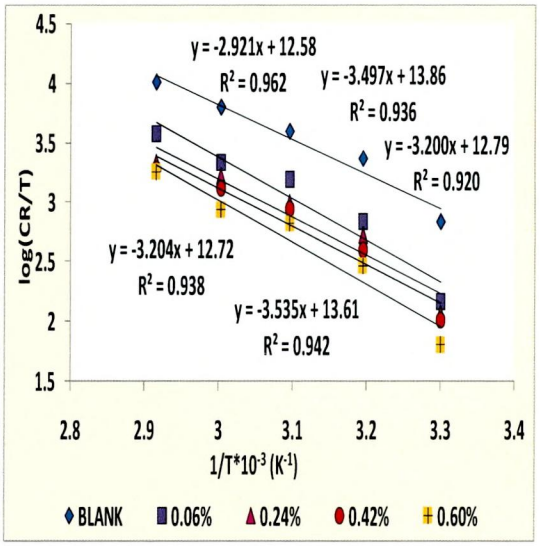

PVATRP

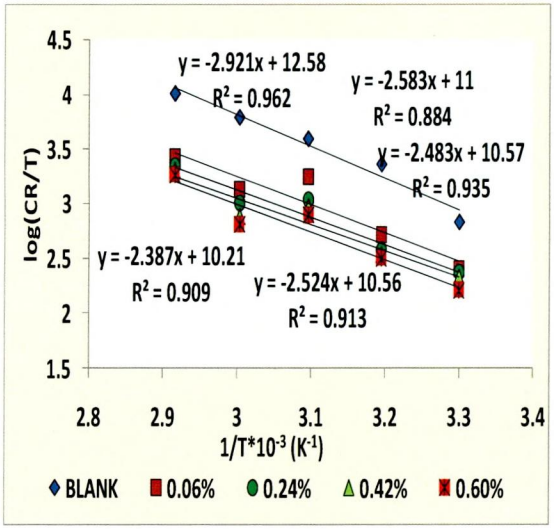

PVATYR

Straight lines are obtained with slope of ($-\Delta H_a/2.303R$) and an intercept of (log R/Nh + $\Delta S_a/2.303R$) from which the values of ΔH_a and ΔS_a respectively were computed and listed in table-26. The enthalpy of activation, ΔH_a and entropy of activation ΔS_a were obtained from Eyring transition state equations (20) and (21) mentioned it methods and materials (Chapter III).

The values of Ea generally in the studied range of polyvinyl alcohol-selected amino acid composites concentration are higher for the inhibited solutions than for the uninhibited solutions, indicating an inhibitive action for the inhibitors by increasing the energy barrier for the inhibitors by increasing the energy barrier for the corrosion process, emphasizing the electrostatic character of the inhibitors adsorption (physisorption) on the mild steel surface.

Table-26 Activation parameters for mild steel in 1M HCl in absence and presence of different concentrations of polyvinyl alcohol-amino acid composites.

S.NO.	Blank/Polymer Composites	Ea KJ/mol	ΔH^o_a KJ/mol	ΔS^o_a J/mol K^{-1}
1.	Blank	53.3	55.9	43.4
2.	PVAALA	59.9	62.6	50.8
3.	PVAVAL	55.9	58.6	38.0
4.	PVAGLN	54.6	57.3	33.7
5.	PVAGLU	72.2	74.9	87.1
6.	PVATYR	44.7	47.3	3.74
7.	PVATRP	60.1	62.8	51.2

In polyvinyl-selected amino acid composites system, the positive signs of the enthalpies (ΔH^o_a) reflect the endothermic nature of the mild steel dissolution process. The positive values of entropies (ΔS^o_a) in the presence of inhibitors imply that the activation complex in the rate determining step represents an association rather than a dissociation step, meaning that an increase in disordering takes place on going from reactants to the activation complex **(Elachouri *et al.,* 1996)**. It is clear that entropy of activation increased in presence of all the studied inhibitors compared to free acid solution. Such variation is associated with the phenomenon of ordering and disordering of inhibitor molecules on the mild steel surface. The increased entropy of activation in the presence of inhibitors indicated that disorderness is increased on going from reactant to activated complex **(Ashish kumar singh et al., 2010b)**.

4.11 Thermodynamic Adsorption Parameters

The temperature increases the rate of all electrochemical processes and influences adsorption equilibria and kinetics as well. Temperature investigations allow

the determination of activation energy, pre-exponential factor and other thermodynamic activation functions in absence and in presence of inhibitors. The obtained results can elucidate the mechanism of corrosion inhibition. In the present work, further insight into the adsorption mechanism is offered by considering the thermodynamic functions for the iron dissolution in 1M HCl solutions in the absence and presence of different concentrations of polyvinyl alcohol-selected amino acid composites.

The values of thermodynamic parameters for the adsorption of inhibitors can provide valuable information about the mechanism of corrosion inhibition. The calculated values of ΔG^{o}_{ads}, ΔH^{o}_{ads}, ΔS^{o}_{ads} at all the temperatures studied (303-343K) using equation (22, 23) at the highest concentration of polymer composites are represented in table-27.

Table - 27 Thermodynamic adsorption parameters for mild steel/ inhibitors in systems at different temperatures in 1M HCl for 0.6%concentration of polymer composites

S.NO.	Polymer Composite Inhibitors	$-\Delta G^{o}_{ads}$ kJ/mol					ΔH^{o}_{ads} J/mol	ΔS^{o}_{ads} J/mol K^{-1}
		303	313	323	333	343		
1.	PVAALA	15.1	16.2	15.6	17.8	16.3	-2418.0	-42.7
2.	PVAVAL	18.4	22.7	22.7	22.1	20.9	-7143.6	-44.0
3.	PVAGLU	18.3	20.7	22.7	20.2	21.7	5266.1	-81.8
4.	PVAGLN	20.0	22.4	20.5	22.2	21.3	-14830.9	-10.8
5.	PVATYR	18.5	21.0	19.4	22.5	22.4	9370.5	-93.2
6.	PVATRP	19.0	20.0	19.5	20.3	21.3	349.9	-55.7

The enthalpy and entropy for the adsorption of polyvinyl alcohol- selected amino acids on mild steel were deduced from the thermodynamic basic equation (24). A plot of ΔG^{o}_{ads} versus T was linear (figure-32) for mild steel acid corrosion in the presence of 0.6% concentration of polymer composites under examination the slope of the straight lines equal to $-\Delta S^{o}_{ads}$ and intercept equal to ΔH^{o}_{ads}. Figure-32 clearly shows the dependence of ΔG^{o}_{ads} on T, indicating the good correlation among thermodynamic parameters. The negative values of ΔG^{o}_{ads} ensure the spontaneity if the adsorption process and stability of the adsorbed layer on the steel surface. Generally, values of ΔG^{o}_{ads} around -20 $kJmol^{-1}$ or lower are consistent with the electrostatic interaction between the charged molecules and the charged metal

(physisorption); those around -40 $kJmol^{-1}$ or higher involve charge sharing or transfer from organic molecules to the metal surface to form a coordinate type of bond (chemisorption).

In the present work, the calculated ΔG^{o}_{ads} values are negative and less than -40 $kJmol^{-1}$ at the same time above -20$kJmol^{-1}$ indicating that the adsorption of the inhibitor molecules is not merely or chemisorption but obeying a comprehensive adsorption (physical and chemical adsorption).

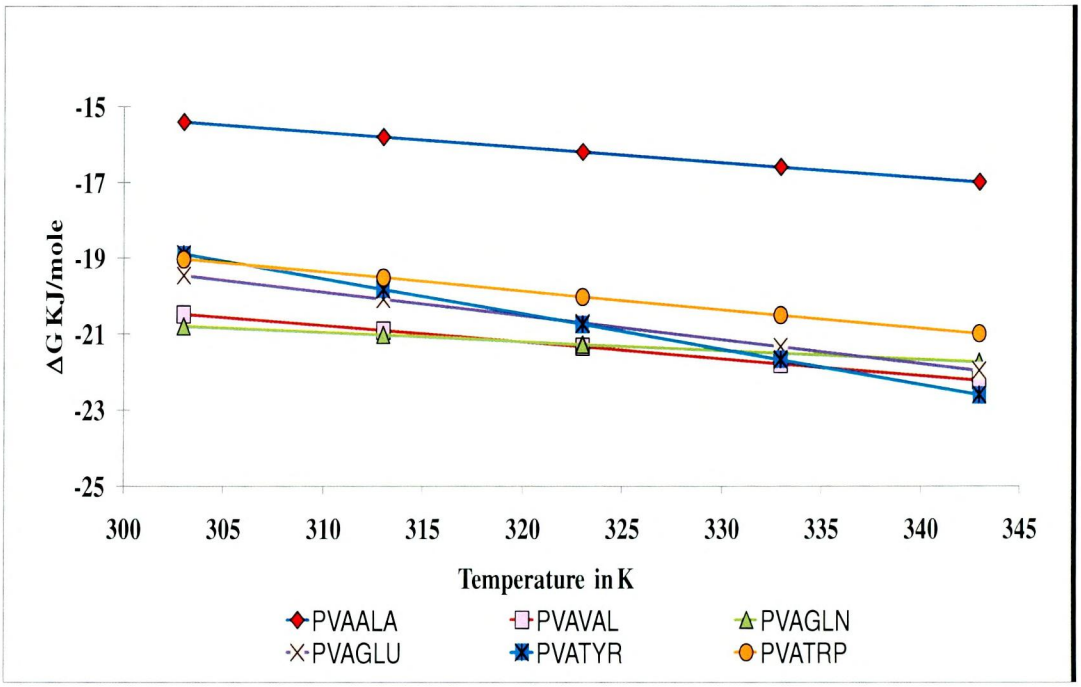

Figure-32 Best fit curves of -ΔG Vs T for 0.6% polyvinyl alcohol-selected amino acids composites in1M HCl

The positive sign of ΔH^{o}_{ads} for the system – PVAGLU, PVATYR and PVATRP composites reflects the endothermic nature of dissolution which suggests the slow dissolution of mild steel. This behaviour can be explained as a result of the replacement process of water molecules during adsorption of PVAGLU, PVATYR and PVATRP composites on the mild steel surface. The entropy of adsorption for the system - PVAGLU, PVATYR and PVATRP composites obtained from equation (24) were negative because inhibitors molecule freely moving in the bulk solution (PVAGLU and PVATYR composites), where adsorption in an orderly fashion onto the mild steel, resulting in a decrease in entropy **(Obi-Egbedi et al., 2010c).**

The sign of enthalpy of adsorption was negative in the presence of PVAVAL, PVAALA, PVATRP and PVAGLN composites. The values of entropy of adsorption are also negative for the above mentioned systems. In fact, it is well known fact the adsorption is an exothermic phenomenon accompanied by decrease in entropy

(Ashish kumar singh *et al.*, 2010c). Inspection of table -27 revealed that decrease in enthalpy and entropy are the driving force for the adsorption of PVAVAL, PVAALA, PVATRP and PVAGLN composites on the mild steel surface **(Umoren *et al.*, 2007a).** The negative values of entropy of adsorption, (ΔS^{o}_{ads}) in the presence of all the studied inhibitors, are attributed to the adsorption process which is accompanied by an increase in order of the system due to the adsorption of the composites on the metal surface **(Gomma *et al.*, 1994).**

4.12 Electrochemical Measurements

Evaluation of inhibition efficiency (%) can also be performed through electrochemical experiments. Electrochemical measurements were carried out using Electrochemical Analyser Solartron -1284 B. Linear Polarization measurements, tafel intercept and electrochemical impedance measurements are carried out for mild steel acid corrosion in the presence of polyvinyl alcohol-selected amino acid composites to predict the nature of the inhibitor- anodic, cathodic or mixed type and to predict a suitable mechanism for inhibition process.

4.12.1 Potentiodynamic Polarization Studies of mild steel in the presence of PVAALA and PVAVAL composites

The potentiodynamic polarization curves of mild steel in 1M HCl with the addition of various concentrations of PVAALA and PVAVAL composites are shown in figure-33 respectively. The corrosion kinetic parameters such as corrosion potential (E_{corr}), corrosion current density (I_{corr}), anodic tafel slope (b_a) and cathodic tafel slope (b_c) deduced from the curves are represented in table-28. The corrosion current density values decreased from 6839.9 $\mu A/cm^2$ of the blank acid to 503.4 and 661.9 $\mu A/cm^2$ respectively for the addition of 0.6% of PVAALA and PVAVAL composites resulting in 92.6% and 90.3 % of inhibition efficiencies. As in the case of weight loss method, the increase in concentration of the inhibitor decrease the I_{corr} values. E_{corr}, b_a, b_c values do not change appreciably with the addition of the inhibitor indicating that the inhibitor is interfering the anodic dissolution or cathodic hydrogen evolution reactions thus acts as a mixed type inhibitor. Moreover, these inhibitors cause no change in the anodic and cathodic tafel slopes, indicating that the inhibitors are first adsorbed onto mild steel surface and therefore impedes by merely blocking the reaction sites of mild steel surface without affecting the anodic and cathodic reaction mechanism **(Brandt *et al.*, 1970).**

Polarisation resistance values (R_p) obtained from the Linear polarization resistance (LPR) method (table-28) showed a steep increase in value from 1.7 ohm/cm^2 for that of blank to 24.0 and 23.2 ohm/cm^2 for the addition of the highest

concentrations of PVAALA and PVAVAL respectively .In accordance with weight loss and tafel polarization methods PVAALA performs better than PVAVAL for a particular concentration added .Increase in R_p with concentration infer that the polymer composites inhibit corrosion of mild steel by adsorption process. Maximum increase in R_p values was noticed at 0.6% in by furnishing a maximum of 93 % in both PVAALA and PVAVAL composites. Increase in inhibition efficiencies with increasing concentration of PVAALA and PVAVAL composites reveals that inhibition action is due to the adsorption on mild steel surface and the adsorption is known to depend on the chemical structure of inhibitors **(Eddy *et al.*, 2010).**

Figure -33 Potentiodynamic Polarization curves for mild steel in 1M HCl in absence and presence of different concentration of PVAALA / PVAVAL composites

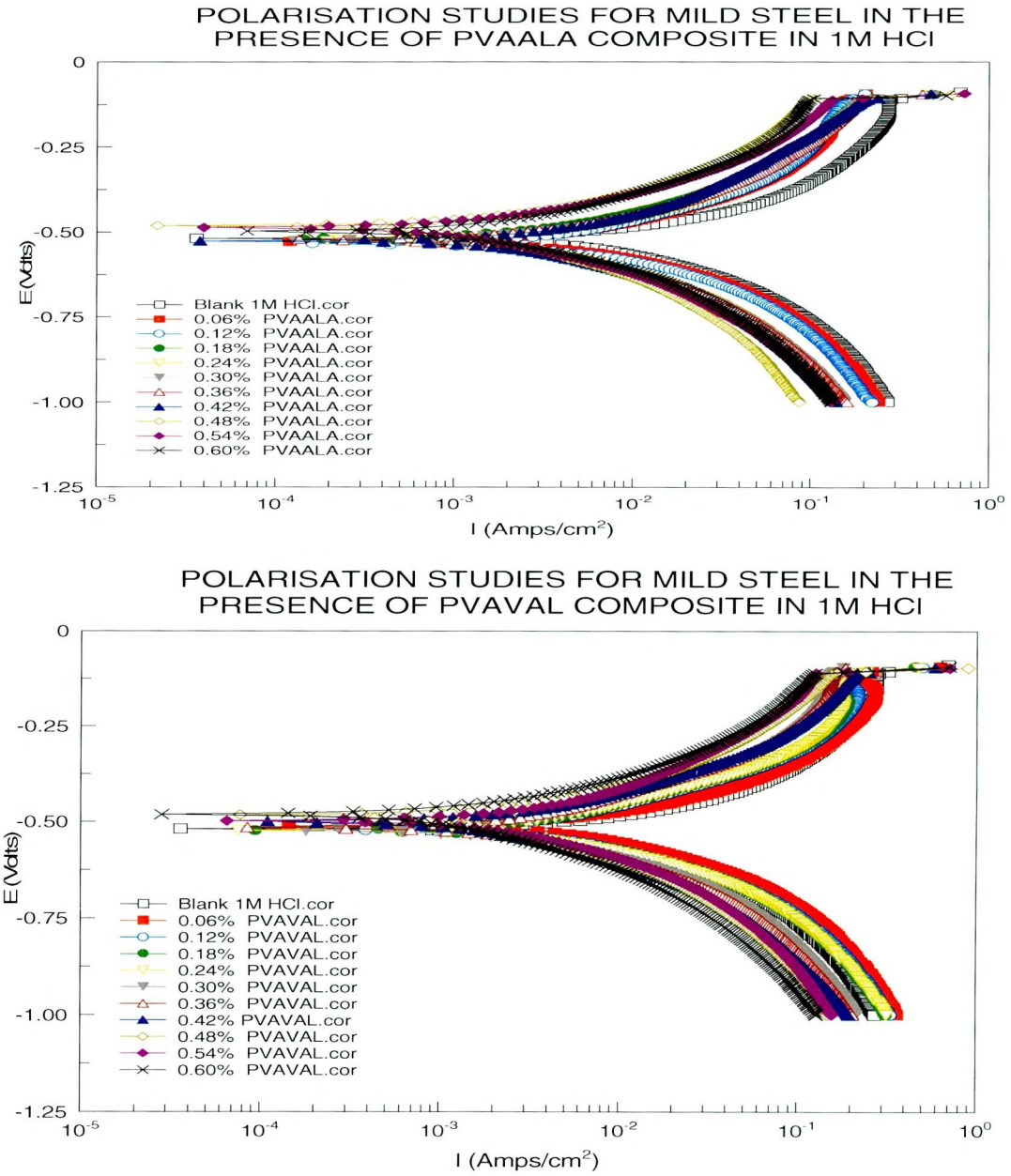

Table-28 Potentiodynamic polarisation parameters for the corrosion of mild steel in 1M HCl in absence and presence of different concentration of PVAALA/PVAVAL composites

S.No.	Conc. of inhibitor in (%) PVAALA	Tafel polarisation parameters					Linear polarisation resistance parameters	
		$-E_{corr}$ mV/ SCE	I_{corr} $\mu A/cm^2$	b_a mV/dec	b_c mV/dec	IE (%)	R_p Ohm/cm^2	IE (%)
1.	Blank	522.6	6839.9	109	114	-	1.73	-
2.	0.06	527.4	3820.4	96	116	44.1	5.88	70.5
3.	0.12	531.8	2077.6	115	85	69.6	6.11	71.6
4.	0.18	523.9	1926.0	63	92	71.8	8.92	80.6
5.	0.24	521.8	1565.1	103	83	77.1	10.75	83.9
6.	0.30	517.1	1125.7	84	89	83.5	11.05	84.3
7.	0.36	519.8	1009.6	80	76	85.2	11.13	84.4
8.	0.42	498.4	849.1	62	87	87.6	14.23	87.8
9.	0.48	481.0	781.2	104	67	88.6	17.45	90.1
10.	0.54	495.7	753.6	64	79	89.0	17.55	90.1
11.	0.60	485.5	503.4	106	92	92.6	23.97	92.8

S.No.	Conc. of inhibitor in (%) PVAVAL	Tafel polarisation parameters					Linear polarisation resistance parameters	
		$-E_{corr}$ mV/ SCE	I_{corr} $\mu A/cm^2$	b_a mV/dec	b_c mV/dec	IE (%)	R_p Ohm/cm^2	IE (%)
1.	Blank	522.7	6839.9	109	114	-	1.73	-
2.	0.06	510.1	4940.9	112	80	27.8	4.07	57.4
3.	0.12	518.8	2743.7	71	86	59.9	6.07	71.4
4.	0.18	522.1	2605.8	68	102	61.9	7.11	75.6
5.	0.24	522.1	2399.7	69	92	64.9	7.32	76.3
6.	0.30	514.0	1527.4	92	103	77.7	7.76	77.6
7.	0.36	520.0	1877.4	96	95	72.6	8.20	78.8
8.	0.42	496.7	1153.7	75	53	83.1	11.71	85.2
9.	0.48	497.7	667.5	68	54	90.2	14.41	88.0
10.	0.54	480.5	697.5	86	50	89.8	16.92	89.7
11.	0.60	480.3	661.9	93	57	90.3	23.18	92.5

4.12.2 Potentiodynamic Polarization Studies of mild steel in the presence of PVAGLU and PVAGLN composites

Polarisation curves of mild steel electrode in 1M HCl without and with the addition of PVAGLU and PVAGLN composites at different concentrations are shown in figure-34. The values of various electrochemical parameters derived by tafel polarization of PVAGLU and PVAGLN composites are given in the tables-29. As it can be seen, both cathodic and anodic reactions of mild steel electrode corrosion were inhibited by the increase of PVAGLU and PVAGLN composites concentrations in 1M HCl suppressed the cathodic reaction as well as the anodic reactions. This

result suggests that the addition of PVAGLU and PVAGLN composites reduce anodic dissolution and also retard the hydrogen evolution reaction. Tafel lines of nearly equal slopes were obtained indicating that the hydrogen evolution reaction was activation-controlled.

Values of corrosion current density (I_{corr}) are enlisted in table-29. The data show that the I_{corr} values decrease considerably in the presence of PVAGLU and PVAGLN composites and decrease with increasing inhibition concentration. Analysis of the values of I_{corr} described in the table-29 highlight a maximum decrease in I_{corr} value at 0.6% in the presence of PVAGLU and PVAGLN composites, thus furnishing maximum IE of 99% and 98.5% in the presence of PVAGLU and PVAGLN composites respectively.

No definite trend was observed in the shift of E_{corr} values, in the presence of various concentrations of these inhibitors in 1M HCl solution. It could be obversed from the table-29 that the E_{corr} values are shifted slightly towards negative side in presence of inhibitors suggesting that the inhibitors inhibit the corrosion of mild steel in acid solution by controlling both anodic and cathodic reactions due to the blocking active sites on the metal surface. It is evident the inhibitors bring about considerable polarization of the cathode as well as anode. It was, therefore, inferred that the inhibitive action is of mixed type. The non-constancy of tafel slopes for different inhibitors concentration reveal that the inhibitor action due to the interference in the mechanism of the corrosion processes at cathode as well as anode. From the polarisation curves, it can be inferred that PVAGLU and PVAGLN composites acted as mixed type inhibitors. Decrease of the corrosion current (I_{corr}) was associated with an appreciable shift of corrosion potential (E_{corr}) to a less negative value. This suggests that though inhibition is of mixed type, it is predominantly anodic **(Samide *et al.*, 2005).**

Linear polarisation resistance (R_p) of mild steel in the absence and presence of PVAGLU and PVAGLN composites are listed in the table-29. From R_p values, it can be inferred that as the concentration of PVAGLU and PVAGLN composites increase, the R_p values also increased. Maximum increases in Rp value at 0.6% infer that the PVAGLU and PVAGLN composites inhibit corrosion of mild steel by adsorption process. Maximum inhibitor efficiencies of PVAGLU and PVAGLN composites were found to be 93 % in both cases. This suggests that the inhibiting action of these compounds occurs by simple blocking at the electrode.

From the results accounted in tables-29, an increase of IE with inhibitor concentrations, reaching a maximum value of 0.6% for both inhibitors was observed, but better performances were obtained by PVAGLU. It can be concluded that the

ability of the molecule to adsorb on the iron surface was dependant on the position of nitrogen and oxygen atom on the PVAGLU and PVAGLN composites. These results are comparable with those calculated from weight loss measurements in tables -29, but a little difference can be observed. This difference can be attributed to the fact that the gravimetric method gives average corrosion rates, whereas the polarisation method gives instantaneous corrosion rates **(Muralidhran *et al.*, 1995)**

Table -29 Potentiodynamic polarisation parameters for the corrosion of mild steel in 1M HCl in absence and presence of different concentration of PVAGLN/PVAGLU composites

S.No.	Conc. of inhibitor in (%) PVAGLN	Tafel polarisation parameters					Linear polarisation resistance parameters	
		$-E_{corr}$ mV/ SCE	I_{corr} μA/cm^2	b_a mV/dec	b_c mV/dec	IE (%)	R_p Ohm/cm^2	IE (%)
1.	Blank	522.7	6839.9	109	114	-	1.7	-
2.	0.06	527.5	2845.9	82	108	58.4	4.2	58.2
3.	0.12	531.4	2389.2	74	110	65.1	8.1	78.6
4.	0.18	531.4	1818.1	57	84	73.4	8.2	78.9
5.	0.24	534.7	1585.2	72	90	76.8	9.6	81.9
6.	0.30	527.4	1293.1	80	92	81.1	10.5	83.5
7.	0.36	524.5	988.9	64	91	85.5	13.5	87.1
8.	0.42	514.8	967.5	109	82	85.9	14.3	87.9
9.	0.48	496.0	990.8	103	63	85.5	14.1	87.7
10.	0.54	488.2	673.4	93	49	90.2	22.9	92.4
11.	0.60	488.3	99.3	34	23	98.5	25.5	93.2

S.No.	Conc. of inhibitor in % PVAGLU	Tafel polarisation parameters					Linear polarisation resistance parameters	
		$-E_{corr}$ mV/ SCE	I_{corr} μA/cm^2	b_a mV/dec	b_c mV/dec	IE (%)	R_p Ohm/cm^2	IE (%)
1.	Blank	522.7	6839.9	109	114	-	1.7	-
2.	0.06	523.7	2115.7	74	106	72.7	4.7	62.9
3.	0.12	526.9	1867.9	69	84	69.1	8.5	79.5
4.	0.18	529.3	1643.3	101	108	76	9.0	80.6
5.	0.24	528.3	1898	112	118	72.3	9.1	81
6.	0.30	526.8	1734.7	72	94	74.6	9.8	82.2
7.	0.36	517.8	1260.9	112	65	81.6	10.7	83.7
8.	0.42	515.7	993.4	96	73	85.5	16.3	89.3
9.	0.48	519.1	519.1	108	59	92.4	21.0	91.7
10.	0.54	484.4	427.0	49	98	93.8	21.2	91.8
11.	0.60	482.9	63.8	88	49	99	24.2	92.8

Figure -34 Potentiodynamic Polarization curves for mild steel in 1M HCl in absence and presence of different concentration of PVAGLN/ PVAGLU composites

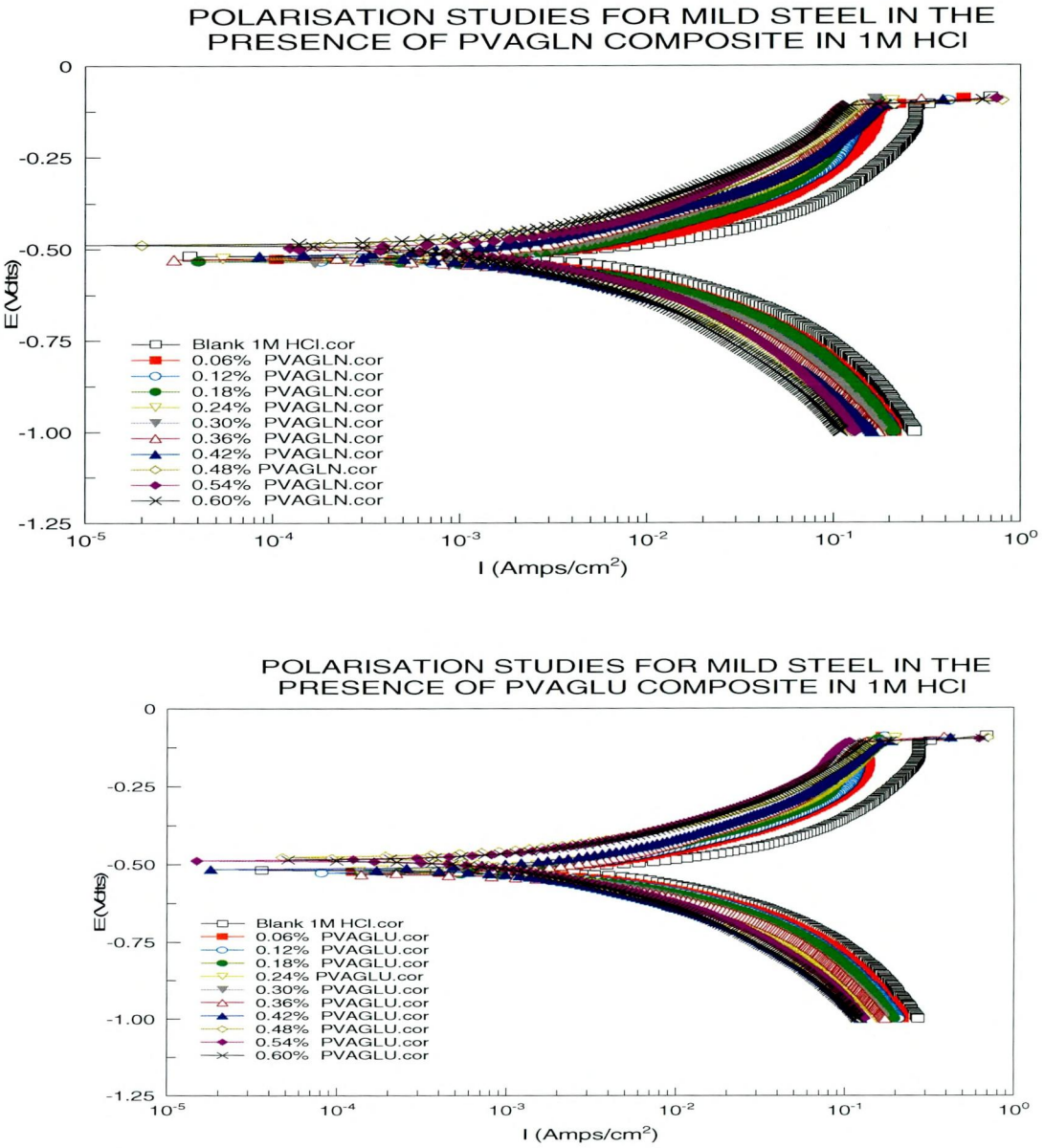

4.12.3 Potentiodynamic Polarization Studies of mild steel in the presence of PVATRP and PVATYR composites

The Tafel polarisation behaviour of mild steel in 1M HCl with the addition of various concentrations of PVATRP and PVATYR composites are shown in figure -35. The kinetic corrosion parameters derived from these curves are presented in table-30. From the tables-30 it is clear that the corrosion current value (I_{corr}) of mild steel decreases with the addition of PVATRP and PVATYR composites in 1M HCl medium. The I_{corr} values decrease considerably in the presence of different concentrations of inhibitors increased. The results show that the inhibitors bring down

I_{corr} value at all concentration and maximum decrease of I_{corr} value was obtained at 0.6% of the inhibitors concentration in IM HCl. It is obvious from the polarisation curves that both anodic as well cathodic curves shift indicating that the inhibitors act in such a manner that both anodic as well as cathodic reactions are influenced by it simultaneously almost to the same extent showing a mixed nature of inhibitors.

Electrochemical parameters and inhibitor efficiency (IE%) for different concentrations are given in table-30. The E_{corr} values are slightly shifted in the presence of inhibitors suggesting that these inhibitors inhibit the corrosion of mild steel in 1M HCl by colltrolling both the anodic and cathodic reactions. In addition no significant change in E_{corr} value was observed with suggests a mixed mode of inhibition.

Anodic and cathodic reaction mechanisms are not affected by the inhibitors because anodic and cathodic tafel slopes do not change appreciably in the presence of the inhibitors. The anodic (b_a) and cathodic (b_c) tafel slopes are approximately constant suggesting the inhibiting action of both PVATYR and PVATRP composites by adsorption at the metal surface according to blocking adsorption mechanism. Hence the both PVATYR and PVATRP composites decrease the surface area available for anodic dissolution and cathodic hydrogen evolution reaction without affecting the reaction mechanism. In the case of PVATYR and PVATRP composites the tafel slope values ba and bc remain almost constant, indicating that they are mixed type of inhibitors.

Linear polarisation resistance (R_p) of mild steel in the absence and presence of PVATYR and PVATRP composites are listed in the table -30. From R_p values, it can be inferred that as the concentration of PVATYR and PVATRP composites increase, the R_p values also increased. Maximum increase in R_p value at 0.6% indicates that the PVATYR and PVATRP composites inhibit corrosion of mild steel by adsorption process. Polarisation resistance values presented in the tables-30 with and without the addition of PVATRP and PVATYR composites describe that the values of R_p increases from 1.7 (blank) to 34.8 ohm/cm^2 and 12.41 ohm/ cm^2 in the presence of PVATRP and PVATYR composites respectively. Inhibition performance of PVATRP and PVATYR composite were found to be 95 and 86 % respectively.

Figure shows the Tafel polarisation curves for mild steel in 1M HCl with the addition of various concentrations of PVATRP and PVATYR composites. The important corrosion parameters obtained from the table -30 shows that the corrosion current density values decrease from 3798.7 to 290.1 μA/cm^2 with the addition of higher concentration of PVATRP composite (0.6%) and from 4142.1 to 910.6 μA/cm^2

with the addition of higher concentration of PVATRP composite (0.6%). The adsorbed inhibitors may form a surface film which acts as a physical barrier to restrict diffusion of ions to or from the metal surface and hence retard the corrosion process. The interactions of the adsorbed inhibitors with surface metal atoms may prevent the metal atoms from participating the cathodic and anodic reaction of corrosion. This simple blocking effect decreases the number of surface metal atoms participating and hence decreases corrosion. Surface coverage is proportional to the inhibition efficiency. The protective effect of the inhibitors is probably due to formation of an insoluble film. Hence the mechanism of the inhibitive action is possibly due to the blocking of cathodic and anodic sites by adsorption, which enables the formation of a protective insoluble film. The increase in inhibition efficiency may be due to the blocking effect of the surface by both adsorption and film formation mechanism which decreases the effective area of attack. The compounds in the present study contain both N and O atoms and exhibit excellent performance on the corrosion of mild steel in 1M HCl, even at a concentration as low as 0.6%. It is also observed that inhibitive power of PVATRP composite in reducing corrosion of mild steel in 1M HCl acid is comparatively higher than that of PVATYR composite. The maximum IE was observed in the case of PVATRP, indicating that PVATRP is a more effective corrosion inhibitor than PVATYR. The highest IE exhibited by these compounds may be attributed to their adsorption on the metal surface through polar groups. This leads to greater coverage of the metal surface by the compounds, there by resulting in higher inhibition efficiency (**Divakarashetty Shetty *et al.*, 2006**).

Table-30 Potentiodynamic polarisation parameters for the corrosion of mild steel in 1M HCl in absence and presence of different concentration of PVATYR/PVATRP composites

S.No.	Conc. of inhibitor in PVATYR	Tafel polarisation parameters					Linear polarisation resistance parameters	
		$-E_{corr}$ mV/ SCE	I_{corr} $\mu A/cm^2$	b_a mV/dec	b_c mV/dec	IE (%)	R_p Ohm/cm^2	IE (%)
1.	Blank	522.7	6839.9	109	114	-	1.7	-
2.	0.06	534.5	4142.1	120	112	39.4	3.6	51.9
3.	0.12	537.3	2986.1	83	115	56.3	6.6	73.8
4.	0.18	536.7	2814.9	118	115	58.8	7.6	77.2
5.	0.24	535.7	2634.8	111	109	61.5	7.8	77.7
6.	0.30	538.1	2269.8	75	98	66.8	8.1	78.7
7.	0.36	531.1	1967.8	79	84	71.2	8.4	79.4
8.	0.42	531.0	1442.1	65	67	78.9	9.3	81.4
9.	0.48	497.8	1357.8	61	70	80.1	9.6	81.9
10.	0.54	485.7	1238.3	96	80	81.9	12.0	85.6
11.	0.60	482.8	910.6	64	45	86.7	12.4	86.0

S.No.	Conc. of inhibitor in % PVATRP	Tafel polarisation parameters					Linear polarisation resistance parameters	
		$-E_{corr}$ mV/ SCE	I_{corr} µA/cm^2	b_a mV/dec	b_c mV/dec	IE (%)	R_p Ohm/cm^2	IE (%)
1.	Blank	522.7	6839.9	109	114	-	1.7	-
2.	0.06	521.9	3798.7	116	103	44.5	4.8	63.8
3.	0.12	523.0	2683.1	95	70	61.5	6.1	71.4
4.	0.18	520.0	2206.2	84	64	67.7	7.0	75.0
5.	0.24	536.3	2036.1	80	75	70.2	7.9	78.0
6.	0.30	536.3	1754.5	72	63	74.3	8.0	78.2
7.	0.36	528.0	1276.1	84	52	81.3	8.2	78.9
8.	0.42	517.4	1173.9	47	46	82.8	8.6	79.7
9.	0.48	502.6	988.0	92	102	85.6	20.4	91.5
10.	0.54	500.5	882.9	119	93	87.1	23.3	92.5
11.	0.60	486.8	290.1	83	32	95.8	34.8	95.0

Figure -35 Potentiodynamic Polarization curves for mild steel in 1M HCl in absence and presence of different concentration of PVATYR and PVATRP composites

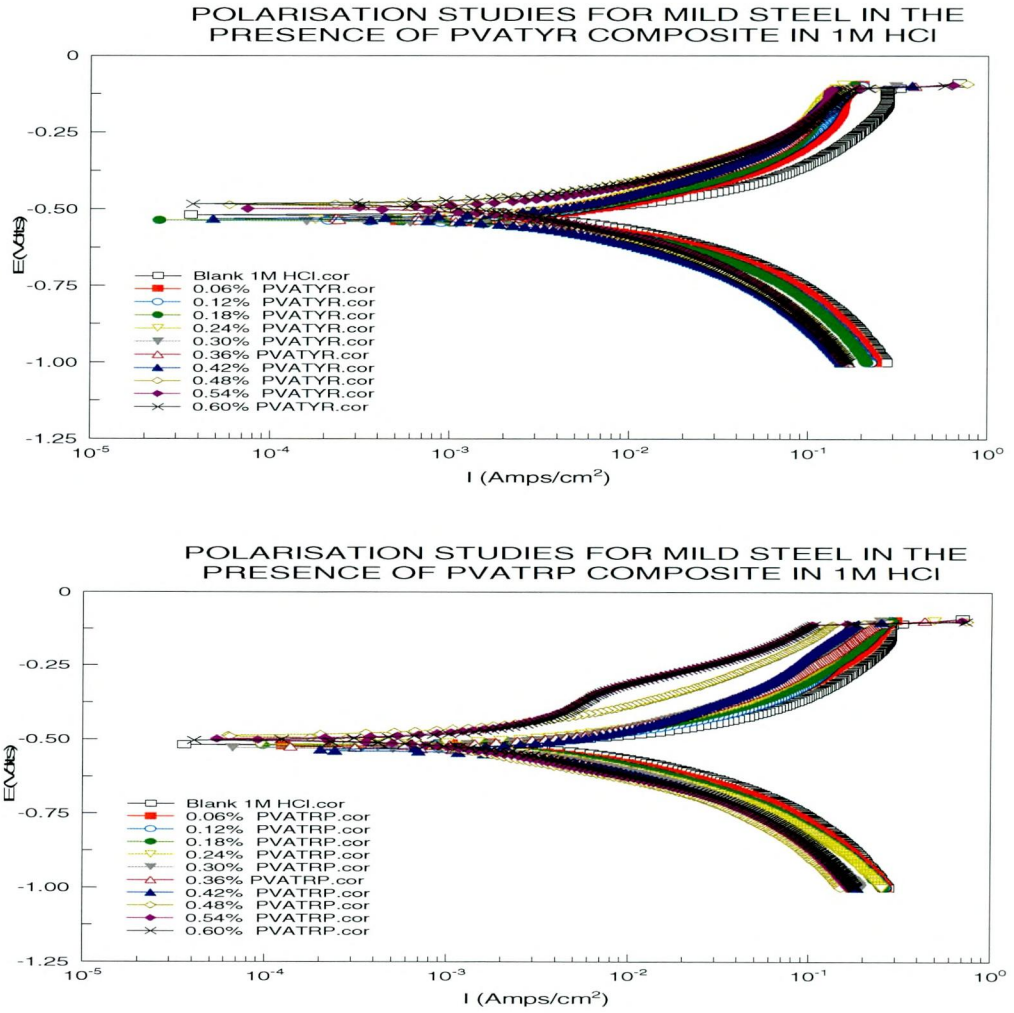

Figure-36 Plot of I_{corr} and R_p with respect to concentrations of polymer composites

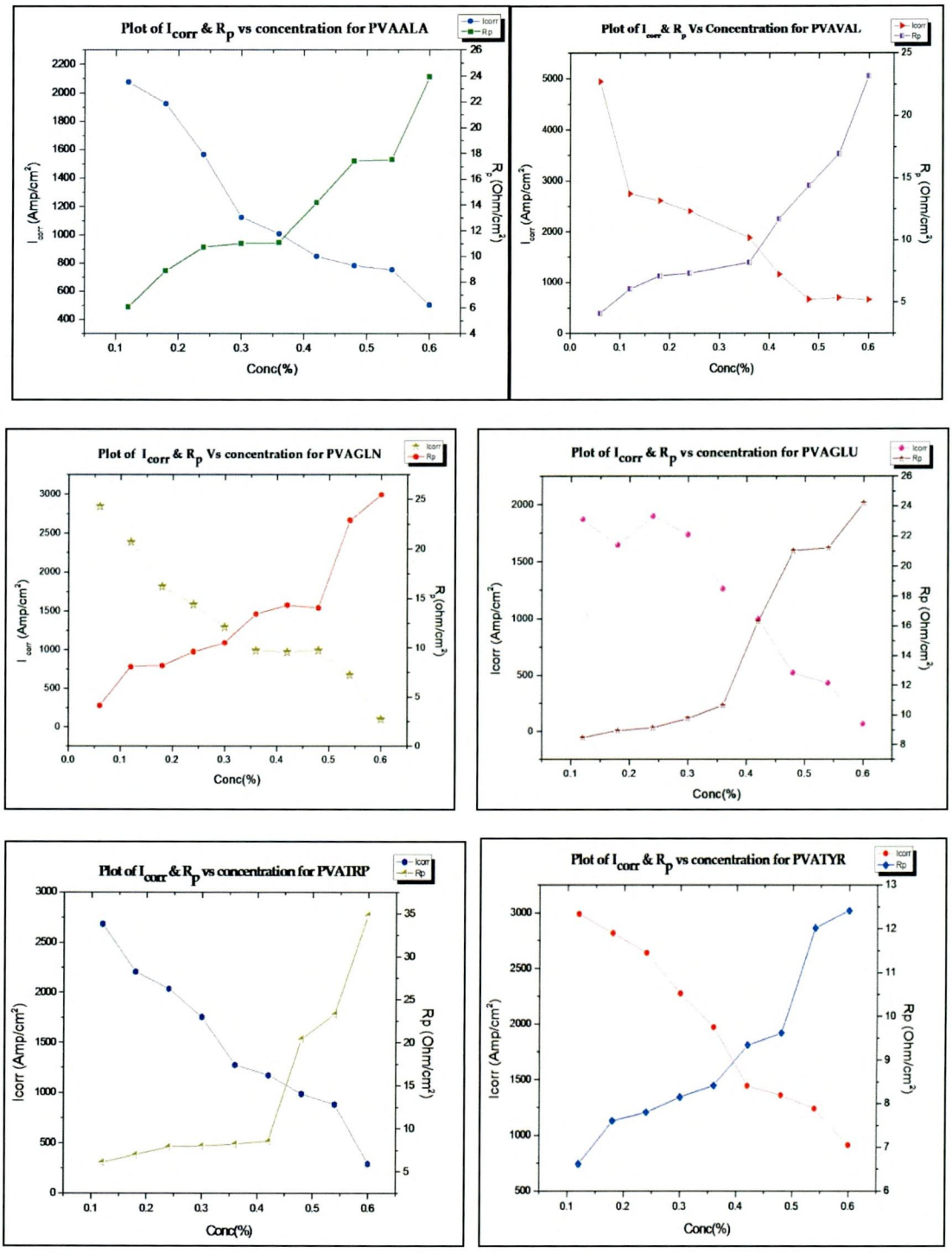

Decrease in Values of I_{corr} and Increase in values of R_p of Mild Steel in the presence of studied inhibitors in both acidic media are pictorially represented in the Figure-36.

4.12.4 Electrochemical Impedance spectroscopy Studies of mild steel in the presence of PVAALA and PVAVAL composites

The Nyquist diagram representation of electrochemical impedance spectroscopic values of mild steel in 1M HCl containing different concentrations of PVAALA and PVAVAL composites are presented in figure-37.

These plots having the shape of semicircle indicate the activation controlled nature of the reactions with single charge transfer process. The existence of depressed nature of semicircle with its centre below the x axis is the characteristics of solid electrodes and is attributed to the increased micro roughness of surface and other inhomogeneities of solid electrode during corrosion **(Sathiyanarayanan *et al.*, 2005a).** The diameter of the semicircle gives the charge transfer resistance R_{ct} equivalent to the polarization resistance R_p which is inversely proportional to the corrosion rate. With the increase in concentration of PVAALA and PVAVAL composites the charge transfer resistance increases .The charge transfer resistance and the interfacial double layer capacitance C_{dl} derived from these curves are summarised in table 31. R_{ct} increase from the value 20.5 ohms for the blank acid to 195.4 and 167.8 ohms for the highest concentrations of PVAALA and PVAVAL composites respectively. Analysis of the data presented in the table-31 reveal maximum of 89.6 and 87.9 % of IE were afforded by PVAALA and PVAVAL polymer composites respectively.

The interfacial double layer capacitance C_{dl} decreases from 3245.0 μF/cm^2 for the blank to 813.9 and 788.2 μF/cm^2 for PVAALA and PVAVAL respectively. Inspection of the data in table 31 infer that the surface coverage of PVAALA and PVAVAL composites on mild steel surface were found to be 0.75 and 0.76 respectively. Decrease in C_{dl} which can result from a decrease in local dielectric constant, and / or a increase in thickness of the electrical double layer, suggests that the PVAALA and PVAVAL composites function by adsorption at the metal- solution interface **(McCafferty *et al.*, 1972).** The change in R_{ct} and C_{dl} values was caused by the gradual replacement of water molecules by the anions of the acid and adsorption of the PVAALA and PVAVAL composites on the metal surface, reducing the extent of dissolution **(Tamil selvi *et al.*, 2003).** The electrochemical experiments reveal that the inhibition efficiencies obtained from electrochemical impedance spectroscopy and potentiodynamic polarization are in reasonably agreement.

Table -31 Impedance parameters for corrosion of mild steel in 1M HCl in the absence and presence of different concentrations of PVAALA/PVAVAL/PVAGLN composites at 303K

s.no	Conc. Of inhibitor in % PVAALA	I_{corr} $\mu A\ cm^{-2}$	IE (%)	R_{ct} (Ohms)	IE (%)	C_{dl} $\mu F/cm^2$	θ
1.	Blank	1187270.5	-	20.4	-	3245.0	-
2.	0.06	943714.8	20.5	24.2	15.7	3229.5	0.0048
3.	0.12	723249.8	39.1	29.3	30.6	3187.4	0.0178
4.	0.18	517444.3	56.4	31.4	35.1	3031.7	0.0657
5.	0.24	428219.7	63.9	46.6	56.3	1238.7	0.6182
6.	0.30	335595.8	71.7	55.9	63.6	1230.7	0.6207
7.	0.36	276123.0	76.7	61.3	66.7	1223.6	0.6229
8.	0.42	241406.9	79.7	65.1	68.7	1098.4	0.6615
9.	0.48	138795.7	88.3	127.5	84.0	1027.5	0.6834
10.	0.54	95552.6	92.0	160.7	87.3	839.0	0.7414
11.	0.60	109437.4	90.8	195.4	89.6	813.9	0.7492

s.no	Conc. Of inhibitor in % PVAVAL	I_{corr} $\mu A\ cm^{-2}$	IE (%)	R_{ct} (Ohms)	IE (%)	C_{dl} $\mu F/cm^2$	θ
1.	Blank	1187270.5	-	20.4	-	3245.0	-
2.	0.06	837989.5	29.4	24.2	15.7	3083.2	0.05
3.	0.12	643526.3	45.8	26.2	22.3	3058.7	0.057
4.	0.18	616939.1	48.0	28.7	29	2824.8	0.129
5.	0.24	381031.9	67.9	44.9	54.6	1524.7	0.53
6.	0.30	444178.1	62.6	47.5	57.1	1607.8	0.505
7.	0.36	340744.1	71.3	60.8	66.5	1274.5	0.61
8.	0.42	202314.3	83.0	66.7	69.4	1165.0	0.641
9.	0.48	167347.8	85.9	78.1	73.9	1140.1	0.649
10.	0.54	111048.3	90.6	123.6	83.5	983.2	0.697
11.	0.60	91411.2	92.3	167.9	87.9	788.2	0.757

s.no	Conc. Of inhibitor in % PVAGLN	I_{corr} $\mu A\ cm^{-2}$	IE (%)	R_{ct} (Ohms)	IE (%)	C_{dl} $\mu F/cm^2$	θ
1.	Blank	1187270.5	-	20.4	-	3245.0	-
2.	0.06	657047.9	44.7	30.8	33.8	2598.6	0.29
3.	0.12	489921.9	58.7	39.2	48.0	2316.2	0.286
4.	0.18	354495.2	70.1	41.6	51.0	2303.9	0.29
5.	0.24	311567.6	73.8	55.7	63.4	1480.2	0.544
6.	0.30	296788.0	75.0	62.6	67.5	1256.0	0.613
7.	0.36	228330.1	80.8	71.5	71.5	1247.1	0.616
8.	0.42	210947.3	82.2	96.3	78.8	1135.7	0.65
9.	0.48	128793.3	89.2	131.8	84.5	1009.0	0.689
10.	0.54	83486.1	93.0	166.9	87.8	926.03	0.725
11.	0.60	33159.7	97.2	179.7	88.7	826.98	0.745

Figure- 37 Nyquist plots for mild steel in 1M HCl in the absence and presence of different concentration of PVAALA and PVAVAL composites

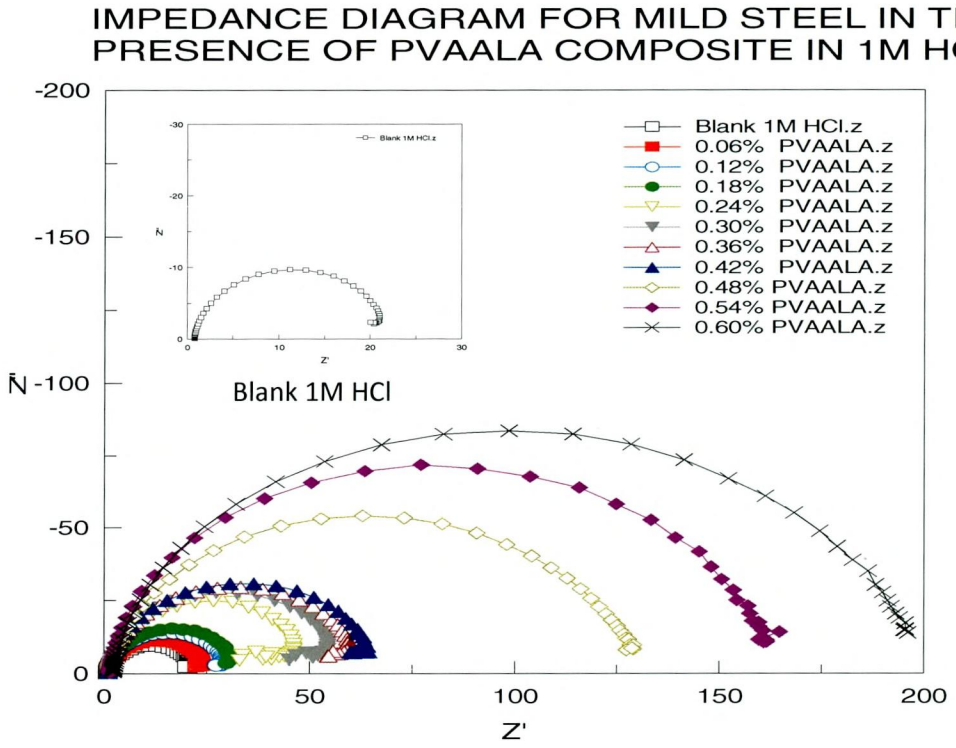

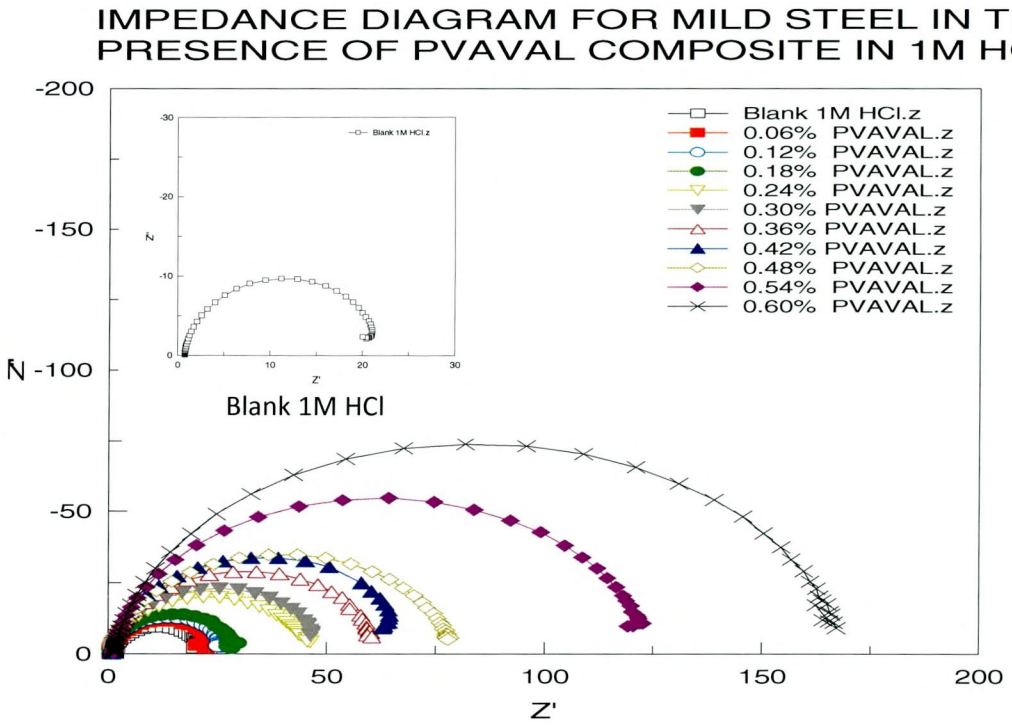

4.12.5 Electrochemical Impedance spectroscopy Studies of mild steel in the presence of PVAGLN and PVAGLU composites

The corrosion behaviour of mild steel in 1M HCl solution in the absence and presence of PVAGLU and PVAGLN composites was also investigated by the electrochemical impedance spectroscopy at 30°C after 30 minutes of immersion. Nyquist plots of mild steel in uninhibited and inhibited acidic solutions (1M HCl) containing various concentrations of PVAGLU and PVAGLN composites are given in figure-38 and table-31, 32.

As it can be seen from the figure-38, the Nyquist plots contain depressed semi circles with the centre under the real axis, whose size increases with the inhibitor concentration, indicating a charge transfer process mainly controlling the corrosion of mild steel. Such behaviour, a characteristic of solid electrodes and often referred to frequency dispersion, has been attributed to roughness and other inhomogeneties of the solid surface. It is apparent, from these plots that the impedance response of mild steel in uninhibited 1M HCl solution has significantly changed after the addition of PVAGLU and PVAGLN composites in the corrosion solutions. This indicated that the impedence of the inhibited substrate has increased with increasing concentration of inhibitors .The characteristic parameters associated to the impedance diagram (R_{ct} and C_{dl}) and IE (%) are given table-31, 32. IE (%) for PVAGLU and PVAGLN has increased with inhibitor concentration. The inhibition efficiencies calculated from AC Impedance results, show the same trend as those obtained from DC Polarisation and weight loss measurements. Comparison of the IE (%) values obtained using those methods show acceptable agreement. The differences are sometimes as high as 5%, but the order of magnitude is the same for all methods.

As it can be seen from table-31, 32, the R_{ct} values increased with the increasing concentration of the inhibitors. On the other hand, the values of C_{dl} decrease with an increase in the inhibitors concentration. This situation was the result of an increase in the surface coverage by the inhibitor which led to an increase in the inhibition efficiency. Values of electrochemical parameters listed in the table-31, 32 reflect the highest inhibition efficiencies of PVAGLU and PVAGLN composites using R_{ct} values (92%for PVAGLU and 89% for PVAGLN). This decrease in the C_{dl}, can result from a decrease in local dielectric constant and /or an increase in the thickness of the electrical double layer, suggest that the PVAGLU and PVAGLN molecules function by adsorption at the metal/solution interface .Thus, the change in C_{dl} values was caused by the gradual replacement of water molecules by the

adsorption of the polymer composites on the metal surface, decreasing the extent of the metal dissolution **(Mc Cafferty *et al.*, 1972).**

Figure- 38 Nyquist plots for mild steel in 1M HCl in the absence and presence of different concentration of PVAGLN and PVAGLU composites

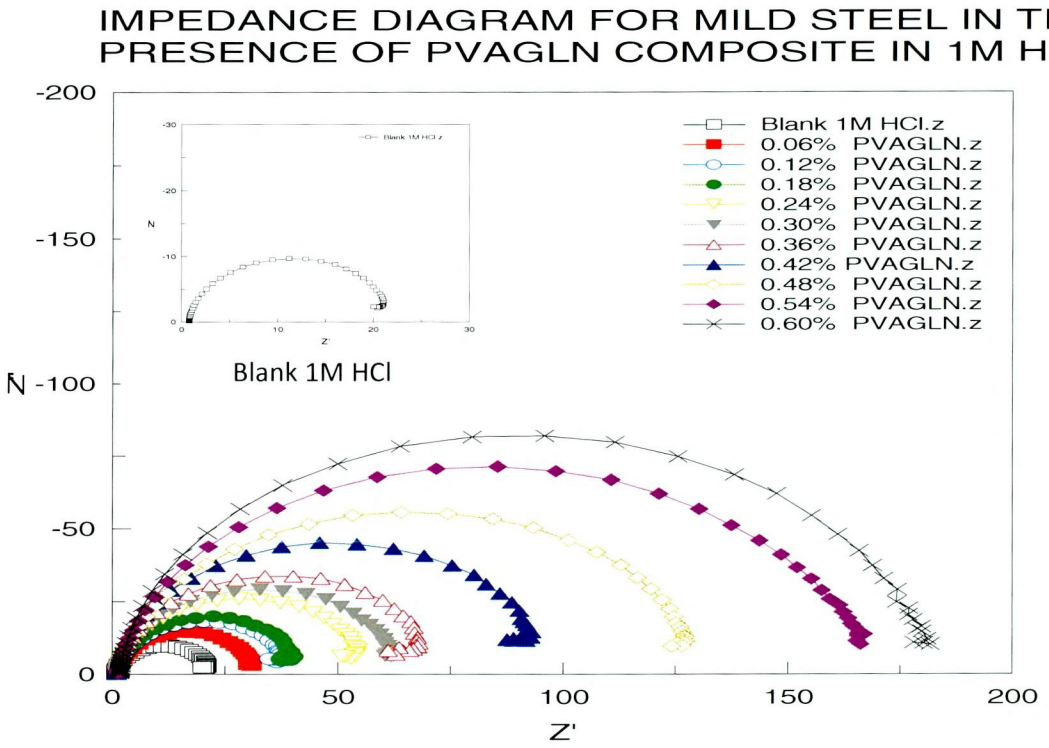

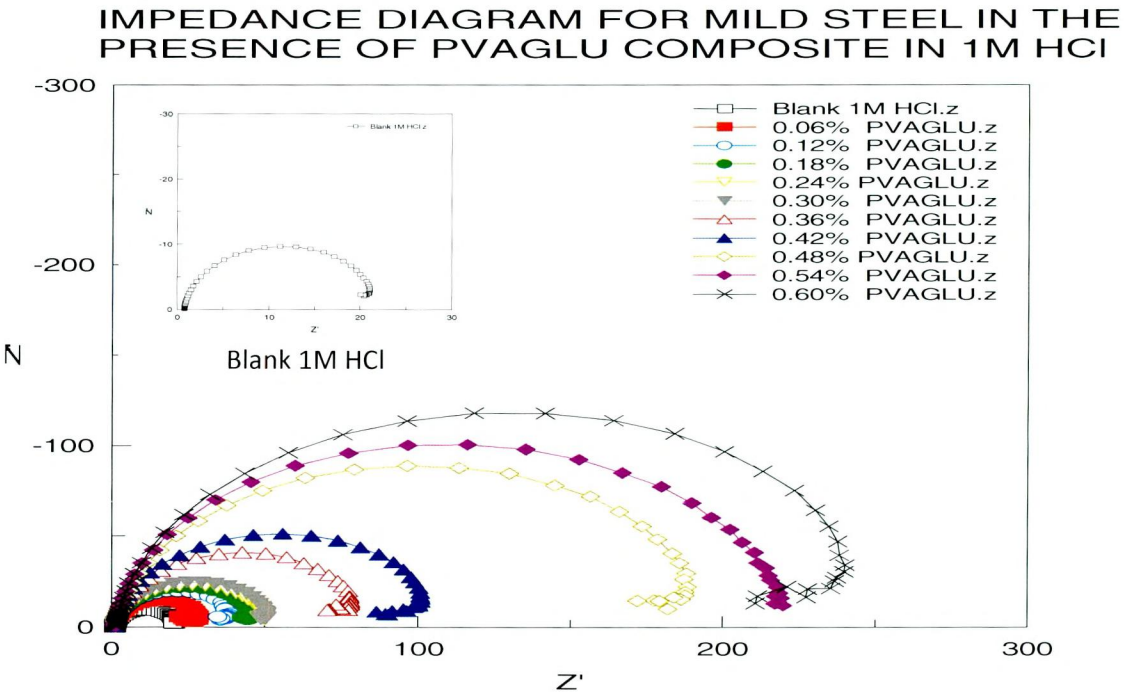

Table-32 Impedance parameters for corrosion of mild steel in 1M HCl in the absence and presence of different concentrations of PVAGLU/PVATYR/PVATRP composites at 303K

s.no	Conc. Of inhibitor in % PVAGLU	I_{corr} ($\mu A\ cm^{-2}$)	IE (%)	R_{ct} (Ohms)	IE (%)	C_{dl} $\mu F/cm^2$	θ
1.	Blank	1187270.5	-	20.4	-	3245.0	-
2.	0.06	650738.7	45.2	29.8	29.9	3014.3	0.071
3.	0.12	412755.5	65.2	39.9	48.9	2935.5	0.095
4.	0.18	489425.3	58.8	46.3	56.0	1975.5	0.391
5.	0.24	492536.9	58.5	50.7	59.8	1970.9	0.393
6.	0.30	342420.2	71.2	51.7	60.6	1728.1	0.468
7.	0.36	220959.7	81.4	80.8	74.8	1055.1	0.675
8.	0.42	170477.6	85.6	105.6	80.7	962.49	0.703
9.	0.48	83891.9	92.9	197.5	80.7	910.41	0.719
10.	0.54	64457.0	94.6	220.1	90.7	874.02	0.731
11.	0.60	53632.8	95.5	254.8	92.0	851.76	0.738

s.no	Conc. Of inhibitor in % PVATYR	I_{corr} $\mu A\ cm^{-2}$	IE (%)	R_{ct} (Ohms)	IE (%)	C_{dl} $\mu F/cm^2$	θ
1.	Blank	1187270.5	-	20.4	-	3245.0	-
2.	0.06	1075166.5	9.4	23.4	12.9	3068.5	0.054
3.	0.12	799400.2	32.7	26.2	22.2	3059.9	0.057
4.	0.18	779247.0	34.4	32.5	37.2	2677.0	0.175
5.	0.24	671822.2	43.4	35.5	42.7	1750.5	0.461
6.	0.30	481141.2	59.5	38.3	46.8	1411.7	0.565
7.	0.36	336147.5	71.7	52.6	61.2	1357.5	0.582
8.	0.42	264363.3	77.7	54.1	62.4	1291.3	0.602
9.	0.48	190624.1	83.9	74.2	72.6	1204.6	0.629
10.	0.54	180436.3	84.8	105.0	80.6	1059.0	0.674
11.	0.60	101773.0	91.4	112.7	81.9	1021.7	0.685

s.no	Conc. Of inhibitor in % PVATRP	I_{corr} $\mu A\ cm^{-2}$	IE (%)	R_{ct} (Ohms)	IE (%)	C_{dl} $\mu F/cm^2$	θ
1.	Blank	1187270.5	-	20.4	-	3245.0	-
2.	0.06	884665.4	25.5	26. 8	23.9	3297.4	0.016
3.	0.12	591383.8	50.2	29.6	31.1	2522.4	0.223
4.	0.18	503788.5	57.6	31.3	34.9	2480.2	0.236
5.	0.24	490583.5	58.7	34.3	40.5	2224.8	0.317
6.	0.30	419363.8	64.7	34.8	41.4	2216.1	0.382
7.	0.36	377061.7	68.2	37.0	44.9	2004.2	0.387
8.	0.42	247132.2	79.2	40.8	50.1	1988.6	0.451
9.	0.48	206605.7	82.6	101.7	80	1781.0	0.451
10.	0.54	179386.8	84.9	126.4	83.9	1529.8	0.529
11.	0.60	51821.6	95.6	193.5	89.5	1439.4	0.556

On the basis of these results, one can conclude that the anodic dissolution process is more strongly affected by the addition of PVAGLU and PVAGLN composites than is the cathodic process. Therefore, the inhibition via the formation of metal-polymer complexes can be expected. Furthermore, the fact that the dissolution of metals is generally inhibited by the polymer composites additives explains the formation of scarcely-soluble complexes on the metal surface. On the other hand, the variation of the inhibition efficiency of the investigated polymer composites. It was also notified that PVAGLU and PVAGLN composites has much greater adsorb ability on the electrode surface. This behaviour could be ascribed to the close packed film formation on the metal surface by PVAGLU and PVAGLN composites. Therefore, one can suggest that a very strong and poorly conducting films is formed on the metal surface in the presence of the additive in question. The observed small shift in corrosion potential (E_{corr}) in the presence of all examined PVAGLU and PVAGLN composites does not reflect any specific interaction although these inhibitors decrease C_{dl} and increase R_p values .This suggests that the inhibiting action of these compounds occurs by simple blocking at the metal surface at the electrode **(Sayed, 1996)**.

4.12.6 Electrochemical Impedance Spectroscopy (PVATYR and PVATRP composites)

The Nyquist representation of the impedance behaviour of mild steel in 1M HCl with and without addition of various concentration of PVATRP and PVATYR composites are given in figure-39. The existence of single semi - circle showed that the single charge transfer process during dissolution which is unaffected by the presence of inhibitor molecules. It is seen that addition of PVATRP and PVATYR composites increases the value of R_{ct} and reduces the value of of C_{dl}. The decrease in C_{dl} is attributed to increase in thickness of electronic double layer. The increase in R_{ct} value is attributed to the formation of protective film on the metal/ solution interface. These observations suggest that PVATRP and PVATYR composites function by adsorption at the metal surface thereby causing the decrease in C_{dl} values and increase in R_{ct} values. The charge transfer resistance (R_{ct}) and the interfacial double layer capacitance (C_{dl}) derived from these curves are given in table-32.

The impedance studies of mild steel in 1M HCl containing PVATRP and PVATYR composites in concentration range 0.06-0.6% are conducted. Figure-39 show the Nyquist plot for mild steel in 1M HCl containing PVATRP and PVATYR composites. The charge transfer resistance values and the double layer capacitance values calculated from the impedance diagram are given in table-32. It is found that

R_{ct} values increases steadily from 26.7 (23.3) to 193.5 (112.7) ohms of PVATRP and PVATYR composites with increased inhibitor concentration from 0.06% to 0.6%, which shows that the inhibition is due to surface adsorption. It is also observed that C_{dl} values decreases from 3297.4(3068.5) μFCm^{-2} to 1439.4 (1021.7) μFCm^{-2} of PVATYR and PVATRP composites with increase in inhibitor concentration, which show that the inhibition is due to be surface adsorption. Maximum inhibition efficiencies of PVATRP and PVATYR composites were noticed using R_{ct} values and the surface coverage values were found to be 0.56 and 0.69 in the presence of PVATRP and PVATYR composites respectively.

The inhibitive property of PVATRP and PVATYR composites is also due to the presence of π electron, quaternary Nitrogen atom and the larger molecular size which ensures greater coverage of the metallic surface. The adsorption of PVATRP and PVATYR composite molecules on the metal surface in the form of (i) a neutral molecule via chemisorption mechanism involving the sharing of electrons between Nitrogen and iron atoms or (ii) the adsorption occurs through π electrons interaction with the metal surface (**Manivel *et al.*, 2004**). It is clear from the data that percentage inhibition efficiency values from electrochemical measurements are in good agreement with those obtained from weight loss methods.

Figure-39 Nyquist plots for mild steel in 1M HCl in the absence and presence of different concentration of PVATYR and PVATRP composites

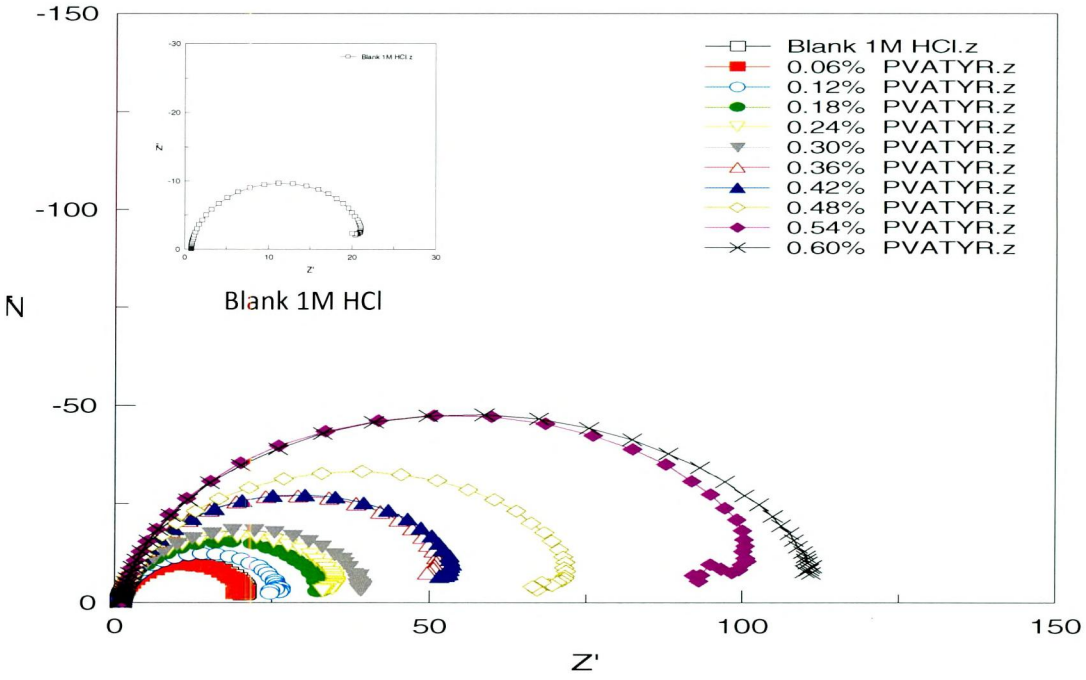

IMPEDANCE DIAGRAM FOR MILD STEEL IN THE PRESENCE OF PVATRP COMPOSITE IN 1M HCl

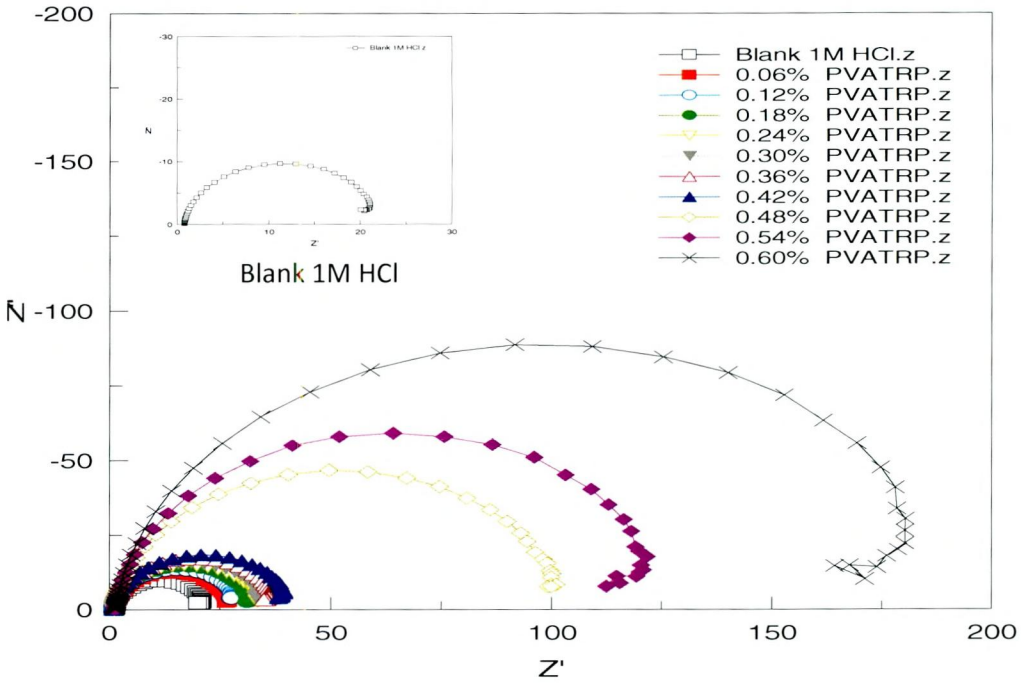

According to the electrochemical theory, R_{ct} is inversely proportional to the corrosion current density (i,e corrosion rate), so it is analogous to the use of polarisation resistance in the stern – Geary equation.

$$I_{corr} = \frac{\beta'}{R_{ct}} \qquad (53)$$

Where $\beta = b_a\, b_c / 2.303 \times R_{ct} \times (b_a + b_c)$

In this work impedance and polarization methods are also correlated. Thus, the corrosion current densities were determined by using the stern-grey equation. These values of R_{ct} have been substituted in the Stern- grey equation to obtain the corrosion current as shown in table-31-32 of polymer composite inhibitors.

As it can be seen from table-31,32, the R_{ct} values increased with the increasing the concentrations of the inhibitors. On the other hand, the values of C_{dl} decreased with an increase in the inhibitors concentration. This situation was the result of an increase of surface coverage by the inhibitor, which led to an increase in the inhibition efficiency (table-31,32). This decrease in the C_{dl}, which can result from a decrease in local dielectric constant and/or an increase in the thickness of the electric double layer suggested that the PVA-selected amino acid composites molecules function by a adsorption at the metal /solution interface. Thus, the change in C_{dl} values was caused by to the gradual replacement of water molecules by the

adsorption of the polymer composites molecules on the metal surface, decreasing the extent of the metal dissolution **(Bentiss *et al.*, 2005)**

The ac impedance investigations show that all investigated polymer composites exhibit excellent inhibitor properties, the best being the PVAGLU. The inhibition efficiency is calculated from Rct as previously described **(Moha Outirite *et al.*, 2011).** It is found that inhibition efficiency increases with the inhibitor concentration (Table 31,32) and it depends on the position of the nitrogen and oxygen atoms on the polyvinyl alcohol and selected amino acids substituent. Based on the inhibitive properties of the tested polyvinyl alcohol -selected amino acid composites, these compounds can be ranked as follows: PVAGLU> PVAALA > PVATRP > PVAGLN > PVAVAL >PVATRY. Therefore, the ability of the molecule to adsorb on the steel surface was dependent on the position of the nitrogen and oxygen atoms polyvinyl alcohol and selected amino acids substituent.

4.12.7 Performance evaluation of studied polyvinyl alcohol-selected amino acid composites at 0.6% concentration for I_{corr}, R_p, R_{ct} and C_{dl}

To substantiate the enhanced corrosion inhibition character of water soluble polymer composites under study a pictorial representation of performance of studied polyvinyl alcohol-selected amino acid composites at 0.6% concentration by using weight loss method and Electrochemical measurement is depicted in the figure-43.

Performance evaluation of polyvinyl alcohol- selected amino acid composites on mild steel acid corrosion in both acidic media by various techniques are depicted in Figure –43

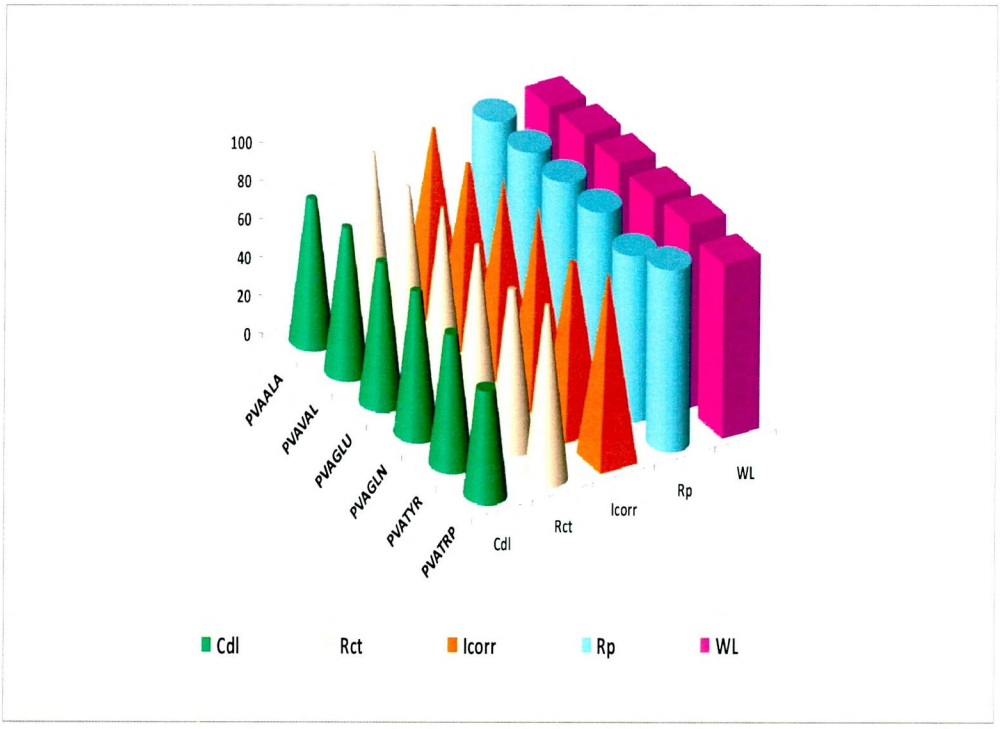

Figure-40 Plot of R_{ct} and C_{dl} with respect to concentrations of polymer composites

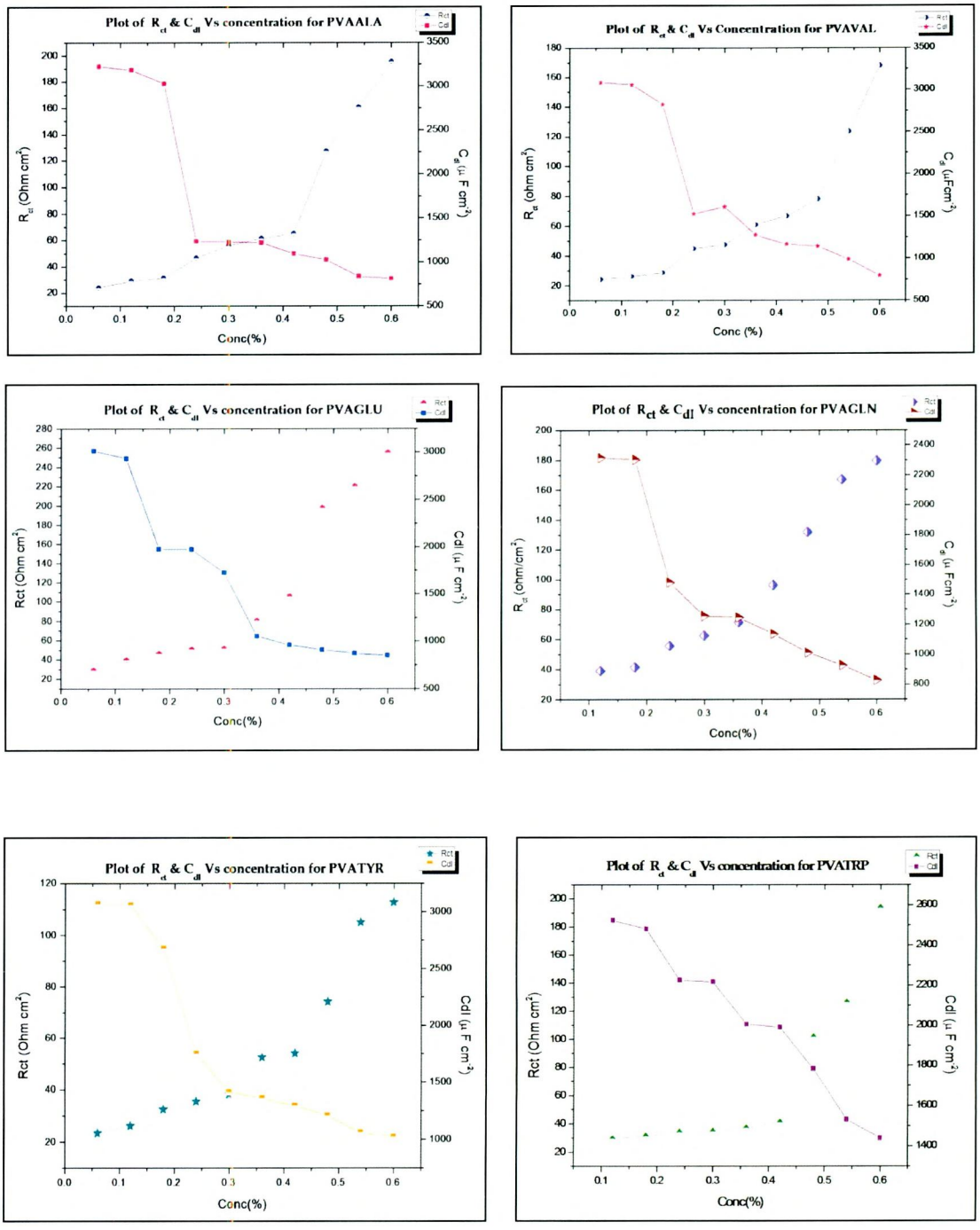

Figure -40 demonstrate the increase in R_{ct} and decrease in C_{dl} of mild steel in the presence of studied inhibitors.

Figure -41 Variation of C_{dl} values with surface coverage (θ) of polymer composites on mild steel surface

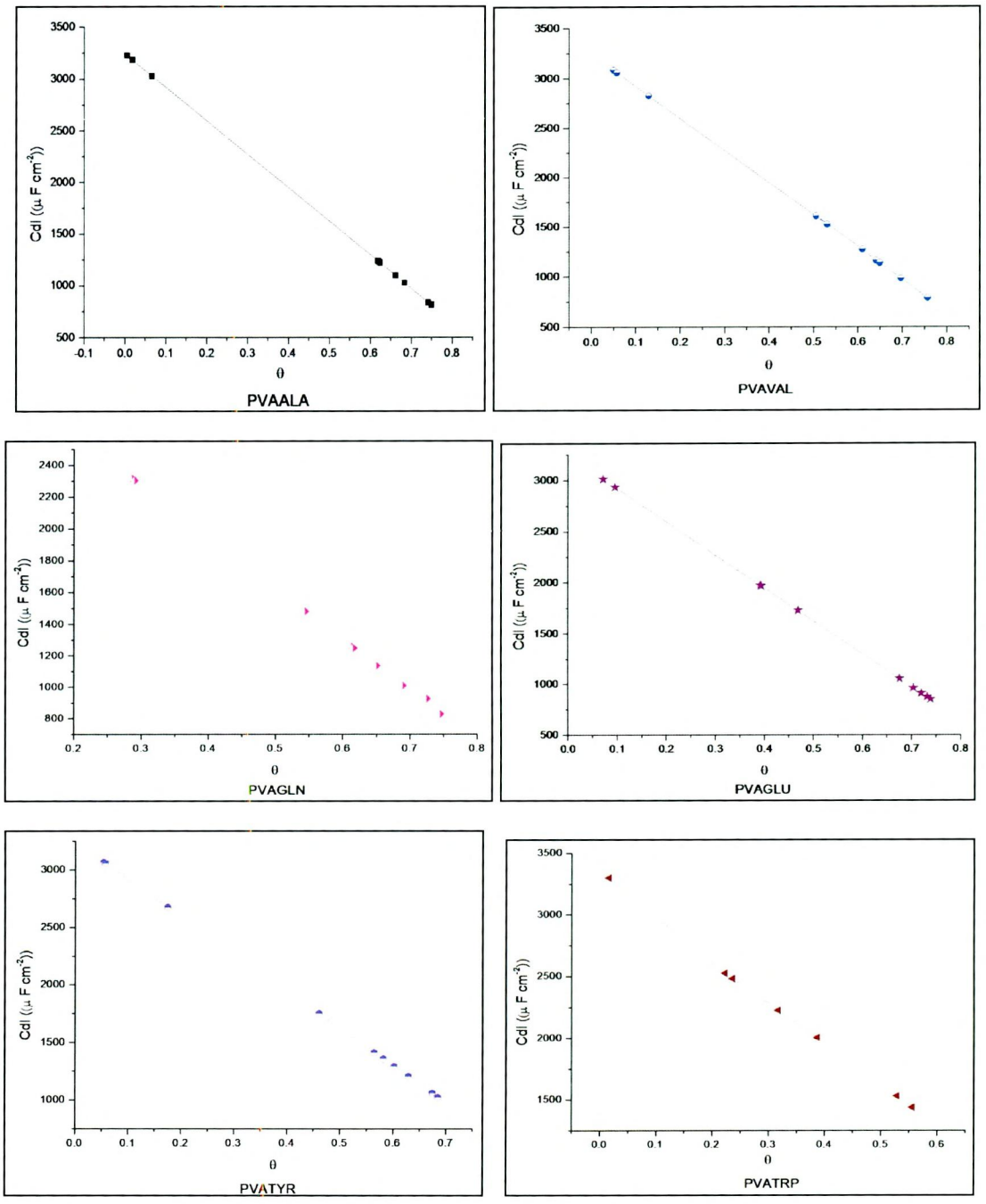

A plot of C_{dl} values versus inhibitors concentration is drawn (figure-41). A straight line is obtained. Similar plots are drawn for all the studied inhibitors which confirm that the inhibitor molecules are adsorbed flatly on the metal surface. **(Martinez *et al.*, 2003).**

Figure-42 Performance Evaluation of PVA-Selected Amino acid composites using Electrochemical measurement

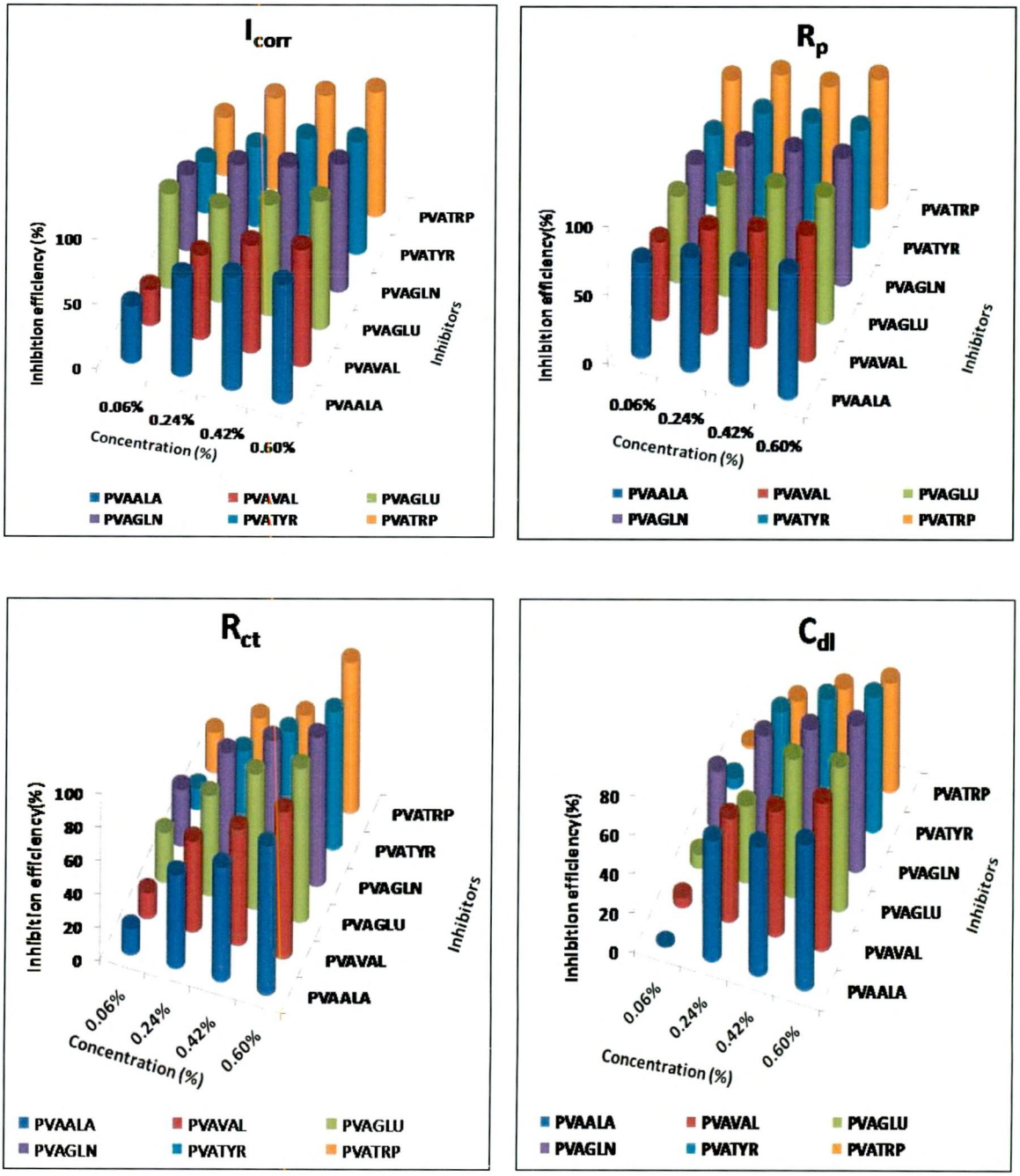

PHASE -III

ANALYSING THE SURFACE OF MILD STEEL IN THE PRESENCE AND ABSENCE OF POLYVINYL ALCOHOL- SELECTED AMINO ACID COMPOSITES BY SURFACE ANALYTICAL TECHNIQUES

In the present investigation, surface of mild steel specimen exposed to the uninhibited and inhibited solutions has been under taken to supplement the results. In this present study, FTIR spectrometry was used to identify whether there was adsorption and to provide new bonding information on the mild steel surface after immersion in inhibited HCl solution. UV-Visible absorption spectra can be used to confirm the protective film formed on the metal surface. The fact that inhibition of corrosion of mild steel in acidic solutions in the presence of PVA-selected Amino acid composites may be due to the formation of film on the metal surface. This is also supported by reflectance studies carried out using a UV-VIS spectrophotometer for different specimens under similar condition. A scanning electron microscope (SEM) was used to evaluate the change in the surface formation caused by contact with the process solutions, and to monitor the effect of adding the inhibitors.

The following surface analytical techniques were used to study the surface of the mild steel in the presence and absence of the inhibitors.

- **Fourier Transform Infra Red Spectroscopy (FTIR)**
- **Ultraviolet-Visible Spectroscopy studies (UV-Visible)**
- **Scanning Electron Microscope (SEM)**

4.13 FTIR SPECTRA STUDY OF THE INHIBITORS

FTIR spectrum has been used to analyze the protective film formed on metal surface.

4.13.1 FTIR spectra of PVAALA composite

FTIR spectrum of the pure PVAALA composite inhibitor was also traced is given in figure-12a. The IR absorption spectrum of PVAALA composite film formed on the surface of the mild steel at immersion time (12h) in 1M HCl acid in the presence of 0.6% PVAALA composite is given in figure-44. It was found that a number of peaks have either disappeared or shifted. Frequencies and peaks of absorption of FTIR of PVAALA composite are presented in table-33. From the results, the FTIR clearly gives the details about the atom which is involved in the coordination with the metal. The presence of characteristic bands for O-H, C=O, COO^-, NH_3^+, N-H, -CONH- and C-N clearly proved that these reaction centres are not involved in the sharing of electrons with the metal. The slight shifts in O-H and N-H bands are observed which may be attributed to the formation of hydrogen bond between them. So, the lone pair electron of oxygen (C=O) may act as electron

donors; forms an complex with Fe^{2+} and prevents corrosion. Other functional groups were missing suggesting that the adsorption of the PVAALA composite inhibitor on the surface of mild steel might have occurred through the missing bonds **(Nnabuk Okon Eddy et al., 2009)**. The weak band at 3753 and 3747 cm^{-1} is attributed to Fe-O bending, which indicate that the coordinate bond is formed by partial transference of electrons from the polar atom (O atom) of PVAALA composite to the metal surface.

Table: 33 Frequency values for FTIR absorption peaks of pure PVAALA composite and adsorbed PVAALA composite on mild steel surface film

S. NO.	Pure PVAALA Composite (cm^{-1})	PVAALA Composite film formation (cm^{-1})	Assgniments
1.	-	3753	Mild steel corroded product
2.	3194	3185	NH_3^+ asym. str., zwitterions, bonded N-H str.
3.	2962,2850	2922	-C-H str. from alkyl group
4.	-	2358	Mild steel corroded product
5.	2013	-	NH_3^+ degenerative deformation
6.	1905,1742	1701	C=O str., amide I band(C=O stretching)
7.	1591	1545	NH_3^+ sym. def., combination NH def. and CN str.
8.	1417	1465	CH_3 bending def. + C-O str. +OH in plane bending
9.	1374	-	Sym. str. of COO^-, C–H/OH bending
10.	1278, 1216	-	CH_2 rocking, rocking of NH_3^+
11.	-	1163, 1115	Mild steel corroded product
12.	1096	1023	C-O str. + C-O-C str. , C-C-N str.
13.	-	866	Mild steel corroded product
14.	790, 712	736	NH wag., COO^-bending
15.	627	670	COO- scissoring

4.13.2 FTIR spectra of PVAVAL composite

FTIR spectroscopy has been used to investigate the nature and center of adsorption by adsorbing the inhibitor on the metal surface. An FTIR spectrum of the pure PVAVAL composite inhibitor was also traced is given in figure-14b. The IR absorption spectrum of PVAVAL composite film formed on the surface of the mild steel at immersion time (12h) in 1M HCl acid in the presence of 0.6% PVAVAL composite is given in figure-44. It was found that a number of peaks have either disappeared or shifted we can conclude that the PVAVAL composite inhibitor is absorbed on the surface of mild steel. Frequencies and peaks of adsorption of FTIR of PVAVAL composite are presented in table-34 The FTIR spectrum of complex prepared by mixing PVAVAL composite and Fe^{2+} is shown in figure-44. Some functional groups were missing, indicating that there is interaction between the PVAVAL composite and the surface of mild steel. This indicates that the electrons

present on the nitrogen, oxygen atoms of PVAVAL composite have coordinated with Fe^{2+} formed on the metal surface resulting in the formation of Fe^{2+}- PVAVAL complex on the anodic sites of the metal surface. The band around 1629 cm^{-1} is attributed to C=O stretching vibration. Appearance of this peak in adsorbed layer indicates that oxygen atom and carbonyl group did not contribute in adsorption process. But the –OH bond (due to carboxylic acid) is missing in the spectrum of the corrosion product, indicating that there is interaction between the surface of mild steel and PVAVAL composite and that the adsorption of PVAVAL composite on the surface of mild steel must have occurred through the missing bond. Also the –OH bond due to hydrogen bond was found in the spectrum of the corrosion product **(Arockia Selvi et al., 2009).**

Table: 34 Frequencies and peaks of FTIR due to corrosion product and PVAVAL composite

S. NO.	Pure PVAVAL Composite (cm^{-1})	PVAVAL Composite (film formation) (cm^{-1})	Assignments
1.	-	3765	Mild steel corroded product
2.	3194	3066	NH_3^+ asym. str., zwitterions, bonded N-H str.
3.	2915, 2846	2917	-C-H str. from alkyl group
4.	-	2393	Mild steel corroded product
5.	2122	-	NH_3^+ degenerative def.
6.	1889	-	C=O Str. Vib., amide I band(C=O str.)
7.	-	1719	Mild steel corroded product
8.	-	-	Mild steel corroded product
9.	1587	1580	NH_3^+ sym. def., combination NH def. and CN str.
10.	1413	-	CH_3 bending def. + C-O str. + OH in plane bending
11.	-	1378	Mild steel corroded product
12.	1293	-	CH_2 rocking, rocking of NH_3^+
13.	-	1160, 1112	Mild steel corroded product
14.	1080	1023	C-O str. + C-O-C str. , C-C-N str.
15.	-	874	Mild steel corroded product
16.	794, 705	739	NH wag., COO^- bending
17.	623	-	COO- scissoring

4.13.3 FTIR spectra of PVAGLU composite

In order to further support the adsorption behaviour of the PVAGLU composite inhibitor on the surface of mild steel, IR spectroscopy was employed. FTIR spectrum of the pure PVAGLU composite inhibitor was also traced is given in figure-15b. The IR absorption spectrum of PVAGLU composite film formed on the surface of the mild steel at immersion time (12h) in 1M HCl acid in the presence of 0.6% PVAGLN composite is given in figure-44. It was found that a number of peaks have either disappeared or shifted. Frequencies and peaks of adsorption of FTIR of

PVAGLU composite are presented in table-35. Some functional groups were missing indicating that there is interaction between PVAGLU composite and Fe in the mild steel and that these functional groups are involved in the formation of bond with Fe in mild steel. The absence of some functional group bands suggest that the lone pair of electron present in the nitrogen is utilized for the bond formation with Fe atoms present in mild steel supporting the protective film formation **(Nnabuk Okon Eddy et al., 2009).**

Table-35 FTIR Spectral data of pure PVAGLU composite and corroded product on mild steel

S. NO.	Pure PVAGLU Composite (cm^{-1})	PVAGLU Composite (film formation) (cm^{-1})	Assignments
1.	-	3747	Mild steel corroded product
2.	3190	3103	NH_3^+ asym. str., zwitterions structure, bonded N-H str.
3.	2973, 2852	2916	-C-H str. from alkyl group
4.	-	2359	Mild steel corroded product
5.	2136	-	NH_3^+ degenerative def.
6.	1884, 1702	1700	C=O str.vib., amide I band(C=O str.)
7.	1581	1542	NH_3^+ sym. def., combination NH def. and CN str.
8.	1415	1464	CH_3 bending def. + C-O str. +OH in plane bending
9.	-	-	Mild steel corroded product
10.	1283	-	CH_2 rocking, rocking of NH_3^+
11.	-	1164	Mild steel corroded product
12.	1082	1021	C-O str. + C-O-C str., C-C-N str.
13.	-	-	Mild steel corroded product
14.	-	874	Mild steel corroded product
15.	795, 710	741	NH wag., COO^- bending
16.	632	669	COO- scissoring

4.13.4 FTIR spectra of PVAGLN composite

In order to evaluate the protective layer formed on the mild steel surface in presence of PVAGLN composite inhibitor and also to provide new bonding information on the mild steel surface, FTIR study has been carried out. FTIR spectrum of the pure PVAGLN composite inhibitor was also traced is given in figure-16b. The IR absorption spectra of PVAGLN composite film formed on the surface of the mild steel at immersion time (12h) in 1M HCl acid in the presence of 0.6% PVAGLN composite is given in figure-44. On comparing the peaks of spectra of PVAGLN composite film formed on the surface of the metal and pure PVAGLN composite spectra, it can be seen that a number of peaks have either disappeared or shifted. Frequencies and peaks of adsorption of FTIR of PVAGLN composite are presented in table-36. From the results, the FTIR clearly gives the details about the

atom which is involved in the coordination with the metal. The shift in the absorption frequencies of the PVAGLN composite on the metal surface strongly support the interaction between oxygen, nitrogen compounds of the inhibitor and metal surface. The reduced intensity of the broad peak at around 3300cm^{-1} designated the reduction of free OH groups, since the proximity of hydroxyl groups enables the PVAGLU to chelate iron ions **(Ramananda Singh et al., 2008)**.

Table-36 FTIR Spectral data of pure PVAGLN composite and corroded product on mild steel

S.NO.	Pure PVAGLN composite (cm^{-1})	PVAGLN Composite (film formation) (cm^{-1})	Assignments
1.	-	3751	Mild steel corroded product
2.	3186	3167	NH_3^+ asym. str., zwitterions structure, bonded N-H str.
3.	2958, 2842	2928	-C-H str. from alkyl group
4.	-	2357	Mild steel corroded product
5.	2145	-	NH_3^+ degenerative def.
6.	1893,1700	1701,1655	C=O str. Vib., amide I band(C=O str.)
7.	1518	1543	NH_3^+ sym. def., combination NH def. and CN str.
8.	1413	1465	CH_3 bending def. + C-O Str. +OH in plane bending
9.	1293	-	CH_2 rocking, rocking of NH_3^+
10.	-	1161	Mild steel corroded product
11.	1080	1021	C-O str. + C-O-C str., C-C-N str.
12.	-	867	Mild steel corroded product
13.	794,705	739	NH wag., COO^- bending
14.	635	671	COO- scissoring

4.13.5 FTIR spectra of PVATYR composite

The FTIR analysis of PVATYR composite and iron complexes has been carried out between 4000 and 400 cm^{-1}. The spectra of pure PVATYR is given in figure-44. The peaks are tabulated in table-37. The IR absorption spectrum of PVATYR composite film formed on the surface of the mild steel at immersion time (12h) in 1M HCl acid in the presence of 0.6% PVATYR composite is given in figure-44. On comparing the spectra of pure PVATYR with the spectra of PVATYR molecule adsorbed over mild steel, it is observed that certain peaks have been disappeared completely and some have shifted to higher frequency region, proving that some adsorption has been taking place over the solid surface. This indicates that this PVATYR inhibitor is adsorbed on the mild steel surface to a certain extent. Since these are adsorbed on the surface, it is anticipated that the adsorption of

these PVATYR composite takes place on the mild steel surface. The broad envelope between 3000 and 3700 cm^{-1} is assigned to the O-H stretch of PVATYR and water. PVATYR molecules may be adsorbed on the mild steel surface and rapidly react with iron cations on or around the surface to form the [PVATYR-Fe-H_2O] complexes on the mild steel surface.

Table: 37 Frequency values for FTIR absorption peaks of pure PVATYR composite and adsorbed PVATYR composite adsorbed on mild steel surface film

S. NO.	Pure PVATYR Composite (cm^{-1})	PVATYR Composite (film formation) (cm^{-1})	Assignments
1.	-	3861, 3744	Mild steel corroded product
2.	3197	-	NH_3^+ asym. str., zwitterion structure , bonded N-H str.
3.	2952, 2852	2920	-C-H str. from alkyl group
4.	-	2357	Mild steel corroded product
5.	2132	-	NH_3^+ degenerative def.
6.	1884	-	C=O Str. Vib., amide I band(C=O str.)
7.	1698	1699	COO^- asym. Str., Substituted benzene ring
8.	1578	1519	NH_3^+ sym.def., combination NH def. and CN str.
9.	1419	-	CH_3 bending def. + C-O Str. +OH in plane bending
10.	1279	-	CH_2 rocking, rocking of NH_3^+
11.	-	-	Mild steel corroded product
12.	1082	1021	C-O str. + C-O-C str. , C-C-N str.
13.	795, 706	-	Mild steel corroded product
14.	628	663	COO- scissoring, Aromatic C-H out of plane bending

Further the intensity of the peaks stretching frequency is decreased which implies that the shifted peaks in this compound is coordinated to Fe^{2+} resulting in the formation of a Fe^{2+}-inhibitor complex on the metal surface. The absence of bands (figure-44) at 2132 and 1884cm^{-1} suggest that the lone pair of electrons present in the nitrogen is utilized for the band formation with Fe atoms present in mild steel supporting the protective film formation. By comparing the spectrum of PVATYR composite film with that of PVATYR composite, we can conclude that the inhibitor is absorbed on the surface of mild steel. The characteristic bands at PVATYR composite found in the PVATYR composite film spectrum confirm the presence of PVATYR composite, or at least, its complex with iron in the formed film. **(Ramananda Singh *et al.*, 2008)**.

4.13.6 FTIR spectra of PVATRP composite

FTIR spectral studies of PVATRP composite on mild steel surface immersed in 1M HCl with 0.6% PVATYR composite are given in table-38 An FTIR spectrum of

the pure PVATRP composite inhibitor is given in figure-18b. The IR absorption spectra of PVATRP composite film formed on the surface of the mild steel at immersion time (12h) in 1M HCl acid in the presence of 0.6% PVATRP composite is given in figure-44. Analysis of the spectrum of the pure inhibitor and the corrosion product reveal that a number of peaks have either disappeared or shifted. This indicates that these components are adsorbed on the mild steel surface to some extent. Since these are adsorbed on the surface, it is anticipated that the adsorption of these PVATRP composite inhibitor takes place on the mild steel surface as well.

NH_2 and O-H stretching vibrations disappeared in the FTIR spectra of adsorbed protective layers it reveals that nitrogen and oxygen atoms can act as active centres in adsorption. An overall investigation of the results suggest that the PVATRP composite has been adsorbed on the mild steel surface, PVATRP composite, as indicated from the spectral data, results in strong adsorption due to donation of lone pair of electrons on oxygen and nitrogen to vacant'd' orbital of the metal which leads to the metal which leads to the formation of metal complexes **(Bahrami et al., 2010).**

Table- 38 Frequency values for FTIR absorption peaks of pure PVATRP composite and adsorbed PVATRP composite adsorption on mild steel surface film

S.NO.	Pure PVATRP composite	PVATRP Composite (film formation)	Assignments
1.	-	3751	Mild steel corroded product
2.	3201	3228	NH_3^+ asym. str., bonded N-H str.
3.	3054	-	NH_3^+ sym. str.
4.	2965, 2841	2923	-C-H str. from alkyl group
5.	-	2336	Mild steel corroded product
6.	2132	-	NH_3^+ degenerative def.
7.	1888	1700	C=O Str. Vib., amide I band(C=O str.)
8.	1578	1543	NH_3^+ sym. def., combination NH def. and CN str.
9.	1407	-	CH_3 bending def. + C-O str. +OH in plane bending
10.	1275	-	CH_2 rocking, rocking of NH_3^+
11.	1176	1113	COO^- symmetric stretching, C-C-C stretching
12.	1082	1022	C-O str. + C-O-C str. , C-C-N str.
13.	-	873	Mild steel corroded product
14.	795706	742	NH wag., COO^-bending
15.	624	-	COO- scissoring, Aromatic C-H out of plane bending

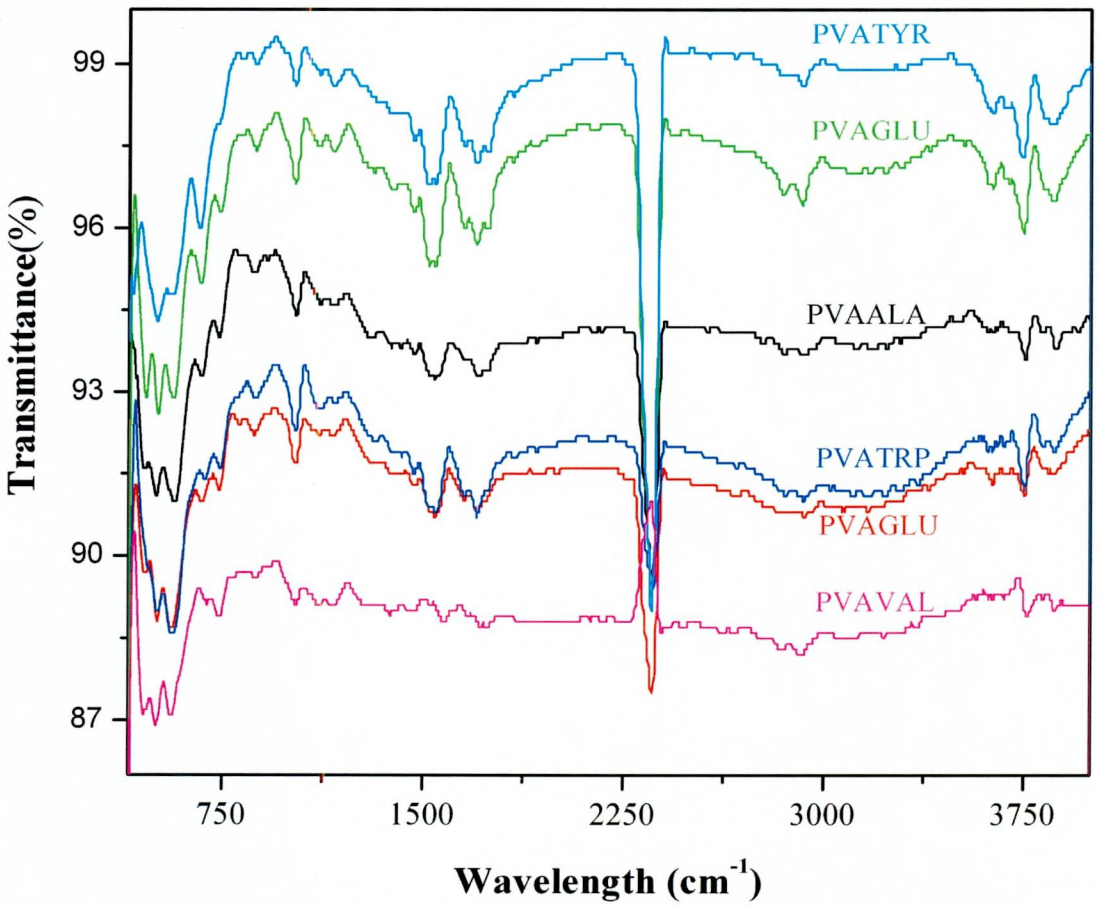

Figure-44 FTIR spectra of PVA-selected amino acid composites and the corrosion product in 1M HCl medium.

4.14 UV-VISIBLE SPECTROSCOPY STUDY OF INHIBITORS

A substantial support for the formation of metal complex is often obtained by UV-Vis spectroscopic investigation. Since there is a certain quantity of metal cation in the solution that is first dissolved from the metal surface, such procedures were conducted in the present work to confirm the possibility of the formation of PVA-selected aminoacid composite complexes as described in several publications (Obi-Egbedi et al.,2010). Furthermore, Abboud et al., 2007 reported the change in position of the absorbance maximum and change in the value of absorbance indicate the formation of complex between two species in solution. In order to confirm the possibility of the formation of PVA- selected amino acid composite- Fe^{2+} complex, UV-Visible absorption spectra was obtained from 1M HCl solution containing 0.6% PVA- selected amino acid composite before and after 12 h of mild steel immersion in figure-45.

The electronic adsorption spectra of the synthesized polymer composites before the mild steel immersion displays

- Two main visible bands at 220nm and 260nm for PVAALA composite (n —> π*
  π —> π* transitions)
- Bands at 220,960nm for PVAGLN and PVAGLU composites (n —> π* transitions)
- Bands at 228,280,310 nm for PVATYR composite (n —> π* π —> π* transitions)
- Bands at 220,960nm for PVATRP composite (n —> π* π —> π* transitions).

These transitions are due to involvement of the whole electronic structure system of the compound with a considerable charge transfer chracter.

After 12h of mild steel immersion UV-Vis spectra of

- PVAALA composite displays two main visible bands at 211nm and 399nm due to n —> π* transitions **(Abboud *et al.*,2007)**
- PVAVAL exhibits a new absorbance peak at 214nm due to n —> π* transition.
- PVAGLU displays new absorbance peaks at 223 and 400nm due to n —> π* and π —> π* transitions
- PVAGLN exhibits an absorbance peak 215nm which may be attributed to n —> π* transitions
- PVATYR displays peaks at 230,280 and 400 nm which may be due to n —> π* and π —> π* transitions
- PVATRP composite displays peaks at 223 and 400nm due to n —> π* and π —> π* transitions

The band maxima for the synthesized polymer composites underwent a blue shift with increase in absorbance suggesting an interaction between the composites and Fe^{2+} ions in solution (Abboud et al.,2007) (chemisorption)

The synthesized polymer composites in aqueous solutions may exist either as neutral molecules or in the form of cations depending upon the concentration of H^+ ions in the solution. In acidic solutions they predominantly exist as cations and adsorb through electrostatic interaction between the positively charged polymer composite and the negatively charged metal surface. In the case of aliphatic amino acid, the interaction between π electron of synthesized polymer

composites and positively charged metal surface also play an important role. The lone pair of e^- density of N atom of the composites and the possibility of e^- donation to the metal via nitrogen is more.

In the case of aromatic amines, the interaction between π electrons of benzene ring and positively charged metal surface also play an important role. The lone pair of electron density of the nitrogen atom is diminished by resonance effect of the synthesized polymer composite (PVATYR & PVATRP) and the possibility of e^- donation to the metal via nitrogen is very less. Hence mild steel surface is positively charged and the interaction between the π electrons of the benzene ring with the mild steel surface is more probable. At low concentration all the synthesized polymer composites offer lower inhibition efficiency. This may be due to the lower coverage of the surface by formation of the quasi complex. The higher efficiency at higher concentration may be due to higher coverage with blockage of the more active sites on the metal surface. The inhibitive property of the polymer composites is mainly due to the adsorption of the polymer molecules on the metal surface in the form of the adsorption through π electron interaction between the composites and the metal surface.

After 12h of immersion time, there was no significant difference in the shape of the bands observed for all the synthesized polymer composites showing a possibility of weak interaction between PVAALA composite and mild steel (Physisorption). These experimental findings give a strong evidence for the possibility of the formation of a complex between the synthesized polymer composites and iron cation in 1M HCl solution.

4.15 SCANNING ELECTRON MICROSCOPY STUDY OF MILD STEEL IN THE PRESENCE OF INHIBITORS

The surface morphology of mild steel surface was studied by scanning electron microscope. In the present investigation, surface chemistry of mild steel specimen exposed to the uninhibited and inhibited solutions has been under taken to supplement the studies.

Figure-45 UV-VISIBLE SPECTRA FOR MILD STEEL TREATED WITH 1M HCl IN THE PRESENCE OF 0.60%PVA-SELECTED AMINO ACID COMPOSITE

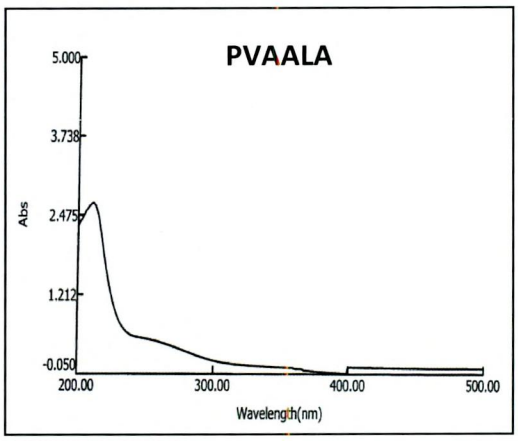

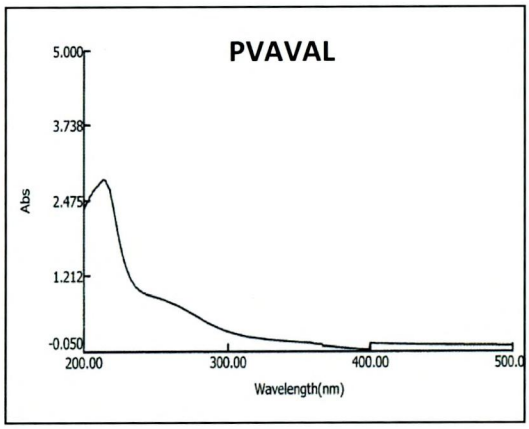

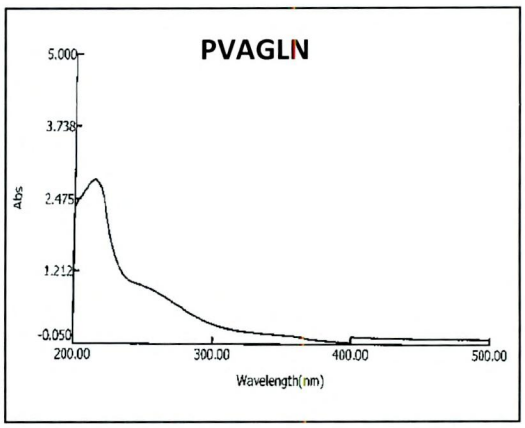

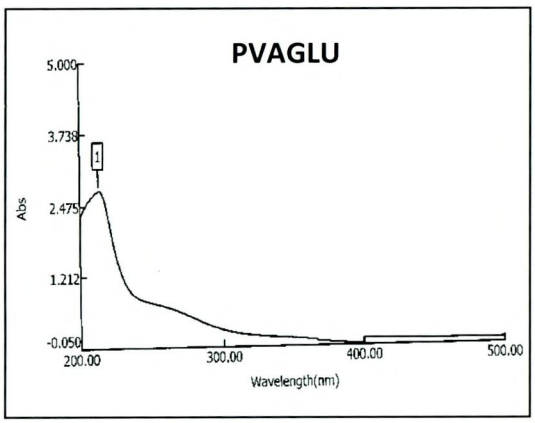

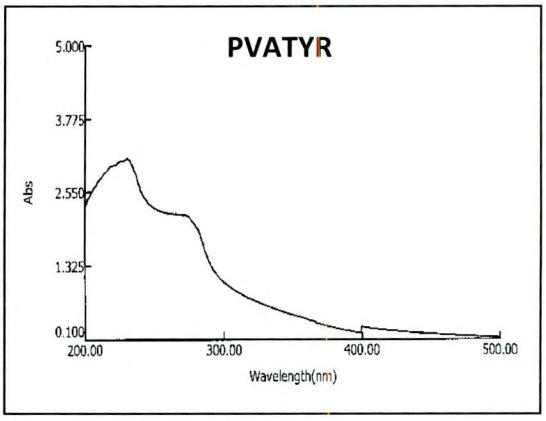

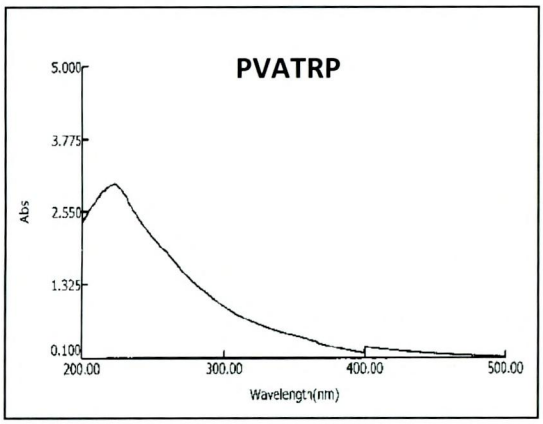

FIGURE-46 SEM IMAGES OF MILD STEEL IN THE PRESENCE AND ABSENCE OF STUDIED INHIBITORS

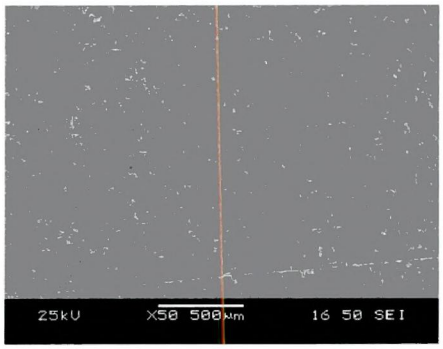

Plain mild steel

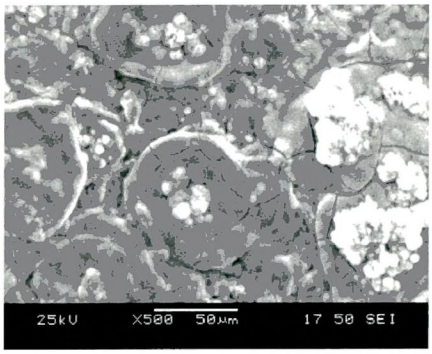

Blank 1M HCl

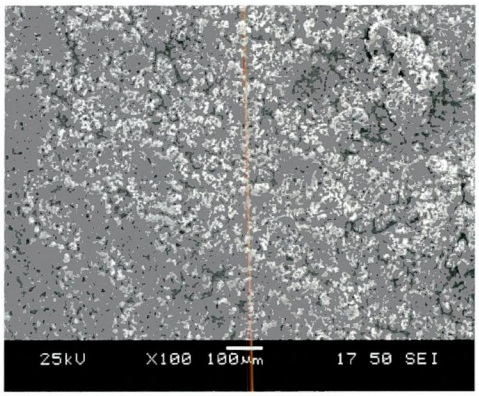

(Mild steel-PVAALA)

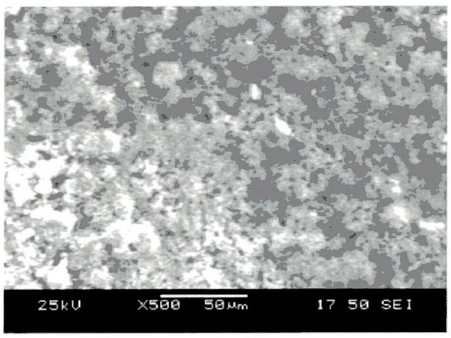

(Mild steel -PVAVAL)

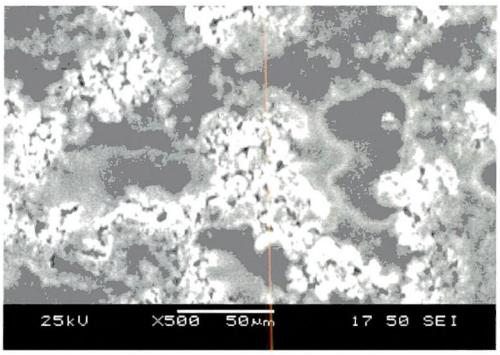

Mild steel -PVAGLN

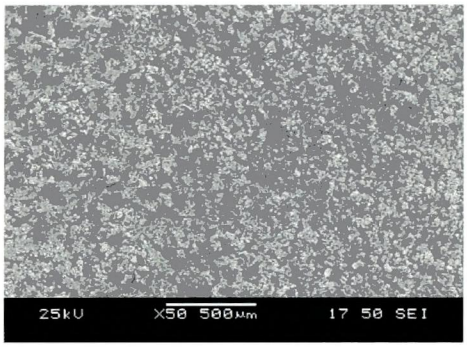

Mild steel -PVAGLU

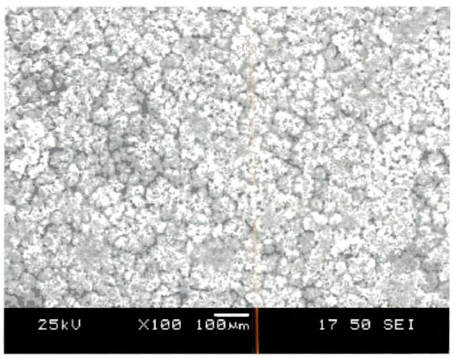

Mild steel -PVATYR

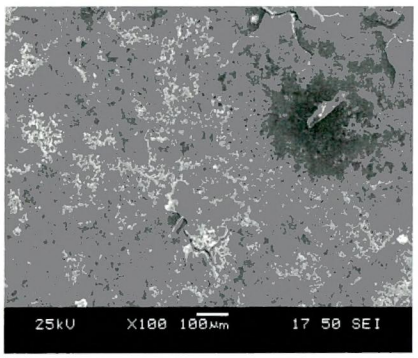

Mild steel -PVATRP

4.15.1 SCANNING ELECTRON MICROSCOPY OF MILD STEEL IN THE PRESENCE OF POLYVINYL ALCOHOL –ALANINE (PVAALA) COMPOSITE:

Figures -46 show the image of mild steel surface immersed in 1M HCl in the absence and presence of PVAALA composite for 6h. Close examination of the SEM coverage in the presence of the inhibitor revealed conditions with smooth surface whereas a corroded rough and coarse uneven surface was observed for the mild steel specimen immersed in 1M HCl acid alone. This observation indicated the corrosion rate is reduced to a very low value in the presence of the PVAALA composite inhibitor. Visual inspection of the mild steel coupons surface shows clearly that application of PVAALA composite inhibitor by immersion methods for 6h in 1M HCl acid /PVAALA composite inhibitor formulation protects the metal surface against further atmospheric corrosion. This might be due the adsorption of inhibitor molecules on the metal surface as protective layer **(Prabhu *et al.,* 2009).**

4.15.2 SCANNING ELECTRON MICROSCOPY OF MILD STEEL IN THE PRESENCE OF POLYVINYL ALCOHOL –VALINE (PVAVAL) COMPOSITE

Scanning electron micrographs of mild steel exposed to 1M HCl solution for 6h in the absence and presence of 0.60% of PVAVAL composite are shown in figure-46 respectively. It is clear from the micrographs that a very rough and corroded surface is obtained in the absence of inhibitor but when the inhibitor is present in 0.60% concentration the efficiency of the inhibitor is quite high, a uniform protective film of the adsorbed inhibitor is obtained on the surface of mild steel. The inhibitor molecule fully covers the metal surface, giving it a high degree of protection against corrosion as proved by the absence of pits on the surface. The surface morphology of PVAVAL composite deposited mild steel clearly shows the presence of non-spherical particles as well as some clusters **(Amin et al., 2010).** It is clear that increasing the chain length increases the inhibition tendency of the inhibitor. That can be attributed to the fact that the increasing the hydrophobic chain length increases the area of metal surface covered by inhibitor molecules. As a result, increasing the covered area by inhibitor molecules increases the inhibition efficiency and dissolution of mild steel decreases.

4.15.3 SCANNING ELECTRON MICROSCOPY OF MILD STEEL IN THE PRESENCE OF POLYVINYL ALCOHOL –GLUTAMIC ACID (PVAGLU) COMPOSITE

SEM photographs obtained for mild steel surface immersed in 1M HCl solutions at room temperature for 6h in the absence and presence of 0.6% of optimum concentration of PVAGLU composite are shown in figure-46 In the absence of PVAGLU composite solution, the corroded metal surface with etched grain

boundaries and corrosion products are clearly seen in figure-46 It can be observed from figure-46, that the specimen surface was strongly damaged in the absence of the inhibitor. But in the presence of inhibitor. SEM image reveals that a good protective adsorbed film is formed on the specimen surface, which suppresses the rate of corrosion, being responsible for the inhibition. The inhibition properties of PVAGLU composite may be to the presence of nitrogenous and oxygen compounds in the PVAGLU composite. This observation clearly proves that the inhibition is due to the formation of an insoluble stable film through the process of adsorption of the PVAGLU composite molecules on the metal surface **(Ganesha Achary *et al.*, 2008).**

4.15.4 SCANNING ELECTRON MICROSCOPY OF MILD STEEL IN THE PRESENCE OF POLYVINYL ALCOHOL –GLUTAMINE (PVAGLN) COMPOSITE:

SEM study (figure-46) show that the inhibited metal surface is found to be smoother than uninhibited metal surface, because the inhibitor gets adsorbed by tightly binding on the metal surface, which shows less abrasion and corrosion on mild steel surface as compared to uninhibited metal surface. This observation indicated that corrosion rate is reduced to a very low value in the presence of the inhibitors. This might be due to the adsorption of inhibitor molecules on the metal surface as a protective layer. These images reveal that the adsorbed inhibitor film present on the mild steel surface mitigated the dissolution of the base metal effectively and thus experience appreciably less corrosion than that of the bare metal. This passive film blocks the active sites present on the mild steel surface. The micrograph shows that in the presence of PVAGLN composite inhibitor, the surface is covered by a heterogeneous layer of products, thereby indicating the inhibiting effect of this film **(Rahim et al., 2008).**

4.15.5 SCANNING ELECTRON MICROSCOPY OF MILD STEEL IN THE PRESENCE OF POLYVINYL ALCOHOL –TYROSINE (PVATYR) COMPOSITE

The typical scanning electron micrograph of the surface of mild steel coupon immersed for 6h in 1M HCl acid medium. Figure-46 show micrograph by SEM by mild steel specimens exposed in 1M HCl of 0.6% PVATYR composite solution at a magnification of ×100.

It is quite apparent from the micrographs the uniform products are also visible. The electron micrograph reveals that the surface was strongly damaged owing to corrosion in absence of the inhibitor, but in the presence of the inhibitor there is a much smaller damage on the surface. This is attributed to the formation of a good protective film on the mild steel surface. The PVATYR composite act as good inhibitor is reduced considerably in the presence of smaller concentrations of PVATYR composite.

The formation of a film is noted which is distributed in a random way on the whole surface of the metal. This may be interpreted as due to the adsorption of the inhibitor on the metal surface incorporating into the passive film in order to block the active site present on the mild steel surface. While the film formed on the metal surface becomes more protective with increase of inhibitor concentration (0.6%) at room temperature. This is attributed to the involvement of PVATYR composite in the interaction with the active sites of metal, so that there is a contact between metal and the aggressive medium. It can be concluded from the figure-46 that corrosion does not occur in presence of inhibitor and hence corrosion was inhibited strongly when the inhibitor was present in the 1M HCl acid medium **(Rafiquee et al., 2007)**.

4.15.6 SCANNING ELECTRON MICROSCOPY OF MILD STEEL IN THE PRESENCE OF POLYVINYL ALCOHOL –TRYPTOPHAN (PVATRP) COMPOSITE

Figure-46 shows scanning electron micrographs of mild steel specimens when exposed to 1M HCl acid solution to 6h in absence and presence of 0.6% of PVATRP composite at room temperature. The polished specimen and the test specimens which are immersed in the blank (1M HCl) and in the inhibitor for 6h, were observed under a metallurgical microscope and photomicrographs are shown in the photograph-46. Photograph-46 show the polished mild steel surface before exposure to the corrosion solution, which is associated with polishing scratches. The specimen surface appears to be roughened extensively by the corrosive environment and porous layer of corrosion product is present. Examination of the figure-46 reveal that the specimens immersed the inhibitor solutions are in better conditions having smooth surfaces compared with that of surface immersed in 1M HCl alone. This indicates that the PVATRP composite compound hinder the dissolution of iron and thereby reduces the rate of corrosion. The smoother surface shown by the coatings indicated the protective behaviour of the coatings against corrosion. By addition of inhibitor to the solution, the corrosion is observed on the surface, but the size and distribution of pits affected by additives structure. The SEM photograph shows that the formation of a film on the metal surface which may be responsible for the corrosion inhibition. It depends on the concentration of the inhibitor solution suggesting that thereby the presence of a protective adsorbed layer of the inhibitor on mild steel surface which impedes corrosion rate of metal appreciably **(Ashassi-Sorkhabi et al., 2005).**

The SEM photograph reveal the formation of a on the metal surface in the presence of current investigated PVA-Selected Amino acids composites and the film formation on metal surface which may be responsible for the corrosion inhibition.

4.16 Mechanism of Inhibition Process:

Mechanism of the inhibition process for studied inhibitors can be discussed on the basis of the experimental findings from weight loss, electrochemical measurements and surface analytical techniques.

In the present investigation corrosion inhibition of mild steel in 1M HCl using the PVA-selected amino acid composites could furnish the following results:

- All the investigated polymer composites obey Langmuir adsorption isotherm indicating that the polymer composites are adsorptive type. The inhibition process is due to the adsorption of the inhibitor molecule onto the mild steel surface.
- The negative values of ΔG_{ads} could confirm that the adsorption process is not merely physical adsorption or chemical adsorption but a comprehensive adsorption.
- Inspection of the data from El Awady adsorption isotherm shows that the reciprocal of Y gives the number of inhibitor molecules occupying one active site (or the number of water molecules replaced by one molecule of inhibitor). Values of 1/Y are more than unity indicating that each molecule of the inhibitor is attached to one active site of the steel surface **(Abd-El Rehim *et al.*, 2001).**
- Values of cathodic and anodic Tafel constant confirm that the investigated PVA-Selected amino acid composites under study act as mixed type of inhibitors.
- Surface analytical techniques using FTIR spectroscopic studies and SEM confirm the adsorption of the polymer composites on the mild steel surface and thus prevents the mild steel corrosion in acid medium.
- UV-Visible spectrophotometer also confirms the adsorption of the inhibitor on the mild steel and formation of iron polymer complex on mild steel surface. From the UV-Visible spectra, the formation of iron polymer complex was confirmed. These iron polymer complex occupy a large surface area of the exposed metal. The absorbed film there by blanket the surface and protect the metal from the aggressive medium.

Corrosion inhibition of mild steel in hydrochloric acid medium by different inhibitors (organic, inorganic, polymers) can be explained on the basis of molecular adsorption. These compounds inhibit corrosion by controlling both anodic as well as cathodic reactions. In most of the cases, the nitrogen/oxygen atom present in the inhibitor molecules can be easily protonated in acidic solution and get converted into quaternary /oxonium ions. These protonated species get adsorbed on the cathodic

sites of the mild steel and decrease the hydrogen evolution and/or to anodic sites through chloride ion inter-bridge thereby decreasing the metal dissolution **(Dileep Kumar Yadav *et al.*, 2010)** The adsorption on anodic sites may also occur through the lone pair electrons of the non protonated nitrogen/oxygen atoms which will decrease the anodic dissolution of the mild steel.

Sulphur-containing compounds are only of minor importance as inhibitor additives in HCl but they are frequently used in H_2SO_4 **(Abd-El Rehim *et al.*, 2001).** As a rule of thumb it holds that S-containing inhibitors are primarily useful in H_2SO_4, whilst N-containing inhibitors exert their best efficiencies in HCl. Some investigators reported that N-containing compounds such as quaternary ammonium salts **(Trabanelli, *et al.*, 1985),** amino acids (**Abdel Rahim *et al.*, 1997)** and aliphatic amines (**Fouda *et al.*, 2005)** are relatively ineffective in prevention corrosion of iron and steel in H_2SO_4 solutions unless certain anions, especially halide (except fluoride) and pseudohalide ions, are present. This gives a strong evidence for the fact that chloride ions of the medium first get adsorbed on the positively charged metal surface.

The process of adsorption of inhibitors are influenced by the nature of the metal surface, the chemical structure of the organic inhibitor, the type of the aggressive electrolyte and the interaction between organic molecules and the metallic surface (**Kertit *et al.*, 1989 and Banerjee *et al.*, 1992**). Many mechanisms have been proposed for the adsorption of organic inhibitors on a metal surface. The inhibitive power of the polymers are also related to the presence of hetero atom (oxygen and nitrogen). These are major active centres for adsorption on the metal surface. Water molecules first get adsorbed on the surface of mild steel immersed in the aqueous medium (**MCCafferty *et al.*, 1972).** The chloride ions from the medium gradually replace the water molecules and get adsorbed on the mild steel surface (**Murakava *et al.*, 1967**).

In the present investigation, polymer composites may interact with the mild steel surface using a number of active centers, good protective layer on the mild steel surface thus retarding further corrosion of the metal in hydrochloric acid. It also exists in the cationic form which can interact with the mild steel surface by electrostatic attraction.

Polymer composites exist in acid solution as neutral molecules or in the form of cations. They can absorb on the metal surface in the form of the neutral molecules via chemisorption **(Quraishi *et al.*, 2000)**.

In acidic medium the OH and NH groups of the polymer composites get protonated. In acidic solution the chloride ions get adsorbed initially on mild steel surface.

The adsorbed chloride ions stimulate the adsorption of protonated polymer composites on the mild steel surface. The adsorbed halide ions acts as an intermediate bridge and enhances the protonated polymer adsorption on the halide adsorbed metal surface. This process is similar to the so-called anion induced adsorption as reported by **(Oguzie et al., 2004)**.

Thus the composites may block the micro-anodes and/or micro-cathodes that are generated on the metal surface in contact with electrolytes and can retard the subsequent dissolution of the metal (**Jayalakshmi *et al.*, 1998)** and represented by the following mechanism (figure-47).

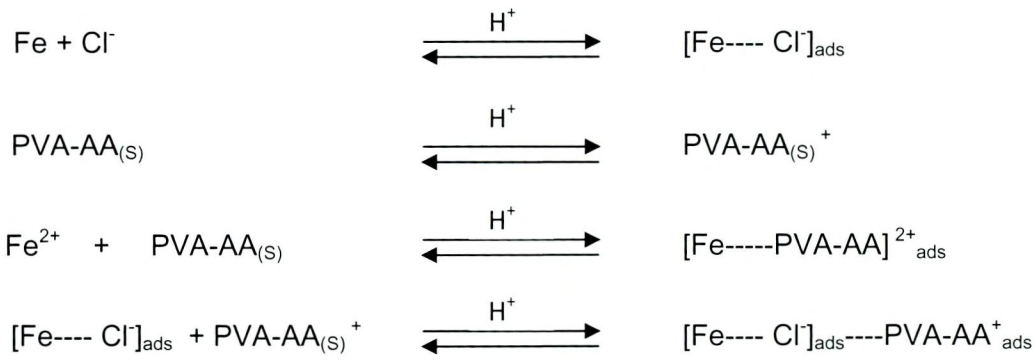

Figure-47 Mechanism of inhibition process

Where PVAAA refers the polymer composite .PVA-AA^+ indicates the protonated polymer composite. [Fe---- $Cl^-]_{ads}$ refers the columbic attraction between Cl^- anion and positively charged metal surface **(Shukla *et al.*, 2011)**. [Fe-----PVA-AA] $^{2+}{}_{ads}$ is the complex formed on the metal surface with polymer composite. [Fe---- Cl^-]$_{ads}$----PVA-$AA^+{}_{ads}$ may be referred an intermediate and it is so called as anion induced adsorption that is chloride ion forms a bridge and enhances the protonated polymer adsorption on the chloride adsorbed on metal surface. The adsorption on anodic sites may also occur through the lone pair electrons of the non protonated nitrogen/oxygen atoms of the composites.

The inhibitive property of polymer composites is also due to the presence of π-electrons, quaternary nitrogen atom and the large molecular size, which ensure greater coverage of the metallic surface.

The adsorption of neutral polymer molecules occurs via donation of the lone pair electrons on nitrogen to iron atoms **(Sathiyanarayanan *et al.*, 2005).**

The high performance of polymer composite is attributed to the presence of nitrogen atom and large number of oxygen atom, larger molecular size and linearity in the polymeric chain. Hence the inhibition process is afforded by virtue of chemical adsorption coupled with physical adsorption (comprehensive adsorption) of PVA-selected amino acid composites into mild steel surface.

Figure-48 Proposed adsorption model for the PVA-amino acid composites is depicted below

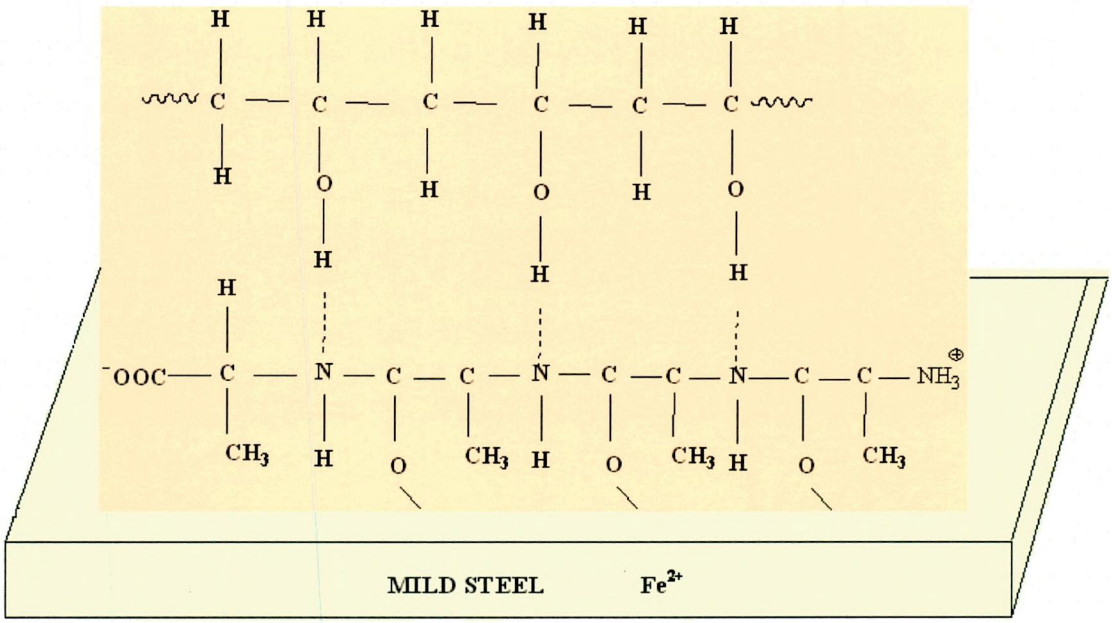

PVAALA COMPOSITE

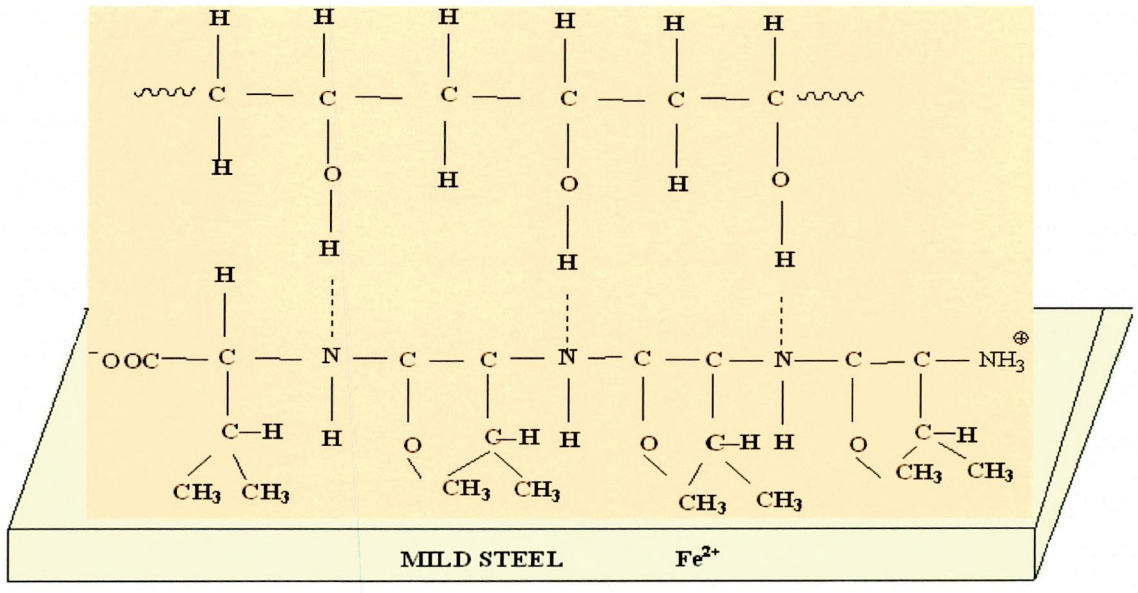

PVAVAL COMPOSITE

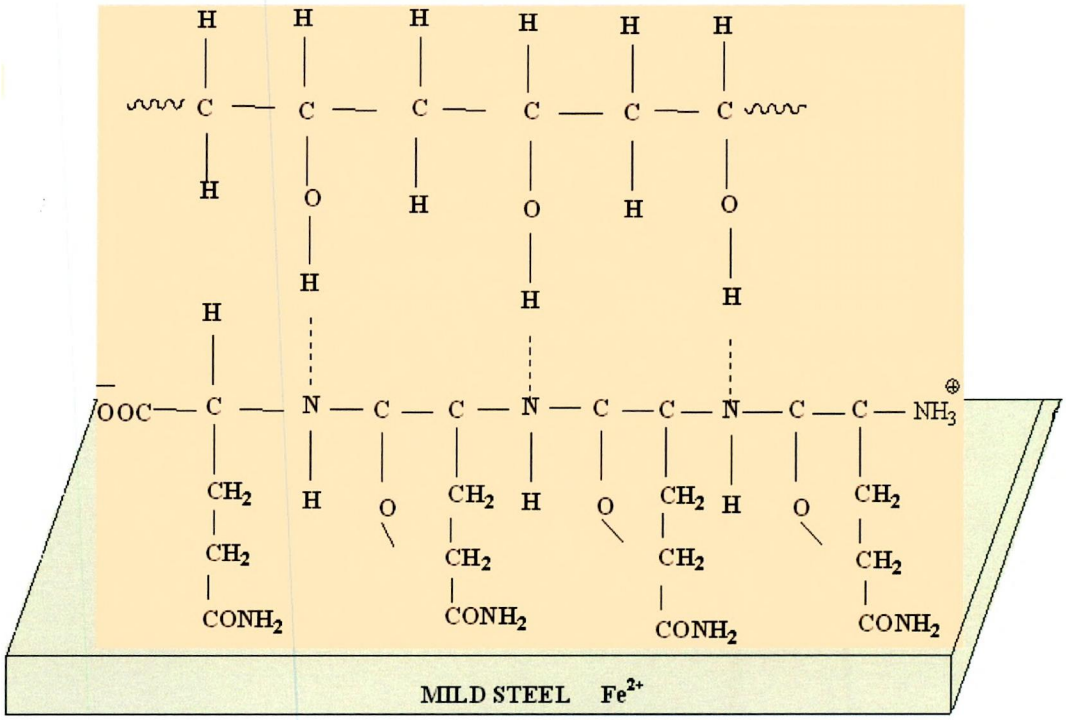

PVAGLN COMPOSITE

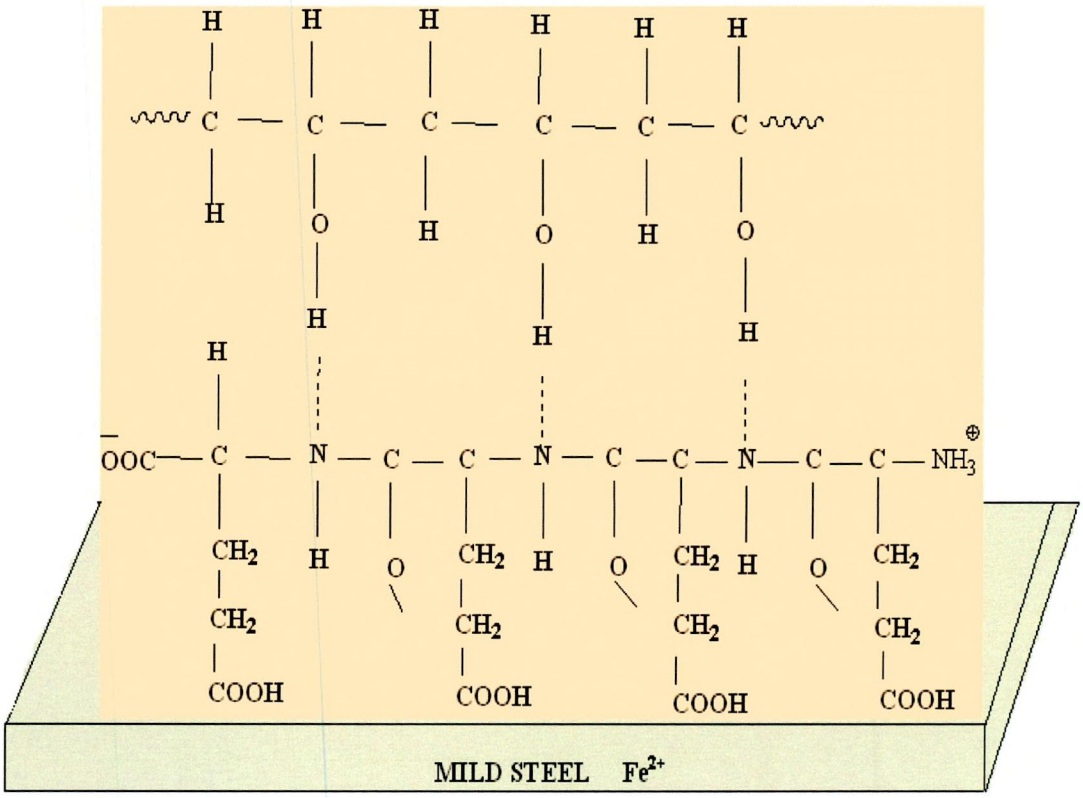

PVAGLU composite

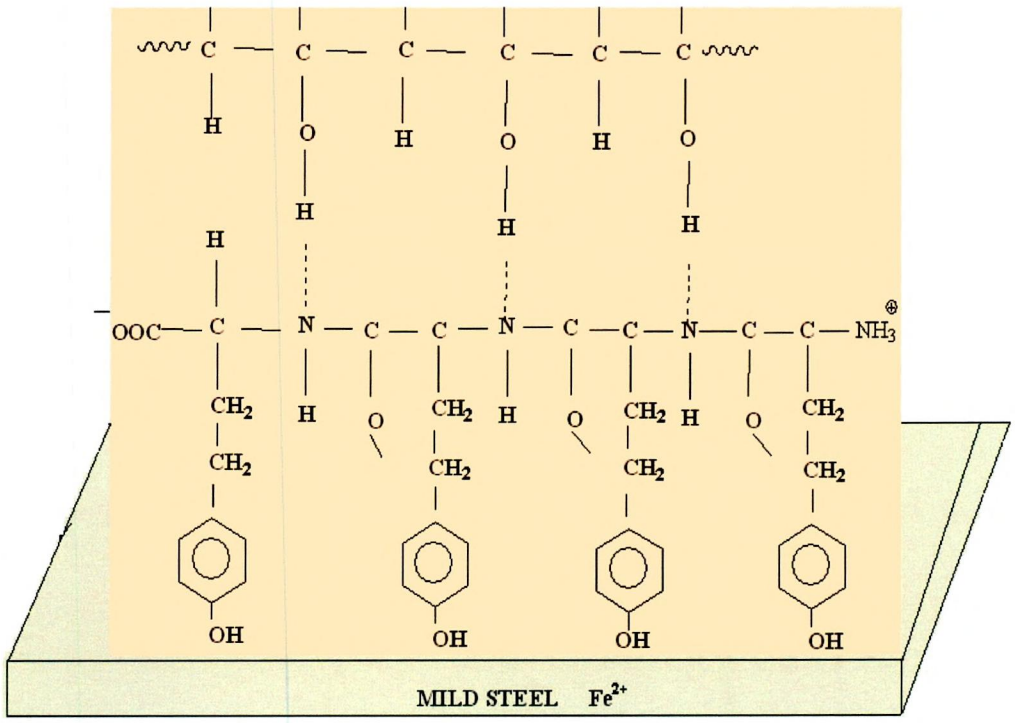

PVATYR composite

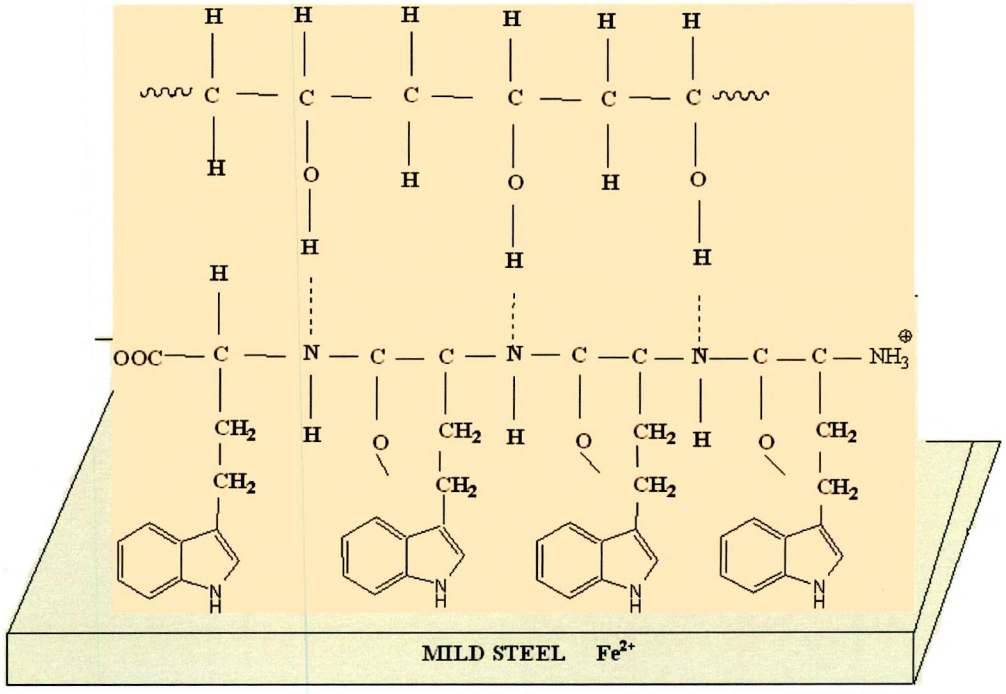

PVATRPCOMPOSITE